Studies of Generation of Acid Sites

on Supported Transition Metal Oxides

TOMOYUKI KITANO

2013

Preface

Studies of "acid-base catalysis on solid surface" started with the discovery of dehydration of alcohol on natural clay by Sir Humphry Davy in 1795. At the present day, this phenomenon is interpreted in terms of dehydration of ethanol to ethane on acid sites on clay surface. In 1901, Kobayashi demonstrated that the natural clay changed the color of Litmus indicator. This is believed to be the first direct evidence of acid property on solid surface. Natural clay minerals consist of mainly hydrated magnesium silicate and aluminosilicates, those are known as solid acids. In 1936, the first industrial process using solid acid catalyst for catalytic cracking began operation by Socony Vaccum Oil Co. Nowadays, in many industrial processes, solid acid catalysts play important and significant roles. Solid acid catalysts have been widely utilized in many important reactions converting petroleum, natural gas, and coal to raw materials for almost all chemical products such as cracking of hydrocarbons, conversion of methanol into hydrocarbons, isomerization, alkylation, acylation, oligomerization, polymerization, hydration, dehydration, and hydrolysis. Therefore, solid acid catalysts are being studied intensively in both academic and applied field to expand their capabilities in a variety of reactions. Indeed, a series of congress focused on acid-base catalysis have been held at regular intervals from 1988.

Solid acid catalysts are promising not only in application to acid-catalyzed reactions but also in material science, including adsorbents, sensors, ceramics etc. Fundamental study of acid-base catalysis on solid surface promotes progress in chemistry of acid-base catalysis by heterogeneous catalysts. Development of the acid-base catalysis may bring to the realization of environmentally benign catalytic process by replacing environmentally unfriendly homogeneous catalysts such as sulfonic acid and sodium hydroxide with heterogeneous ones.

In the case of heterogeneous catalysts including solid acid and base catalysts, the catalytic properties are totally dependent on the surface properties of the catalysts. It has been though that the surface structure of the catalysts is one of the key factors to control the surface properties like acid and base property. Although the relationship between the structure, acid property, and catalytic performance of solid surface is widely investigated, and based on this relationship, there have been attempts to understand the mechanism of generation of acid sites on solid surface, the

generation mechanism of acid sites is still under discussion. Fundamental studies of the generation mechanism of acidic and basic property on solid surface, the author believes, are essentially important at present to develop and design new and effective solid acid and base catalysts for many fascinating reactions.

The main themes of the present thesis are to clarify acidic property and the generation mechanism of some new solid acid catalysts. From this point of view, the author commenced to study structure, acid property, and nature of the catalyst of alumina-supported niobium oxide (Nb_2O_5/Al_2O_3) calcined at various temperatures with various Nb_2O_5 loadings. The author found the generation of thermally stable Brønsted acid sites on Nb_2O_5/Al_2O_3 calcined at high temperatures above 1000 K. The relationship between structure of niobium oxide supported on alumina and its acidic property are investigated and the generation mechanism of acid sites is discussed. In addition, the author demonstrated that other transition metal oxides (Ta, Mo, and W) supported on alumina calcined at high temperatures (1073 - 1223 K) also exhibits Brønsted acid sites as well as Nb_2O_5/Al_2O_3, and characterized the structure of these transition metal oxides supported on alumina.

Generally, acid sites on solid acid surface disappear when solid acids are heated at higher temperatures than 1000 K due to decomposition of acid sites and/or phase transition of solid acid to a stabilized phase. In contrast, supported transition metal oxides (Nb_2O_5, Ta_2O_5, MoO_3, and WO_3) on alumina maintain Brønsted acid sites even after calcined at high temperatures. Because of specific acidic and structural characters of supported transition metal oxides on alumina, the author focused these supported transition metal oxides and investigated to reveal their acidic property and the origins.

CONTENTS

General Introduction

Current Situation of Acid Catalyst

Catalyst is a fundamental material for chemical industry. Catalyst is used not only for converting petroleum and natural gas to new materials but also for cleaning exhaust gas from cars and factories and generating electricity from hydrogen and oxygen.[1-4] Above all, acid-base catalyst plays an important role in the chemical industry. Acid-base catalyzed reaction is one of the reactions utilized most continually in all of the industrial reactions. Producing raw materials from fossil fuel exclusively depends on acid-base reactions and converting raw materials to end products depend on various reactions such as oxidation, reduction, and polymerization. Acid-base catalysts are used for many reactions to produce raw materials such as isomerization, alkylation, acylation, dehydration, and hydration. To develop highly-efficient and lean acid-catalyzed reactions, many researchers have studied acid-base catalysts.

The first person finding catalytic action is Joseph Priestley. In the end of 18th, he noticed that ethyl alcohol changed into a gas which is different from ethyl alcohol when ethyl alcohol passed through natural clay. It is said that dehydration of ethyl alcohol occurred. The phenomenon was called as "catalysis" by Jons Jakob Berzelius in 1836 and catalytic reaction was started to be recognized from this period. "Catalyst" is defined as the material changing reaction rate and not changing equilibrium regardless of consumption by Friedrich Wilhelm Ostwald in 1896. Acid-catalyzed reaction process commercially began in 1936. Oil cracking process using natural clay is the first industrial reaction process using solid acid catalyst on a large scale. Since 1936, various industrial reaction processes using solid acid catalysts have been developed and study of catalyst started kicking in from this period.

Catalyst is broadly divided into heterogeneous catalyst and homogeneous catalyst. In the case of acid catalyst, liquid acid catalysts such as H_2SO_4 and HF belong to homogeneous catalyst and solid acid catalysts such as zeolite and cation exchanged resin belong to heterogeneous catalyst. Liquid acid catalyst is used for many liquid phase reactions because liquid acid catalyst shows high activity and selectivity at low temperature, low investment and better flexibility. However, because

liquid acid catalyst is difficult to be separated from solution and has toxicity and corrosivity, acid-catalyzed reaction process using solid acid catalyst is ideal.

Solid acid catalyst is estimated in terms of activity, selectivity, mechanical strength, and life of the catalyst. Above all, Activity and selectivity are important factors for solid acid catalysts and strongly depend on acid property of the catalyst. Acid property is evaluated by three factors, acid amount, acid strength, and acid type (Brønsted acid or Lewis acid). Because acid amount and acid strength concern with activity and acid strength and acid type concern with selectivity, it is necessary for development of solid acid catalyst to investigate the factors in parts. Acid property strongly depends on structure of the catalyst. Therefore, many researchers study the structure of solid acid catalyst and relationship between the acid property and the structure of the catalyst and try to clarify the generation mechanism of acid sites.

Study of Mixed Metal Oxides

There are many kinds of solid acid catalysts such as cation exchange resins, metal oxides, metal salts, and mixed metal oxides.[5] Above all, mixed metal oxides are often used for industrial acid-catalyzed reactions. In the Tanabe's[6] and Busca's report,[7] most of gas phase reactions concerning petroleum (alkylation, isomerization, dehydration, hydration, and esterification) proceed on mixed metal oxides. Industrial acid-catalyzed reaction processes mainly proceed on zeolite, which is one of the most popular mixed metal oxides used for acid-base reactions, such as Y zeolite, ZSM-5 zeolite, and Mordenite zeolite. In addition, amorphous SiO_2-Al_2O_3 and TiO_2-SiO_2 are also used for industrial acid-catalyzed reactions. Therefore, mixed metal oxides play an important role in the solid acid catalysts. Mixed metal oxide takes the central role not only in oil cracking but also in MTO (Methanol To Olefin) and complex acid-catalyzed reaction such as selective hydration of nitriles.[4] In addition, some researchers reported that some mixed metal oxides are active for reactions from biomass feedstock, which is a new energy source alternative to fossil fuel, and the mixed metal oxides are expected to open up new industrial reaction processes.[8]

On the demand for development of industrial acid-catalyzed reaction processes, the acid property of mixed metal oxide has been studied. Basically, few simple metal oxide exhibit strong

acid property except for niobic acid and hydrated tantalum oxide.[9-12] However, many researchers have found various mixed metal oxides (TiO_2-SiO_2, SiO_2-MgO, Al_2O_3-TiO_2, etc.) exhibiting acid property, and then a hypothesis predicting the generation of acid sites on binary metal oxides was proposed by Tanabe et al..[5,13] The hypothesis expects whether a binary metal oxide generates acid property or not and whether Brønsted acid sites or Lewis acid sites generate on a binary metal oxide. According to the hypothesis, acid sites generation is caused by excess of a negative or positive charge in the model structure of a binary metal oxide. Very good agreement between the predictions of Tanabe et al.'s hypothesis with the experimental results was shown and the hypothesis explains well the mechanism of the acid site generation only on amorphous binary metal oxides.

The Acid Property of Heterogeneously Mixed Metal Oxide

There are two types of mixed metal oxides, homogeneously mixed metal oxide such as zeolite and heterogeneously mixed metal oxide such as supported metal oxide and ion-exchanged metal oxide. In the most of the cases, homogeneously mixed metal oxide are used for industrial acid-catalyzed reactions and commercial reaction processes using supported metal oxides and ion-exchanged metal oxide are a few. Therefore, the acid property and the structure of homogeneously mixed metal oxides are often studied. On the other hand, though supported metal oxides and ion-exchanged metal oxides are really used commercially, some supported metal oxides and ion-exchanged metal oxides are reported to show unique acidic property. Okuhara et al. reported that MoO_3/ZrO_2 showed high activity for water-concerning reactions such as hydrolysis, dehydration, and esterification and the surface hydrophobicity was the important factor to the activity of water-concerning reactions.[14-16] They found that addition of water accelerated the water-concerning reactions on the catalyst, but the mechanism of acceleration and the structure of acid sites were still unclear. Kaneda et al. and Onaka et al. reported that ion-exchanged montmorillonite showed high activities for various acid-catalyzed reactions.[17-20] Kaneda et al. reported that copper and scandium ion-exchanged montmorillonite showed high catalytic activities for carbon-carbon bond-forming reaction (Michael reaction, Sakurai-Hosomi allylation, and the Diels-Alder reaction) promoted on Lewis acid sites.[18] Onaka et al. found that tin and titanium ion-exchanged montmorillonite showed

high reactivity for esterification between triose and methanol and cyanation of alcohol and exhibited Brønsted acid property.[19,20] They proposed that a chainlike structured metal oxide were formed in the layer of montmorillonite and the chainlike structured metal oxides generated Lewis acid sites or Brønsted acid sites. Arata et al. reported that superacid sites were generated on WO_3/ZrO_2, MoO_3/ZrO_2, WO_3/SnO_2, WO_3/TiO_2, WO_3/Fe_2O_3, and B_2O_3/ZrO_2 etc..[21-23] The acid strength of such catalysts is higher than 100 % H_2SO_4 and the catalysts promote isomerization of alkanes which needs strong acid sites. The structure of acid sites having super acidic property have been characterized but the detail is now under discussion.

Though these mixed metal oxides exhibit unique acid property, Tanabe et al.'s hypothesis cannot explain the generation of acid property on these catalysts because the catalysts are heterogeneously mixed metal oxides and the hypothesis assumes that two kinds of metal oxides are dispersed in the catalysts homogeneously. And the hypothesis has a disadvantage that the hypothesis cannot explain the acid strength. Many kinds of heterogeneously mixed metal oxides exhibiting acid property were found and expected to be utilized for industrial reactions and the acid property of the catalysts also cannot be explained by Tanabe's hypothesis. Due to controlling and developing the acid property of mixed metal oxides, other kinds of hypothesis about generation of acid sites on such mixed metal oxides are necessitated.

The Effect of Local Structure on Generation of Acid Sites

Some interesting speculations on generation of mixed metal oxides were reported. Both amorphous SiO_2-Al_2O_3 and zeolites are composed from SiO_2 and Al_2O_3, but the acid property is quite different. In addition, the acid property of zeolites strongly depend on zeolite type such as Y, mordenite, and ZSM-5 etc..[7,24] Considering Tanabe's hypothesis, these alumino silicates are expected to exhibit the same acid property. Niwa et al. reported that H-Y zeolite had four kinds of structurally different Brønsted acid sites. Using IRMS-TPD of ammonium, in which IR and MS on line work together to measure the behavior of adsorbed ammonia species as well as the desorbed ammonia, they found four kinds of acidic hydroxyl regions and calculated each of heat of ammonia adsorption. From the results, they concluded that the Brønsted acid sites on H-Y zeolite were

generated on different sites (super cage, sodalite cage, and hexagonal cage) and exhibited different acid strength.[25] Each site has different Si-OH-Al angles and Al-O bond length and such geometrical parameters are supposed to be the key of decision of acid property. Some researchers investigated correlation between Brønsted acid property of zeolites and the structure of Al incorporated in the framework of zeolite and concluded that the acid property depended on Si-OH-Al angles more strongly than Al-O length and kind of extra framework cation.[26,27] These facts indicate that "distortion" is the important factor for generation of acid sites and acid strength, because it is often considered that active sites generate on unstable structured sites. Some researchers show that "distortion" plays an essential role in generation of acid sites and decision of acid strength. SiO_2 is known to be inactive material but FSM-16 and MCM-41, which are mesoporous silica with regular one-dimensional pore structure, exhibit acid property.[28-31] Yamamoto et al. expected that weakly perturbed isolated silanol groups acted as Brønsted acid sites and strained siloxane bridges acted as Lewis acid sites.[28,30,32] On the other hand, no paper suggests that SBA-15, which is also one of mesoporous silica with regular one-dimensional pore structure and the pore size is a little larger than that of FSM-16 and MCM-41, has acid property. It is supposed that the difference of pore size cause the difference of acid property, and in other words, the trigger of generation of acid sites is "distortion" due to smaller Si-O-Si angle. TiO_2 has only weak acid sites but TiO_2 nanotube shows high activity for Friedel-Crafts alkylation and dehydration. Kitano et al. also supposed that distortion of local structure caused generation of acid sites.[33] It is often said that niobic acid has water-torelant acid sites.[15,34,35] Niobic acid is composed of distorted NbO_6 octahedra and NbO_4 tetrahedra and recently, Hara and colleagues suggested that the NbO_4 tetrahedra acted as water-tolerant Lewis acid sites from the results of Raman spectra.[36] In this case, it is supposed that low coordination number causes generation of acid sites as "distortion".

Characterization of Supported Metal Oxide

It is generally said that generation of acid sites on supported metal oxide also needs distortion of local structure of metal oxide. As described above, WO_3/ZrO_2, MoO_3/ZrO_2, WO_3/SnO_2, WO_3/TiO_2, WO_3/Fe_2O_3, and B_2O_3/ZrO_2 exhibit super strong acid property. Above all, WO_3/ZrO_2

showed the highest strong acid property ($H_0 \leq -14.6$) in all of the mixed metal oxides.[21,23] WO_3/ZrO_2 has received considerable attention as a strong solid acid catalyst for the isomerization of light alkanes at low temperature and is considered as an alternative catalyst for many practical industrial applications. A large number of groups have investigated the acid property and the structure of tungsten oxide on WO_3/ZrO_2. It has been often suggested that catalytic performance strongly depends on the surface density of WO_x species on the zirconia surface, and WO_x species supported on $ZrO_x(OH)_{4-2x}$ can have considerably superior acid property than WO_x species supported on well-defined ZrO_2 crystallite.[37,38] It is generally considered that WO_3/ZrO_2 exhibits the highest catalytic activity when WO_x is loaded as 7-8 W nm^{-2}, which is a little larger than the value corresponding to monolayer surface coverage and at that loading amount, WO_3 forms two-dimensional WO_3 domains and crystalline WO_3 nanoparticles.[37,39,40] Scheithauer and colleagues favored a fully oxidized poly-tungstate Keggin-like network structure incorporating trace levels of surface-exposed Zr^{4+} as the active species because of electron-withdrawing effect by adjacent WO_x units.[41] Wachs and colleagues assigned the structure of active site to distorted Zr-stabilized WO_3 nanoparticles.[37] Afanasiev and colleagues proposed a model in which several tungsten oxoanions surround a hydrated zirconium oxide group with OH groups attached to Zr atoms being responsible for the strong acid sites.[42] The detailed atomic-scale structure of the catalytic active site is still a controversial subject, several active sites models having been proposed in the literature because supported metal oxide forms a lot of sites in which geometric parameter (coordination number, bond length, and bond angle) differs from each other and it is difficult to decide which site exhibits acid property. However, each case indicates that specific local structures (poly-tungstate incorporating Zr^{4+}, Zr-stabilized distorted WO_3 nanoparticles, and Zr atoms surrounded by several tungsten oxoanions) are needed to generate acid sites and it is supposed that "distortion" occurs on such specific local structures.

Outline of the Present Thesis

The author found that binary-metal oxides exhibit unique acid property. Most solid acid catalysts calcined at higher temperature than 873 K lose their acid property. Niobic acid, which

shows water-tolerance and strong acid property, also loses the acid property when the catalyst is calcined at 673 K. However, niobium oxide supported on alumina calcined at high temperature (1123 K) shows activities for Friedel-Crafts alkylation, cumene cracking, and isomerization of α-pinene and generates thermally stable Brønsted acid property. There are few reports discussing solid acid catalysts calcined at high temperature exhibiting acid property, especially Brønsted acid property. The generation of such acid sites on these catalysts can not be explained by Tanabe's hypothesis because niobium oxide and alumina are not mixed homogeneously. Even if Tanabe's hypothesis is applied for this catalyst, Tanabe's hypothesis does not indicate generation of Brønsted acid sites. Because thermally stable solid acid catalyst is promising material, investigation of the structure of thermally stable acid sites and clarification of generation mechanism of thermally stable acid property are important.

In this thesis, the author discovered some translated metal oxide (Nb, Ta, Mo, and W) supported on alumina and calcined at high temperature (1073 - 1223 K) generated Brønsted acid sites and focused attention on the relation between acid property and structure of translated metal oxide supported on alumina calcined at high temperature. The results of structural characterization such as X-ray photoelectron spectroscopy (XPS), Fourier transformed infrared (FT–IR) spectroscopy, and energy-dispersive X-ray (EDX) analysis suggested that translated metal oxides are supported on alumina as two-dimensional metal oxide monolayer domains. And considering the change in the acid property with calcination temperature and loading amount, the author concluded the generation mechanism of thermally stable Brønsted acid sites as described below. 1) Raise of calcination temperature and loading amount cause increase of the amount of metal oxide monolayer domains. 2) Around monolayer coverage of the monolayer domains, the domains contact with other domains. 3) At the contact point, "distorted" M-O-M bonding is formed (M = Nb, Ta, Mo, and W) and Brønsted acidic hydroxyl groups are generated on the bonding (M-OH-M).

References

(1)   Kikuchi, E.; Segawa, K.; Tada, A.; Imizu, Y.; Hattori, H. *Atarashii Syokubai Kagaku*, Sankyo Syuppan, Tokyo, 2007.

(2)   Misono, M.; Saito, Y. *Syokubai Kagaku*, Maruzen, Tokyo, 2009.

(3)   Tanabe, K. *Syokubai no Hataraki*, Kagaku Dojin, Kyoto, 1988.

(4)   Syokubaigakkai *syokubaibinran*, Kodansha, Tokyo, 2008.

(5)   Tanabe, K.; Misono, M.; Ono, Y.; Hattori, H. *New Solid Acids and Bases*, Kodansha, Tokyo, 1989.

(6)   Tanabe, K.; Holderich, W. F. *Appl. Catal. A,* **1999**, *181*, 399.

(7)   Busca, G. *Chem. Rev.,* **2007**, *107*, 5366.

(8)   Corma, A.; Iborra, S.; Velty, A. *Chem. Rev.,* **2007**, *107*, 2411.

(9)   Nowak, I.; Ziolek, M. *Chem. Rev.,* **1999**, *99*, 3603.

(10)   Tanabe, K. *Catal. Today,* **1990**, *8*, 1.

(11)   Iizuka, T.; Ogasawara, K.; Tanabe, K. *Bull. Chem. Soc. Jpn.,* **1983**, *56*, 2927.

(12)   Ushikubo, T.; Wada, K. *Appl. Catal.,* **1990**, *67*, 25.

(13)   Tanabe, K.; Sumiyosh.T; Shibata, K.; Kiyoura, T.; Kitagawa, J. *Bull. Chem. Soc. Jpn.,* **1974**, *47*, 1064.

(14)   Li, L. S.; Yoshinaga, Y.; Okuhara, T. *Phys. Chem. Chem. Phys.,* **2002**, *4*, 6129.

(15)   Okuhara, T. *Chem. Rev.,* **2002**, *102*, 3641.

(16)   Li, L. S.; Yoshinaga, Y.; Okuhara, T. *Phys. Chem. Chem. Phys.,* **1999**, *1*, 4913.

(17)   Ebitani, K.; Kawabata, T.; Nagashima, K.; Mizugaki, T.; Kaneda, K. *Green Chem.,* **2000**, *2*, 157.

(18)   Kawabata, T.; Kato, M.; Mizugaki, T.; Ebitani, K.; Kaneda, K. *Chem. Eur. J.,* **2004**, *11*, 288.

(19)   Wang, J.; Masui, Y.; Onaka, M. *Acs Catal.,* **2011**, *1*, 446.

(20)   Wang, J.; Masui, Y.; Onaka, M. *Appl. Catal. B,* **2011**, *107*, 135.

(21)   Arata, K. *Appl. Catal. A,* **1996**, *146*, 3.

(22)   Arata, K.; Nakamura, H.; Shouji, M. *Appl. Catal. A,* **2000**, *197*, 213.

(23)   Arata, K.; Matsuhashi, H.; Hino, M.; Nakamura, H. *Catal. Today,* **2003**, *81*, 17.

(24)   Lee, C.; Parrillo, D. J.; Gorte, R. J.; Farneth, W. E. *J. Am. Chem. Soc.,* **1996**, *118*, 3262.

(25)   Suzuki, K.; Katada, N.; Niwa, M. *J. Phys. Chem. C,* **2007**, *111*, 894.

(26)   Katada, N.; Suzuki, K.; Noda, T.; Sastre, G.; Niwa, M. *J. Phys. Chem. C,* **2009**, *113*, 19208.

(27)   Sastre, G.; Fornes, V.; Corma, A. *J. Phys. Chem. B,* **2000**, *104*, 4349.

(28)   Yamamoto, T.; Tanaka, T.; Funabiki, T.; Yoshida, S. *J. Phys. Chem. B,* **1998**, *102*, 5830.

(29)   Iwamoto, M.; Tanaka, Y.; Sawamura, N.; Namba, S. *J. Am. Chem. Soc.,* **2003**, *125*, 13032.

(30)   Yamamoto, T.; Mori, S.; Shishido, T.; Kawai, J.; Tanaka, T. *Top. Catal.,* **2009**, *52*, 657.

(31)   Tanaka, Y.; Sawamura, N.; Iwamoto, M. *Tetrahedron Lett.,* **1998**, *39*, 9457.

(32)   Yamamoto, T.; Tanaka, T.; Inagaki, S.; Funabiki, T.; Yoshida, S. *J. Phys. Chem. B,* **1999**, *103*, 6450.

(33)   Kitano, M.; Nakajima, K.; Kondo, J. N.; Hayashi, S.; Hara, M. *J. Am. Chem. Soc.,* **2010**, *132*, 6622.

(34)   Tanabe, K.; Okazaki, S. *Appl. Catal. A-Gen.,* **1995**, *133*, 191.

(35)   Tanabe, K. *Catal. Today,* **2003**, *78*, 65.

(36)   Nakajima, K.; Baba, Y.; Noma, R.; Kitano, M.; Kondo, J. N.; Hayashi, S.; Hara, M. *J. Am. Chem. Soc.,* **2011**, *133*, 4224.

(37)   Ross-Medgaarden, E. I.; Knowles, W. V.; Kim, T.; Wong, M. S.; Zhou, W.; Kiely, C. J.; Wachs, I. E. *J. Catal.,* **2008**, *256*, 108.

(38)   Santiesteban, J. G.; Vartuli, J. C.; Han, S.; Bastian, R. D.; Chang, C. D. *J. Catal.,* **1997**, *168*, 431.

(39)   Barton, D. G.; Soled, S. L.; Meitzner, G. D.; Fuentes, G. A.; Iglesia, E. *J. Catal.,* **1999**, *181*, 57.

(40)   Zhou, W.; Ross-Medgaarden, E. I.; Knowles, W. V.; Wong, M. S.; Wachs, I. E.; Kiely, C. J. *Nat. Chem.,* **2009**, *1*, 722.

(41)   Scheithauer, M.; Grasselli, R. K.; Knozinger, H. *Langmuir,* **1998**, *14*, 3019.

(42)   Afanasiev, P.; Geantet, C.; Breysse, M.; Coudurier, G.; Vedrine, J. C. *J. Chem. Soc., Faraday Trans.,* **1994**, *90*, 193.

Chapter 1

Brønsted Acid Property of Alumina-Supported Niobium Oxide

Calcied at High Temperatures : Characterization

by Acid-Catalyzed Reactions and Spectroscopic Methods

Abstract

The acidic properties of alumina-supported niobium oxide (Nb_2O_5/Al_2O_3) calcined at high temperatures, with Nb_2O_5 loadings of 5-30 wt % as Nb_2O_5, were investigated using acid-catalyzed reactions (benzylation of anisole, cumene cracking, and isomerization of α-pinene), and Fourier-transform infrared spectroscopy. Structural characterization was carried out using X-ray diffraction (XRD), Raman spectroscopy, X-ray photoelectron spectroscopy (XPS), and X-ray absorption fine structure (XAFS) analysis. The relation between acidic properties and structure is discussed. The addition of niobium to γ-Al_2O_3 generates Brønsted acid sites, where acid-catalyzed reactions take place. The catalytic activity depends on calcination temperature and niobium loading. In a series of Nb_2O_5/Al_2O_3 catalysts, 16 wt % Nb_2O_5/Al_2O_3 calcined at 1123 K exhibited the highest activity. Nb_2O_5/Al_2O_3 showed significant catalytic activity in the isomerization of α-pinene to camphene and limonene, even after evacuation at 1173 K, indicating high thermal stability of the Brønsted acid sites. XPS and XAFS revealed that a niobic oxide monolayer with distorted octahedral NbO_6 units was formed and stabilized on alumina. Brønsted acid sites are probably generated at boundaries between two niobic oxide monolayer domains. When the Nb_2O_5 loading was sufficient to form two-dimensional niobium oxide overlayers (>16 wt %), some of the Brønsted acid sites on Nb_2O_5/Al_2O_3 were deposited by $AlNbO_4$ having no Brønsted acid site, resulting in a lowering of the catalytic activity.

Introduction

Niobium compounds are of great interest in various types of heterogeneous catalysis such as acid-base catalysis,[1-6] oxidation-reduction catalysis,[7-11] and photocatalysis,[12-15] where they are used as catalyst components or are added in small amounts to catalysts. The acidic properties of niobium acid ($Nb_2O_5 \cdot nH_2O$, hydrated niobium oxide) have been widely investigated. Niobic acid calcined at moderate temperatures of 373-573 K exhibits Brønsted acid properties ($H_0 < -5.6$),[3,4] and is effective for reactions that relate to aqueous media including esterification, olefin hydration, and alcohol dehydration.[1-6,16-18] Niobium oxide is an amorphous metal oxide composed mainly of distorted NbO_6 octahedra and NbO_4 tetrahedra. Since the Nb-O bonds in these distorted polyhedral are highly polarized, some of the surface OH groups function as Brønsted acid sites. Nakajima et al. reported that NbO_4 tetrahedra in niobium acid act as effective Lewis acid sites, which catalyze the allylation of benzaldehyde with tetraallyl tin, and the conversion of glucose to 5-(hydroxymethyl)furfural in the presence of water.[18] However, as a result of the dehydration of niobic acid, the compound became almost neutral when heated at temperatures higher than 673 K.[19,20]

Because a supported metal oxide often shows different catalytic properties from those of the bulk oxide, much research on supported niobium oxide has been carried out in attempts to control the catalytic properties and the structures of the surface niobium species, using different supporting metal oxides, niobium precursors (chloride, oxalate, ethoxide, niobium acid, and niobium complexes), and preparation methods.[14,15,21-36] Wachs and co-workers investigated the acidic properties of supported niobium oxide catalysts with Nb_2O_5 loadings below 20 wt % and found Lewis acid sites on Nb_2O_5/SiO_2, Nb_2O_5/Al_2O_3, Nb_2O_5/MgO, Nb_2O_5/TiO_2, and Nb_2O_5/ZrO_2, whereas Brønsted acid sites were only detected on Nb_2O_5/SiO_2 and Nb_2O_5/Al_2O_3.[28] Asakura et al. also reported that a monolayer of niobium oxide on SiO_2 catalyzes dehydration of ethanol,[30] suggesting formation of Brønsted acid sites on Nb_2O_5/SiO_2. Onfroy and co-workers characterized the acidic properties of Nb_2O_5/TiO_2 and Nb_2O_5/ZrO_2, using Fourier-transform infrared (FT-IR) spectra of the adsorption of pyridine and lutidine, and Raman spectroscopy.[31-34] They observed generation of Brønsted acid sites on Nb_2O_5/TiO_2 and Nb_2O_5/ZrO_2, and a direct correlation between the number of Brønsted acid sites and the catalytic activity of isopropanol dehydration to propylene. The generation

of Lewis and Brønsted acid sites on Nb_2O_5/Al_2O_3 with 17.2 wt % of Nb_2O_5 was reported by de la Cruz et al. on the basis of FT-IR spectra of adsorbed pyridine.[35,36] They concluded that Brønsted acid sites on Nb_2O_5/Al_2O_3 exhibit catalytic activity for benzylation of anisole.

The calcination temperature is an important parameter in controlling the structure and catalytic properties of supported niobium oxide catalysts. However, in most cases, supported niobium oxide catalysts have been calcined at moderate temperatures, 673-773 K, and there have only been a few investigations of acidic properties and catalysis of supported niobium oxide calcined at high temperatures (>1000 K). It is important to assess the relations among acid properties, structures, and catalytic properties of supported niobium oxide calcined at high temperatures, but these are still unclear.

Our previous X-ray absorption fine structure (XAFS) study of alumina-supported niobium oxide[23] showed that a niobic acid-like compound was stabilized on the Al_2O_3 surface at temperatures higher than 673 K at high loadings of niobium oxide, and we therefore supposed that highly loaded Nb_2O_5/Al_2O_3 would act as a stable Brønsted acid catalyst. We recently reported that highly loaded Nb_2O_5/Al_2O_3 calcined at 1173 K acts as an effective catalyst for benzylation of anisole, which is promoted on Brønsted acid sites.[37] This is in marked contrast to the evidence that calcination of niobium oxide itself at temperatures higher than 773 K does not result in Brønsted acidity.

In the present study, we investigated a series of aluminasupported niobium oxide catalysts with various loadings of Nb_2O_5 and calcined at various temperatures to clarify the relation among their acidic properties, catalytic performances, and local structures around niobium species. Benzylation of anisole, cracking of cumene, and isomerization of α-pinene were used as test reactions for acidic properties. It is known that benzylation of anisole (Friedel-Crafts reaction of anisole with benzyl alcohol) is promoted on Brønsted acids.[35,36,38-40] Cracking of cumene has been used as a test reaction as it has been established that this reaction is only catalyzed by Brønsted acid sites. The isomerization of α-pinene is an excellent test reaction for acid-base catalysts. Over a solid basic catalyst, only an equilibrium reaction between α-pinene and β-pinene occurs. In contrast, various bicyclic and monocyclic products are formed over acid catalysts, and the selectivities depend on the maximum acid strength.[41-47]

Experimental

Preparation

A series of Nb_2O_5/Al_2O_3 catalysts were prepared by impregnation of γ-alumina (JRC-ALO-8) with an aqueous solution of niobium oxalate (CBMM) and calcination at various temperatures for 3 h in dry air. Aluminum niobate ($AlNbO_4$; monoclinic, a = 1.215 nm, b = 0.3735 nm, c = 0.6438 nm, α = γ = 90°, β = 107°) was synthesized from $Al(NO_3)_3·9H_2O$ and niobium oxalate.[48] $Al(NO_3)_3·9H_2O$ was dissolved in an aqueous solution, and then oxalic acid (Wako, Osaka, Japan) and 28% ammonia solution were added to pH values of 1.0 and 3.0, respectively. An aqueous solution of niobium oxalate was added to an aluminum solution in a ratio of Al/Nb = 1.0, and refluxed at 413 K for 1 h. The white paste obtained by removing water was dried at 423 K for 15 h, and $AlNbO_4$ was formed by calcination of the solid at 1273 K for 3 h. Niobic acid ($Nb_2O_5·nH_2O$) was supplied by CBMM and pretreated by calcination at 473 K. Sulfated zirconia (JRC-SZ-1), silica-alumina (JRC-SAL-2, Si/Al atomic ratio = 5.3), HZSM-5 (JRC-Z5-90H(1), Si/Al atomic ratio = 40), H-Y (JRC-Z-HY5.6(2), Si/Al atomic ratio = 2.8), H-Mor (JRC-ZHM15(1), Si/Al atomic ratio =7.7), and H-β (JRC-Z-HB(25), Si/Al atomic ratio =12.5) were supplied by the Catalysis Society of Japan as reference catalysts.

Reactions

Benzylation of anisole (Friedel-Crafts alkylation of anisole with benzylalcohol), cumene cracking, and isomerization of α-pinene were used as test reactions to examine the acidic properties of Nb_2O_5/Al_2O_3.

Benzylation of anisole was examined in the liquid phase. The catalyst (0.2 g) was pretreated in a N_2 flow at 473 K for 1 h and then added to a mixture of benzyl alcohol (6.25 mmol) and anisole (92.5 mmol) in a 100-mL flask for 3 h. The reaction was carried out at 413 K, and the products were determined by GLC (GC-14B with a flame ionization detector, Shimadzu, Kyoto, Japan) and GC-MS (Shimadzu GC-MS QP-5050), using a CBP10 column.

Cumene cracking was examined in a fixed-bed pulse-reactor. The catalyst (0.05 g) was placed in the reactor and pretreated at 673 K for 1 h in 14.3 vol % O_2 diluted with He. The reaction was carried out at 673 K in a He flow (30 mL min^{-1}), and cumene (0.5 μL) was injected into the

reactor. The products were analyzed by GLC (Shimadzu GC-8A with a thermal conductivity detector), using a PEG-20 M column.

Isomerization of α-pinene was carried out under a dry N_2 atmosphere using a stirred batch reactor. Prior to each run, 0.1 g of catalyst was pretreated at 673 K under 13.3 kPa of O_2 for 1 h, followed by evacuation at the same temperatures for 1 h. α-Pinene (12.5 mmol) was added in the reactor and stirred at 343 K for 3 h. The products were determined using GLC (Shimadzu GC-2014 with a flame-ionization detector), using a CBP20 column.

Characterizations

The Brunauer-Emmett-Teller (BET) specific surface area was estimated from N_2 isotherm at 77 K. The N_2 adsorption isotherm measurements were carried out using a BELSORP 28SA (BEL Japan, Osaka, Japan) at 77 K. Prior to the measurement, each sample was evacuated at 573 K for 2 h.

X-ray diffraction (XRD) patterns were obtained using a MultiFlex DR powder X-ray diffractometer (Rigaku, Tokyo, Japan), using Cu Kα radiation ($\chi = 1.5405$ Å).

Laser Raman spectra were obtained using a NRS-2000 Raman spectrometer (JASCO, Tokyo, Japan), using 514.5 nm line of an argon laser. The spectral resolution was 4 cm^{-1}.

FT-IR spectra were recorded using a SPECTRUM ONE FTIR spectrometer (Perkin-Elmer, Walthham, MA) with a resolution of 4 cm^{-1}. Each sample (12.5 mg) was pressed into a self-supporting wafer (diameter 13 mm). The catalysts were pretreated under 13.3 kPa of O_2 for 1 h at 673 K and then evacuated for 1 h at 673 K. For determination of the number of Brønsted and Lewis acid sites on Nb_2O_5/Al_2O_3, the wafer was exposed to 0.667 kPa of pyridine vapor at 298 K for 10 min followed by evacuation at 423 K for 10 min.

X-ray photoelectron spectra (XPS) of the catalysts were acquired using an ULVAC PHI 5500MT system equipped with a hemispherical energy analyzer. Samples were mounted on indium foil and then transferred to an XPS analyzer chamber. The residual gas pressure in the chamber during data acquisition was less than 1.33×10^{-6} Pa. The spectra were measured at room temperature using Mg Kα radiation. The electron take-off angle was set at 45 deg. The binding energy was referenced to the O 1s level.

X-ray absorption experiments were carried out on the BL01B1 at SPring-8 (Hyogo, Japan). The ring energy was 8 GeV, and the stored current was 99.5 mA. The Nb K-edge (19.0 keV) X-ray

absorption spectra were recorded in transmission mode in air or in N_2 at room temperature. A Si (311) and Si (111) two crystal monochromator was used to obtain a monochromatic X-ray beam. The data reduction was performed using the REX2000 Ver.2.5.9 (Rigaku) and FEFF8.40 programs.[49]

Results and discussion

Catalysis

Figure 1a shows the results of benzylation of anisole over 16 wt% Nb_2O_5/Al_2O_3 calcined at various temperatures. Benzyl anisole is produced on Brønsted acid sites.[35,36,38-40,50,51] Mainly, *p*- and *o*-benzyl anisole was produced. Formation of multiply alkylated products was not observed. The amount of dibenzyl ether, which is formed via intermolecular dehydration on Lewis acid sites, was less than 0.7 mmol in every reaction. The yield of benzyl anisole depended strongly on the calcination temperature, and increased approximately linearly with increasing calcination temperature up to 1123 K. Calcination at temperatures higher than 1123 K caused a reduction in the yield of benzyl anisole. Niobic acid calcined at 473 K showed low activity, which indicates that the acidic properties of Nb_2O_5/Al_2O_3 are quite different from those of niobic acid. The ratio of *p*-benzyl anisole to *o*-benzyl anisole was ca. 3/2 regardless of the calcination temperature.

The results of benzylation over Nb_2O_5/Al_2O_3 calcined at 1123 K with various Nb_2O_5 loadings are shown in Figure 2a. The Nb_2O_5 loading affects the activity of benzylation of anisole. Alumina (without Nb) was almost inactive. No significant changes in the yields of benzyl anisole occurred until the Nb_2O_5 loading was 5 wt %; above 10 wt % Nb_2O_5 loading, the yield of benzyl anisole increased rapidly with increasing Nb_2O_5 loading. The 16 wt % Nb_2O_5/Al_2O_3 exhibited the highest activity, and then the activity decreased significantly. The selectivities for pand *o*- benzyl anisole were almost constant (the *p/o* ratio was ca. 3/2) regardless of the Nb_2O_5 loading. This suggests that the acid strength was independent of the Nb_2O_5 loading, although the number of acid sites varied.
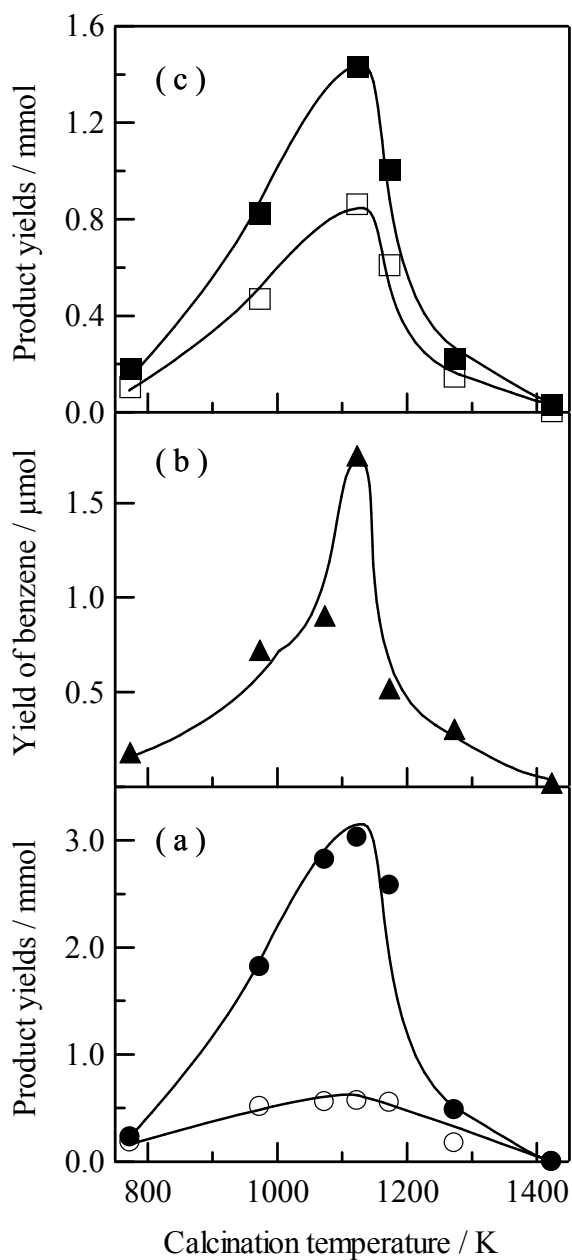
Figure 1. Activity of 16 wt% Nb_2O_5/Al_2O_3 calcined at various temperatures (a) for Friedel–Crafts alkylation (($\bullet$) benzyl anisole and ($\circ$) dibenzyl ether), (b) for cracking of cumene, and (c) for isomerization of α-pinene (($\blacksquare$) camphene and ($\square$) limonene).
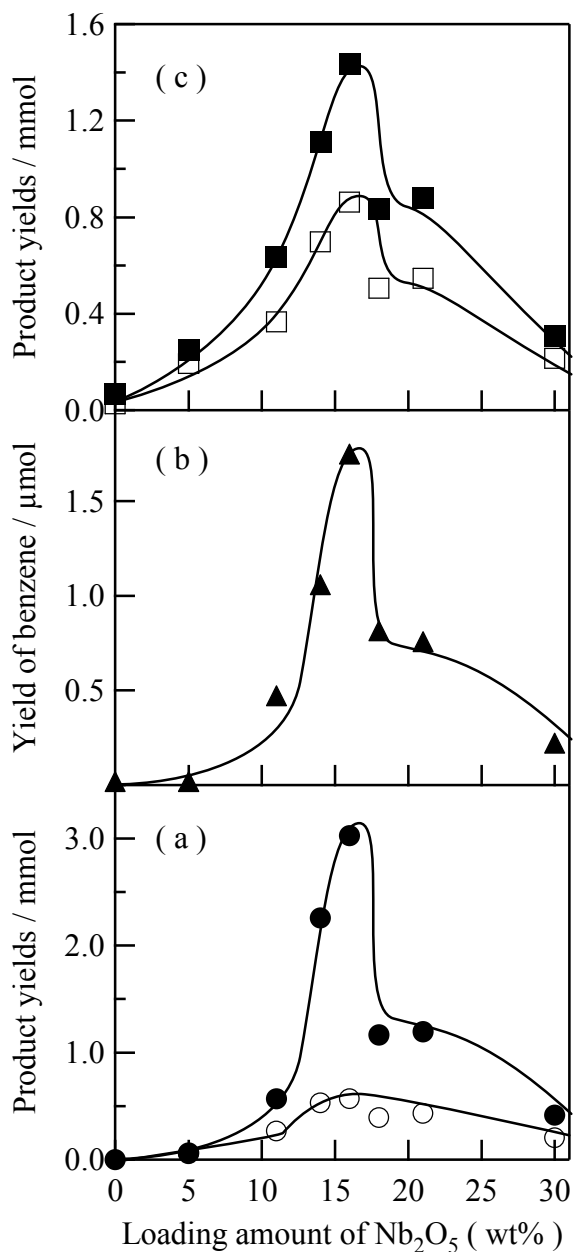
Figure 2. Activity of Nb_2O_5/Al_2O_3 calcined at 1123 K with various loadings (a) for Friedel–Crafts alkylation (($\bullet$) benzyl anisole and ($\circ$) dibenzyl ether), (b) for cracking of cumene, and (c) for isomerization of α-pinene (($\blacksquare$) camphene and ($\square$) limonene).

Figure 1b shows the benzene yield in the cracking of cumene over Nb_2O_5/Al_2O_3 calcined at various temperatures. The Nb_2O_5 loading was fixed at 16 wt %. The effect of Nb_2O_5 loading on the yield of benzene on Nb_2O_5/Al_2O_3 calcined at 1123 K is shown in Figure 2b. The first pulse data are summarized in Figures 1b and 2b. It has been reported that cracking of cumene proceeds on Brønsted acid sites.[52-54] The first pulse data may indicate the performance of the fresh catalyst.[55] Indeed, as a result of carbon deposition, the yield of benzene decreased with the pulse number (data not shown). The products were benzen e and propylene. As shown in Figure 1c, the activity strongly depends on the calcination temperature. The activity is enhanced by raising the calcination temperature, up to 1123 K. Calcination at temperatures higher than 1123 K results in a decline in activity. The effect of calcination temperature on the activity of cumene cracking over Nb_2O_5/Al_2O_3 was similar to that on benzylation of anisole, but the change in activity at around 1123 K was sharper than that for benzylation of anisole (Figure 1a). The Nb_2O_5 loading also has an effect on the activity. No activity was observed on alumina, and 5 wt % Nb_2O_5/Al_2O_3 was almost inactive, suggesting that there are no Brønsted acid sites on 5 wt % Nb_2O_5/Al_2O_3. Above 5 wt % Nb_2O_5 loading, the activity increased with increasing Nb_2O_5 loading until the Nb_2O_5 loading reached 16 wt %. Above 16 wt %, the activity rapidly decreased.

Table 1 shows the results of α-pinene isomerization over Nb_2O_5/Al_2O_3 calcined at various temperatures. It is known that α-pinene isomerization is an excellent test reaction for acid-base catalysts, and the products of α-pinene isomerization can be classified into three groups, as shown in Scheme 1. The first composed of monocyclic products (e.g., limonene, terpinolene, α-terpinene, γ-terpinene). Over solid basic catalysts such as MgO and SrO, only equilibrium between α-pinene and β-pinene is observed. In contrast, acid catalysts promote the reactions producing all three groups, and the selectivities depend on the maximum acid strength. Ohnishi[42] and Yamamoto[47] reported that monocyclic and bicyclic compound such as camphene and limonene are produced on Brønsted acid sites. The main products over Nb_2O_5/Al_2O_3 were camphene and limonene, and the selectivities were ca. 50% and 28%, respectively. The minor products were β-pinene, fenchene, α-terpinene, γ-terpinene, and terpinolene. The selectivities in α-pinene isomerization on Nb_2O_5/Al_2O_3 catalysts indicate that the generated active sites were acid sites, probably Brønsted acid sites. Figure 1c shows the change in the yields of camphene and limonene with calcination temperature.
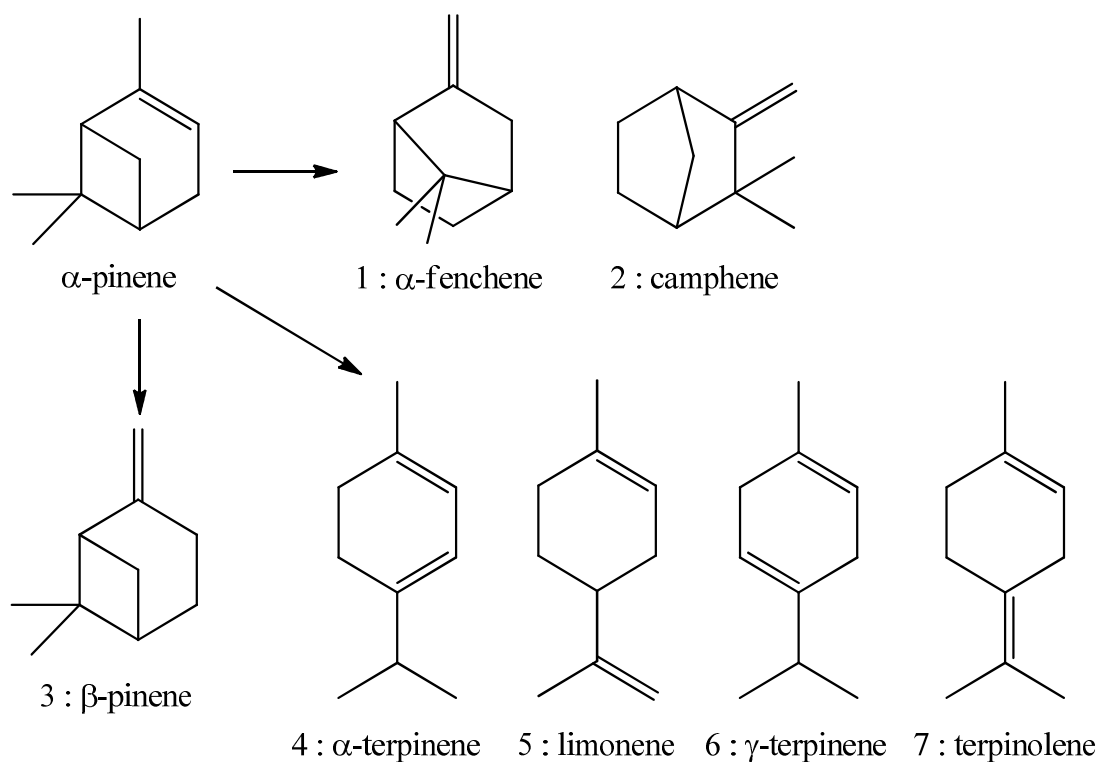
Scheme 1. α-Pinene isomerization.

Table 1. Results for α-pinene isomerization on 16 wt% Nb_2O_5/Al_2O_3 calcined at various temperatures.

Calcination temperature / K	Conversion (%)	Selectivity[a] (%)							
		1	2	3	4	5	6	7	8
973	22.1	4	50	5	1	28	2	7	3
1123	26.4	4	51	3	2	30	1	6	3
1173	21.9	4	49	5	2	29	2	7	2
1273	10.2	3	40	13	2	26	3	8	5
1423	3.4	2	44	28	1	3	tr	tr	22

[a] 1 : α-fenchene, 2 : camphene, 3 : β-pinene, 4 : α-terpinene, 5 : limonene, 6 : γ-terpinene,

7 terpinolene, 8 others.

The yields increased for calcination temperatures up to 1123 K and then dropped. The selectivities for camphene and limonene were almost constant up to 1123 K. Above 1123 K, the selectivities for camphene and limonene declined, and the amount of β-pinene increased slightly (Table 1). These results suggest that the number of acid sites increased up to 1123 K, although the acid strength did not change. In contrast, calcination above 1173 K may result in changes not only in the number of acid sites but also in the acid strength.

Table 2 and Figure 2c show the results of α-pinene isomerization on Nb_2O_5/Al_2O_3 calcined at 1123 K with various Nb_2O_5 loadings. The reaction scarcely proceeded on alumina, and the selectivities to camphene, β-pinene, and terpinolene were relatively high. As in the case of benzylation of anisole and cumene cracking, increased Nb_2O_5 loadings up to 16 wt % improved the activity, and then the activity decreased. The selectivities for camphene and limonene were almost constant, between 11 and 21 wt %, suggesting that the number of acid sites changed without varying the acid strength.

Table 2. Results for α-pinene isomerization on Nb_2O_5/Al_2O_3 calcined at 1123 K with various Nb_2O_5 loadings

Loading amount of Nb_2O_5 (wt%)	Conversion (%)	Selectivity[a] (%)							
		1	2	3	4	5	6	7	8
0	4.0	tr	30	16	11	11	13	19	tr
5	7.4	3	37	11	2	28	4	10	5
11	15.1	4	49	8	1	28	1	6	3
14	22.8	4	49	4	1	30	2	7	3
16	26.4	4	51	3	2	30	1	6	3
18	20.8	4	49	6	1	30	2	7	1
21	23.7	4	48	3	2	29	2	8	4
30	14.2	3	41	9	2	29	3	8	5

[a] 1 : α-fenchene, 2 : camphene, 3 : β-pinene, 4 : α-terpinene, 5 : limonene, 6 : γ-terpinene, 7 terpinolene, 8 others.

Acidic properties

As mentioned above, 16 wt% Nb_2O_5/Al_2O_3 calcined at 1123 K showed good catalytic activities for benzylation of anisole, cumene cracking, and α-pinene isomerization. To investigate the generation of Brønsted acid sites on Nb_2O_5/Al_2O_3 calcined at 1123 K, the acid sites were characterized using FT-IR spectra of pyridine adsorbed on the catalysts. Figure 3 shows the IR spectra of pyridine adsorbed on 16 wt % Nb_2O_5/Al_2O_3 calcined at 1123 K and on bare γ-Al_2O_3. The spectrum of γ-Al_2O_3 exhibited four bands, at 1447, 1490, 1578, and 1609 cm^{-1}. These four bands correspond to pyridine adsorbed on Lewis acid sites. Nb_2O_5/Al_2O_3 gave a band at 1545 cm^{-1}, corresponding to pyridine adsorbed on Brønsted acid sites. These results clearly indicate that Brønsted acid sites are generated by the addition of niobium on alumina, and are maintained even after calcination at high temperatures.

To determine whether Brønsted acidity controlled the activities of benzylation of anisole, cumene cracking, and α-pinene isomerization, we evaluated the specific amounts of pyridinium ions adsorbed on Brønsted acid sites and of pyridine coordinated to Lewis acid sites on each Nb_2O_5/Al_2O_3 catalyst. The number of Brønsted acid sites titrated by pyridine was calculated using an integrated molar adsorption coefficient value of ε = 1.67 cm μmol^{-1} for the band area at 1545 cm^{-1} of protonated pyridine.[56,57] The number of Lewis acid sites was also calculated using an integrated molar
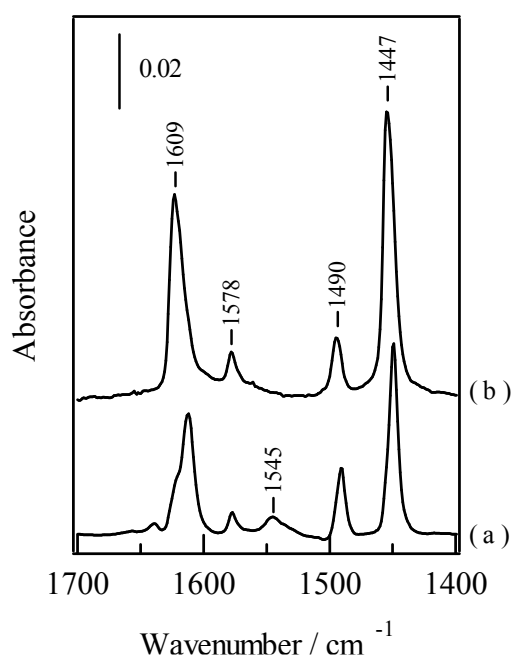

Figure 3. IR spectra of pyridine adsorbed on (a) 16 wt% Nb_2O_5/Al_2O_3 calcined at 1123 K and (b) γ-Al_2O_3.

adsorption coefficient value of $\varepsilon = 2.22$ cm μmol^{-1} for the band area at 1450 cm^{-1} of coordinated pyridine. Figure 4 shows that the number of Brønsted acid sites increased with calcination temperature up to 1123 K, but the calcination at temperatures higher than 1123 K resulted in a reduction in the number of Brønsted acid sites. It is interesting that Brønsted acid sites are still present on the Nb_2O_5/Al_2O_3 calcined at temperatures above 1100 K, and that high-temperature calcination results in the generation of Brønsted acid sites. In contrast, the number of Lewis acid sites decreased monotonically with calcination temperature (see Figure 5).
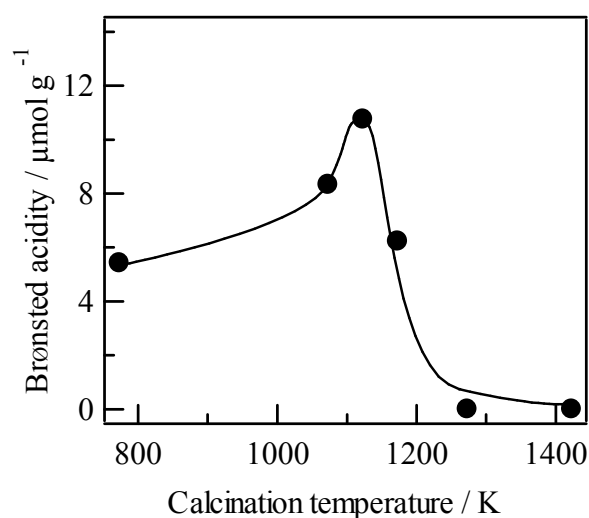

Figure 4. Brønsted acidity over 16 wt% Nb_2O_5/Al_2O_3 calcined at various temperatures.

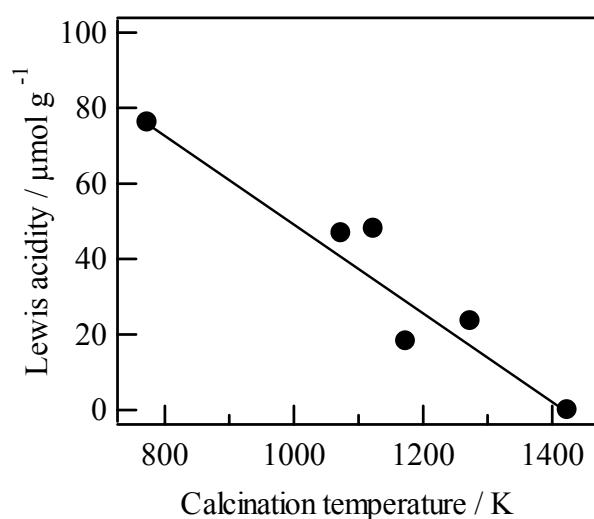**Figure 5.** Lewis acidity over 16 wt% Nb_2O_5/Al_2O_3 calcined at various temperatures.

The number of Brønsted acid sites on Nb_2O_5/Al_2O_3 calcined at 1123 K varied with the Nb_2O_5 loading. When the Nb_2O_5 loading was less than 5 wt %, the number of Brønsted acid sites was negligible. The number increased with increasing Nb_2O_5 loading, and peaked at 16 wt % Nb_2O_5 (Figure 6). An approximately linear decrease in the concentration of Lewis acid sites with increasing Nb_2O_5 loading was observed (see Figure 7), meaning that the Lewis acid sites on the surface of the support disappear in proportion to the fraction of the surface occupied by the deposited niobium oxide.
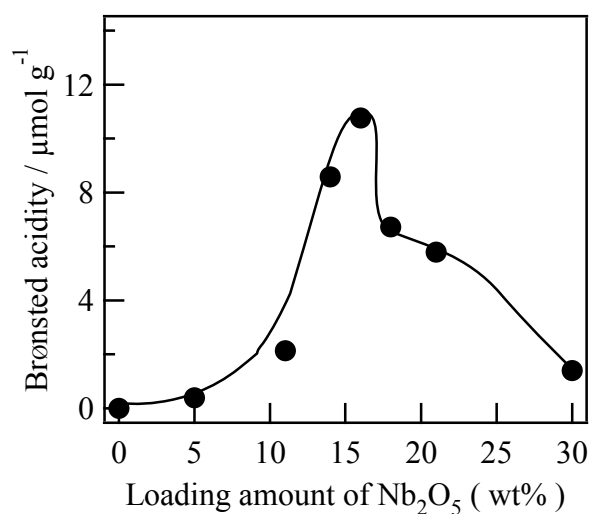
Figure 6. Brønsted acidity over Nb_2O_5/Al_2O_3 calcined at 1123 K with various loadings.
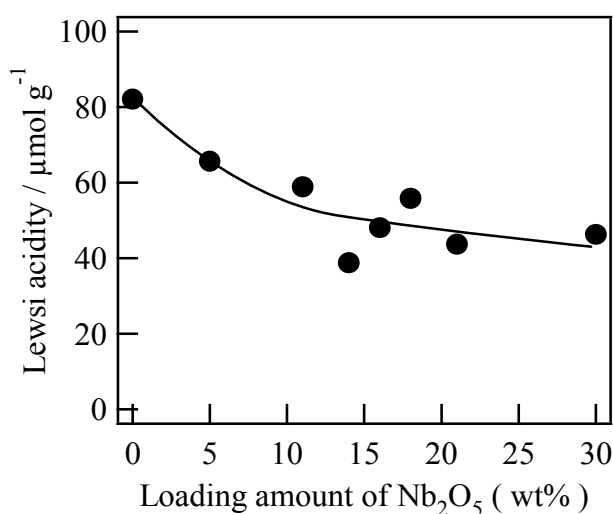
Figure 7. Lewis acidity over Nb_2O_5/Al_2O_3 calcined at 1123 K with various loadings.

Figure 8 shows the correlation between the catalytic activities and numbers of Brønsted acid sites on Nb_2O_5/Al_2O_3 with various Nb_2O_5 loadings. The activities for benzylation of anisole (Figure 8a), cumene cracking (Figure 8b), and α-pinene isomerization (Figure 8c) over Nb_2O_5/Al_2O_3 calcined at 1123 K were proportional to the Brønsted acidity, indicating that these reactions were promoted on the Brønsted acid sites on the Nb_2O_5/Al_2O_3 catalysts.
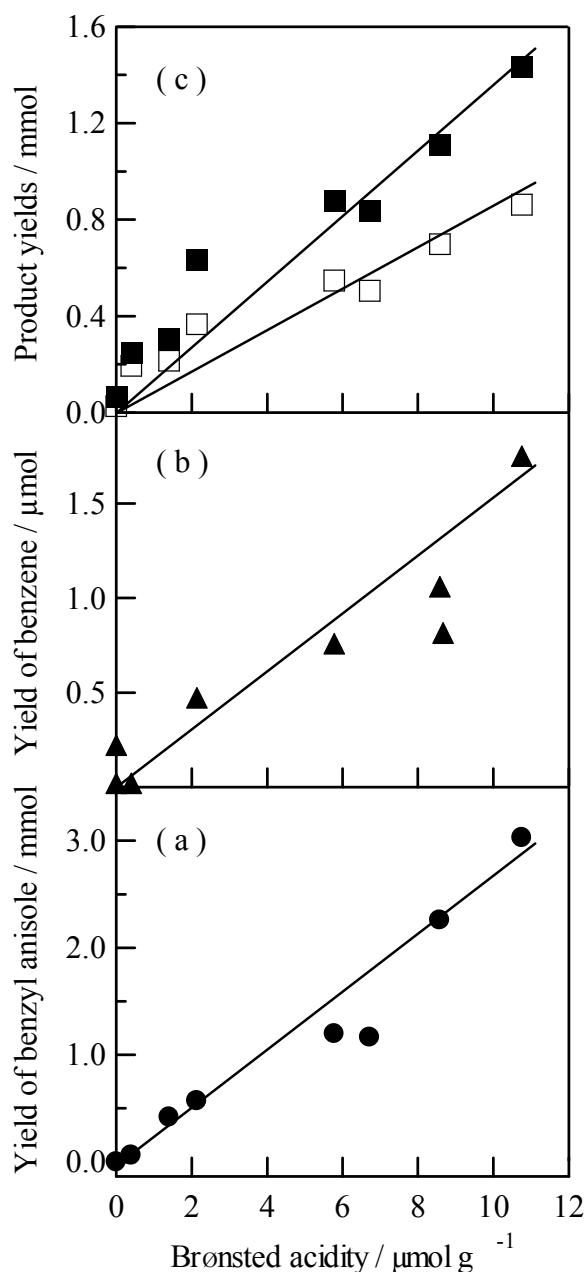
Figure 8. Correlation between catalytic activities over Nb_2O_5/Al_2O_3 calcined at 1123 K with various loadings and Brønsted acidity of samples. (a) Benzylation of anisole, (b) Cracking of cumene, (c) Isomerization of α-pinene ((■) camphene and (□) limonene).

The effect of pretreatment temperature on the activities in α-pinene isomerization over 16 wt % Nb_2O_5/Al_2O_3 calcined at 1173 K was examined to assess the thermal stability of the Brønsted acid sites on the Nb_2O_5/Al_2O_3 catalysts. The results are shown in Table 3 and Figure 9. The conversion increased with increasing pretreatment temperature up to 673 K, and the conversion and selectivity were almost constant from 673 to 1173 K. The yields of camphene and limonene increased significantly with increasing pretreatment temperature up to 673 K, and then the yields were constant (Figure 9), which indicates that Brønsted acid sites are maintained despite evacuation at high temperatures such as 1173 K.

The thermal stability of Nb_2O_5/Al_2O_3 was compared with those of various acidic catalysts (Figure 10). The activities of zeolites (HZSM-5, H-Mor, H-β), sulfated zirconia, silica-alumina, and niobic acid pretreated at 1173 K were much lower than the activities of those pretreated at 673 K. Acidic hydroxyls on the H-β zeolite are broken by heating at 823 K,[58] and sulfated zirconia calcined at over 873 K loses its acidic properties as a result of decomposition to sulfate ions.[59,60] In contrast, the activity of Nb_2O_5/Al_2O_3 was almost maintained even after pretreatment at 1173 K. On the basis of these results, it is concluded that Brønsted acid sites on Nb_2O_5/Al_2O_3 calcined at 1123 K are thermally stable.

Table 3. Results for α-pinene isomerization of 16 wt% Nb_2O_5/Al_2O_3 calcined at 1123 K pretreated at various temperatures

Pretreatment temperature / K	Conversion (%)	Selectivity[a] (%)							
		1	2	3	4	5	6	7	8
298	18.9	4	52	9	tr	27	1	5	2
373	10.3	4	48	8	1	27	2	6	4
473	22.8	3	50	4	2	30	2	7	2
573	26.0	4	50	3	2	30	1	7	3
673	26.4	4	51	3	2	30	1	6	3
773	25.9	4	49	4	1	32	1	7	2
973	27.0	4	49	3	2	31	1	7	3
1173	23.4	4	52	3	2	31	2	6	tr

[a] 1 : α-fenchene, 2 : camphene, 3 : β-pinene, 4 : α-terpinene, 5 : limonene, 6 : γ-terpinene, 7 terpinolene, 8 others.
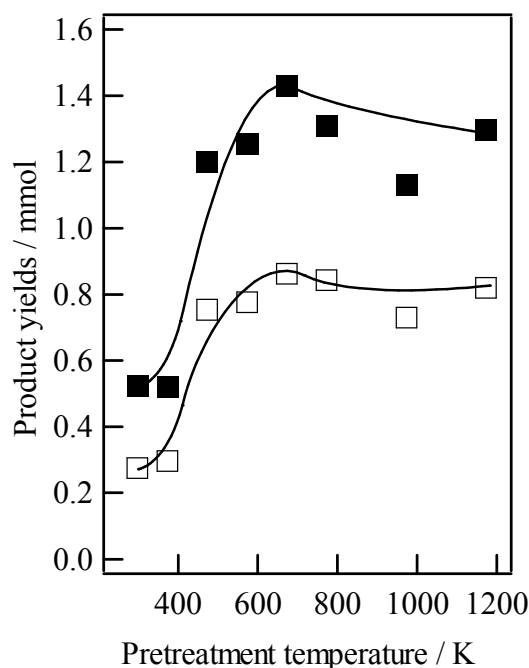
Figure 9. Activity of 16 wt% Nb_2O_5/Al_2O_3 calcined at 1123 K pretreated at various temperature for isomerization of α-pinene. (■) camphene and (□) limonene.
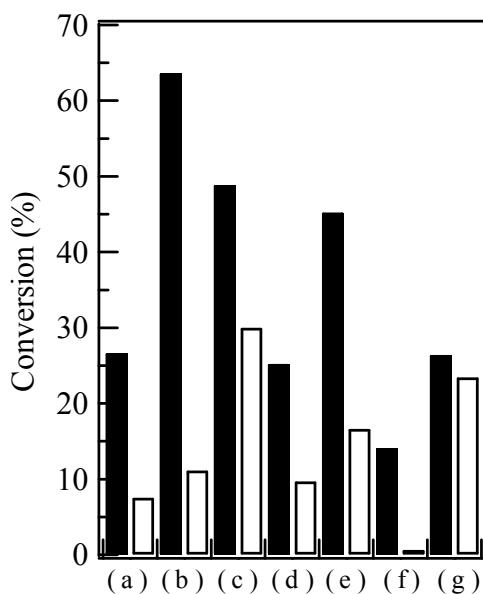
Figure 10. Activity of various solid acid catalysts pretreated at (■) 673 K and (□) 1173 K for isomerization of α-pinene. (a) H-β : 0.01 g, (b) H-M : 0.1 g, (c) H-ZSM-5 : 0.1 g, (d) Sulfated zirconia : 0.1 g, (e) Silica-alumina : 0.01 g, (f) Niobic acid : 0.1 g, and (g) 16 wt% Nb_2O_5/Al_2O_3 calcined at 1123 K : 0.1 g.

Characterizations

X-ray diffraction patterns and Raman spectra

Figures 11 and 12 show the XRD patterns and Raman spectra of 16 wt % Nb_2O_5/Al_2O_3 calcined at various temperatures. When 16 wt % Nb_2O_5/Al_2O_3 was calcined at temperatures below 1123 K, the niobium oxide was amorphous. Calcination at 1173 K results in formation of aluminum niobate ($AlNbO_4$) and the θ-Al2O3 phase. Niobic acid exhibits an amorphous phase,[6,19,20] but niobic acid is converted to TT-Nb_2O_5 by heating at 773 K. In the cases of Nb_2O_5/Al_2O_3 catalysts, calcination up to 1123 K does not cause formation of niobium oxide crystallites (TT-Nb_2O_5) or $AlNbO_4$ crystallites as shown by powder XRD and Raman spectroscopy, indicating that the amorphous phase is stabilized on alumina, even on heating at 1123 K. $AlNbO_4$ was completely inert for benzylation of anisole, cumene cracking and α-pinene isomerization, and no acid sites were detected in the FT-IR spectra of adsorbed pyridine.[37] It is therefore concluded that the formation of $AlNbO_4$ accounts for the decrease in the number of Brønsted acid sites and the catalytic activity.
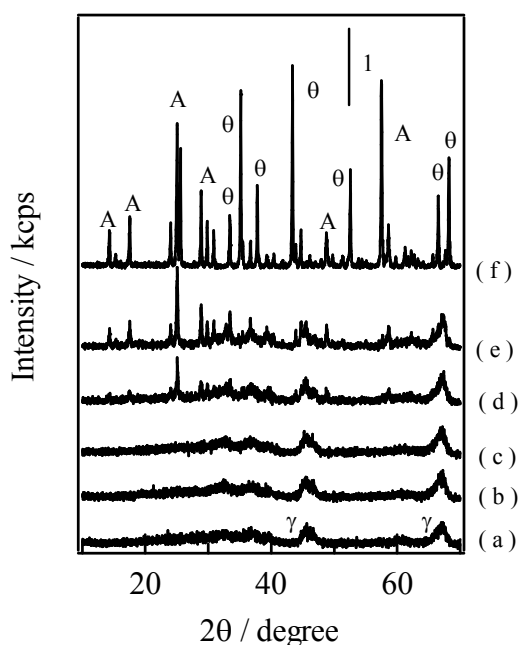
Figure 11. XRD patterns of 16 wt% Nb_2O_5/Al_2O_3 calcined at various temperatures. (a) 773 K, (b) 1073 K, (c) 1123 K, (d) 1173 K, (e) 1 273 K, and (f) 1423 K.
$\gamma = \gamma$-Al_2O_3; $\theta = \theta$-Al_2O_3; A = $AlNbO_4$.

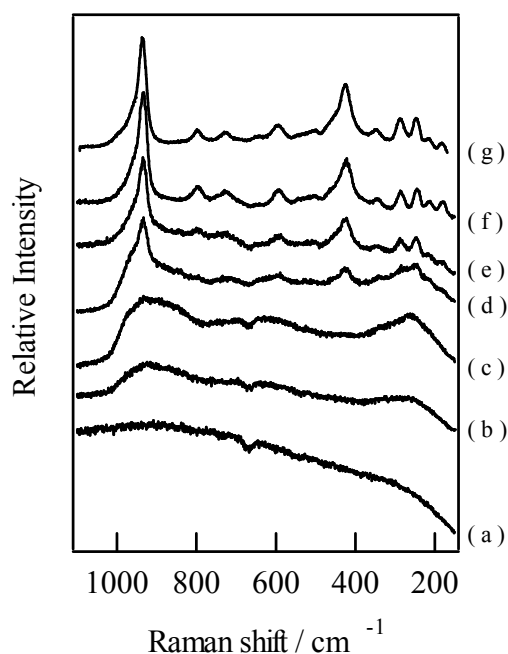**Figure 12.** Raman spectra of 16 wt% Nb_2O_5/Al_2O_3 calcined at various temperatures. (a) 773 K, (b) 1073 K, (c) 1123 K, (d) 1173 K, (e) 1273 K, (f) 1423 K, and (g) $AlNbO_4$.

Figures 13 and 14 show the XRD patterns and Raman spectra of Nb_2O_5/Al_2O_3 calcined at 1123 K with various Nb_2O_5 loadings. No diffraction line and Raman peak attributable to TT-Nb_2O_5 and $AlNbO_4$ appeared until the Nb_2O_5 loading reached 18 wt %. However, above 18 wt %, both the XRD patterns and Raman spectra show the formation of $AlNbO_4$. The formation of an inert $AlNbO_4$ phase results in a reduction in the catalytic activity and Brønsted acidity of Nb_2O_5/Al_2O_3. Moreover, we concluded that the niobium oxide on alumina available for acid-catalyzed reactions is not in a crystalline state, such as the TT- and T-Nb_2O_5 phases, but is in an amorphous state.

Surface composition estimated by X-ray photoelectron spectroscopy

The surface Nb/Al ratios on the Nb_2O_5/Al_2O_3 catalysts were estimated from the areas in the Nb 3d and Al 2p XP spectra. The binding energies of Nb $3d_{5/2}$ and $3d_{3/2}$ peaks were 208.0 and 210.6 eV, and the position of these peaks did not change regardless of the calcination temperature and Nb_2O_5 loading.

Figure 13. XRD patterns of Nb_2O_5/Al_2O_3 calcined at 1123 K with various loadings. (a) 5 wt%, (b) 11 wt%, (c) 14 wt%, (d) 16 wt%, (e) 18 wt%, (f) 21 wt%, and (g) 30 wt%.
$\gamma = \gamma$-Al_2O_3; A = $AlNbO_4$.

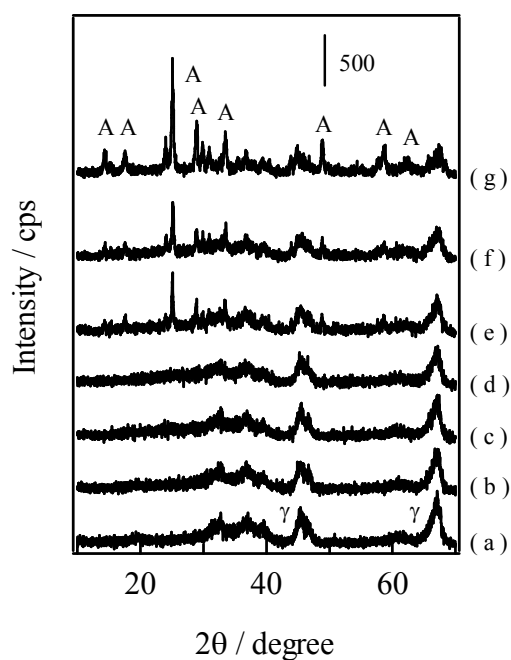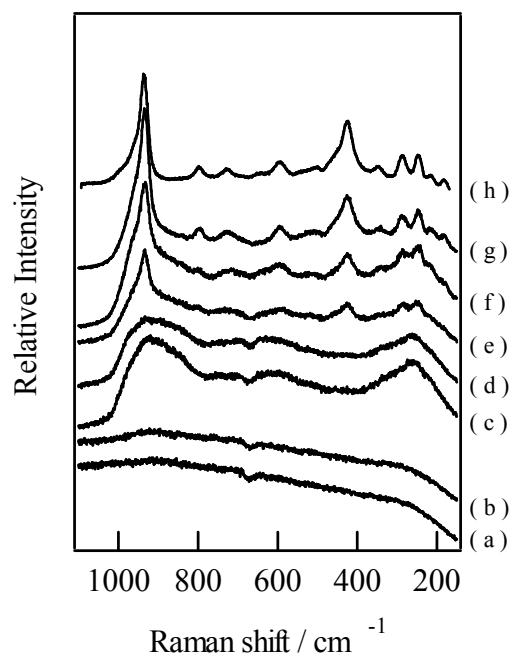**Figure 14.** Raman spectra of Nb_2O_5/Al_2O_3 calcined at 1123 K with various loadings. (a) 5 wt%, (b) 11 wt%, (c) 14 wt%, (d) 16 wt%, (e) 18 wt%, (f) 21 wt%, (g) 30 wt%, and (h) $AlNbO_4$.

On the basis of these binding energies, the valence of niobium in Nb_2O_5/Al_2O_3 catalysts was assigned as Nb^{5+}. The surface Nb/Al ratio of 16 wt % Nb_2O_5/Al_2O_3 was independent of the calcination temperature, which suggests that Nb atoms are located near the alumina surface, even after heating at 1423 K. That is, $AlNbO_4$ was formed on the catalyst surface. Figure 15 shows the surface Nb/Al ratio for Nb_2O_5/Al_2O_3 calcined at 1123 K, with various loadings. The surface Nb/Al ratio shows a linear increase with increasing Nb_2O_5 loading up to 16 wt %, but then the increase becomes gradual. On the basis of the cross-sectional area of the NbO_6 octahedral unit (0.16 nm^{-2}) and the surface area of the catalyst, it is estimated that the surface of the Nb_2O_5/Al_2O_3 catalyst is completely covered with a monolayer of niobium oxide when the niobium content is 16 wt % as Nb_2O_5. These results strongly suggest that a monolayer of niobic oxide was formed on 16 wt % Nb_2O_5/Al_2O_3. Taking into account the effect of Nb_2O_5 loading on the number of Brønsted acid sites, we conclude that a stabilized monolayer of niobic oxide on Al_2O_3 accounts for the generation of Brønsted acid sites.
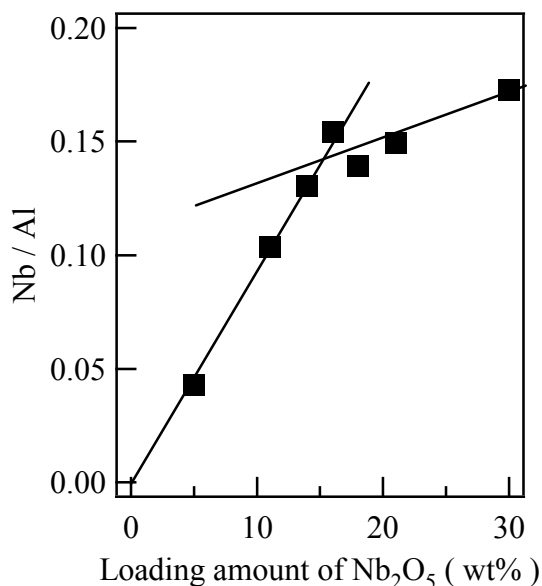

Figure 15. Atomic ratio of Nb_2O_5/Al_2O_3 calcined at 1123 K with various loadings.

Characterization of local structure of niobium oxide by X-ray absorption fine structure

Figure 16 shows the Nb K-edge X-ray absorption near-edge structure (XANES) spectra of Nb_2O_5/Al_2O_3 calcined at 1123 K with various loadings and of reference samples. The pre-edge peak in the Nb K-edge XANES, which is assigned to 1s to d-p orbital transitions, is sensitive to symmetry. X-ray absorptions have often been used to provide information on local symmetry.[24,61,62] The niobium oxide unit on a sample is distorted from an ideal octahedral symmetry, and the pre-edge peak at the Nb K-edge XANES of the sample is intense. The pre-edge peak of $YbNbO_4$ (NbO_4 tetrahedral) is much more intense than that of niobic acid (distorted NbO_6 octahedral), and that of $NaNbO_3$ (NbO_6 octahedral) is much less intense than that of niobic acid. When the Nb_2O_5 loading is lower than 16 wt %, the pre-edge peak areas of Nb_2O_5/Al_2O_3 are almost constant and larger than that of $NaNbO_3$ but smaller than that of $YbNbO_4$, indicating that the coordination symmetry around Nb in Nb_2O_5/Al_2O_3 is distorted NbO_6 octahedral. Above 18 wt %, this value gradually increased and approached that of $AlNbO_4$. This indicates that formation of $AlNbO_4$ occurred when the loading was larger than 18 wt %.
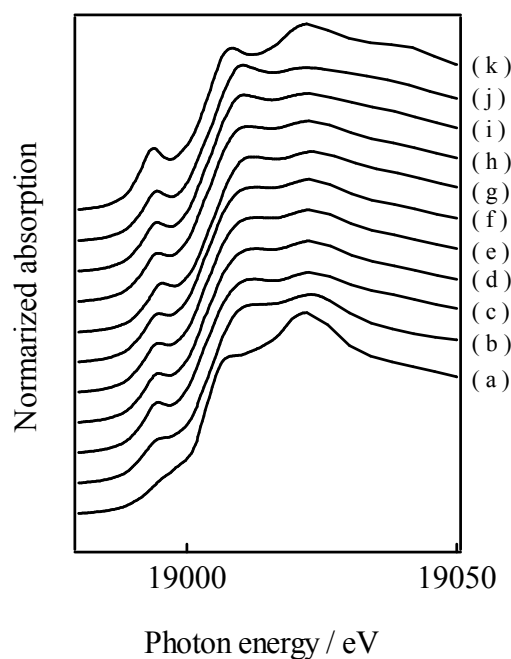

Figure 16. Nb K-edge XANES spectra of reference samples and Nb_2O_5/Al_2O_3 calcined at 1123 K with various loadings.
(a) Sr_2GaNbO_6, (b) $Nb_2O_5 \cdot nH_2O$, (c) 5 wt%, (d) 11 wt%, (e) 14 wt%, (f) 16 wt%, (g) 18 wt%, (h) 21 wt%, (i) 30 wt%, (j) $AlNbO_4$, and (k) $YbNbO_4$.

Figure 17 shows the Nb K-edge k^3-weighted EXAFS spectra of Nb_2O_5/Al_2O_3 catalysts with various loadings, and of reference samples. No significant changes in the EXAFS spectra of each catalyst appeared until the Nb_2O_5 loading was 16 wt %. The oscillation amplitude decreased monotonically with k, and a weaker oscillation than that of niobium acid was observed in the k region above 10 Å^{-1}. Moreover, the oscillation period was similar to that of niobium acid. These results indicate that a smaller Nb-(O)-Nb contribution than that in niobium oxide exists in the catalyst sample. In contrast, the configuration changed in the EXAFS spectra of 18-30 wt % Nb_2O_5/Al_2O_3. Appreciable oscillation appeared in the k region higher than 10 Å^{-1}, and the oscillation is similar to that of $AlNbO_4$, indicating that there is a Nb-(O)-Al contribution on the catalyst. The oscillation amplitude in the k region higher than 6 Å^{-1} increased monotonically with increasing Nb_2O_5 loading, which indicates growth of the $AlNbO_4$ domain. This could be seen more clearly in the radial structure function (RSF; Figure 18). The RSFs of the Nb_2O_5/Al_2O_3 samples gave three peaks, at 1.4, 3.0, and 3.4 Å. The first peak corresponds to a Nb-O linkage. The second and third peaks correspond to Nb-(O)-Nb or Nb-(O)-Al linkages. To determine whether these peaks correspond to Nb-(O)-Nb or Nb-(O)-Al linkages, we analyzed the backscattering amplitudes and the phase shifts. Because the atomic numbers of Al and Nb are 13 (third period) and 41 (fifth period), the backscattering amplitude of Al and the phase shift of the Nb-Al pair are quite different from those of the Nb-(O)-Nb pair. On the basis of this analysis, in the cases of 18, 21, and 30 wt % Nb_2O_5/Al_2O_3 samples, Al scatterers mainly contribute to the peak at 3.0 Å. This result agrees with the XRD, Raman, and XPS results. However, below 16 wt %, Nb scatterers probably cause the second and third peaks. These structural analyses strongly suggest that Nb atoms were supported on alumina in a two-dimensional (monolayer) form with Nb-(O)-Nb linkages. The shape of the second coordination sphere of Nb_2O_5/Al_2O_3 with Nb_2O_5 loadings higher than 18 wt % was identical to that of $AlNbO_4$.
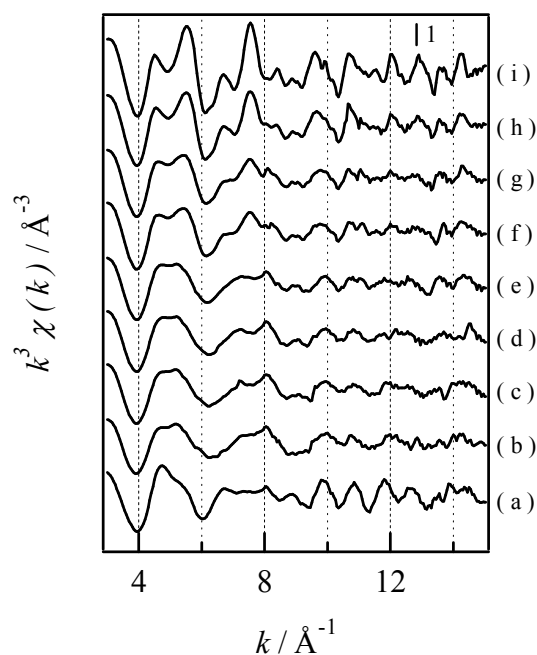
Figure 17. Nb K-edge k^3-weighted EXAFS of reference samples and Nb_2O_5/Al_2O_3 calcined at 1123 K with various loadings.
(a) $Nb_2O_5 \cdot nH_2O$, (b) 5 wt%, (c) 11 wt%, (d) 14 wt%, (e) 16 wt%, (f) 18 wt%, (g) 21 wt%, (h) 30 wt%, and (i) $AlNbO_4$.
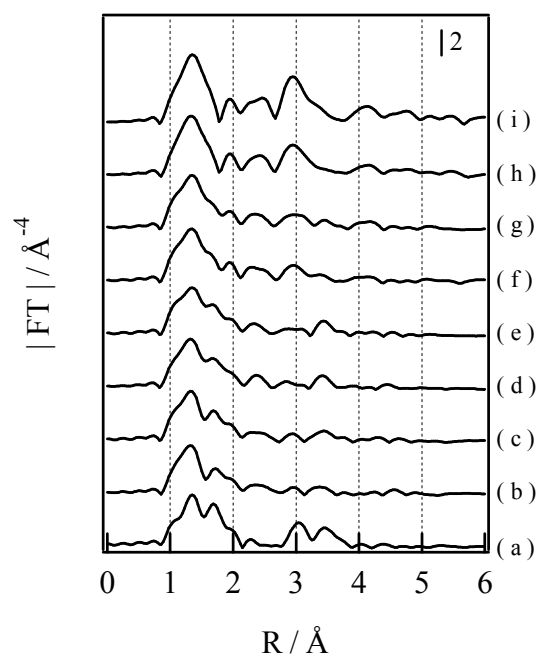
Figure 18. Fourier transforms of Nb K-edge k^3-weighted EXAFS of reference samples and Nb_2O_5/Al_2O_3 calcined at 1123 K with various loadings.
(a) $Nb_2O_5 \cdot nH_2O$, (b) 5 wt%, (c) 11 wt%, (d) 14 wt%, (e) 16 wt%, (f) 18 wt%, (g) 21 wt%, (h) 30 wt%, and (i) $AlNbO_4$.

An EXAFS spectrum consists of a linear combination of many kinds of simple sine waves, which correspond to each scatter-scatterer pair. We assume that there are two types of Nb species on Al_2O_3: a two-dimensional (monolayer) form with Nb-(O)-Nb linkages (island form of niobium oxide) and $AlNbO_4$ crystallites. If this assumption is correct, EXAFS spectra of highly loaded catalysts could be reproduced by convolution of each standard spectrum. As a standard spectrum of two-dimensional (monolayer) form, we adopted that of 10 wt % Nb_2O_5/Al_2O_3. The result of convolution analysis to 30 wt% Nb_2O_5/Al_2O_3 is shown in Figure 19. The EXAFS spectrum could be reproduced with those of 10 wt % Nb_2O_5/Al_2O_3 (35%) and $AlNbO_4$ (65%), indicating that 35% of the supported Nb was in a two-dimensional (monolayer) form and the residue (65%) was $AlNbO_4$ crystallites. Similarly, on the basis of the convolution analysis, it is estimated that 30% and 35% of the niobium were in $AlNbO_4$ crystallites on the 18 and 21 wt % Nb_2O_5/Al_2O_3 catalysts, respectively. Nb species are therefore supported on alumina in a two-dimensional (monolayer) form until Nb_2O_5 species completely cover the alumina surface, and the excess Nb species are deposited to form $AlNbO_4$ crystallites.

Figure 19. The results of convolution analysis on Nb K-edge k^3-weighted EXAFS of 30 wt% Nb_2O_5/Al_2O_3 calcined at 1123 K.
(a) 10 wt% Nb_2O_5/Al_2O_3 calcined at 1123 K, (b) 30 wt% Nb_2O_5/Al_2O_3 calcined at 1123 K (solid black curve : measured spectrum, dotted red curve : fitted spectrum), (c) $AlNbO_4$.

Structure of active sites

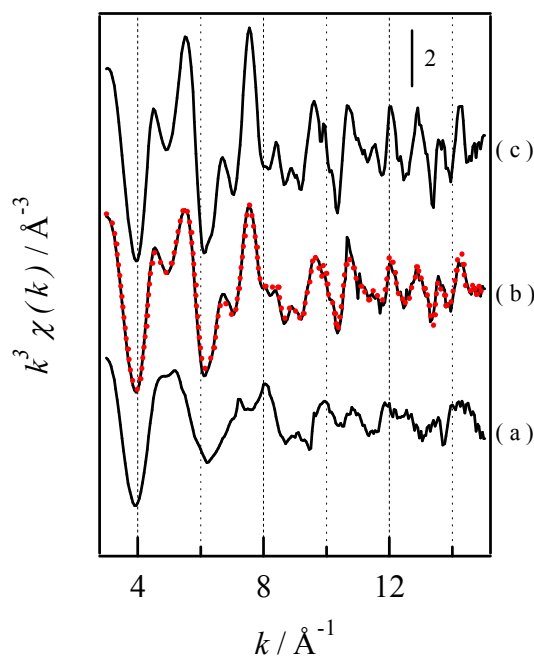Table 4 summarizes the BET specific surface areas. The catalyst areas include that of the Al_2O_3 carrier. S_0 is the surface area $g(Al_2O_3)^{-1}$ of a carrier, and was calculated from the BET specific surface area and Nb_2O_5 content. Soccupied is the estimated area occupied by NbO_6 units according to three assumptions described below. The first assumption is that all Nb atoms exist as NbO_6 octahedra. The second assumption is that all NbO_6 units have the same crosssection. The third assumption is that the cross-section is 0.16 nm^2 per NbO_6 unit (0.32 nm^2 per Nb_2O_5 unit), estimated from the crystal structure of H-Nb_2O_5.[63] The surface area gradually decreased with increasing Nb_2O_5 loading up to 21 wt %, and then decreased significantly. In the cases of 11-16 wt % Nb_2O_5/Al_2O_3 catalysts, the areas occupied by NbO_6 units ($S_{occupied}$) were calculated to be 89.6-138 m^2 $g(Al_2O_3)^{-1}$. This value is lower than or comparable to the surface areas $g(Al_2O_3)^{-1}$ of carriers and the area of Al_2O_3 pretreated at 1123 K. The surface density of Nb atom for 16 wt % Nb_2O_5/Al_2O_3 calcined at 1123 K was estimated to be 6.4 atoms nm^{-2}. Iwasawa[64] and Bell[65] reported that the surface density of Nb atoms in monolayer coverage with Nb_2O_5 was 6.3 atoms nm^{-2} in the cases of Nb_2O_5/SiO_2 and Nb_2O_5/TiO_2. These results show that (1) a monolayer of niobium oxide was formed on the Al_2O_3 surface and (2) most of the Al_2O_3 surface was covered with a monolayer of niobium oxide when the Nb_2O_5 loading was 16 wt %.

Table 4. Physical properties of Nb_2O_5/Al_2O_3 calcined at 1123 K

Nb content		Area[b] / m^2g^{-1}	S_0[c] / m^2	$S^d_{occupied}$ / m^2 $g(cat)^{-1}$	$S^d_{occupied}$ / m^2 $g(Al_2O_3)^{-1}$
mmol $g(Al_2O_3)^{-1}$	(wt%)[a]				
0	0	124	124	0	0
0.20	5	136	143	36.2	38.1
0.46	11	123	138	79.7	89.6
0.72	16	106	126	116	138
0.82	18	98.1	120	130	159
1.0	21	104	132	152	193
1.6	30	74.2	106	217	311

[a] As Nb_2O_5
[b] BET specific surface area
[c] Surface area of $g(Al_2O_3)^{-1}$ carrier
[d] Occupied area by Nb_2O_5 unit (0.32 nm^2)

Table 5 summarizes the specific activities per Brønsted acid site for benzylation of anisole, cumene cracking, and α-pinene isomerization over Nb_2O_5/Al_2O_3 calcined at 1123 K. The estimated turnover numbers per Brønsted acid site are almost equal over 11-30 wt % Nb_2O_5/Al_2O_3 catalysts. This shows that each Brønsted acid site, for Nb_2O_5 loadings between 11 and 30 wt %, exhibits similar specific catalytic activity. The results showing that the specific activities and selectivities were quite similar indicate that the structures of the active sites (Brønsted acid sites) resemble each other. As mentioned above, there are very few Brønsted acid sites on 5 wt % Nb_2O_5/Al_2O_3 (Figure 6), suggesting that the formation of Nb-(O)-Nb linkages (niobium oxide islands) is necessary for the generation of Brønsted acid sites. The activities increased up to 16 wt % Nb_2O_5 loading. This tendency is consistent with the results reported by Wachs and co-workers. They reported that Brønsted acid sites appeared on Nb_2O_5/Al_2O_3 calcined at 773 K when the niobium oxide species reaches a critical surface coverage (~0.5 monolayer), and then increased linearly as the surface coverage increased until a maximum was reached at less than a monolayer.[28] In the case of 21 wt % Nb_2O_5/Al_2O_3, the calculated $S_{occupied}$ is 193 m^2 $g(Al_2O_3)^{-1}$, which exceeds the carrier area and the excess Nb atoms deposited on the monolayer of niobium oxide to form $AlNbO_4$. The formed $AlNbO_4$ blocks some of the Brønsted acid sites, resulting in reduced catalytic activities.

Table 5. Specific activity per Brønsted acid site of Nb_2O_5/Al_2O_3 calcined at 1123 K in Friedel-Crafts alkylation, cumene cracking, and α-pinene isomerization.

Loading amount of Nb_2O_5 (wt%)	TON		
	Friedel-Crafts alkylation[a]	cracking of cumene[b]	α-pinene isomerization[c]
0	0	0	—
5	157	0	1126
11	267	0.214	468
14	263	0.121	211
16	281	0.161	213
18	173	0.118	200
21	207	0.128	247
30	297	0.144	372

[a] (yield of benzyl anisole) / (Brønsted acidity)
[b] (yield of benzene) / (Brønsted acidity)
[c] (yield of camphene and limonene) / (Brønsted acidity)

Several researchers have reported that two-dimensional metal oxides exhibit acidic properties. WO_3/ZrO_2 is known as solid superacid,[66] and some groups have reported that superacid sites are generated on tungsten oxide supported two-dimensionally on zirconium oxide.[67,68] Although amorphous silica is completely inert and alumina exhibits only Lewis acidic properties, Niwa reported that a thin silica layer on alumina prepared by chemical vapor deposition exhibited Brønsted acid sites.[69] They suggested that silanols on the silica layer attached to alumina act as Brønsted acid sites. Takagaki et al. reported the generation of Brønsted acid sites on HNb_3O_8, which has a two-dimensional $Nb_3O_8^-$ anion nanosheet composed of NbO_6 octahedra. They showed that bridging hydroxyl groups, Nb-(OH)-Nb, of the HNb_3O_8 nanosheets function as strong Brønsted acid sites, which are available for hydrolysis of ethyl acetate as well as niobic acid.[70] They also reported that various kinds of mixed metal oxide nanosheet such as $HTiNbO_5$, $HTiTaO_5$, $HNbMoO_6$, $HNbWO_6$, and $HTaWO_6$ show strong Brønsted acidic properties.[51,70-81] In contrast, bulk Nb_2O_5 is almost neutral. These results clearly indicate that the local structure of niobium oxide species has an effect on the generation of Brønsted acid sites.

XPS and Nb K-edge XAFS results for Nb_2O_5/Al_2O_3 calcined at 1123 K show that a monolayer of niobium oxide covered the surface of Nb_2O_5/Al_2O_3 calcined at 1123 K, and the surface is completely covered with a monolayer of niobium oxide at 16 wt% Nb_2O_5 loading. The number of Brønsted acid sites increased up to 16 wt % Nb_2O_5 loading, and the number of Lewis acid sites decreased nonlinearly with Nb_2O_5 loading, which suggests that new Brønsted acid sites are formed in Nb_2O_5/Al_2O_3 catalysts as existing sites are occupied by niobium oxide. However, the number of Brønsted acid sites is much smaller than the number of supported Nb atoms. The independence of the selectivities in acid-catalyzed reactions with respect to Nb_2O_5 loading shows that the acid strength distributions of Nb_2O_5/Al_2O_3 catalysts resemble each other. High-temperature calcination causes strong interactions between niobium oxide with distorted NbO_6 units and alumina, and stabilizes the niobium oxide monolayer, resulting in generation of Brønsted acid sites on highly loaded Nb_2O_5/Al_2O_3. On the basis of the results mentioned above, we concluded that a two-dimensional structured niobium oxide monolayer is the key to the generation of Brønsted acid sites; this gives several possibilities for the structures and locations of Brønsted acid sites, as shown in Figure 20. The first model is isolated or bridged hydroxyl groups on a niobium oxide monolayer

(Nb-OH or Nb-(OH)-Nb). In the second model these groups are located at the edges of niobium oxide islands (niobium oxide domain; Nb-(OH)-Al), and in the third model they are located at the boundaries of niobium oxide islands. The relation between the number of Brønsted acid sites and the Nb content strongly suggests that model 3, isolated or bridged hydroxyl groups located at the boundaries of niobium oxide islands, is the most reliable among the proposed models. Generation of Brønsted acid sites by calcination at high temperatures is assumed to be due to (1) the formation of monolayer of niobium oxide on the surface of alumina, and (2) the formation of boundaries of domains of niobium oxide monolayer. The shrink of alumina by calcination at high temperatures contributes to the reduction of surface area of alumina. As a result, the distance between domains of niobium oxide monolayer becomes shorter, and then, boundaries of niobium oxide monolayers form to generate Brønsted acid sites. Detailed characterization of the hydroxyl groups is under investigation to determine the locations of the hydroxyl groups on Nb_2O_5/Al_2O_3 catalysts.
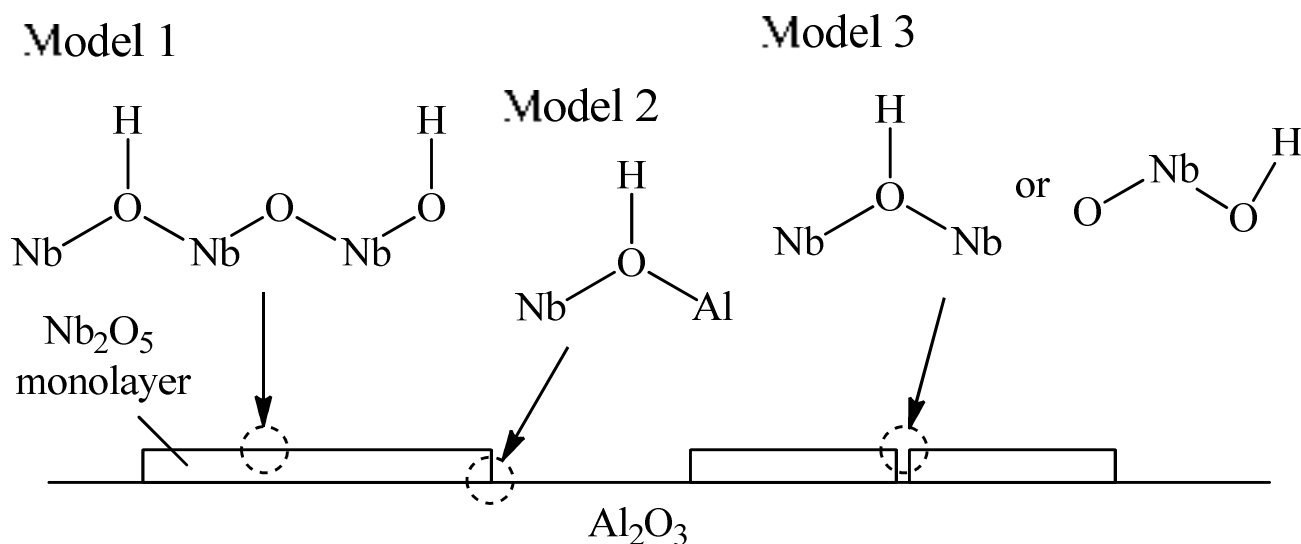
Figure 20. Structure models of Brønsted acid sites on Nb_2O_5/Al_2O_3.

Conclusions

Alumina-supported niobium oxide catalysts calcined at 1123 K exhibit Brønsted acid properties and catalyze benzylation of anisole, cumene cracking, and isomerization of α-pinene. The catalytic activity depends on both the calcination temperature and the niobium loading; 16 wt % Nb_2O_5/Al_2O_3 calcined at 1123 K exhibited the highest activity. Interestingly, Nb_2O_5/Al_2O_3 showed significant catalytic activity in the isomerization of α-pinene to camphene and limonene even after pretreatment at 1173 K; this shows the high thermal stability of Brønsted acid site generated on Nb_2O_5/Al_2O_3. A monolayer of niobic oxide with distorted octahedral NbO_6 units was formed and stabilized on alumina. Brønsted acid sites are probably generated at boundaries between two domains of the niobic oxide monolayer. When the Nb_2O_5 loading exceeded the amount needed to form a two-dimensional niobium oxide overlayer (>16 wt %), inert $AlNbO_4$ crystallites formed and were deposited on some of the Brønsted acid sites on Nb_2O_5/Al_2O_3, resulting in a lowering of the catalytic activity.

References

(1)   Iizuka, T.; Ogasawara, K.; Tanabe, K. *Bull. Chem. Soc. Jpn* **1983**, *56*, 2927.

(2)   Tanabe, K. *Catal. Today* **1990**, *8*, 1.

(3)   Tanabe, K.; Okazaki, S. *Appl. Catal. A-Gen.* **1995**, *133*, 191.

(4)   Tanabe, K. *Catal. Today* **2003**, *78*, 65.

(5)   Okuhara, T. *Chem. Rev.* **2002**, *102*, 3641.

(6)   Nowak, I.; Ziolek, M. *Chem. Rev.* **1999**, *99*, 3603.

(7)   Grasselli, R. K.; Burrington, J. D.; Buttrey, D. J.; DeSanto, P.; Lugmair, C. G.; Volpe, A. F.; Weingand, T. *Top. Catal.* **2003**, *23*, 5.

(8)   Millet, J. M. M.; Roussel, H.; Pigamo, A.; Dubois, J. L.; Jumas, J. C. *Appl. Catal. A-Gen.* **2002**, *232*, 77.

(9)   Grasselli, R. K. *Catal. Today* **1999**, *49*, 141.

(10)   Ushikubo, T.; Oshima, K.; Kayou, A.; Hatano, M. In *Spillover and Migration of Surface Species on Catalysts*; Li, C., Xin, Q., Eds. 1997; Vol. 112, p 473.

(11)   Ushikubo, T. *Catal. Today* **2003**, *78*, 79.

(12)   Hitoki, G.; Takata, T.; Kondo, J. N.; Hara, M.; Kobayashi, H.; Domen, K. *Electrochemistry* **2002**, *70*, 463.

(13)   Yoshida, H.; Murata, C.; Hattori, T. *J. Catal.* **2000**, *194*, 364.

(14)   Tanaka, T.; Nojima, H.; Yamamoto, T.; Takenaka, S.; Funabiki, T.; Yoshida, S. *Phys. Chem. Chem. Phys.* **1999**, *1*, 5235.

(15)   Tanaka, T.; Nojima, H.; Yoshida, H.; Nakagawa, H.; Funabiki, T.; Yoshida, S. *Catal. Today* **1993**, *16*, 297.

(16)   Paulis, M.; Martin, M.; Soria, D. B.; Diaz, A.; Odriozola, J. A.; Montes, M. *Appl. Catal. A-Gen.* **1999**, *180*, 411.

(17)   Tanabe, K. *Catal. Today* **1993**, *16*, 289.

(18)   Nakajima, K.; Baba, Y.; Noma, R.; Kitano, M.; Kondo, J. N.; Hayashi, S.; Hara, M. *J. Am. Chem. Soc.* **2011**, *133*, 4224.

(19)   Ohuchi, T.; Miyatake, T.; Hitomi, Y.; Tanaka, T. *Catal. Today* **2007**, *120*, 233.

(20)   Ushikubo, T. *Catal. Today* **2000**, *57*, 331.

(21)   Ko, E. I.; Bafrali, R.; Nuhfer, N. T.; Wagner, N. J. *J. Catal.* **1985**, *95*, 260.

(22)   Burke, P. A.; Ko, E. I. *J. Catal.* **1991**, *129*, 38.

(23)   Tanaka, T.; Yoshida, T.; Yoshida, H.; Aritani, H.; Funabiki, T.; Yoshida, S.; Jehng, J. M.; Wachs, I. E. *Catal. Today* **1996**, *28*, 71.

(24)   Yoshida, H.; Tanaka, T.; Yoshida, T.; Funabiki, T.; Yoshida, S. *Catal. Today* **1996**, *28*, 79.

(25)   Wachs, I. E.; Chen, Y.; Jehng, J. M.; Briand, L. E.; Tanaka, T. *Catal. Today* **2003**, *78*, 13.

(26)   Jehng, J. M.; Turek, A. M.; Wachs, I. E. *Appl. Catal. A-Gen.* **1992**, *83*, 179.

(27)   Jehng, J. M.; Wachs, I. E. *Catal. Today* **1993**, *16*, 417.

(28)   Datka, J.; Turek, A. M.; Jehng, J. M.; Wachs, I. E. *J. Catal.* **1992**, *135*, 186.

(29)   Beutel, T.; Siborov, V.; Tesche, B.; Knozinger, H. *J. Catal.* **1997**, *167*, 379.

(30)   Asakura, K.; Iwasawa, Y. *J. Phys. Chem.* **1991**, *95*, 1711.

(31)   Onfroy, T.; Clet, G.; Bukallah, S. B.; Hercules, D. M.; Houalla, M. *Catal. Lett.* **2003**, *89*, 15.

(32)   Onfroy, T.; Clet, G.; Houalla, M. *J. Phys. Chem. B,* **2005**, *109*, 14588.

(33)   Onfroy, T.; Clet, G.; Bukallah, S. B.; Visser, T.; Houalla, M. *Appl. Catal. A-Gen.* **2006**, *298*, 80.

(34)   Onfroy, T.; Manoilova, O. V.; Bukallah, S. B.; Hercules, D. M.; Clet, G.; Houalla, M. *Appl. Catal. A-Gen.* **2007**, *316*, 184.

(35)   de la Cruz, M. H. C.; da Silva, J. F. C.; Lachter, E. R. *Catal. Today* **2006**, *118*, 379.

(36)   de la Cruz, M. H. C.; Abdel-Rehim, M. A.; Rocha, A. S.; da Silva, J. F. C.; Faro, A. D.; Lachter, E. R. *Catal. Commun.* **2007**, *8*, 1650.

(37)   Shishido, T.; Kitano, T.; Teramura, K.; Tanaka, T. *Catal. Lett.* **2009**, *129*, 383.

(38)   Yamashita, K.; Hirano, M.; Okumura, K.; Niwa, M. *Catal. Today* **2006**, *118*, 385.

(39)   Okumura, K.; Yamashita, K.; Hirano, M.; Niwa, M. *Chem. Lett.* **2005**, *34*, 716.

(40)   Okumura, K.; Yamashita, K.; Hirano, M.; Niwa, M. *J. Catal.* **2005**, *234*, 300.

(41)   Stanisla.A; Yeddanap.Lm *Can. J. Chem.* **1972**, *50*, 113.

(42)   Ohnishi, R.; Tanabe, K.; Morikawa, S.; Nishizak.T *Bull. Chem. Soc. Jpn.* **1974**, *47*, 571.

(43)   Corma, A.; Garcia, H. *Catal. Today* **1997**, *38*, 257.

(44)   Severino, A.; Esculcas, A.; Rocha, J.; Vital, J.; Lobo, L. S. *Appl. Catal. A-Gen.* **1996**, *142*, 255.

(45)   Yamamoto, T.; Tanaka, T.; Funabiki, T.; Yoshida, S. *J. Phys. Chem. B* **1998**, *102*, 5830.

(46)   Yamamoto, T.; Matsuyama, T.; Tanaka, T.; Funabiki, T.; Yoshida, S. *Phys. Chem. Chem. Phys.* **1999**, *1*, 2841.

(47)   Yamamoto, T.; Tanaka, T.; Matsuyama, T.; Funabiki, T.; Yoshida, S. *J. Phys. Chem. B* **2001**, *105*, 1908.

(48)   Deoliveira, P. G. P.; Lefebvre, F.; Primet, M.; Eon, J. G.; Volta, J. C. *J. Catal.* **1991**, *130*, 293.

(49)   Ankudinov, A. L.; Ravel, B.; Rehr, J. J.; Conradson, S. D. *Phys. Rev. B* **1998**, *58*, 7565.

(50)   Cseri, T.; Bekassy, S.; Figueras, F.; Cseke, E.; Demenorval, L. C.; Dutartre, R. *Appl. Catal. A-Gen.* **1995**, *132*, 141.

(51)   Tagusagawa, C.; Takagaki, A.; Hayashi, S.; Domen, K. *J. Am. Chem. Soc.* **2008**, *130*, 7230.

(52)   Decanio, S. J.; Sohn, J. R.; Fritz, P. O.; Lunsford, J. H. *J. Catal.* **1986**, *101*, 132.

(53)   Richardson, J. T. *J. Catal.* **1967**, *9*, 182.

(54)   Shishido, T.; Hattori, H. *J. Catal.* **1996**, *161*, 194.

(55)   Hino, M.; Kurashige, M.; Matsuhashi, H.; Arata, K. *Thermochimica Acta* **2006**, *441*, 35.

(56)   Barzetti, T.; Selli, E.; Moscotti, D.; Forni, L. *Journal Of The Chemical Society-Faraday Transactions* **1996**, *92*, 1401.

(57)   Emeis, C. A. *J. Catal.* **1993**, *141*, 347.

(58)   Jia, C.; Massiani, P.; Barthomeuf, D. *J. Chem. Soc.-Faraday Trans.* **1993**, *89*, 3659.

(59)   Sikabwe, E. C.; Coelho, M. A.; Resasco, D. E.; White, R. L. *Catal. Lett.* **1995**, *34*, 23.

(60)   Arata, K.; Matsuhashi, H.; Hino, M.; Nakamura, H. *Catal Today* **2003**, *81*, 17.

(61)   Yamamoto, T.; Orita, A.; Tanaka, T. *X-Ray Spectrometry* **2008**, *37*, 226.

(62)   Yoshida, S.; Tanaka, T.; Hanada, T.; Hiraiwa, T.; Kanai, H.; Funabiki, T. *Catal. Lett.* **1992**, *12*, 277.

(63)   Gatehouse, B. M.; Wadsley, A. D. *Acta Crystallographica* **1964**, *17*, 1545.

(64)   Asakura, K.; Iwasawa, Y. *Chem. Lett.* **1986**, 859.

(65)   Pittman, R. M.; Bell, A. T. *J. Phys. Chem.* **1993**, *97*, 12178.

(66)   Arata, K. *Appl. Catal. A-Gen.* **1996**, *146*, 3.

(67)   Boyse, R. A.; Ko, E. I. *J. Catal.* **1997**, *171*, 191.

(68)   Barton, D. G.; Soled, S. L.; Meitzner, G. D.; Fuentes, G. A.; Iglesia, E. *J. Catal.* **1999**, *181*, 57.

(69)   Niwa, M.; Katada, N.; Murakami, Y. *J. Phys. Chem.* **1990**, *94*, 6441.

(70)   Takagaki, A.; Lu, D. L.; Kondo, J. N.; Hara, M.; Hayashi, S.; Domen, K. *Chem. Mat.* **2005**, *17*, 2487.

(71)   Takagaki, A.; Tagusagawa, C.; Hayashi, S.; Hara, M.; Domen, K. *Energy Environ. Sci.* **2010**, *3*, 82.

(72)   Tagusagawa, C.; Takagaki, A.; Takanabe, K.; Ebitani, K.; Hayashi, S.; Domen, K. *J. Catal.* **2010**, *270*, 206.

(73)   Tagusagawa, C.; Takagaki, A.; Iguchi, A.; Takanabe, K.; Kondo, J. N.; Ebitani, K.; Hayashi, S.; Tatsumi, T.; Domen, K. *Angew. Chem.-Int. Edit.* **2010**, *49*, 1128.

(74)   Takagaki, A.; Sasaki, R.; Tagusagawa, C.; Domen, K. *Topics in Catalysis* **2009**, *52*, 592.

(75)   Tagusagawa, C.; Takagaki, A.; Takanabe, K.; Ebitani, K.; Hayashi, S.; Domen, K. *J. Phys. Chem. C* **2009**, *113*, 17421.

(76)   Tagusagawa, C.; Takagaki, A.; Hayashi, S.; Domen, K. *Catal. Today* **2009**, *142*, 267.

(77)   Tagusagawa, C.; Takagaki, A.; Hayashi, S.; Domen, K. *J. Phys. Chem. C* **2009**, *113*, 7831.

(78)   Takagaki, A.; Tagusagawa, C.; Domen, K. *Chem. Commun.* **2008**, 5363.

(79)   Takagaki, A.; Toda, M.; Okamura, M.; Kondo, J. N.; Hayashi, S.; Domen, K.; Hara, M. *Catal. Today* **2006**, *116*, 157.

(80)   Takagaki, A.; Yoshida, T.; Lu, D. L.; Kondo, J. N.; Hara, M.; Domen, K.; Hayashi, S. *J. Phys. Chem. B* **2004**, *108*, 11549.

(81)   Takagaki, A.; Sugisawa, M.; Lu, D. L.; Kondo, J. N.; Hara, M.; Domen, K.; Hayashi, S. *J. Am. Chem. Soc.* **2003**, *125*, 5479.

Chapter 2

Characterization of Thermally Stable Bronsted Acid Sites

on Alumina-Supported Niobium Oxide Calcined at High Temperature

Abstract

Thermally stable Brønsted acid sites were generated on alumina-supported niobium oxide (Nb_2O_5/Al_2O_3) by calcination at high temperatures such as 1123 K. Structural characterization of thermally stable Brønsted acid sites on Nb_2O_5/Al_2O_3 was carried out using Fourier transformed infrared (FT-IR) spectroscopy, transmission electron microscopy (TEM), scanning transmission electron microscopy (STEM), and energy-dispersive X-ray (EDX) analysis. The results of FT–IR, TEM, STEM, and EDX measurements indicated that Nb_2O_5 monolayer domains were highly dispersed on alumina at low Nb_2O_5 loading such as 5 wt% and no Brønsted acid sites were presents. The coverage of Al_2O_3 with Nb_2O_5 monolayer domains increased as the Nb_2O_5 loading was increased, and was almost fully covered at a loading of 16 wt%. A sharp increase in the number of hydroxyl groups, which act as Brønsted acid sites, was observed at this loading. The relationship between acidic property and structure suggested that bridging hydroxyl groups (Nb–(OH)–Nb) formed at the boundaries between domains of Nb_2O_5 monolayer act as thermally stable Brønsted acid sites.

Introduction

Niobic acid ($Nb_2O_5 \cdot nH_2O$, hydrated niobium oxide) is a useful solid acid catalyst and its acidic properties have been widely investigated.[1-7] Niobic acid calcined at moderate temperatures of 373–573 K behaves as a Brønsted acid properties ($H_0 < -5.6$),[1-3] and is effective for reactions that relate to aqueous media including esterification, olefin hydration, and alcohol dehydration.[2-6] Niobium oxide (Nb_2O_5) is an amorphous metal oxide composed mainly of distorted NbO_6 octahedra and NbO_4 tetrahedra. Because the Nb-O bonds in these distorted polyhedra are highly polarized, some of the surface OH groups function as Brønsted acid sites. Nakajima et al. reported that NbO_4 tetrahedra in niobic acid act as effective Lewis acid sites, which catalyze the allylation of benzaldehyde with tetraallyl–tin, and the conversion of glucose to 5-(hydroxymethyl)furfural in the presence of water.[8] However, the acidic properties of $Nb_2O_5 \cdot nH_2O$ also lost following treatment at 673 K because of a structural change with phase transition to the TT-phase.[9,10]

Supported niobium oxide has been widely studied in attempts to control its catalytic properties and the structure of surface niobium species, by using different supporting metal oxides, and niobium precursors.[11-20] Although calcination temperature affects the structure and catalytic properties of supported niobium oxide catalysts, in most cases, such catalysts have been calcined at moderate temperatures of 673–773 K. There have only been a few investigations of the acidic properties and catalysis of supported niobium oxide calcined at high temperature (> 1000 K).

Recently, we reported that Nb_2O_5/Al_2O_3 containig a high loading of Nb_2O_5 calcined at 1123 K acts as an effective acid catalyst for benzylation of anisole, cumene cracking, and isomerization of α-pinene.[21-23] The activities of Nb_2O_5/Al_2O_3 for these reactions were proportional to its Brønsted acidity, indicating that these reactions occured at the Brønsted acid sites on the Nb_2O_5/Al_2O_3 catalysts. The Brønsted acidity of Nb_2O_5/Al_2O_3 catalysts depends on both the calcination temperature and the loading of niobium oxide. Among the Nb_2O_5/Al_2O_3 catalysts tested, 16 wt% Nb_2O_5/Al_2O_3 calcined at 1123 K exhibited the largest Brønsted acidity. This is in marked contrast to the evidence that calcination of niobium oxide itself at temperature higher than 773 K results in disappearance of Brønsted acidity.[14] Interestingly, Nb_2O_5/Al_2O_3 showed significant catalytic activity in the isomerization of α-pinene to camphene and limonene even after pretreatment at 1173 K. This clearly

demonstrates that the high thermal stability of Brønsted acid sites generated on Nb_2O_5/Al_2O_3 calcined at high temperature. Structural analysis revealed that niobium oxide was present as a monolayer on 16 wt% Nb_2O_5/Al_2O_3 calcined at 1123 K, and this niobium oxide monolayer plays an important role in the generation of Brønsted acid sites. However, the detailed structure of the monolayer of niobium oxide and the location of Brønsted acid sites are still unclear.

In the present study, a series of alumina-supported niobium oxide catalysts with various loading of Nb_2O_5 and calcined at different temperatures was characterized to determine the location and structure of thermally stable Brønsted acid sites generated by high temperature calcination. For this purpose, the relationship between the distribution and structure of niobium oxide on alumina surface and acidic properties was examined using Fourier transformed infrared (FT–IR) spectroscopy, transmission electron microscopy (TEM), scanning transmission electron microscopy (STEM), and energy-dispersive X-ray (EDX) analysis.

Experimental

Preparation

A series of Nb_2O_5/Al_2O_3 catalysts was prepared by impregnation of γ-alumina (JRC-ALO–8) with an aqueous solution of niobium oxalate (CBMM, Brazil) and calcination at various temperatures for 3 h in dry air. Aluminum niobate ($AlNbO_4$; monoclinic, $a = 1.215$ nm, $b = 0.3735$ nm, $c = 0.6438$ nm, $\alpha = \gamma = 90°$, $\beta = 107°$) was synthesized from $Al(NO_3)_3 \cdot 9H_2O$ and niobium oxalate.[24] $Al(NO_3)_3 \cdot 9H_2O$ was dissolved in water and then oxalic acid (Wako, Osaka, Japan) and 28% ammonia solution were added to the solution at pH of 1.0 and 3.0, respectively. An aqueous solution of niobium oxalate was added to an aluminum solution with a molar ratio of Al/Nb = 1.0, and then heated under refluxed at 413 K for 1 h. The white paste obtained after removing water was dried at 423 K for 15 h. $AlNbO_4$ was formed by calcination of the solid at 1273 K for 3 h.

Characterizations

The Brunauer–Emmett–Teller (BET) specific surface areas of catalysts were estimated from N_2 isotherms at 77 K. N_2 adsorption isotherms were measured at 77 K using an adsorption analyzer (BELSORP 28SA, BEL Japan, Osaka, Japan). Prior to measurement, each sample was evacuated at

573 K for 2 h. The surface area was determined from six points of data (adsorption amount *vs.* relative pressures (P/P_0) ranging from 0.05 to 0.2) in each isotherm.

FT–IR spectra were recorded using an FT–IR spectrometer (SPECTRUM ONE, Perkin–Elmer, Walthham, MA, USA) with a resolution of 4 cm^{-1}. Each sample (12.5 mg) was pressed into a self-supporting wafer with a diameter of 13 mm. Catalysts were pretreated under 13.3 kPa of O_2 for 1 h at 673 K and then evacuated for 1 h at 673 K. To determine the amount of Brønsted and Lewis acid sites on samples, each wafer was exposed to 0.667 kPa of pyridine vapor at 298 K for 10 min and then was evacuated at various temperatures for 10 min.

TEM, STEM, and EDX mapping images were obtained with a JEOL JEM–2100F transmission electron microscope operating at an accelerating voltage of 200 kV. TEM samples were prepared by depositing drops of a methanol suspension containing small amounts of the powders onto a carbon-coated copper grid (Okenshoji Co. Ltd.) and allowing the methanol to evaporate in air.

Results

Physical properties

The physical properties of Nb_2O_5/Al_2O_3 prepared under various conditions are summarized in Table 1. The areas of the catalysts include the Al_2O_3 carrier. S_0 is the surface area $g(Al_2O_3)^{-1}$ of the carrier and was calculated from the BET specific surface area and Nb_2O_5 content. $S_{occupied}$ is the estimated area occupied by NbO_6 units according to the following three assumptions: 1) All Nb atoms exist as NbO_6 octahedra. 2) All NbO_6 units have the same cross-section. 3) The cross-section estimated from the crystal structure of $H–Nb_2O_5$ is 0.16 nm^2 per NbO_6 unit (0.32 nm^2 per Nb_2O_5 unit).[25] The surface area decreases as the calcination temperature and loading of Nb_2O_5 increase. Calcination above 1123 K or with a Nb_2O_5 loading higher than 21 wt% caused a sharp decrease of surface area. In a previous report, XRD patterns showed that amorphous niobium oxide transformed to crystalline aluminum niobate ($AlNbO_4$) by calcination above 1123 K or Nb_2O_5 loading > 21 wt%, indicating that crystallization of $AlNbO_4$ results in a sharp decrease of surface area.[23] On 16 wt% Nb_2O_5/Al_2O_3 catalysts calcined at 1073 K and 1123 K, S_0 was comparable to $S_{occupied}$. The surface density of Nb atom on 16 wt% Nb_2O_5/Al_2O_3 calcined at 1123 K was estimated to be 6.4 atoms nm^{-2}.

In the cases of Nb_2O_5/SiO_2 and Nb_2O_5/TiO_2, Iwasawa[17] and Bell[13] respectively reported that the surface density of Nb atoms in monolayer coverage with Nb_2O_5 was 6.3 atoms nm^{-2}. These results suggest that most of the Al_2O_3 surface was covered with a monolayer of niobium oxide when the Nb_2O_5 loading was 16 wt%. As mentioned above, Nb_2O_5 crystals were not formed regardless of Nb_2O_5 loading and calcination temperature, but $AlNbO_4$ was formed on the catalyst when the calcination temperature was > 1123 K or the Nb_2O_5 loading was above 16 wt%. This fact indicates that $AlNbO_4$ is more stable than Nb_2O_5 crystals on γ-Al_2O_3 and the interaction between Nb and Al is stronger than that between Nb and Nb. It appears that the strong interaction between Nb and Al helps to form a monolayer of niobium oxide on the alumina surface.

Table 1. Physical properties of Nb_2O_5/Al_2O_3

Nb content		Calcination	$Area^b$	S_0^c / m^2	$S^d_{occupied}$
mmol $g(Al_2O_3)^{-1}$	$(wt\%)^a$	temperature / K	$/ m^2 g^{-1}$		$/ m^2 g(Al_2O_3)^{-1}$
0	0	1123	124	124	0
0.20	5	1123	136	143	38.1
0.46	11	1123	123	138	89.6
0.72	16	773	155	185	138
		973	138	164	138
		1073	123	146	138
		1123	106	126	138
		1173	91	108	138
		1273	58	69	138
		1423	6	7	138
0.82	18	1123	98.1	120	159
1.0	21	1123	104	132	193
1.6	30	1123	74.2	106	311

^{a} As Nb_2O_5
^{b} BET specific surface area
^{c} Surface area of $g(Al_2O_3)^{-1}$ carrier
^{d} Occupied area by Nb_2O_5 unit (0.32 nm^2)

Surface coverage estimated from FT-IR spectra

To estimate the coverage of the niobium oxide monolayer on Al_2O_3, the amount of Lewis acid sites attributed to Al_2O_3 on Nb_2O_5/Al_2O_3 calcined at 1123 K with various loadings of Nb_2O_5 were evaluated based on FT-IR spectra of adsorbed pyridine. The amount of Lewis acid sites on Al_2O_3 was then correlated with the surface coverage of Al_2O_3 by an niobium oxide monolayer. Figure 1 shows an FT-IR spectrum of pyridine adsorbed on γ-Al_2O_3 calcined at 1123 K. The FT–IR spectra of adsorbed pyridine after evacuation at 423 K are widely used as a quantitative measurement of the amounts of Lewis and Brønsted acid sites.[26-29] The band at around 1600 cm^{-1} corresponds to the 8a ring vibration mode of pyridine coordinated to Lewis acid sites.[30-32] Because ring vibration of pyridine is quite sensitive to coordination environment, the position of this band reflects the local environment of Lewis acid sites. In the case of γ-Al_2O_3, the band at around 1600 cm^{-1} can be divided into two bands corresponding to pyridine coordinated to different Lewis acid sites. Morterra et al. [31-34] reported that γ-Al_2O_3 has three types of Lewis acid sites: vacancies on octahedral Al sites (Al^L_o), vacancies shared by tetrahedral Al and octahedral Al cations pair ($Al^L_{t,o}$), and vacancies on tetrahedral Al sites (Al^L_t). They proposed that the bands at 1598, 1610-1620, and, 1625 cm^{-1} correspond to pyridine coordinated to Al^L_o, $Al^L_{t,o}$, and Al^L_t, respectively. According to their results,

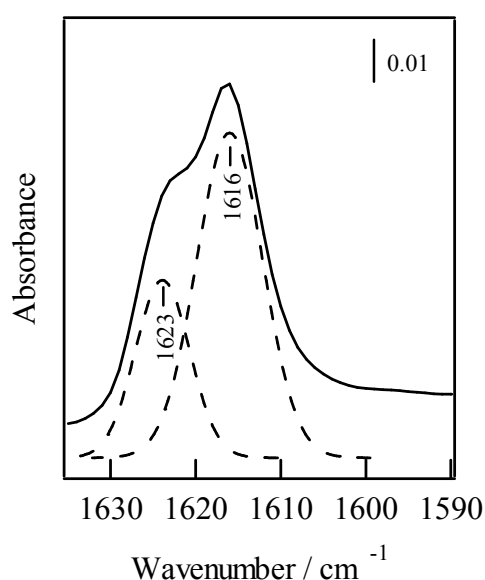**Figure 1.** FT-IR spectrum of pyridine adsorbed on the Lewis acid sites of γ-Al_2O_3 calcined at 1123 K. The sample was exposed to pyridine at 298 K, and then evacuated at 423 K.

we assigned the band at 1616 cm^{-1} to pyridine coordinated to Al$^L_{t,o}$ and the band at 1623 cm^{-1} to Al^L_t.

An FT-IR spectrum of pyridine adsorbed on 16 wt% Nb$_2$O$_5$/Al$_2$O$_3$ calcined at 1123 K is shown in Figure 2. The band at around 1620 cm^{-1} is divided into two bands at 1612 cm^{-1} and 1623 cm^{-1}. The new band at 1612 cm^{-1} appeared upon loading with Nb$_2$O$_5$. Yamamoto et al. reported that new Lewis acid sites were generated on lanthanide (Ln) oxides (Ln such as La, Ce, Eu, Tb, and Yb) supported on alumina by using pyridine adsorption FT-IR experiments.[35,36] They showed that new bands appeared at around 1610 cm^{-1} upon loading of Ln oxide, and assigned these new bands are to Lewis acid sites formed on Ln with Ln-O-Al linkages. Because the alumina surface is covered with a monolayer of niobium oxide, the band at 1612 cm^{-1} is assigned to pyridine coordinated to Lewis acid sites on niobium oxide (Nb^L).

Figure 3 shows FT-IR spectra of pyridine adsorbed on Nb$_2$O$_5$/Al$_2$O$_3$ calcined at 1123 K with various Nb$_2$O$_5$ loadings as well as reference spectra (γ-Al$_2$O$_3$, niobic acid (Nb$_2$O$_5$•nH$_2$O), and AlNbO$_4$). Niobic acid showed a band related to pyridine coordinated to Lewis acid sites at 1610 cm^{-1}. In contrast, AlNbO$_4$ did not show a band caused by pyridine coordinated to Lewis acid sites. As the Nb$_2$O$_5$ loading increased up to 16 wt%, the intensity of the bands at 1616 and 1623 cm^{-1} decreased and a new band at 1612 cm^{-1} appeared and increased in intensity.
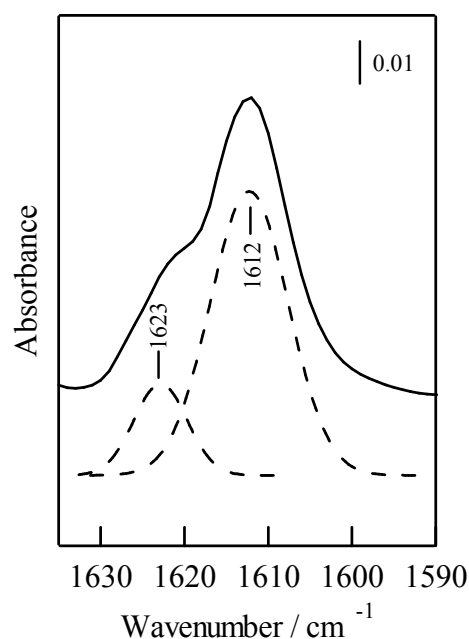

Figure 2. FT-IR spectrum of pyridine adsorbed on the Lewis acid sites of 16 wt% Nb$_2$O$_5$/Al$_2$O$_3$ calcined at 1123 K. The sample was exposed to pyridine at 298 K, and then evacuated at 423 K.

These results clearly indicate that the number of Lewis acid sites on alumina decreased and those on niobium oxide increased through loading of Nb_2O_5 on alumina. However, over a loading of 16 wt%, the bands at 1623 and 1612 cm^{-1}decreased in intensity as the Nb_2O_5 loading increased. Figure 4 shows the change in the amounts of each Lewis acid site on Nb_2O_5/Al_2O_3 calcined at 1123 K with various loadings. The amount of each Lewis acid site was determined using the method outlined below. First, the total amount of Lewis acid sites was calculated using an integrated molar adsorption coefficient value of $\varepsilon = 2.22$ cm μmol^{-1} for the band area at 1450 cm^{-1} of coordinated pyridine.[37,38] Then, assuming that the adsorption coefficient values of each band at 1612, 1616, and 1623 cm^{-1} areas the same, the amounts of each Lewis acid site were determined based on the area of each band.[32,33] As the Nb_2O_5 loading increased, a sharp decrease of $Al^L_{t,o}$ and gradual decrease of Al^L_t were observed. In contrast, Nb^L increased linearly up to 16 wt%. The surface Nb/Al ratio determined by XPS increased linearly with increasing Nb_2O_5 loading up to 16 wt%.[23] These results suggest that a monolayer of niobium oxide formed preferentially on $Al^L_{t,o}$ and new Lewis acid sites were generated on this monolayer. Above 16 wt%, Nb^L decreased slightly and Al^L_t increased a little.
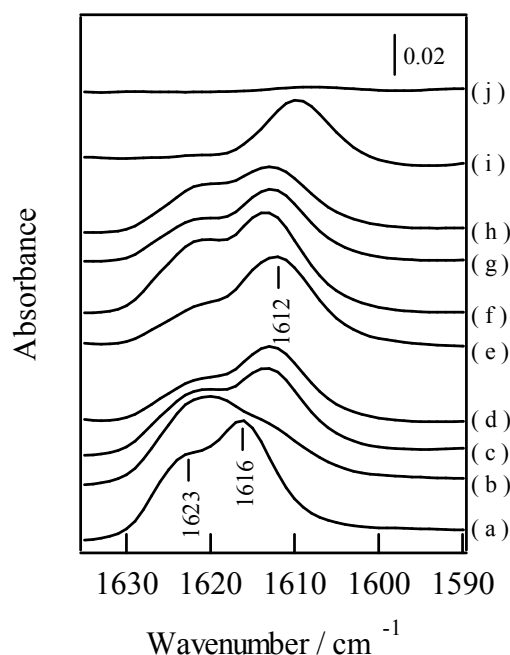

Figure 3. FT-IR spectra of pyridine adsorbed on Lewis acid sites of Nb_2O_5/Al_2O_3 calcined at 1123 K with various loadings. Reference spectra are also shown. (a) γ-Al_2O_3. Nb_2O_5 loadings of (b) 5 wt%, (c) 11 wt%, (d) 14 wt%, (e) 16 wt%, (f) 18 wt%, (g) 21 wt%, and (h) 30 wt%. Reference spectra of (i) $Nb_2O_5 \cdot nH_2O$, and (j) $AlNbO_4$.

These findings may be related to the aggregation of the monolayer of niobium oxide to form $AlNbO_4$ crystals.

Figure 5 depicts the ratio of Lewis acid sites occupied by the monolayer of niobium oxide ($Al_{L,occupied}$) to the total number of Lewis acid sites on Al_2O_3 ($Al^L_{t,o} + Al^L_t$) and the surface coverage of the monolayer of niobium oxide against Nb_2O_5 loading. Generally, the Lewis acid sites on alumina, $Al^L_{t,o}$ and Al^L_t, are uniformly dispersed on alumina surface. Therefore, the ratio of $Al_{L,occupied}$ reflects covering behavior of niobium oxide monolayer domains on an alumina surface.

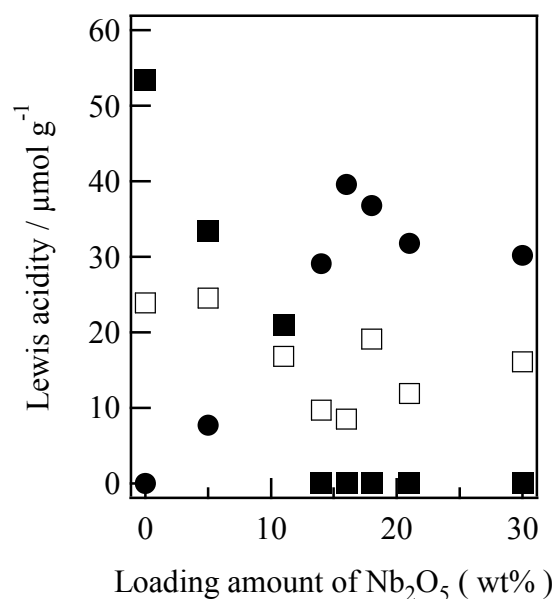**Figure 4.** Amount of each Lewis acid site on Nb_2O_5/Al_2O_3 calcined at 1123 K with various loadings. (■) $Al^L_{t,o}$, (□) Al^L_t, (●) Nb^L.
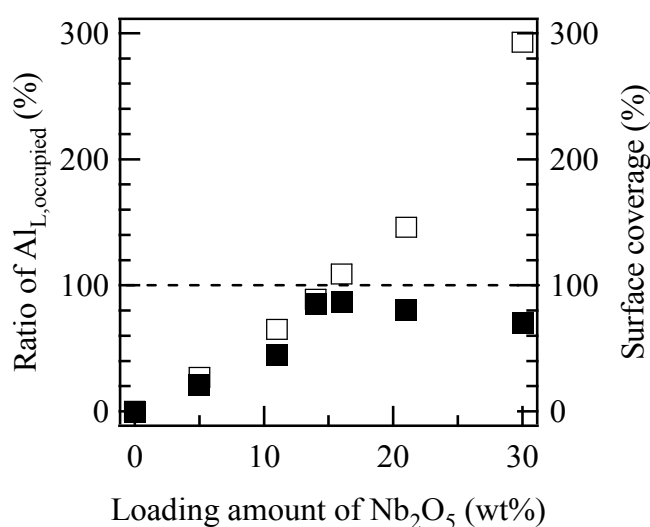
Figure 5. Correlation between the ratio of $Al_{L,occupied}$ (■) and surface coverage (□) of Nb_2O_5/Al_2O_3 calcined at 1123 K with various loadings.

Both the ratio of Lewis acid sites occupied by the monolayer of niobium oxide to the total number of Lewis acid sites on Al_2O_3 and the surface coverage of niobium oxide monolayer increased linearly as the Nb_2O_5 loading increased up to 16 wt%. The surface coverage was higher than the ratio of $Al_{L,occupied}$ regardless of Nb_2O_5 loadings. Although the surface coverage increased above 100% at 16 wt%, the ratio of $Al_{L,occupied}$ was ca. 87 %. If NbO_6 units are uniformly dispersed on an alumina surface to form a niobium oxide monolayer, the ratio of $Al_{L,occupied}$ would be 100 % when the surface coverage is 100 %. Therefore, these results indicate an inhomogeneous distribution of NbO_6 unit; that is, the formation of multilayer Nb_2O_5 species through the aggregation of NbO_6 units or the formation of bonded interface via the collision of two niobium oxide monolayer domains.

The average ratio of Nb atoms per $Al_{L,occupied}$ as a function of Nb_2O_5 loading (Nb atoms/$Al_{L,occupied}$) is presented in Figure 6. Nb atoms/$Al_{L,occupied}$ was around 23 up to 16 wt%, and then increased linearly with increasing Nb_2O_5 loading. Figure 3 indicates that 77.3 $\mu mol\ g^{-1}$ of Lewis acid sites are dispersed on the surface of γ-Al_2O_3 (124 m^2g^{-1}). Based on the Lewis acidity and surface area, the occupied area by each Lewis acid site on Al_2O_3 was calculated to be 2.67 nm^2. In contrast, the occupied area (cross section) of each niobium oxide monolayer domain composed of 23 Nb atoms is estimated to be 3.90 nm^2 (Figure 7).[25] The area of each niobium oxide monolayer domain composed of 23 Nb atoms is larger than the occupied area for each Lewis acid site on Al_2O_3. If the niobium oxide monolayer domains are loaded on two adjacent Lewis acid sites on Al_2O_3, these two domains will conflict with each other. These results strongly suggest that Lewis acid sites on Al_2O_3 were covered with niobium oxide monolayer domains.
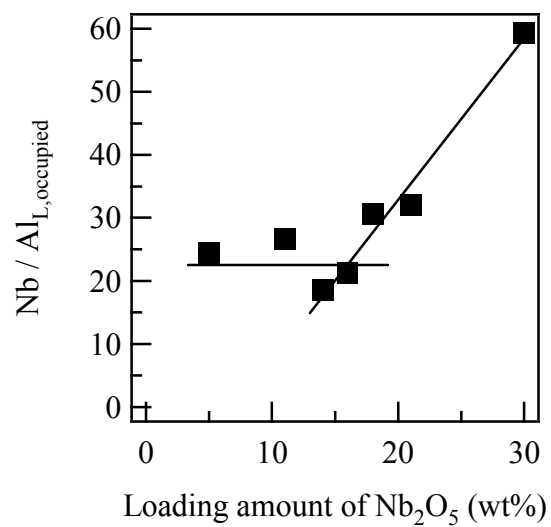
Figure 6. Average number of Nb atoms per $Al_{L,occupied}$ as a function of Nb_2O_5 loading.
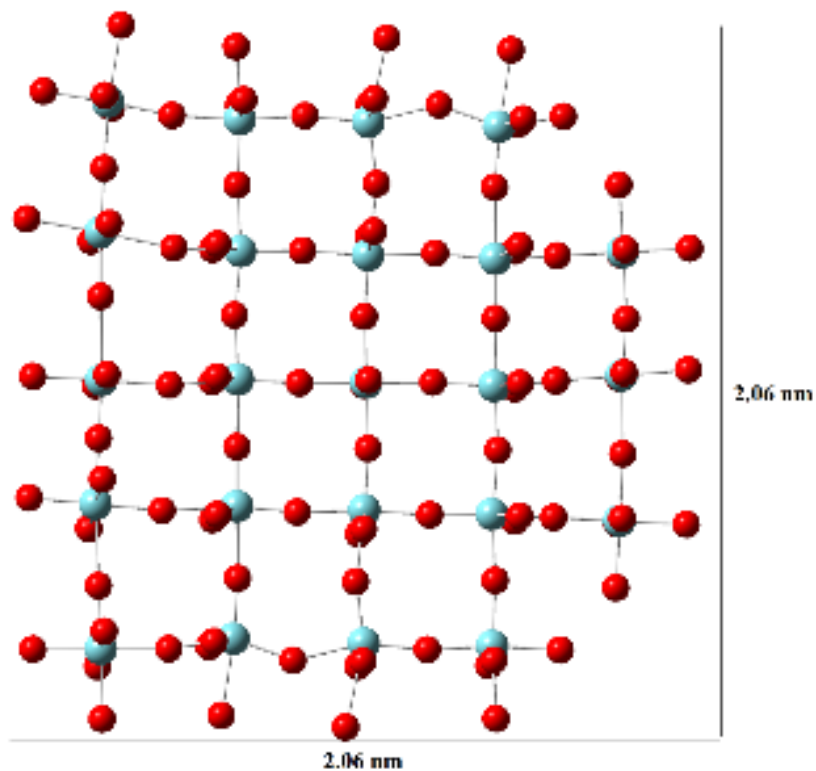
Figure 7. Structural model of an Nb_2O_5 monolayer domain.

Characterization of local structure of niobium oxide by electron microscopy

Figure 8 shows TEM images of Al_2O_3 and 5, 16, and 30 wt% Nb_2O_5/Al_2O_3 calcined at 1123 K. In the TEM image of Al_2O_3, (111) $\gamma-Al_2O_3$ fringes with a spacing of 0.455 nm can be clearly observed.[39] The fringes assigned to $\gamma-Al_2O_3$ become unclear on some parts of the particle in the 5 and 16 wt% Nb_2O_5/Al_2O_3 samples, because of the presence of niobium oxide. On the other hand, (011) $AlNbO_4$ fringes with a spacing of 0.572 nm are observed in the image of 30 wt% Nb_2O_5/Al_2O_3.[24]
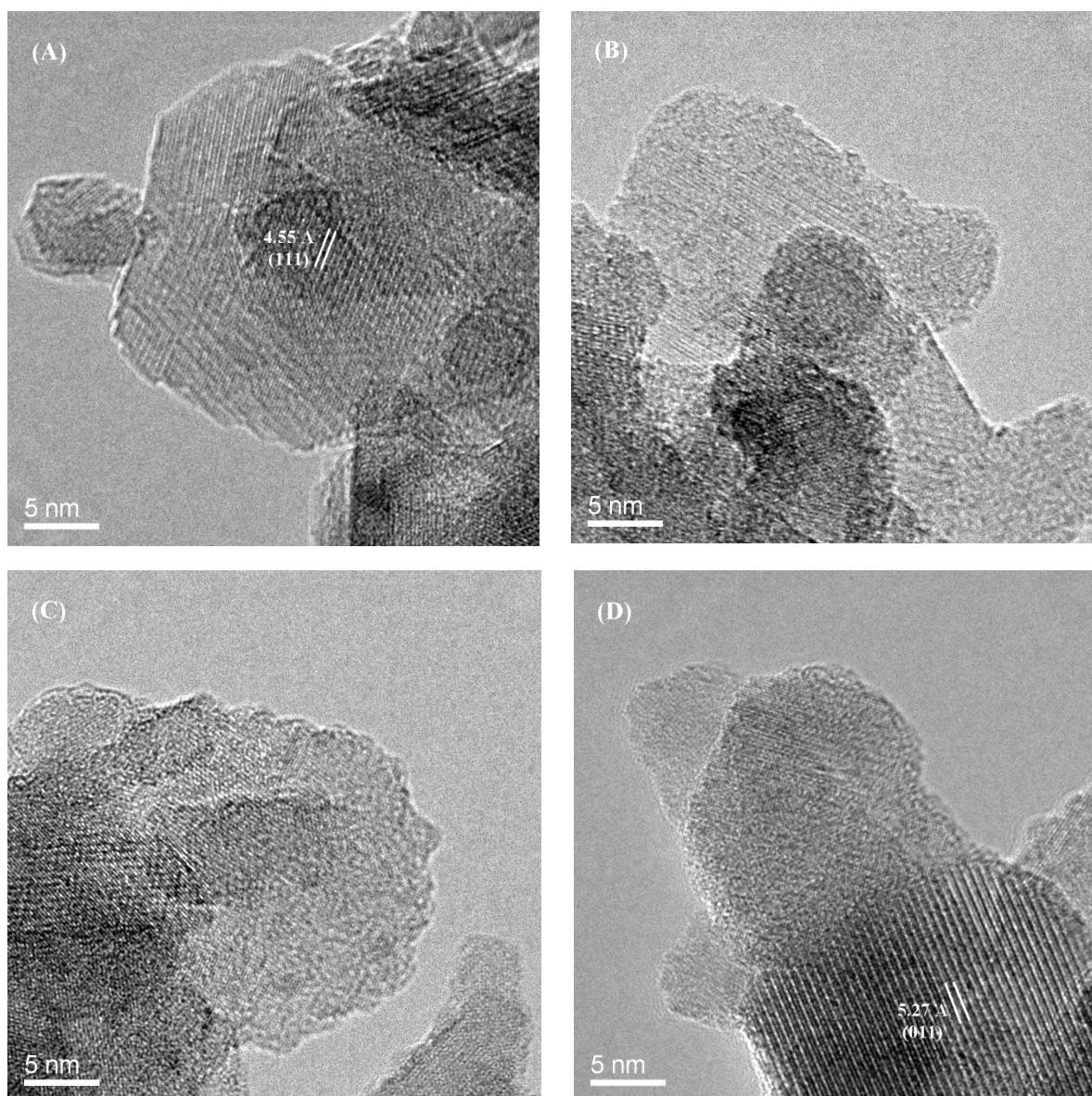
Figure 8. TEM images of (A) $\gamma-Al_2O_3$, and (B) 5 wt%, (C) 16 wt%, and (D) 30 wt% Nb_2O_5/Al_2O_3 calcined at 1123 K.

Figure 9(A) and (B) shows an STEM image and the results of EDX line analysis for 5 wt% Nb_2O_5/Al_2O_3 calcined at 1123 K, respectively. The dots on the line in Figure 9(A) indicate observation points in EDX. The change in intensity of Al (Al Kα) showed a volcano shape, whereas the intensity of Nb (Nb Lα) had two peaks at around points *a* and *b*. These results indicate an inhomogeneous distribution of Nb and suggest that niobium oxide domains were supported on alumina around points *a* and *b*. Because the length of the interval between two dots is 0.9 nm and each peak covers three dots, the domain size is estimated to be ca. 2 nm from EDX line analysis; this is similar to that calculated from the results of FT-IR spectra (Figure 7).

Figure 9. (A) STEM image and (B) the results of EDS analysis of 5 wt% Nb_2O_5/Al_2O_3 calcined at 1123 K. Green line : Nb, red line : Al.

Figure 10(A) and (B) shows an STEM image and the results of EDX analysis of 16 wt% Nb_2O_5/Al_2O_3 calcined at 1123 K, respectively. The change in intensity of Al (Al Kα) showed a volcano shape like 5 wt% Nb_2O_5/Al_2O_3. In contrast, the intensity of Nb (Nb Lα) was almost constant over the whole of the particle investigated. This tendency indicates that the surface of alumina was homogeneously covered with niobium oxide monolayer domains, and no segregation of niobium oxide took place.

Figure 10. (A) STEM image and (B) the results of EDS analysis of 16 wt% Nb_2O_5/Al_2O_3 calcined at 1123 K. Green line : Nb, red line : Al.

Figure 11(A) and (B) shows an STEM image and the result of EDX analysis of 30 wt% Nb_2O_5/Al_2O_3 calcined at 1123 K, respectively. The intensity of the Nb signal showed two peaks at points *a* and *b*. Considering the formation of $AlNbO_4$ crystals on this catalyst, it is thought that part of the niobium oxide monolayer domains aggregated to form $AlNbO_4$ crystals on alumina at around points *a* and *b*.
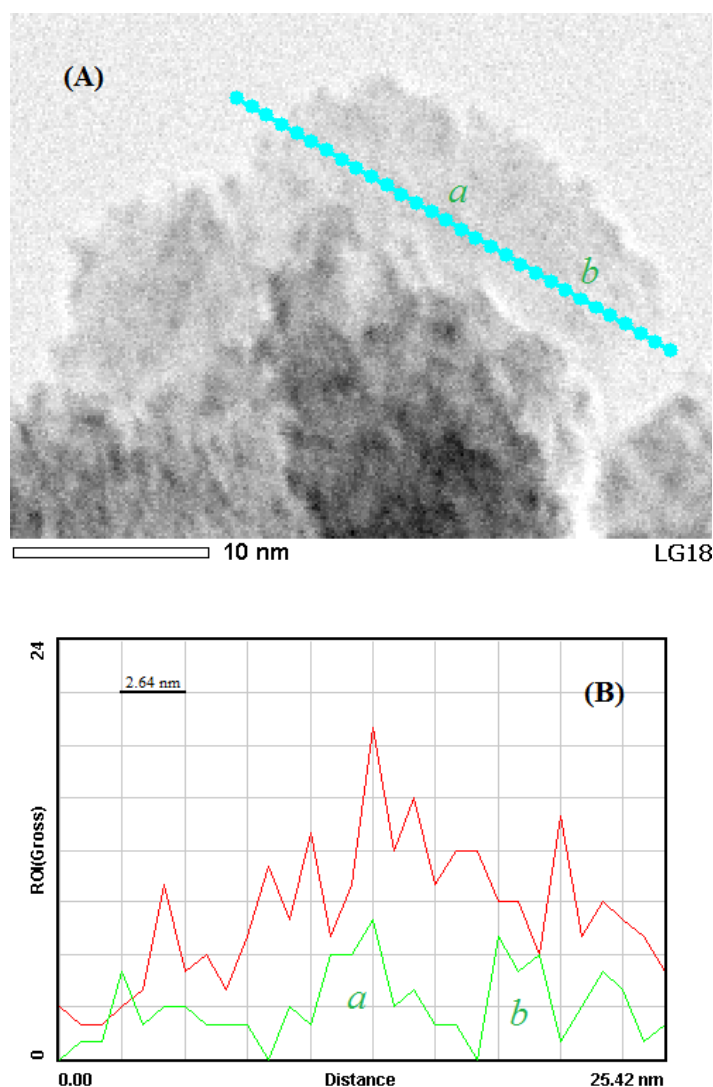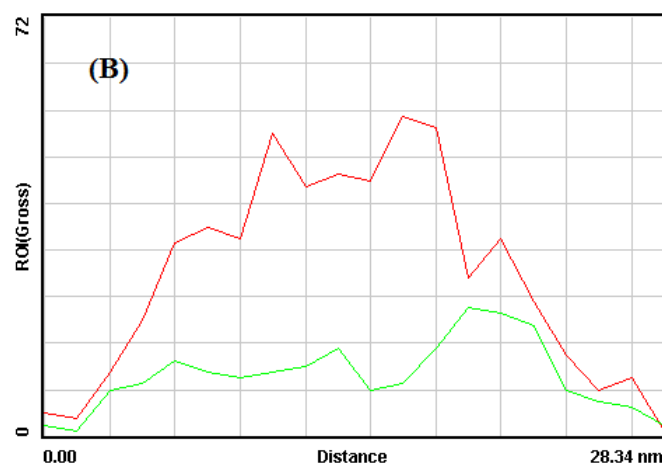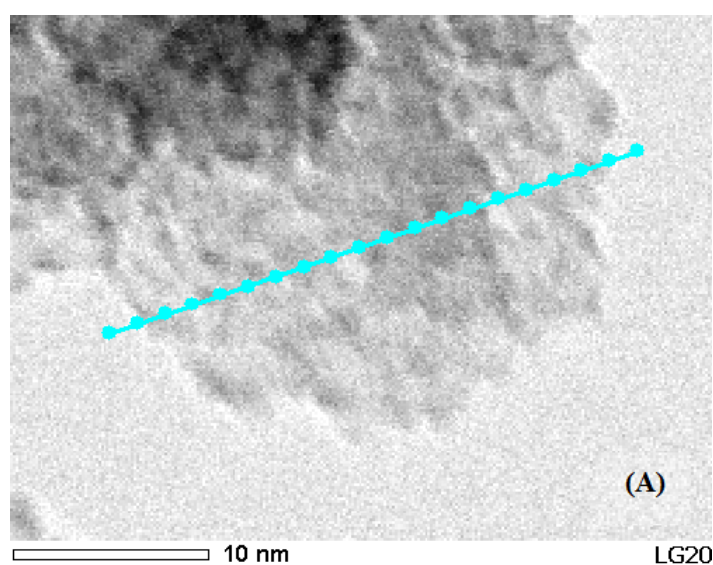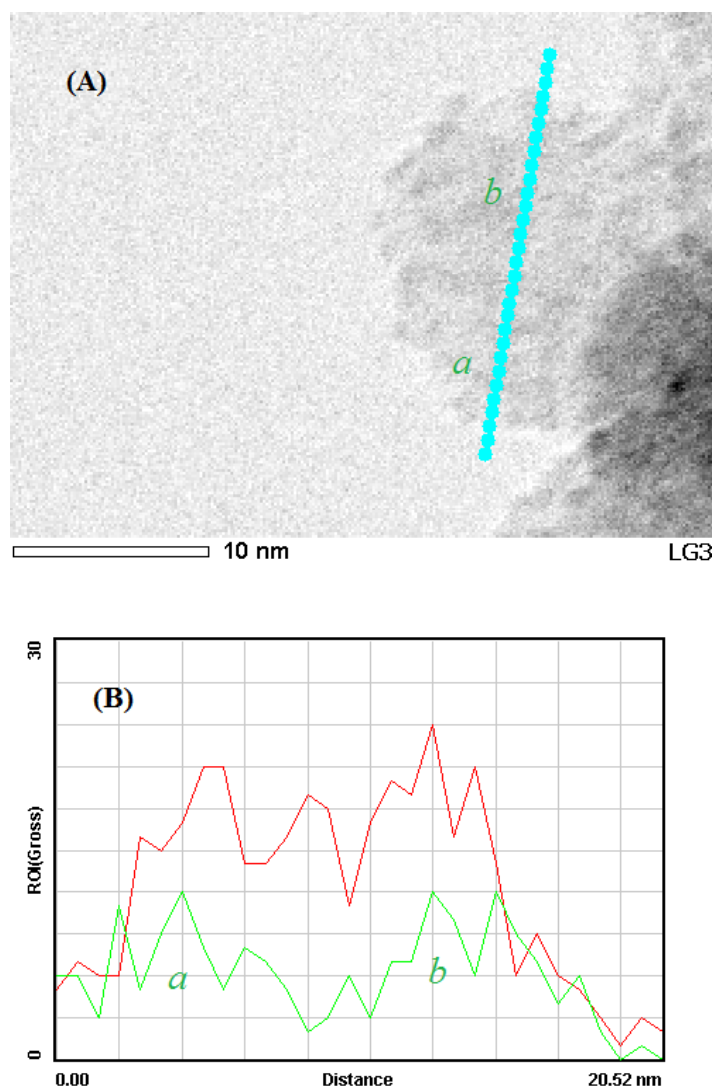

Figure 11. (A) STEM image and (B) the results of EDS analysis of 30 wt% Nb_2O_5/Al_2O_3 calcined at 1123 K. Green line : Nb, red line : Al.

Overall, these TEM, STEM and EDX results indicate that 1) niobium oxide monolayer domains are formed on alumina surface even at a Nb_2O_5 loading of 5wt%, 2) the coverage of alumina with niobium oxide increases as the Nb_2O_5 loading increases, 3) the surface of alumina is almost fully covered with niobium oxide monolayer domains at a Nb_2O_5 loading of 16 wt%, and 4) $AlNbO_4$ forms at Nb_2O_5 loading above 16 wt%.

Structure of Brønsted acid sites

To characterize the location and structure of Brønsted acid sites generated by loading of niobium oxide monolayer domains on an alumina surface, the change in the absorption bands of hydroxyl groups was investigated using the adsorption of pyridine. Figure 12(A) shows FT–IR spectra (OH region, 3650–3800 cm^{-1}) of γ-Al_2O_3 calcined at 1123 K before and after pyridine adsorption. After pretreatment at 673 K, two bands at 3726, and 3687 cm^{-1} appeared. The band at 3726 cm^{-1} was assigned to hydroxyl groups containing oxygen atoms coordinated to tetrahedral Al and octahedral Al, and the band at 3687 cm^{-1} was assigned to hydroxyl groups with oxygen atoms coordinated to three octahedral Al.[31,40] Figure 12(B) shows the difference spectra to clarify the change in the hydroxyl groups of Al_2O_3 upon adsorption of pyridine. When pyridine was adsorbed on Al_2O_3, the band at 3726 cm^{-1} decreased in intensity significantly; the intensity of this band was recovered upon evacuation at 373 K. In contrast, the intensity of the band at 3687 cm^{-1} increased upon evacuation at 423 K. These results indicate that isolated hydroxyl groups interacted with pyridine to form hydrogen–bonding hydroxyl groups. Figure 12(C) shows difference spectra (1430–1560 cm^{-1}) of pyridine adsorbed on Al_2O_3. A band at 1450 cm^{-1} assigned to pyridine adsorbed on Lewis acid sites appeared, whereas a band at around 1545 cm^{-1} from pyridinium ions adsorbed on Brønsted acid sites did not.[37,38] These results indicate that Al_2O_3 has no Brønsted acid sites, so the hydroxyl groups identified at 3726 cm^{-1} do not act as Brønsted acid sites.
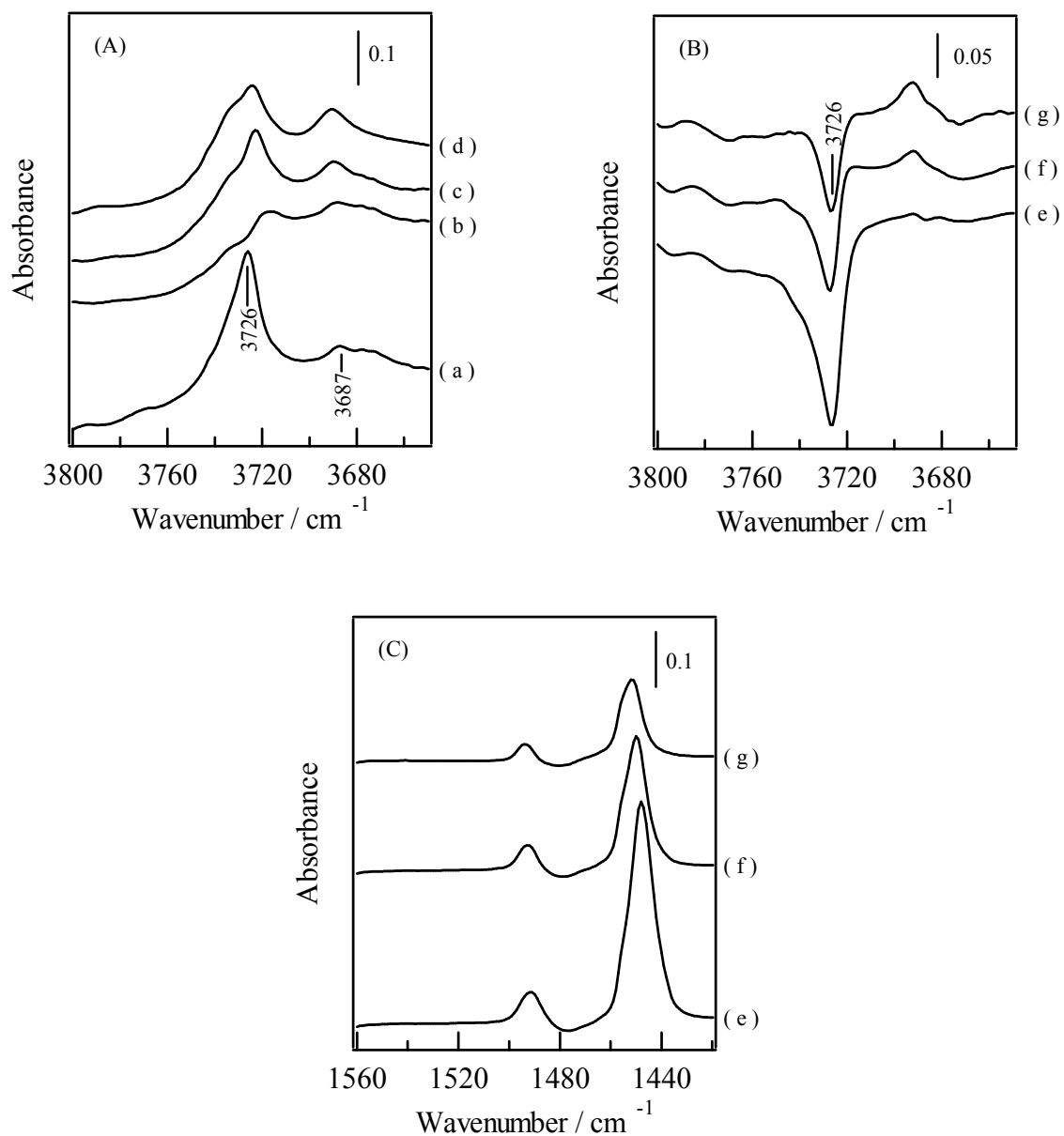
Figure 12. (A) FT-IR spectra of (a) γ-Al$_2$O$_3$, and γ-Al$_2$O$_3$ with adsorbed pyridine and subsequent evacuation at (b) 298 K, (c) 373 K, and (d) 423 K. (B), (C) Difference spectra of pyridine adsorbed on Al$_2$O$_3$; (e) : (b)-(a), (f) : (c)-(a), and (g) : (d)-(a).

The OH regions of FT–IR spectra of 16 wt% Nb_2O_5/Al_2O_3 calcined at 1123 K before and after adsorption of pyridine are shown in Figure 13(A). A sharp band appeared at 3743 cm^{-1} and a broad band was observed around 3713 cm^{-1}. Figure 13(B) shows difference spectra from 3650 to 3800 cm^{-1} of adsorbed pyridine on 16 wt% Nb_2O_5/Al_2O_3 calcined at 1123 K. After adsorption of pyridine, negative bands appeared at 3743 and 3713 cm^{-1}. After evacuation at 423 K, a partial reversal of the intensity of the bands at 3743 and 3713 cm^{-1} occurred. Figure 13(C) shows difference spectra from 1420 to 1560 cm^{-1} of IR spectra of pyridine adsorbed on 16 wt% Nb_2O_5/Al_2O_3 calcined at 1123 K. A band at 1545 cm^{-1} assigned to pyridinium ions adsorbed at Brønsted acid sites appeared, and the intensity of this band decreased as the evacuation temperature increased. These results indicate that the hydroxyl groups observed at 3713 and 3743 cm^{-1} on 16 wt% Nb_2O_5/Al_2O_3 calcined at 1123 K act as Brønsted acid sites.
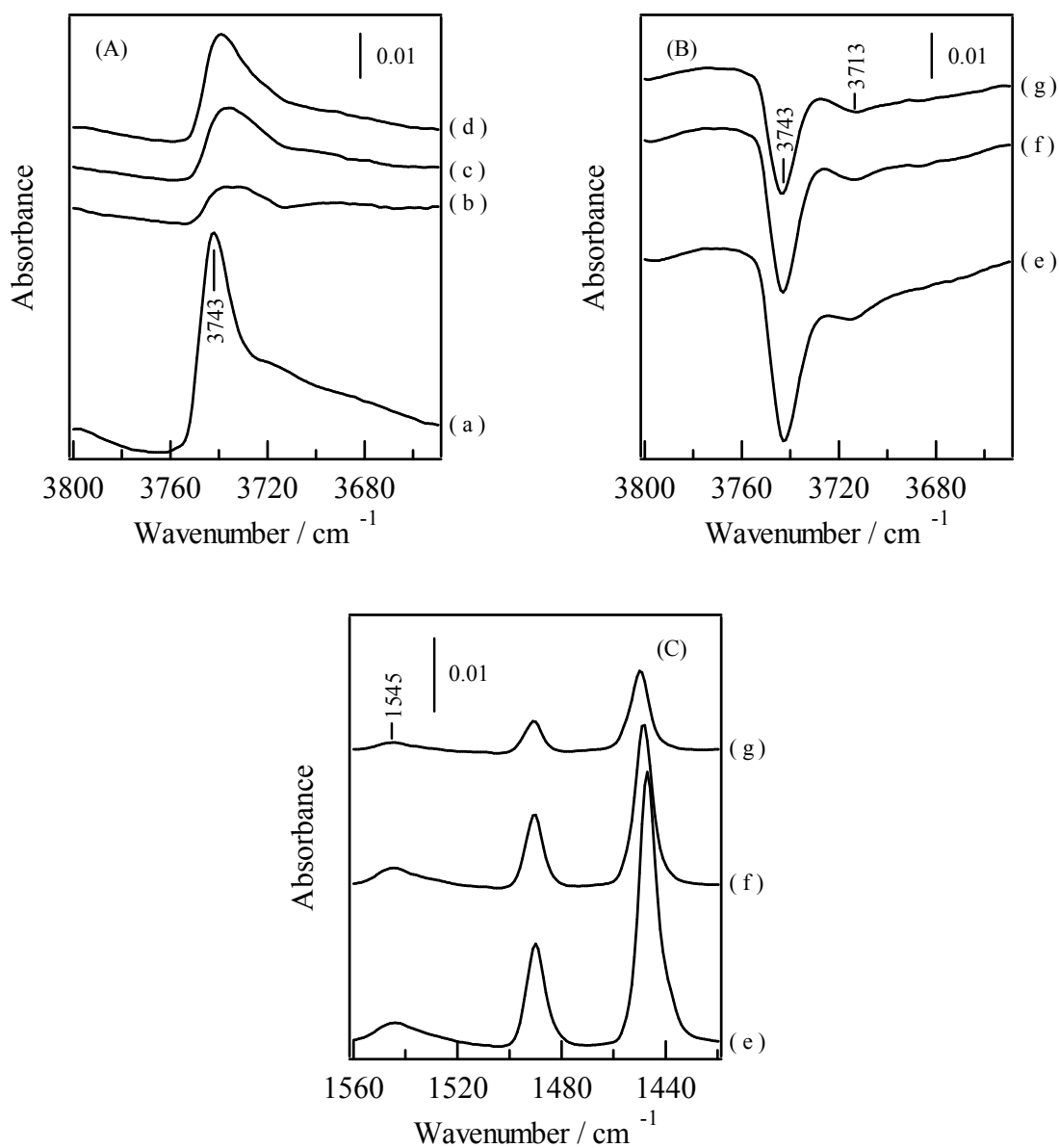
Figure 13. (A) FT-IR spectra of (a) 16 wt% Nb_2O_5/Al_2O_3 calcined at 1123 K, and 16 wt% Nb_2O_5/Al_2O_3 calcined at 1123 K with adsorbed pyridine and subsequent evacuation at (b) 298 K, (c) 373 K, and (d) 423 K. (B), (C) Difference spectra of pyridine adsorbed on 16 wt% Nb_2O_5/Al_2O_3 calcined at 1123 K (e): (b)-(a), (f): (c)-(a), and (g): (d)-(a).

Figure 14 shows IR spectra of hydroxyl groups on Nb_2O_5/Al_2O_3 calcined at 1123 K with various Nb_2O_5 loadings. As the Nb_2O_5 loading increased up to 16 wt%, the band at 3726 cm^{-1} decreased in intensity and new bands appeared at 3713 and 3743 cm^{-1}. These bands increased in intensity with Nb_2O_5 loading up to 16 wt%. Over 16 wt%, the band at 3743 cm^{-1} decreased in intensity until a loading of 30 wt%. Based on the results of XPS, XRD, XAFS, TEM, and STEM–EDX measurements, we concluded that niobium oxide monolayer domains are formed on Nb_2O_5/Al_2O_3 calcined at 1123 K with an Nb_2O_5 loading of up to 16 wt%. When the Nb_2O_5 loading exceeds 16 wt%, $AlNbO_4$, which has no hydroxyl groups and/or Brønsted acid sites, is formed. This results in a decrease of Brønsted acid sites. Figure 15 shows difference spectra of hydroxyl groups on Nb_2O_5/Al_2O_3 calcined at 1123 K with various loadings. Two negative bands at 3713 and 3743 cm^{-1} increased in intensity with Nb_2O_5 loading up to 16 wt%, and then decreased in intensity over 16 wt%. Because the intensity of the band at 3726 cm^{-1} decreased with increased Nb_2O_5 loading, in other words, as the coverage of niobium oxide monolayer domains increased, this band is attributed to hydroxyl groups on Al_2O_3. The bands at 3713 and 3743 cm^{-1} are assigned to hydroxyl groups, which act as Brønsted acid sites, on niobium oxide monolayer domains.
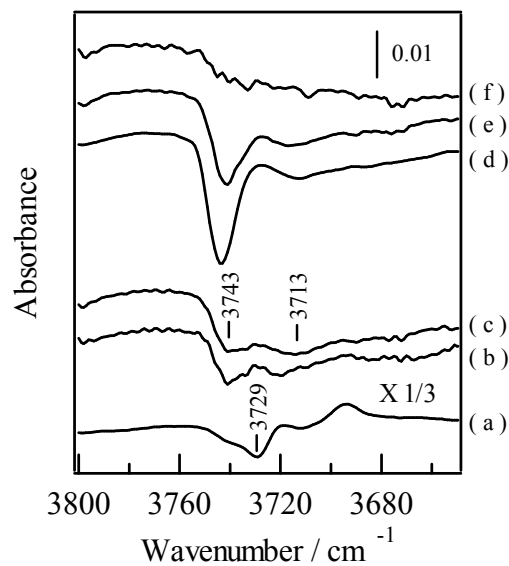
Figure 14. FT-IR spectra of Nb_2O_5/Al_2O_3 calcined at 1123 K with various Nb_2O_5 loadings. (a) γ-Al_2O_3, (b) 5 wt%, (c) 14 wt%, (d) 16 wt%, (e) 18 wt%, (f) 30 wt% Nb_2O_5 loading.
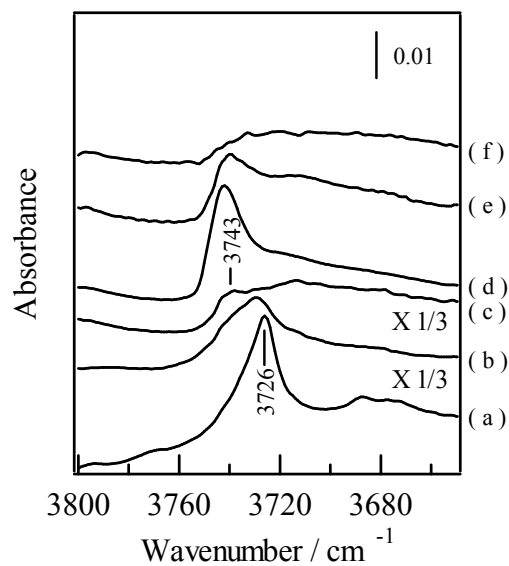
Figure 15. FT-IR spectra of Nb_2O_5/Al_2O_3 calcined at 1123 K with various Nb_2O_5 loadings after pyridine adsorption and subsequent evacuation at 423 K. (a) 5 wt%, (b) 11 wt%, (c) 14 wt%, (d) 16 wt%, (e) 18 wt%, and (f) 30 wt% Nb_2O_5.

Figure 16 shows FT–IR spectra of hydroxyl regions on 16 wt% Nb_2O_5/Al_2O_3 calcined at various temperatures. The band at 3732 cm^{-1} decreased upon calcination at higher temperatures exceeding 773 K. In contrast, a new band appeared at 3743 cm^{-1} that increased in intensity with increased calcination temperature until 1123 K, then the intensity of this band began to decrease. Figure 17 shows difference spectra of hydroxyl groups on 16 wt% Nb_2O_5/Al_2O_3 calcined at various temperatures. Two negative bands at 3714 and 3741 cm^{-1} increased in intensity with calcination temperature up to 1123 K; these bands disappeared above 1123 K because of the formation of $AlNbO_4$ crystals. These bands are attributed to the hydroxyl groups of niobium oxide monolayer domains. The intensity of the band at 3743 cm^{-1} increased significantly between 1073 and 1123 K (spectra (b) and (c), respectively), indicating that high temperature calcination such as 1123 K is required to generate Brønsted acid sites on Nb_2O_5/Al_2O_3. High–temperature calcination induces strong interactions between Nb_2O_5 with distorted NbO_6 units and alumina, and stabilizes the niobium oxide monolayer, resulting in generation of Brønsted acid sites on Nb_2O_5/Al_2O_3 containing a high loading of Nb_2O_5.
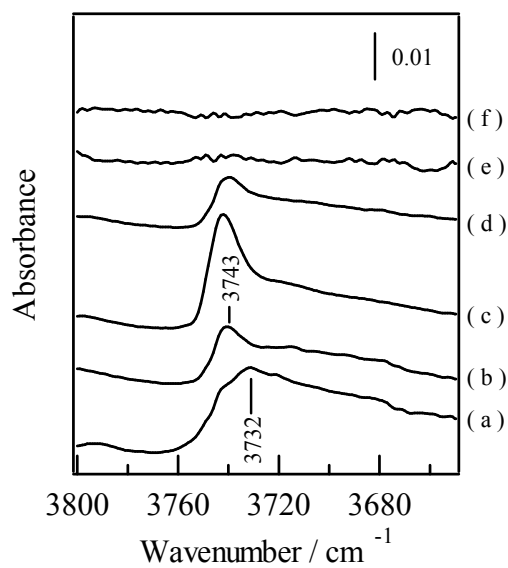
Figure 16. FT-IR spectra of 16 wt% Nb_2O_5/Al_2O_3 calcined at (a) 773 K, (b) 1073 K, (c) 1123 K, (d) 1173 K, (e) 1423 K, and (f) $AlNbO_4$.

Figure 17. FT-IR spectra of 16 wt% Nb_2O_5/Al_2O_3 calcined at (a) 773 K, (b) 1073 K, (c) 1123 K, (d) 1173 K, and (e) 1423 K after adsorption of pyridine and subsequent evacuation at 423 K.

The positions of the bands of hydroxyl groups did not change as the calcination temperatures and loading amount were varied. This suggests that the amount of Brønsted acid sites is affected by calcinat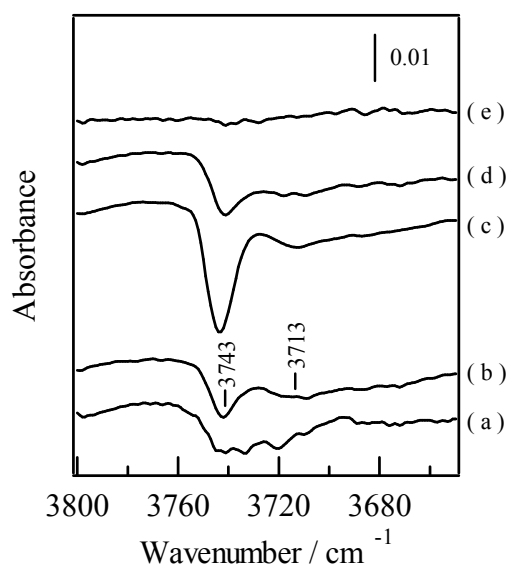ion temperature and loading, but the acid strength is almost constant. It seems that there is no difference of acid strength between the two bands, because the absorption bands due to both hydroxyl groups completely recovered when the catalyst was evacuated at 473 K.

Discussions

Recently, we reported that the catalytic activity depended on calcination temperature and niobium oxide loading.[31-33] In a series of Nb_2O_5/Al_2O_3 catalysts, 16wt% Nb_2O_5/Al_2O_3 calcined at 1123 K exhibited the highest activity. Nb_2O_5/Al_2O_3 exhibited catalytic activities for benzylation of anisole, cumene cracking, and isomerization of α-pinene that were proportional to the Brønsted acidity, indicating that these reactions were promoted on the Brønsted acid sites on the Nb_2O_5/Al_2O_3 catalysts. In the case of 5 wt% Nb_2O_5/Al_2O_3, no Brønsted acid sites were generated and niobium oxide monolayer domains were highly dispersed. This strongly suggests that the bridging hydroxyl groups located at the edges of niobium oxide monolayer domains (Nb–(OH)–Al) are not Brønsted acid sites on Nb_2O_5/Al_2O_3.

For Nb_2O_5 loadings from 14 to 16 wt%, a sharp increase in the amount of hydroxyl groups, which act as Brønsted acid sites, was observed as the loading increased. In this region, the coverage of alumina with niobium oxide monolayer domains increased until almost the entire surface of alumina was covered for 16 wt% Nb_2O_5/Al_2O_3. Above 18 wt%, the amount of Brønsted acid sites decreased and part of the Nb_2O_5 monolayer domains were converted into $AlNbO_4$ crystals. High temperature calcination such as at 1123 K appears essential to generate Brønsted acid sites on Nb_2O_5/Al_2O_3. Based on these results, we propose that a niobium oxide monolayer with two-dimensional structure is important to the generation of Brønsted acid sites. It seems that isolated or bridging hydroxyl groups on a niobium oxide monolayer (Nb–OH or Nb–(OH)–Nb) are candidates for the structures and locations of Brønsted acid sites. However, this model is not consistent with the fact that the ratio of the amount of Brønsted acid sites to loaded Nb_2O_5 is about 0.02 on 16 wt% Nb_2O_5/Al_2O_3 calcined at 1123 K. Therefore, we concluded that bridging hydroxyl

groups on a niobium oxide monolayer (Nb–OH or Nb–(OH)–Nb) located at the boundaries of niobium oxide islands act as Brønsted acid sites. The surface area of alumina is reduced by calcination at high temperatures. As a result, the distance between domains of niobium oxide monolayer decreases and then boundaries form to generate bridging hydroxyl groups that act as Brønsted acid sites.

The nature of hydroxyl groups on niobium oxide monolayer domains has been widely investigated. Various metal oxides, such as TiO_2, SiO_2, ZrO_2, and Al_2O_3, possess several kinds of hydroxyl groups. TiO_2 has two types of isolated hydroxyl groups with FT-IR bands at 3700 and 3670 cm^{-1} that are assigned to bridging and terminal hydroxyl groups, respectively.[41-44] In the case of ZrO_2, there are two kinds of isolated hydroxyl groups with signals at 3780 and 3680 cm^{-1} that are attributed to terminal and bridging hydroxyl groups, respectively.[45,46] On SiO_2, there are two types of hydroxyl groups with peaks at 3750 and 3740 cm^{-1}, which are assigned to isolated and vicinal pairs of hydroxyl groups, respectively.[47-49] In contrast, Al_2O_3 has five kinds of isolated hydroxyl groups with bands at 3800, 3775, 3745, 3730, and 3700 cm^{-1} that are assigned to terminal hydroxyl groups coordinated to a single octahedral Al cation, terminal hydroxyl groups coordinated to a single tetrahedral Al cation, bridging hydroxyl groups that link two octahedral Al cations, bridging hydroxyl groups that link one octahedral Al cation and one tetrahedral Al cation, and bridging hydroxyl groups that link three octahedral Al cations, respectively.[31,40] The structure of the hydroxyl groups on Nb_2O_5/Al_2O_3 with FT-IR signals at 3743 and 3713 cm^{-1} are bridging hydroxyl groups. Because the position of the peak from bridging hydroxyl groups that link two octahedral Al cations is higher than that linking one octahedral Al cation and one tetrahedral Al cation on Al_2O_3, the structures of the hydroxyl groups with signals at 3743 and 3713 cm^{-1} are bridging hydroxyl groups that link two octahedral Nb cations (Nb_o), and those that link one octahedral Nb cation and one tetrahedral Nb cation (Nb_t), respectively (Figure 18). At low Nb_2O_5 loading (5 wt%), domains of niobium oxide monolayer are dispersed on alumina and there are no boundaries between each domain. As the loading is increased, the number of domains increases and boundaries form between domains. At that time, bridging hydroxyl groups working as Brønsted acid sites are formed at the boundaries between domains. At 16 wt%, the domains just cover most of the alumina surface, so the Brønsted acidity is the largest because of the formation of boundaries between domains. Above 16

wt%, Nb_2O_5 domains change to inert $AlNbO_4$ and the Brønsted acidity decreases because the boundaries between niobium oxide domains disappear.
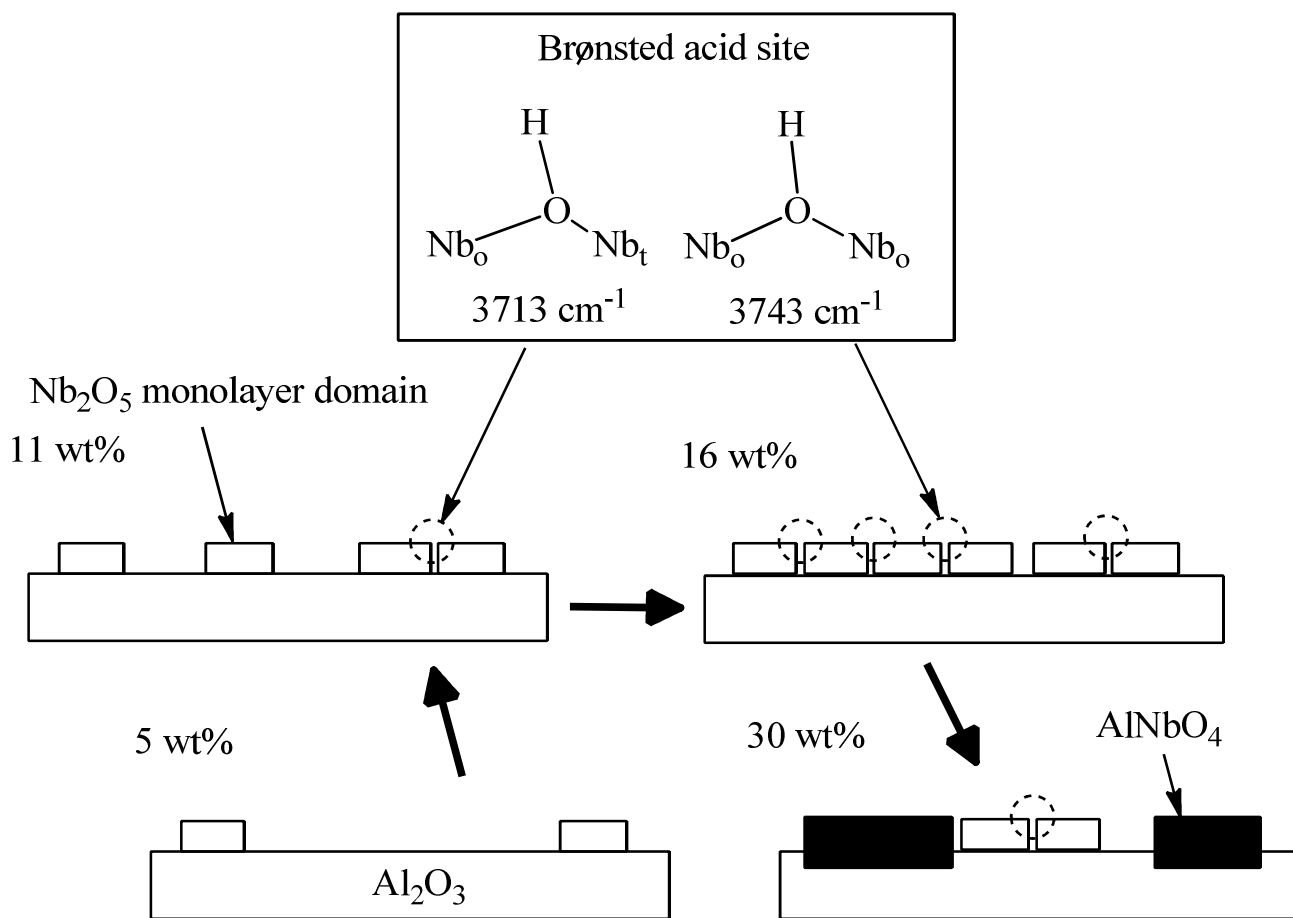

Figure 18. Structural models of the Brønsted acid sites on Nb_2O_5/Al_2O_3.

Conclusions

We prepared Nb_2O_5/Al_2O_3 samples with various loadings of Nb_2O_5 that were calcined at different temperatures and characterized the niobium oxide monolayer supported on alumina to clarify the structure of Brønsted acid sites generated on the catalyst. The results of FT-IR, TEM, STEM, and EDX measurements revealed that a niobium oxide monolayer is present as domains and Brønsted acid sites are generated at the boundary between these domains. At low Nb_2O_5 loading, domains of niobium oxide monolayer are dispersed on the alumina surface and there are no boundaries between domains. As the loading is increased, the number of domains increases and boundaries form between domains. At that time, bridging hydroxyl groups (Nb–(OH)–Nb) acting as Brønsted acid sites are formed at the boundaries between domains. At 16 wt% Nb_2O_5, the domains cover most of the alumina surface and Brønsted acidity is maximized because of the formation of boundaries between domains. Above 16 wt%, niobium oxide domains change to inert $AlNbO_4$ and Brønsted acidity decreases because of the disappearance of the boundaries between niobium oxide domains.

References

(1)   Iizuka, T.; Ogasawara, K.; Tanabe, K. *Bull. Chem. Soc. Jpn.,* **1983**, *56*, 2927.

(2)   Tanabe, K. *Mater. Chem. Phys.,* **1987**, *17*, 217.

(3)   Tanabe, K. *Catal. Today,* **1990**, *8*, 1.

(4)   Tanabe, K.; Okazaki, S. *Appl., Catal., A,* **1995**, *133*, 191.

(5)   Tanabe, K. *Catal. Today,* **2003**, *78*, 65.

(6)   Okuhara, T. *Chem. Rev.,* **2002**, *102*, 3641.

(7)   Nowak, I.; Ziolek, M. *Chem. Rev.,* **1999**, *99*, 3603.

(8)   Nakajima, K.; Baba, Y.; Noma, R.; Kitano, M.; Kondo, J. N.; Hayashi, S.; Hara, M. *J. Am. Chem. Soc.,* **2011**, *133*, 4224.

(9)   Ohuchi, T.; Miyatake, T.; Hitomi, Y.; Tanaka, T. *Catal. Today,* **2007**, *120*, 233.

(10)   Ushikubo, T.; Wada, K. *Appl. Catal.,* **1990**, *67*, 25.

(11)   Burcham, L. J.; Datka, J.; Wachs, I. E. *J. Phys. Chem. B,* **1999**, *103*, 6015.

(12) Datka, J.; Turek, A. M.; Jehng, J. M.; Wachs, I. E. *J. Catal.,* **1992**, *135*, 186.

(13) Pittman, R. M.; Bell, A. T. *J. Phys. Chem.,* **1993**, *97*, 12178.

(14) Onfroy, T.; Clet, G.; Bukallah, S. B.; Hercules, D. M.; Houalla, M. *Catal. Lett.,* **2003**, *89*, 15.

(15) Onfroy, T.; Manoilova, O. V.; Bukallah, S. B.; Hercules, D. M.; Clet, G.; Houalla, M. *Appl., Catal., A,* **2007**, *316*, 184.

(16) Ushikubo, T.; Koike, Y.; Wada, K.; Lei, X.; Wang, D. Z.; Guo, X. X. *Catal. Today,* **1996**, *28*, 59.

(17) Asakura, K.; Iwasawa, Y. *Chem. Lett.,* **1986**, 859.

(18) Asakura, K.; Iwasawa, Y. *J. Phys. Chem.,* **1991**, *95*, 1711.

(19) Tanaka, T.; Yoshida, T.; Yoshida, H.; Aritani, H.; Funabiki, T.; Yoshida, S.; Jehng, J. M.; Wachs, I. E. *Catal. Today,* **1996**, *28*, 71.

(20) Yoshida, H.; Tanaka, T.; Yoshida, T.; Funabiki, T.; Yoshida, S. *Catal. Today,* **1996**, *28*, 79.

(21) Shishido, T.; Kitano, T.; Teramura, K.; Tanaka, T. *Catal. Lett.,* **2009**, *129*, 383.

(22) Shishido, T.; Kitano, T.; Teramura, K.; Tanaka, T. *Top Catal.,* **2010**, *53*, 672.

(23) Kitano, T.; Shishido, T.; Teramura, K.; Tanaka, T. *J. Phys. Chem. C,* **2012**, *116*, 11615.

(24) Deoliveira, P. G. P.; Lefebvre, F.; Primet, M.; Eon, J. G.; Volta, J. C. *J. Catal.,* **1991**, *130*, 293.

(25) Gatehouse, B. M.; Wadsley, A. D. *Acta Crystallogr.,* **1964**, *17*, 1545.

(26) Jacobs, P. A.; Leeman, H. E.; Uytterho.Jb. *J. Catal.,* **1974**, *33*, 17.

(27) Parry, E. P. *J. Catal.,* **1963**, *2*, 371.

(28) Okumura, K.; Yamashita, K.; Hirano, M.; Niwa, M. *J. Catal.,* **2005**, *234*, 300.

(29) Okumura, K.; Nishigaki, K.; Niwa, M. *Microporous Mesoporous Mater.,* **2001**, *44*, 509.

(30) Digne, M.; Sautet, P.; Raybaud, P.; Euzen, P.; Toulhoat, H. *J. Catal.,* **2004**, *226*, 54.

(31) Morterra, C.; Magnacca, G. *Catal. Today,* **1996**, *27*, 497.

(32) Morterra, C.; Chiorino, A.; Ghiotti, G.; Garrone, E. *J. Chem. Soc., Faraday Trans 1,* **1979**, *75*, 271.

(33) Morterra, C.; Coluccia, S.; Chiorino, A.; Boccuzzi, F. *J. Catal.,* **1978**, *54*, 348.

(34) Morterra, C.; Emanuel, C.; Cerrato, G.; Magnacca, G. *J. Chem. Soc., Faraday Trans.,* **1992**,

88, 339.

(35)   Yamamoto, T.; Tanaka, T.; Matsuyama, T.; Funabiki, T.; Yoshida, S. *J. Phys. Chem. B,* **2001**, *105*, 1908.

(36)   Yamamoto, T.; Hatsui, T.; Matsuyama, T.; Tanaka, T.; Funabiki, T. *Chem. Mater.,* **2003**, *15*, 4830.

(37)   Emeis, C. A. *J. Catal.,* **1993**, *141*, 347.

(38)   Barzetti, T.; Selli, E.; Moscotti, D.; Forni, L. *J. Chem. Soc., Faraday Trans.,* **1996**, *92*, 1401.

(39)   Zhou, R. S.; Snyder, R. L. *Acta Crystallogr. B,* **1991**, *47*, 617.

(40)   Knozinger, H.; Ratnasamy, P. *Catal. Rev.-Sci. Eng.,* **1978**, *17*, 31.

(41)   Yates, D. J. *J. Phys. Chem.,* **1961**, *65*, 746.

(42)   Primet, M.; Pichat, P.; Mathieu, M. V. *J. Phys. Chem.,* **1971**, *75*, 1216.

(43)   Tanaka, K.; White, J. M. *J. Phys. Chem.,* **1982**, *86*, 4708.

(44)   Jackson, P.; Parfitt, G. D. *Trans. Faraday Soc.,* **1971**, *67*, 2469.

(45)   Agron, P. A.; Fuller, E. L.; Holmes, H. F. *J. Colloid Interf. Sci.,* **1975**, *52*, 553.

(46)   Yamaguchi, T.; Nakano, Y.; Tanabe, K. *Bull. Chem. Soc. Jpn.,* **1978**, *51*, 2482.

(47)   Morrow, B. A.; McFarlan, A. J. *Langmuir,* **1991**, *7*, 1695.

(48)   Morrow, B. A.; McFarlan, A. J. *J. Phys. Chem.,* **1992**, *96*, 1395.

(49)   Zecchina, A.; Bordiga, S.; Spoto, G.; Marchese, L.; Petrini, G.; Leofanti, G.; Padovan, M. *J. Phys. Chem.,* **1992**, *96*, 4991.

Chapter 3

The Acid Property of Alumina-Supported Niobium Oxide Prepared by Impregnation Method Using Niobium Oxalate Solution: Effect of pH of Solution on the Structure and Acid Property

Abstract

5 and 16 wt% Nb_2O_5/Al_2O_3 catalysts were prepared by impregnation method using niobium oxalate solution with various pH values. The acid property of 16 wt% Nb_2O_5/Al_2O_3 was examined by benzylation of anisole and pyridine adsorbed Fourier transform infrared (FT-IR) spectra. The structure of niobium oxide monolayer domains on 5 and 16 wt% Nb_2O_5/Al_2O_3 were characterized using X-ray diffraction (XRD), Raman spectroscopy, and pyridine adsorbed FT-IR spectra. The acid property of 16 wt% Nb_2O_5/Al_2O_3 depended on the pH values in the preparation solution. As increase of pH value in the preparation solution, the size of niobium oxide monolayer domains increased whereas the number of domains decreased. The number of Brønsted acid sites was larger on Nb_2O_5/Al_2O_3 having large niobium oxide domains than that having small niobium oxide domains. These results suggest that Brønsted acid sites were generated on the boundaries between large niobium oxide monolayer domains, and imply that the strong distortion of Nb–(OH)–Nb bond is necessary to generate Brønsted acid property.

Introduction

In the previous report, we demonstrated that Brønsted acid sites were generated on Nb_2O_5/Al_2O_3 calcined at 1123 K. Ordinal solid acid catalysts lose the acid property when calcined above 1000 K. Acid property of niobic acid ($Nb_2O_5 \cdot nH_2O$), which is a unique solid acid catalyst exhibiting reaction activity for water-relating reactions[1-5] and strong acid property ($H_0 < -5.6$),[1,2,6] also disappears by calcination at higher temperatures than 773 K due to phase transformation.[7,8] In contrast, Nb_2O_5/Al_2O_3 calcined at 1123 K maintains Brønsted acid sites despite of high temperature calcination.[9-11] From the results of optimization of preparation condition, 16 wt% Nb_2O_5/Al_2O_3 calcined at 1123 K exhibited the highest activity and Brønsted acidity. Moreover, the Brønsted acid sites generated on the catalyst were thermally stable because no decline of the activity for isomerization of α-pinene was observed even after pretreatment at 1173 K. The acid property of Nb_2O_5/Al_2O_3 depended on both calcination temperature and loading amount of Nb_2O_5 due to structural change of niobium oxide supported on alumina. Based on structural characterization of Nb_2O_5/Al_2O_3, we revealed that niobium oxide was loaded as two-dimensional monolayer domains on alumina, and the number of domains increased without change in the domain size as Nb_2O_5 loading amount increased.[12] Furthermore, we proposed that Brønsted acid sites were generated on the boundaries between the niobium oxide monolayer domains.

The size effect of supported metal particle on the reaction activity has been reported by many researchers.[13-17] Generally, gold is known as inert metal. However, Au nanoparticle supported on titania exhibited reaction activity for various reactions, such as selective oxidation and hydrogenation, and the reaction activity strongly depended on the particle size.[13-15] Tsukuda et al. also reported that Au clusters stabilized by poly(N-vinyl-2-pyrrolidone), which was smaller than 1.5 nm, exhibited high reaction activity for selective oxidation by aerobic oxygen. They also suggested that the activity strongly depends on the particle size.[16,17]

Reaction activity on supported metal oxide is also affected by aggregation state. Two-dimensional domains of molybdenum oxide supported on alumina promote oxidative dehydration of propane and polymeric molybdenum oxide on alumina is active for epoxidation of allyl alcohol, these reactions do not proceed on monomeric molybdenum oxide well.[18,19] In the case

of WO_3/ZrO_2, superacid sites are not generated on monomeric tungsten oxide but on polymeric tungsten oxide.[20-22] For the purpose of controlling aggregational state, preparation method has been well investigated. Controlling the pH value in the preparation solution is one of the most utilized methods to control the aggregational state. Tanaka et al.[23,24] reported that the selectivity of propene photo-oxidation on Nb_2O_5/SiO_2 change by verifying the pH value in the niobium oxalate solution due to change in the structure of niobium oxide. These facts imply that the size of metal oxide monolayer domains is one of the factors to control the Brønsted acid property.

In the present study, we prepared 5 and 16 wt% Nb_2O_5/Al_2O_3 prepared by impregnation method using niobium oxalate aqueous solution with various pH values, and investigated change in acidic property and structure of niobium oxide supported on alumina. To clarify the effect of pH value on the acid property and the structure of niobium oxide monolayer domains, the acid property of Nb_2O_5/Al_2O_3 was evaluated by benzylation of anisole and pyridine adsorbed FT-IR spectra. The structure of niobium monolayer domains on Nb_2O_5/Al_2O_3 was characterized using XRD, Raman spectroscopy, and pyridine adsorbed FT-IR spectra.

Experimental

Preparation

A series of 5 and 16 wt% Nb_2O_5/Al_2O_3 were prepared by impregnation of γ-alumina (JRC–ALO-8) with an aqueous solution of niobium oxalate (CBMM) of various pH values (pH 0.7–4.1) as below. 33 ml of aqueous solution of niobium oxalate was used as preparation solution. 0.177 g or 0.567 g of niobium oxalate was dispersed in the solution for 5 or 16 wt% Nb_2O_5/Al_2O_3, respectively. The pH value in the preparation solution was changed in the range from 0.7 to 4.1 by oxalic acid and aqueous ammonium solution. 0.95 g or 0.84 g of γ-alumina was mixed to the solution as support for 5 or 16 wt% Nb_2O_5/Al_2O_3, respectively and stirred for 2 h at 353 K. Then, the solution was dried up and kept at 353 K overnight. After drying, the precursor was calcined at 1123 K for 3 h in a dry air.

Reactions

Benzylation of anisole (Friedel-Crafts alkylation of anisole with benzylalcohol) was

employed as test reaction to examine the acid property of Nb_2O_5/Al_2O_3. Benzylation of anisole was examined in a liquid phase as follows : 0.2 g of the catalyst was pretreated in N_2 flow at 473 K for 1 h and then added to a mixture of benzyl alcohol (6.25 mmol) and anisole (92.5 mmol) in a 100 ml flask. The reaction was carried out at 413 K and products were determined by GLC (Shimadzu GC-14B with a flame ionization detector) and GC-MS (Shimadzu GC-MS QP-5050), using a CBP10 column.

Characterizations

X-ray diffraction (XRD) patterns were obtained using a MultiFlex DR powder X-ray diffractometer (Rigaku, Tokyo, Japan), using Cu Kα radiation (χ = 1.5405 Å).

Laser Raman spectra were obtained using a NRS-2000 Raman Spectrometer (JASCO, Tokyo, Japan), using 514.5-nm line of an argon laser. The spectral resolution was 4 cm^{-1}.

Characterization was performed for the obtained catalysts by FTIR. FTIR spectra were recorded with Perkin-Elmer SPETRUM ONE Fourier transform infrared spectrometer with the resolution of 4 cm^{-1}. Each sample (12.5 mg) was pressed into a self-supporting wafer (13 mm in a diameter). The catalysts were pretreated under 13.3 kPa of O_2 for 1 h at 673 K and then evacuated for 1 h at the same temperature. For determination of the amount of Brønsted and Lewis acid sites over samples, the wafer was exposed to 0.667 kPa of pyridine vaper at 298 K for 10 min followed by evacuation at 423 K for 10 min.

Results

Acidic properties

Figure 1 shows the activities for benzylation of anisole over 16 wt% Nb_2O_5/Al_2O_3 prepared with various pH values. The main products were *o*-benzyl anisole and *p*-benzyl anisole, and the minor was dibenzyl ether. No polymerized product appeared. Benzyl anisole is produced on Brønsted acid sites.[25-31] The yield of benzyl anisole strongly depended on pH value. Increase of pH value up to 1.7 resulted in raise of the yield of benzyl anisole and the yield decreased above pH 1.7. On the other hand, no change in the yield of dibenzyl ether was observed regardless of pH value. We showed that the yield of benzyl anisole correlate with Brønsted acidity.[11,32] These results indicate

that the pH value in niobium oxalate aqueous solution affects Brønsted acid property of Nb_2O_5/Al_2O_3, and Brønsted acidity becomes the maximum at pH 1.7.

Using pyridine adsorbed FT-IR spectra, the change in Brønsted acid property of Nb_2O_5/Al_2O_3 prepared at various pH values was evaluated. The amount of Brønsted acid sites was estimated from the specific amount of the adsorbed pyridinium ions on Brønsted acid sites over each Nb_2O_5/Al_2O_3. Figure 2 shows the change in Brønsted acidity of Nb_2O_5/Al_2O_3 against pH values. The amount of Brønsted acid sites was calculated using an integrated molar adsorption coefficient value of $\varepsilon = 1.67$ cm μmol^{-1} for the band area at 1545 cm^{-1} of protonated pyridine. Indeed, Brønsted acidity on Nb_2O_5/Al_2O_3 prepared at pH 1.7 was the largest.

Characterizations

Figure 3 and 4 show the XRD patterns and Raman spectra of 16 wt% Nb_2O_5/Al_2O_3 prepared by impregnation method using niobium oxalate aqueous solution with various pH values. When the pH value was below 1.7, the supported niobium oxide was amorphous. Formation of aluminum niobate ($AlNbO_4$) occurred on Nb_2O_5/Al_2O_3 when the pH value was above 1.7. $AlNbO_4$ was completely inert for benzylation of anisole and no acid sites were detected in the FT-IR spectra of adsorbed pyridine.[11] Considering change in acid property with pH value, the formation of $AlNbO_4$ accounts for the decrease of Brønsted acidity and the catalytic activity.
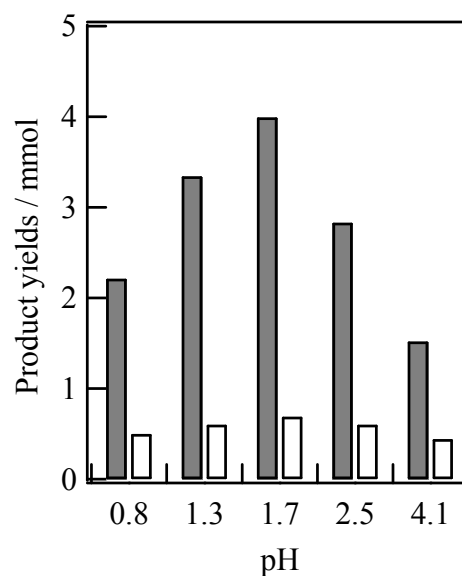
Figure 1. Activity of 16 wt% Nb_2O_5/Al_2O_3 calcined 1123 K prepared from the solution of various pH values. (■) Benzyl anisole and (□) dibenzyl ether.
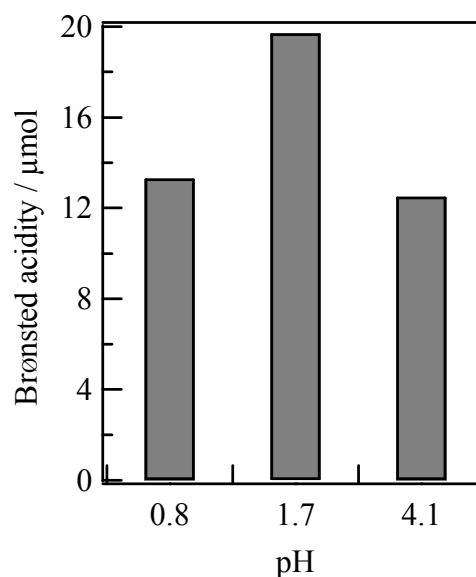
Figure 2. Brønsted acidity of 16 wt% Nb_2O_5/Al_2O_3 calcined 1123 K prepared from the solution of various pH values.
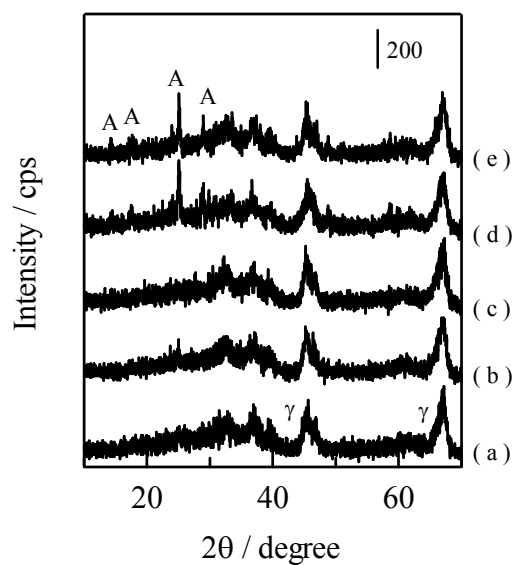
Figure 3. XRD patterns of 16 wt% Nb_2O_5/Al_2O_3 calcined at 1123 K prepared from the solution of pH (a) 0.8, (b) 1.3, (c) 1.7, (d) 2.5, and (e) 4.1.

γ = γ-Al_2O_3; A = $AlNbO_4$
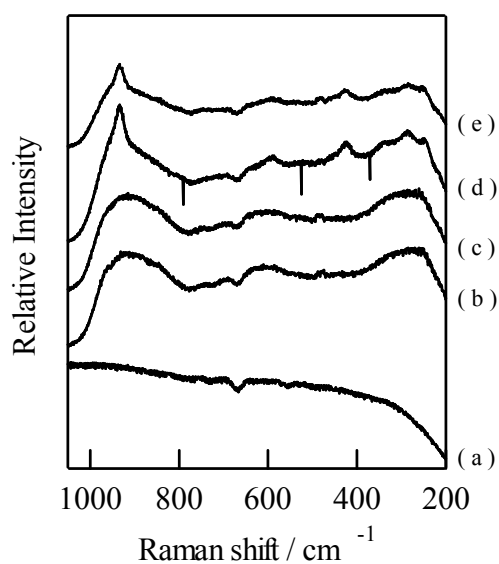
Figure 4. Raman spectra of 16 wt% Nb_2O_5/Al_2O_3 calcined at 1123 K prepared from the solution of pH (a) 0.8, (b) 1.3, (c) 1.7, (d) 2.5, and (e) 4.1.

To estimate the coverage of the niobium oxide monolayer on Al_2O_3, the amount of Lewis acid sites attributed to Al_2O_3 on Nb_2O_5/Al_2O_3 were evaluated based on FT-IR spectra of adsorbed pyridine. The FT-IR spectra of adsorbed pyridine after evacuation at 423 K are widely used as quantitative measurement of the amount of Lewis and Brønsted acid sites.[29,33-35] The 8a ring vibration mode of pyridine coordinated to Lewis acid sites appears at around 1600 cm^{-1}.[36-38] This band is quite sensitive to coordination environment and the position of the band reflects the local environment of Lewis acid sites. Morterra and co-workers[37-40] reported that γ-Al_2O_3 has three types of Lewis acid sites: vacancies on octahedral Al sites (Al^L_o), vacancies shared by tetrahedral Al and octahedral Al cations pair ($Al^L_{t,o}$), and vacancies on tetrahedral Al sites (Al^L_t) and proposed that bands at 1598, 1610-1620, and 1625 cm^{-1} correspond to pyridine coordinated to Al^L_o, $Al^L_{t,o}$, and Al^L_t, respectively. Yamamoto et al. reported that new Lewis acid sites were generated on lanthanide (Ln) oxides (Ln such as La, Ce, Eu, Tb, and Yb) supported on alumina by using pyridine adsorption FT-IR experiments.[41,42] They showed that new bands appeared at around 1610 cm^{-1} upon loading of Ln oxide, and assigned these new bands are to Lewis acid sites formed on Ln with Ln-O-Al linkages. We reported that an FT-IR spectrum of pyridine adsorbed on γ-Al_2O_3 calcined at 1123 K showed two bands at 1616 and 1623 cm^{-1} assigned to pyridine coordinated to $Al^L_{t,o}$ and Al^L_t, respectively.[12] On the other hand, An FT-IR spectrum of pyridine adsorbed on 16 wt% Nb_2O_5/Al_2O_3 calcined at 1123 K showed a new band at 1612 cm^{-1} assigned to pyridine coordinated to Lewis acid sites on niobium oxide (Nb^L). Using this method, we estimated surface coverage of two-dimensional niobium oxide monolayer on 16 wt% Nb_2O_5/Al_2O_3 prepared from the solution of various pH values. Figure 5 shows difference spectra (1590–1635 cm^{-1}) of pyridine adsorbed on 16 wt% Nb_2O_5/Al_2O_3 with various pH values as well as reference spectra (γ-Al_2O_3 and niobic acid ($Nb_2O_5 \cdot nH_2O$)). The spectrum of niobic acid showed a band at 1610 cm^{-1} and that of Al_2O_3 showed two bands at 1616 and 1623 cm^{-1}. These bands are assigned to pyridine coordinated to Nb^L, $Al^L_{t,o}$, and Al^L_t, respectively. Only one band at 1612 cm^{-1} was shown in the spectrum of 16 wt% Nb_2O_5/Al_2O_3 prepared at pH 0.8, and the other band at 1623 cm^{-1} appeared and increased with increase of pH value. These results indicate that pH value affected both Lewis acid property and surface coverage by niobium oxide monolayer domains. Figure 6 shows the change in the amounts of Al^L_t and Nb^L on 16 wt% Nb_2O_5/Al_2O_3 prepared at various pH values and the ratio of Lewis acid sites occupied by the monolayer of niobium oxide
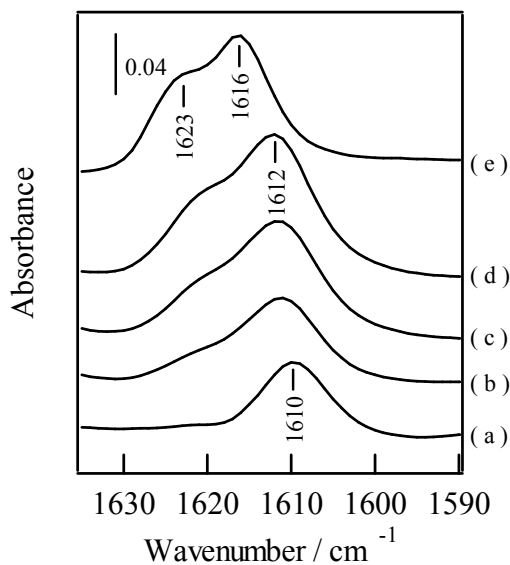
Figure 5. IR spectra of pyridine adsorbed on (a) niobic acid, 16 wt% Nb_2O_5/Al_2O_3 calcined at 1123 K prepared from the solution of pH (b) 0.8, (c) 1.7, (d) 4.1, and (e) γ-Al_2O_3. Evacuation temperature : 423 K.
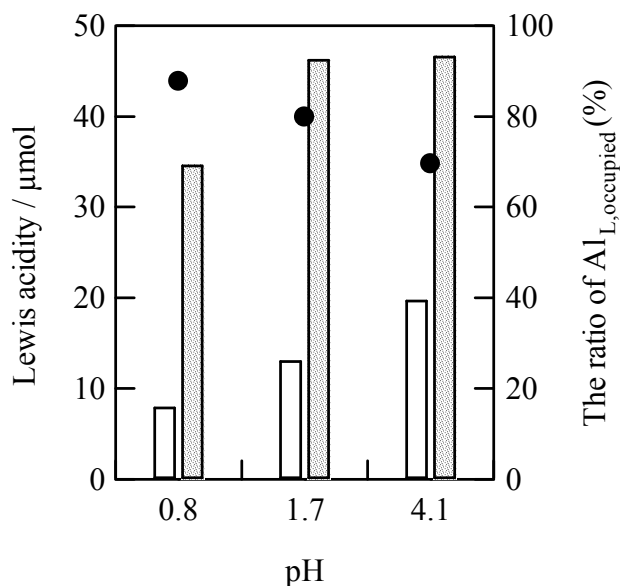
Figure 6. Amount of each Lewis acid site (($\square$) Al^L_t and (▦) Nb^L) and the ratio of $Al_{L,occupied}$ ($\bullet$) on 16 wt% Nb_2O_5/Al_2O_3 calcined at 1123 K prepared from the preparation solution of various pH value.

($Al_{L,occupied}$) to the total number of Lewis acid sites on Al_2O_3 support against pH values. Generally, the Lewis acid sites on alumina, $Al^L_{t,o}$ and Al^L_t, are uniformly dispersed on alumina surface. Therefore, the ratio of $Al_{L,occupied}$ reflects covering behavior of niobium oxide monolayer domains on an alumina surface. The amount of Al^L_t and Nb^L was determined using the method outlined below.

First, the total amount of Lewis acid sites was calculated using an integrated molar adsorption coefficient value of $\varepsilon = 2.22$ cm μmol^{-1} for the band area at 1450 cm^{-1} of coordinated pyridine.[43,44] Then, assuming that the adsorption coefficient values of each band at 1612, 1616, and 1623 cm^{-1} are as the same, the amounts of each Lewis acid site were determined based on the area of each band.[38] The ratio of Al$_{L,occupied}$ was calculated using Lewis acidity on alumina surface (77.3 μmol g^{-1}). Increase of pH value caused increase of Al$^L_{t,o}$ and Nb^L and decrease of the ratio of Al$_{L,occupied}$. These results suggest that larger surface area was covered by niobium oxide monolayer domains on Nb$_2$O$_5$/Al$_2$O$_3$ prepared at pH 0.8 than that at 1.7. The formation of AlNbO$_4$ caused aggregation of Nb, resulting in increasing the area of exposed bare Al$_2$O$_3$ surface in the case of Nb$_2$O$_5$/Al$_2$O$_3$ prepared at pH 4.1. Considering pH value influence the structure of niobium oxalate in preparation solution, it is supposed that change in the structure of niobium oxide monolayer domains caused change in coverage of Al$_2$O$_3$ surface with niobium oxide monolayer domains.

To confirm the effect of pH value on the structure of niobium oxide monolayer domains, the surface coverage of Al$_2$O$_3$ with niobium oxide monolayer domains on 5 wt% Nb$_2$O$_5$/Al$_2$O$_3$ catalysts prepared at various pH values was estimated by FT-IR spectra of adsorbed pyridine. In the case of 5 wt% Nb$_2$O$_5$/Al$_2$O$_3$, niobium oxide monolayer domains are dispersed (coverage; ca. 27 %, vide infra). This is quite different from 16 wt% Nb$_2$O$_5$/Al$_2$O$_3$, on which niobium oxide monolayer domains cover almost of alumina surface. Therefore, in the case of 5 wt% Nb$_2$O$_5$/Al$_2$O$_3$, the effect of interaction between domains is able to be ignored in considering the size of niobium oxide monolayer domains. Figure 7 shows difference IR spectra (1590–1635 cm^{-1}) of pyridine adsorbed on 5 wt% Nb$_2$O$_5$/Al$_2$O$_3$ prepared at various pH values. The band position shifted from 1616 cm^{-1} to 1619 cm^{-1} and the band area increased with increase of pH value. The result also indicates that pH value affects Lewis acid property and surface coverage with niobium oxide monolayer domains.

Figure 8 shows the change in the amounts of Al$^L_{t,o}$+Al^L_t and Nb^L on 5 wt% Nb$_2$O$_5$/Al$_2$O$_3$ against pH values. The ratio of Al$_{L,occupied}$ to the total number of Lewis acid sites on Al$_2$O$_3$ support against pH values is also demonstrated. The result shows increase of Lewis acidity on alumina and decrease of the ratio of Al$_{L,occupied}$ with increase of pH value. The amount of Nb^L did not change with the pH value. If niobium oxide monolayer domains are loaded on alumina randomly, the ratio of Al$_{L,occupied}$ will be smaller than 27%, which is the surface coverage of 5 wt% Nb$_2$O$_5$/Al$_2$O$_3$ estimated
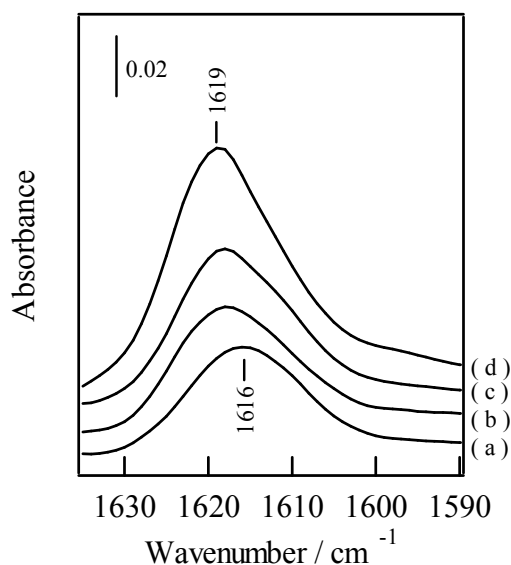
Figure 7. IR spectra of pyridine adsorbed on 5 wt% Nb_2O_5/Al_2O_3 calcined at 1123 K prepared from the solution of pH (a) 0.7, (b) 1.0, (c) 1.3, and (d) 1.7. Evacuation temperature : 423 K
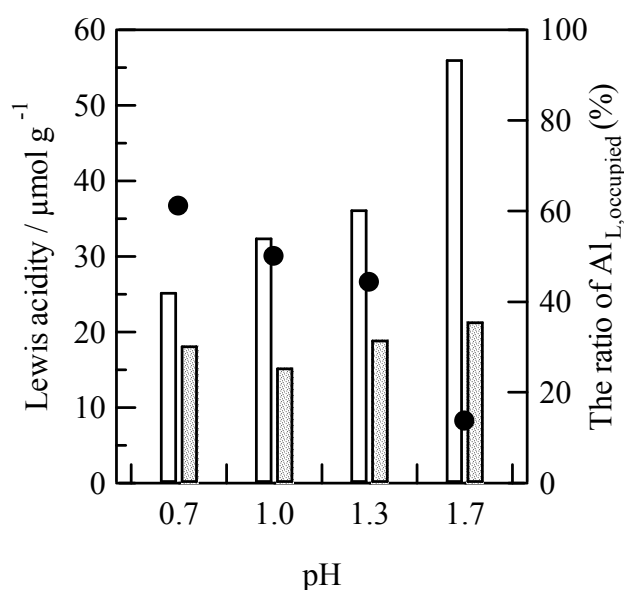
Figure 8. Amount of each Lewis acid site (($\square$) $Al^L_{t,o}+Al^L_t$ and (▦) Nb^L) and the ratio of $Al_{L,occupied}$ (●) on 16 wt% Nb_2O_5/Al_2O_3 calcined at 1123 K prepared from the preparation solution of various pH value.

from the cross-sectional area of the NbO_6 octahedral unit. However, the ratio of $Al_{L,occupied}$ was larger than 27% on 5 wt% Nb_2O_5/Al_2O_3 prepared at pH of 0.7, 1.0, and 1.3, indicating that niobium oxide monolayer domains were loaded on Lewis acid sites on Al_2O_3 surface, preferentially. Moreover, the decrease of the ratio of $Al_{L,occupied}$ clearly indicates increase of the size of niobium oxide monolayer domains but decrease of the number of niobium oxide monolayer domains.

Discussions

We demonstrated that Nb_2O_5/Al_2O_3 calcined at high temperatures exhibited catalytic activity and generated thermally stable Brønsted acid sites.[9-12] We revealed that niobium oxide is supported as two-dimensional monolayer domains on alumina and the niobium oxide monolayer domains increase with increase of loading amount of Nb_2O_5 until the domains cover almost of alumina surface. We concluded that a bridging hydroxyl groups (Nb–(OH)–Nb) acting as Brønsted acid sites are formed on the boundaries between niobium oxide monolayer domains.

It is expected that Brønsted acidity would increase if the domain size becomes smaller and the number of domains becomes larger because Brønsted acid sites are generated on the boundaries between niobium oxide monolayer domains. Tanaka and co-workers[23,24] reported that the structure of niobium oxide supported on silica can be controlled by pH of the preparation solution. Niobium oxalates in aqueous solution prepared at pH 0.8 exist as monomer species $[NbO(C_2O_4)_2H_2O]^-$ and at pH 5 exist as dimer species $[Nb_2O_4(C_2O_4)_2(H_2O)_2]^{2-}$. The structural change of niobium oxalate in the preparation solution with various pH values caused the adsorbed state of niobium species on silica surface before calcination and the dispersion of niobium species after calcination. Only dispersed monomeric tetrahedron of niobium oxide is obtained on Nb_2O_5/SiO_2 prepared at pH 0.8, while small oligomer comprised of the tetrahedral species on silica is obtained on Nb_2O_5/SiO_2 prepared at pH 4. This report indicates that pH value has the potential to control the size of niobium oxide monolayer domains on Nb_2O_5/Al_2O_3 and increase the domain size with raise of pH value. Actually, the results of pyridine adsorbed FT-IR spectra of 5 and 16 wt% Nb_2O_5/Al_2O_3 prepared at various pH values showed the change in the size of niobium oxide monolayer domains and increase of niobium oxide domain size as pH value increased up to 1.7. Therefore, the amount of domains and boundaries between domains on 16 wt% Nb_2O_5/Al_2O_3 prepared at pH 0.8 is larger than at pH 1.7. Because Brønsted acid sites are generated on the boundaries between domains, the Brønsted acidity on 16 wt% Nb_2O_5/Al_2O_3 prepared at pH 0.8 is expected to be higher than at pH 1.7. However, the activity and Brønsted acidity was larger on Nb_2O_5/Al_2O_3 prepared at pH 1.7 than at pH 0.8. The decrease of activity and Brønsted acidity with increase of the number of niobium oxide monolayer domains is supposed to be caused by the difference of strength of distortion.

There are some reports suggesting that distortion concerns with the generation of acid sites. Niwa et al. reported that the Brønsted acid sites on H-Y zeolite were generated on different sites (super cage, sodalite cage, and hexagonal cage) and exhibited different acid strength.[45] Each site has different Si–OH–Al angles and Al–O bond length and the acid property depended on Si–OH–Al angles and Al–O length. The effect of Si–OH–Al angles on acid property is stronger than Al–O length and kind of extra framework cation.[46,47] SiO_2 is known to be inactive material but FSM-16 and MCM-41, which are mesoporous silica with regular one-dimensional pore structure, exhibit acid property.[48-50] Yamamoto et al. expected that weakly perturbed isolated silanol groups acted as Brønsted acid sites and strained siloxane bridges acted as Lewis acid sites. On the other hand, no paper suggests that SBA-15, which is also one of mesoporous silica with regular one-dimensional pore structure and the pore size is a little larger than that of FSM-16 and MCM-41, has acid property.[48,50,51] It is supposed that the difference of pore size cause the difference of acid property, and in other words, the trigger of generation of acid sites is "distortion" due to smaller Si–O–Si angle. TiO_2 has only weak acid sites but TiO_2 nanotube shows high activity for Friedel-Crafts alkylation and dehydration. Kitano et al. also supposed that distortion of local structure caused generation of acid sites.[52] The distortion of local sites on Nb_2O_5/Al_2O_3 is also assumed to act an important role for generation of Brønsted acid sites. When the size of niobium oxide monolayer domains is small, the distortion of the boundaries between domains caused by shrink of alumina support due to calcination is weak. On the other hand, overlapping and wounding on the boundaries between niobium oxide monolayer domains is considered to occur when the size of domains is large. We concluded that the generation of Brønsted acid sites demands such strong distortion on the boundaries between niobium oxide monolayer domains and the strong distortion needs the boundaries between certain sized niobium oxide monolayer domains.(Figure 9)
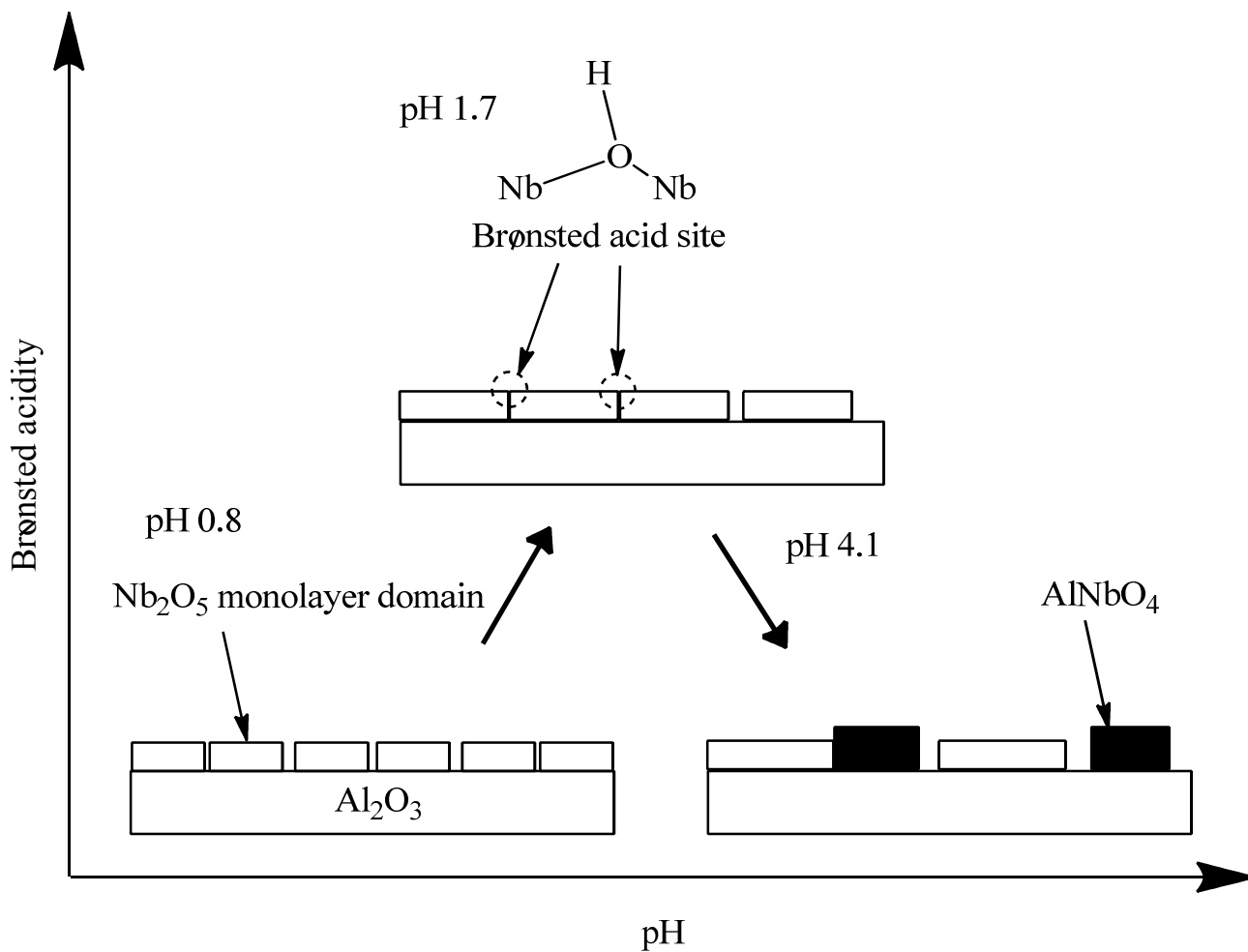
Figure 9. Structural model for generation of Brønsted acid sites on 16 wt% Nb_2O_5/Al_2O_3

Conclusions

The pH of niobium oxalate aqueous solution largely affected the catalytic activity and Brønsted acid property of 16 wt% Nb_2O_5/Al_2O_3 calcined at 1123 K. Increase of pH value up to 1.7 caused raise of the catalytic activity and Brønsted acidity, and above pH of 1.7, decreased due to the formation of inert $AlNbO_4$. As increase of pH value up to 1.7, the size of niobium oxide monolayer domains increased and the amount of domains decreased. Smaller the size of niobium oxide monolayer domains is, weaker distortion between niobium oxide monolayer domains is. Brønsted acidity is larger on large niobium oxide domains supported on alumina than on small niobium oxide domains. These results suggest that Brønsted acid sites were generated on the boundaries between large niobium oxide monolayer domains, and imply that the strong distortion of Nb–(OH)–Nb bond is necessary to generate Brønsted acid property.

References

(1)   Tanabe, K. *Mater. Chem. Phys.,* **1987**, *17*, 217.

(2)   Tanabe, K. *Catal. Today,* **1990**, *8*, 1.

(3)   Tanabe, K.; Okazaki, S. *Appl. Catal. A-Gen.,* **1995**, *133*, 191.

(4)   Tanabe, K. *Catal. Today,* **2003**, *78*, 65.

(5)   Okuhara, T. *Chem. Rev.,* **2002**, *102*, 3641.

(6)   Iizuka, T.; Ogasawara, K.; Tanabe, K. *Bull.Chem. Soc. Jpn.,* **1983**, *56*, 2927.

(7)   Ohuchi, T.; Miyatake, T.; Hitomi, Y.; Tanaka, T. *Catal. Today,* **2007**, *120*, 233.

(8)   Ushikubo, T.; Wada, K. *Appl. Catal.,* **1990**, *67*, 25.

(9)   Shishido, T.; Kitano, T.; Teramura, K.; Tanaka, T. *Catal. Lett.,* **2009**, *129*, 383.

(10)   Shishido, T.; Kitano, T.; Teramura, K.; Tanaka, T. *Top. Catal.,* **2010**, *53*, 672.

(11)   Kitano, T.; Shishido, T.; Teramura, K.; Tanaka, T. *J. Phys. Chem. C,* **2012**, *116*, 11615.

(12)   Kitano, T.; Shishido, T.; Teramura, K.; Tanaka, T. *to be submitted.*

(13)   Haruta, M.; Date, M. *Appl. Catal. A-Gen.,* **2001**, *222*, 427.

(14)   Hayashi, T.; Tanaka, K.; Haruta, M. *J. Catal.,* **1998**, *178*, 566.

(15)   Valden, M.; Lai, X.; Goodman, D. W. *Science,* **1998**, *281*, 1647.

(16)   Tsunoyama, H.; Ichikuni, N.; Tsukuda, T. *Langmuir,* **2008**, *24*, 11327.

(17)   Tsunoyama, H.; Ichikuni, N.; Sakurai, H.; Tsukuda, T. *J. Am. Chem. Soc.,* **2009**, *131*, 7086.

(18)   Imamura, S.; Sasaki, H.; Shono, M.; Kanai, H. *J. Catal.,* **1998**, *177*, 72.

(19)   Chen, K.; Xie, S.; Bell, A. T.; Iglesia, E. *J. Catal.,* **2001**, *198*, 232.

(20)   Barton, D. G.; Soled, S. L.; Meitzner, G. D.; Fuentes, G. A.; Iglesia, E. *J. Catal.,* **1999**, *181*, 57.

(21)   Ross-Medgaarden, E. I.; Knowles, W. V.; Kim, T.; Wong, M. S.; Zhou, W.; Kiely, C. J.; Wachs, I. E. *J. Catal.,* **2008**, *256*, 108.

(22)   Scheithauer, M.; Grasselli, R. K.; Knozinger, H. *Langmuir,* **1998**, *14*, 3019.

(23)   Tanaka, T.; Nojima, H.; Yoshida, H.; Nakagawa, H.; Funabiki, T.; Yoshida, S. *Catal. Today,* **1993**, *16*, 297.

(24)   Yoshida, H.; Tanaka, T.; Yoshida, T.; Funabiki, T.; Yoshida, S. *Catal. Today,* **1996**, *28*, 79.

(25)   de la Cruz, M. H. C.; Abdel-Rehim, M. A.; Rocha, A. S.; da Silva, J. F. C.; Faro, A. D.; Lachter, E. R. *Catal. Commun.,* **2007**, *8*, 1650.

(26)   de la Cruz, M. H. C.; da Silva, J. F. C.; Lachter, E. R. *Catal. Today,* **2006**, *118*, 379.

(27)   Yamashita, K.; Hirano, M.; Okumura, K.; Niwa, M. *Catal. Today,* **2006**, *118*, 385.

(28)   Okumura, K.; Yamashita, K.; Hirano, M.; Niwa, M. *Chem. Lett.,* **2005**, *34*, 716.

(29)   Okumura, K.; Yamashita, K.; Hirano, M.; Niwa, M. *J. Catal.,* **2005**, *234*, 300.

(30)   Cseri, T.; Bekassy, S.; Figueras, F.; Cseke, E.; Demenorval, L. C.; Dutartre, R. *Appl. Catal. A-Gen.,* **1995**, *132*, 141.

(31)   Tagusagawa, C.; Takagaki, A.; Hayashi, S.; Domen, K. *J. Am. Chem. Soc.,* **2008**, *130*, 7230.

(32)   Kitano, T.; Okazaki, S.; Shishido, T.; Teramura, K.; Tanaka, T. *Catal. Today,* **2012**, *192*, 189.

(33)   Jacobs, P. A.; Leeman, H. E.; Uytterho.Jb. *J. Catal.,* **1974**, *33*, 17.

(34)   Parry, E. P. *J. Catal.,* **1963**, *2*, 371.

(35)   Okumura, K.; Nishigaki, K.; Niwa, M. *Microporous Mesoporous Mater.,* **2001**, *44*, 509.

(36)   Digne, M.; Sautet, P.; Raybaud, P.; Euzen, P.; Toulhoat, H. *J. Catal.,* **2004**, *226*, 54.

(37)   Morterra, C.; Magnacca, G. *Catal. Today,* **1996**, *27*, 497.

(38)   Morterra, C.; Chiorino, A.; Ghiotti, G.; Garrone, E. *J. Chem. Soc. Faraday Trans 1,* **1979**, *75*, 271.

(39)   Morterra, C.; Coluccia, S.; Chiorino, A.; Boccuzzi, F. *J. Catal.,* **1978**, *54*, 348.

(40)   Morterra, C.; Emanuel, C.; Cerrato, G.; Magnacca, G. *J. Chem. Soc. Faraday Trans,* **1992**, *88*, 339.

(41)   Yamamoto, T.; Tanaka, T.; Matsuyama, T.; Funabiki, T.; Yoshida, S. *J. Phys. Chem. B,* **2001**, *105*, 1908.

(42)   Yamamoto, T.; Hatsui, T.; Matsuyama, T.; Tanaka, T.; Funabiki, T. *Chem. Mater.,* **2003**, *15*, 4830.

(43)   Emeis, C. A. *J. Catal.,* **1993**, *141*, 347.

(44)   Barzetti, T.; Selli, E.; Moscotti, D.; Forni, L. *J. Chem. Soc. Faraday Trans,* **1996**, *92*, 1401.

(45)   Suzuki, K.; Katada, N.; Niwa, M. *J. Phys. Chem. C,* **2007**, *111*, 894.

(46)   Katada, N.; Suzuki, K.; Noda, T.; Sastre, G.; Niwa, M. *J. Phys. Chem. C,* **2009**, *113*, 19208.

(47)   Sastre, G.; Fornes, V.; Corma, A. *J. Phys. Chem. B,* **2000**, *104*, 4349.

(48)   Yamamoto, T.; Tanaka, T.; Funabiki, T.; Yoshida, S. *J. Phys. Chem. B,* **1998**, *102*, 5830.

(49)   Iwamoto, M.; Tanaka, Y.; Sawamura, N.; Namba, S. *J. Am. Chem. Soc.,* **2003**, *125*, 13032.

(50)   Yamamoto, T.; Mori, S.; Shishido, T.; Kawai, J.; Tanaka, T. *Top. Catal.,* **2009**, *52*, 657.

(51)   Yamamoto, T.; Tanaka, T.; Inagaki, S.; Funabiki, T.; Yoshida, S. *J. Phys. Chem. B,* **1999**, *103*, 6450.

(52)   Kitano, M.; Nakajima, K.; Kondo, J. N.; Hayashi, S.; Hara, M. *J. Am. Chem. Soc.,* **2010**, *132*, 6622.

Chapter 4

Generation of Brønsted Acid Sites on Alumina-Supported Tantalum Oxide Calcined at High Temperature

Abstract

An alumina-supported tantalum oxide (Ta_2O_5/Al_2O_3) calcined at 1223 K promoted both Benzylation of anisole (Friedel-Crafts alkylation of anisole with benzylalcohol) and isomerization of α-pinene, and exhibited Brønsted acidity despite the high temperature calcination. Among the Ta_2O_5/Al_2O_3 catalysts tested, 33 wt% Ta_2O_5/Al_2O_3 calcined at 1223 K showed the highest activity. A monolayer of tantalum acid-like compound, which has distorted octahedral symmetry, was stabilized over 33 wt% Ta_2O_5/Al_2O_3 catalyst calcined at 1223 K. The two-dimensional Ta–O–Ta network of stabilized tantalum acid-like compound probably accounts for the generation of Brønsted acid.

Introduction

Tantalum acid ($Ta_2O_5 \cdot nH_2O$, hydrated tantalum oxide) shows mainly Lewis acid properties in the absence of water,[1,2] but Brønsted acid sites are generated by treatment with steam at 373 K. Compared to niobic acid ($Nb_2O_5 \cdot nH_2O$, hydrated niobium oxide), which is known as a water-tolerant solid acid catalyst that exhibits strong Brønsted acidity and is effective for reactions in aqueous media such as esterification, olefin hydration, and alcohol dehydration,[3-7] tantalum acid retains its strong acidity after calcination at higher temperatures. In the case of niobic acid, dehydration leads to lose of its acid property by heating above 773 K.[8] On the other hand, tantalum acid maintains its acidic property up to 1073 K. Generally, high temperature calcination usually causes solid acid catalysts to lose the acid property. Ordinary solid acid catalysts, such as aluminosilicate, zeolite and binary oxides, pretreated at >873 K lose their acid property,[9-11] except in some cases like SiO_2/Al_2O_3 prepared with CVD method,[12] highly siliceous zeolites and layered mixed oxide.[13-15] High stability is one of the important factors on useful solid acid catalyst, because the life of solid acid catalyst strongly depends on the stability. If a solid acid could be prepared by calcination at high temperatures required for the formation of ceramics (>1173 K), it would be a useful acidcatalyst even under strict conditions because of its high stability.

We have reported that a solid acid prepared with high loading of Nb_2O_5 on an Al_2O_3 support and calcined at 1173 K exhibited Brønsted acid property despite the high temperature calcination. This strongly suggests that the alumina support stabilizes the Brønsted acid sites during calcination at high temperature.[16,17] Amount of Brønsted acid site on Nb_2O_5/Al_2O_3 changed depending on both calcination temperature and loading amount of Nb_2O_5. This strongly suggests that the structural change around niobium is expected to have a major impact on Brønsted acid property. We have proposed that the stabilized niobic acid-like compound which has two-dimensional Nb–O–Nb network of probably account for the generation of Brønsted acid site. Very recently, we reported that alumina-supported tantalum oxide (Ta_2O_5/Al_2O_3) calcined at high temperature such as 1223 K with high loading of Ta_2O_5 exhibited Brønsted acid property,[18] suggesting that Ta_2O_5/Al_2O_3 would also act as a stable Brønsted acid catalyst. However, the relationship between the structural change around tantalum and generation of Brønsted acid site on Ta_2O_5/Al_2O_3 catalyst is still unclear. Here,

we have prepared a series of Ta_2O_5/Al_2O_3 solid acids and the relationship between the local structure of tantalum species in Ta_2O_5/Al_2O_3 solid acids and acid property is investigated.

Experimental

Preparation

A series of Ta_2O_5/Al_2O_3 solid acids were prepared by impregnation of α-alumina (JRC-ALO-8, 148 m^2 g^{-1}) with an ethanol solution of tantalum ethoxide ($Ta(OC_2H_5)_5$), followed by calcination at various temperatures for 3 h in dry air. Ta_2O_5 loading amount was changed from 10 wt% to 50 wt%, and calcination temperature was changed from 773 K to 1423 K. Aluminum tantalate, $AlTaO_4$, was synthesized from tantalum ethoxide and aluminum isopropoxide ($Al(OC_3H_7)_3$) according to an established procedure.[19] Hydrated tantalum oxide ($Ta_2O_5 \cdot nH_2O$) was prepared from tantalum ethoxide by calcination at 573 K according to the literature.[1,2] Crystalline T-phase Ta_2O_5 was prepared from $Ta_2O_5 \cdot nH_2O$ by calcination at 1223 K.

Reactions

Benzylation of anisole and isomerization of α-pinene were carried out as test reactions to investigate the acidic properties of Ta_2O_5/Al_2O_3. Benzylation of anisole was examined in the liquid phase. The catalyst (0.15 g) was pretreated at 473 K for 1 h in N_2 flow and added to a mixture of benzyl alcohol (6.25 mmol) and anisole (92.5 mmol) in a 100 mL flask. The mixture was allowed to react at 433 K. Isomerization of α-pinene was also examined in the liquid phase. The catalyst (0.10 g) was pretreated at 573 K under 13.3 kPa of O_2 for 1 h and evacuated at the same temperature for 1 h. Then the sample was added to α-pinene (12.5 mmol) in a 20 mL container. The reaction was carried out at 353 K. Products were analyzed by FID-GC (Shimadzu GC-14B, Kyoto, Japan) and GC-MS (Shimadzu QP-5050). Tridecane was used for the internal standard in the both of reactions. The carbon balance was above 90% in the both alkylation and isomerization.

Characterization

Specific surface area was evaluated by BET method at 77 K (liquid nitrogen temperature) with BEL Japan BELSORP28 28A. The surface area was determined from six points of data (adsorption amount vs relative pressures (P/P_0) ranging from 0.05 to 0.2) in the isotherm.

X-ray diffraction (XRD) was performed on an X-ray diffractometer (Rigaku MultiFlex DR Powder X-ray diffractometer) using Cu Kα radiation (χ = 1.5405Å). For the measurement of XRD patterns, the scanning rate and was 0.067 s^{-1} and the resolution was 0.02 deg.

Laser Raman spectra were taken with the 514.5 nm line of the argon laser (JASCO NRS-2000 Raman Spectrometer). The scan number, the acquisition time and the resolution were 16 scans, 70 s and resolution 3.8 cm^{-1}, respectively. The laser power was 100 mW.

Infrared spectra of adsorbed lutidine (2,6-dimethylpyridine) were recorded with Perkin-Elmer Spectrum One Fourier transform infrared spectrometer, and used to elucidate the generation of Brønsted acid sites over Ta_2O_5/Al_2O_3. The sample (13 mg) was pressed into a self-supporting disk (Ø 13 mm) and pretreated under 13.3 kPa of O_2 for 1 h at 773 K, and then evacuated for 1 h at 773 K. Then the sample was exposed to 0.53 kPa of lutidine vapor at 298 K for 10 min followed by evacuation at 473 K for 10 min. The amount of Brønsted acid sites was calculated based on the amount of adsorbed lutidine. The amount of adsorbed lutidine was estimated by using the integrated molar adsorption coefficient value of ε = 6.8 cm μmol^{-1} for the band at 1628 cm^{-1} and 1647 cm^{-1} of protonated lutidine as reported by Onfloy et al..[20]

X-ray photoelectron spectra (XPS) were acquired using an ULVAC PHI 5500MT. XPS samples were mounted on indium foil and the spectra were measured using Mg Ka radiation (15 kV, 400 W) in a chamber with the base pressure of ca. 1×10^{-8} Torr. The takeoff angle was set at 45 deg. Binding energies were referenced to Al(2p) level at 74.0 eV.

Ta L_3- and L_1-edges (9.9 and 11.7 keV, respectively) XAFS data were collected at a facility of the BL01B1 beam line at the SPring-8, of the Japan Synchrotron Radiation Research Institute, Japan in the transmission mode in air at room temperature. Incident X-ray flux and transmitted flux were measured with ionization chambers. Si (311) two crystal monochromator for Ta L_1-edge and Si (111) two crystal monochromator for Ta L_3-edge were used to obtain monochromatic X-ray beam. Energy was calibrated by Ta foil, and the energy step of measurement in the XANES region was 0.5 eV. The absorption was normalized to 1.0 at an energy position of ca. 100 eV higher than the absorption edge. The data reduction was performed by the REX2000 Ver.2.5.9 (Rigaku) and FEFF 8.40 programs.[21]

Results and discussion

Catalytic activity

The catalytic activities of Ta_2O_5/Al_2O_3 catalysts have been investigated as a function of calcination temperature. Loading amount of tantalum oxide was 33 wt%. Figure 1(A) shows the effect of the calcination temperature on the product yields in benzylation of anisole. The main products were *o*- and *p*-benzyl anisole isomers, which were presumably formed on the Brønsted acid sites, and by-product was dibenzyl ether produced mostly on the Lewis acid sites.[14,22-26] The ratio of orthoto para-benzyl anisole was approximately 48:52 throughout the reaction. The yield of benzyl anisole increased as the calcination temperature increased to 1223 K. Increasing the calcination above 1223 K resulted in a reduction of yield of benzyl anisole. The yield of dibenzyl ether was independent of the calcination temperature. These results strongly suggest that Brønsted acid sites are generated on Ta_2O_5/Al_2O_3 by calcination at high temperatures such as 1223 K. No benzyl anisole was formed on tantalum acid and trace of dibenzyl ether (0.02 mmol) was obtained under this condition.
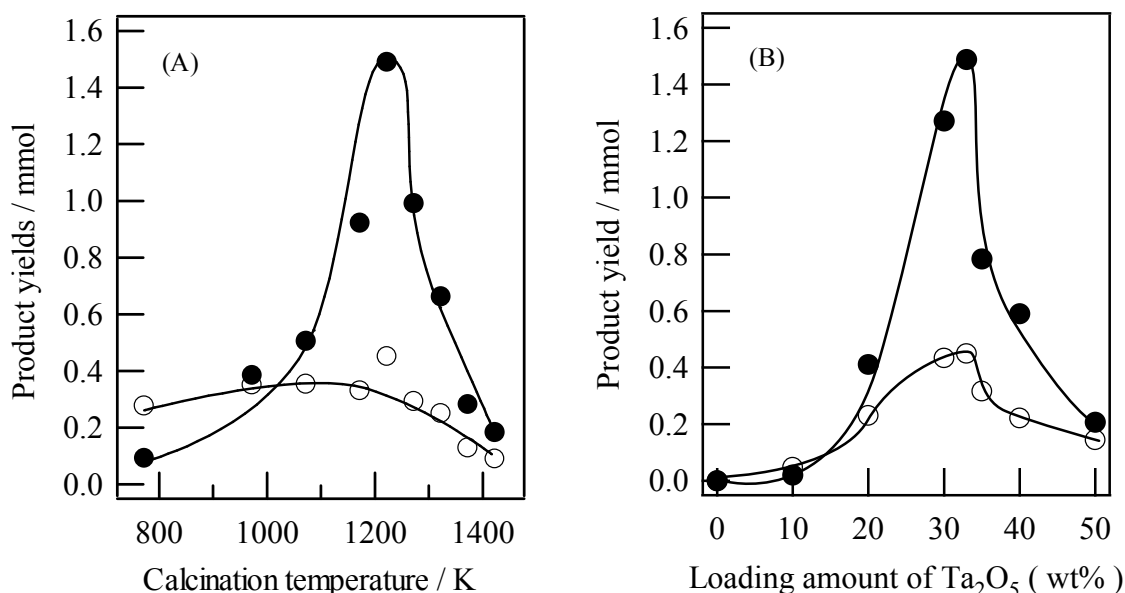

Figure 1. Activity of Ta_2O_5/Al_2O_3 for Friedel–Crafts alkylation of benzyl alcohol with anisole. (A) Calcined at various temperatures, Ta_2O_5 loading: 33 wt%, (B) with various Ta_2O_5 loadings. Calcination temperature: 1223 K, reaction temperature: 433 K, reaction time: 1 h. (●) Benzyl anisole and (○) dibenzyl ether.

Figure 2(A) shows the effect of the calcination temperature on the product yields in isomerization of α-pinene. The main products were camphene and limonene. A small amount of terpinene, terpinolene, fenchene, and β-pinene was formed as by-products. The yield of camphene was almost twice to that of limonene regardless of the calcination temperature. The change in yields of products has the same tendency as that in yield of benzyl anisole in benzylation of anisole. The yields of camphene and limonene increased with increasing calcination temperature up to 1223 K and the calcination at higher temperatures than 1273 K results in the reduction of yields of these products. This result strongly suggests that camphene and limonene were formed on Brønsted acid sites as well as benzyl anisole in benzylation of anisole. Tantalum acid gave a small amount of camphene (0.14 mmol) and limonene (0.05 mmol), respectively.
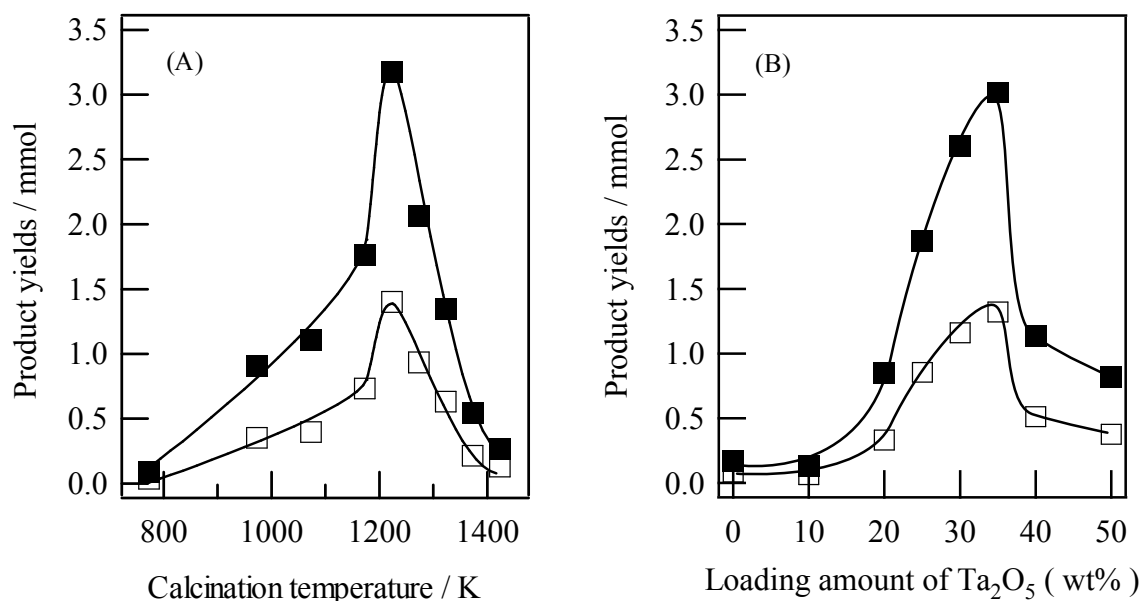

Figure 2. Activity of Ta_2O_5/Al_2O_3 for isomerization of α-pinene. (A) Calcined at various temperatures, Ta_2O_5 loading: 33 wt%, (B) with various Ta_2O_5 loadings. Calcination temperature: 1223 K, reaction temperature: 353 K, reaction time: 3 h. (■) Camphene and (□) limonene.

The results of benzylation of anisole over Ta_2O_5/Al_2O_3 solid acids with various Ta_2O_5 loadings and calcined at 1223 K are shown in Figure 1(B). Figure 2(B) demonstrates the effect of loading amount of Ta_2O_5 on the yields of camphene and limonene in isomerization of α-pinene. The calcination temperature was fixed at 1223 K. The 33 wt% Ta_2O_5/Al_2O_3 catalyst exhibited the highest activity in both benzylation of anisole and isomerization of α-pinene. In the case of 33 wt% Ta_2O_5/Al_2O_3 catalyst calcined at 1223 K, the TOFs were 110 h^{-1} for benzylation of anisole and 106 h^{-1} for isomerization of α-pinene, respectively.

Brønsted acidity

To examine the generation of Brønsted acid sites on Ta_2O_5/Al_2O_3 calcined at 1223 K, the acid sites were characterized based on FTIR spectra of lutidine adsorbed on the catalysts. Figure 3 shows the IR spectra of lutidine adsorbed on 33 wt% Ta_2O_5/Al_2O_3 calcined at 1223 K and bare γ-Al_2O_3. The bands at 1580 and 1608 cm^{-1} were assignable to lutidine adsorbed on Lewis acid sites, and the bands at 1628 and 1647 cm^{-1} can be assigned to lutidine adsorbed on Brønsted acid sites.[20,27,28] In the case of 33 wt% Ta_2O_5/Al_2O_3, in addition to the bands at 1580 and 1608 cm^{-1}, the bands at 1628 and 1647 cm^{-1} appeared. This result clearly indicates that Brønsted acid sites are generated on Ta_2O_5/Al_2O_3 calcined at such high temperature in addition to Lewis acid sites. On the other hand, in the case of Al_2O_3, the bands at 1580 cm^{-1} and 1608 cm^{-1} due to lutidine adsorbed on Lewis acid sites appeared. The bands at 1632 cm^{-1} and 1635 cm^{-1} are assigned to hydrogen-bonding lutidine. Therefore it can be though that only Lewis acid sites exist on Al_2O_3. This makes a great difference to the evidence that tantalum acid itself calcined at higher temperatures than 1073 K loses acid property, and that tantalum acid exhibits mainly Lewis acid properties in the absence of water.[1,2]

Figure 4 shows the correlation between the yield of benzyl anisole and the Brønsted acidity, which was evaluated from FT-IR spectra of adsorbed lutidine, of Ta_2O_5/Al_2O_3 calcined at 1223 K with various Ta_2O_5 loadings. The yield of benzyl anisole correlated with the Brønsted acidity. The yield of benzyl anisole increased with increasing the amount of Brønsted acid site. This indicates that the Friedel–Crafts reaction is promoted on the Brønsted acid sites. As shown in Figure 1 and Figure 2, the activities for Friedel–Crafts alkylation and isomerization of α-pinene changed depending on the change of calcinations temperature and loading amount of Ta_2O_5. The tendency of change in activity for isomerization of α-pinene against the calcination temperature or loading amount of Ta_2O_5

was almost similar to that for the Friedel–Crafts alkylation. This indicates that isomerization of α-pinene to camphene and limonene also takes place on Brønsted acid sites. These results strongly suggest that both calcination temperature and Ta_2O_5 amount affected the amount of Brønsted acid site. This suggests that structural changes around the tantalum species have a major impact on the Brønsted acidic property.
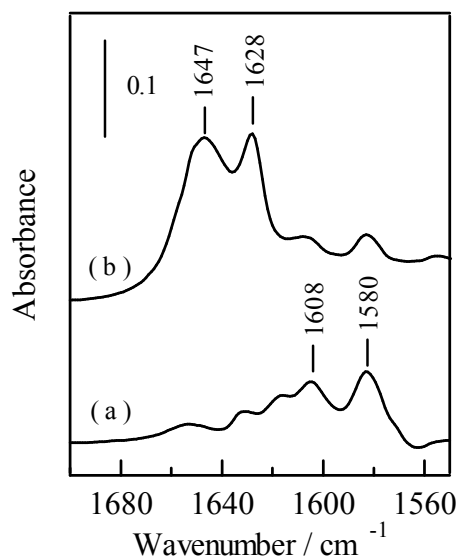

Figure 3. IR spectra of lutidine adsorbed on (a) alumina, and (b) 33 wt% Ta_2O_5/Al_2O_3 calcined at 1223 K.
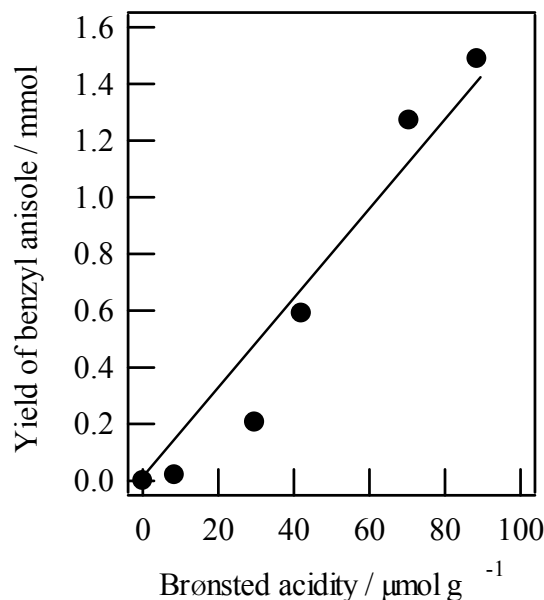

Figure 4. The correlation between Brønsted acidity and the yield of benzyl anisole. Calcination temperature: 1223 K.

Interestingly, Brønsted acid sites were still detected for the Ta_2O_5/Al_2O_3 catalysts even after the calcination at 1223 K. 33 wt% Ta_2O_5/Al_2O_3 calcined at 1223 K exhibited the highest Brønsted acidity and By contrast, pure Ta_2O_5 calcined at higher temperatures (>1073 K, T-Ta_2O_5) does not exhibit both Brønsted and Lewis acid property at all. This is consistent with the previous report.[1,2]

XRD patterns and Raman spectra

Figure 5 and Figure 6 show the XRD patterns and Raman spectra of 33 wt% Ta_2O_5/Al_2O_3 calcined at various temperatures. Calcination at up to 1223 K did not cause crystallization of tantalum oxide (T-Ta_2O_5) or aluminum tantalate ($AlTaO_4$). By contrast, the XRD patterns and Raman spectra of Ta_2O_5/Al_2O_3 calcined at 1273 K or above exhibited the formation of T-Ta_2O_5 and $AlTaO_4$. Ushikubo et al. reported that amorphous $Ta_2O_5 \cdot nH_2O$ crystallized to T-Ta_2O_5 after calcination at 1073 K.[1,2] Therefore, it appears that Al_2O_3 support stabilizes amorphous tantalum oxide cluster and prevents it from crystallizing during calcination even at 1223 K. Corresponding to the crystallization results, the specific surface area of Ta_2O_5/Al_2O_3 v ery gradually decreased from 150 to 100 m^2 g^{-1} with an increase in calcination temperature up to 1223 K, and drastically decreased to 50 m^2 g^{-1} with calcination at higher temperatures (1273–1423 K).
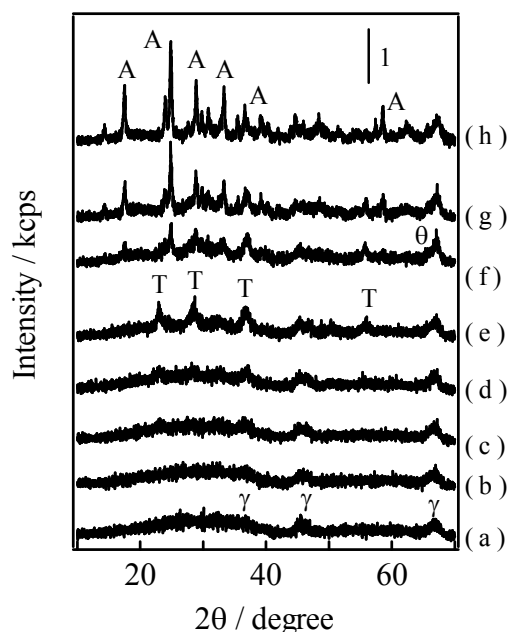

Figure 5. XRD patterns of Ta_2O_5/Al_2O_3 catalysts calcined at various temperatures. (a)773 K, (b) 973 K, (c) 1173 K, (d) 1223 K, (e) 1273 K, (f) 1323 K, (g) 1373 K, and (h)1423 K. Ta_2O_5 loading: 33 wt%, (A) $AlTaO_4$, (T) T-Ta_2O_5, (γ) γ-Al_2O_3 and (θ) θ-Al_2O_3.

In this region, the formation of $AlTaO_4$ proceeded and increasing the calcination temperature resulted in drastically decreasing the yields of benzyl anisole, camphene and limonene. $AlTaO_4$ was completely inert for both Friedel–Crafts alkylation and isomerization of α-pinene. Moreover, even after the exposure to lutidine, IR spectrum of $AlTaO_4$ showed no band due to adsorbed lutidine. This result indicates that both Brønsted and Lewis acid sites are absent on $AlTaO_4$. These results strongly suggest that the formation of inert $AlTaO_4$ phase by calcination at high temperatures (>1273 K) reduces the catalytic activity. XRD patterns and Raman spectra of with various loadings calcined at 1223 K are shown in Figure 7 and Figure 8. These results indicated that $T-Ta_2O_5$ was not present in Ta_2O_5/Al_2O_3 catalysts with Ta_2O_5 mass fraction of less than 33%. Above 35%, the larger the mass fractions of Ta_2O_5, the increasing the intensity and the decreasing of the full width at half maximum of the diffraction lines for $T-Ta_2O_5$ occurred. These results indicate that the amorphous Ta_2O_5 supported on γ-Al_2O_3 crystallized to $T-Ta_2O_5$ and the crystallite size increased. When the Ta_2O_5 mass fraction was >35%, the activities for Friedel–Crafts alkylation and isomerization of α-pinene were greatly reduced. Friedel–Crafts alkylation and isomerization of α-pinene did not proceed over $T-Ta_2O_5$.
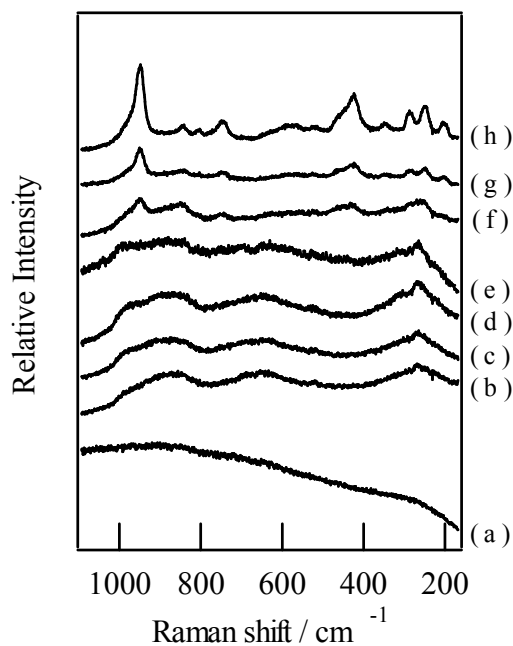
Figure 6. Raman spectra of Ta_2O_5/Al_2O_3 catalysts calcined at various temperatures.(a) 773 K, (b) 973 K, (c) 1173 K, (d) 1223 K, (e) 1273 K, (f) 1323 K, (g) 1373 K, and (h) 1423 K. Ta_2O_5 loading: 33 wt%,
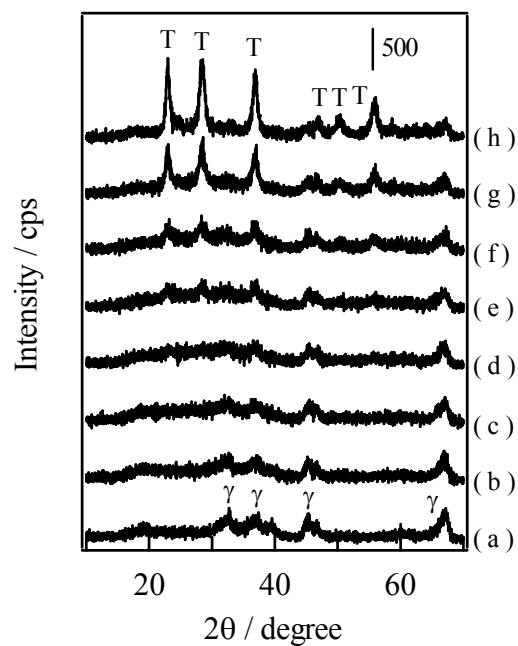
Figure 7. XRD patterns of Ta_2O_5/Al_2O_3 catalysts with various loadings. (a) 10 wt%, (b)20 wt%, (c) 30 wt%, (d) 33 wt%, (e) 35 wt%, (f) 40 wt%, and (g) 50 wt%. Calcination temperature: 1223 K, (γ) γ-Al_2O_3 and (T) T-Ta_2O_5.
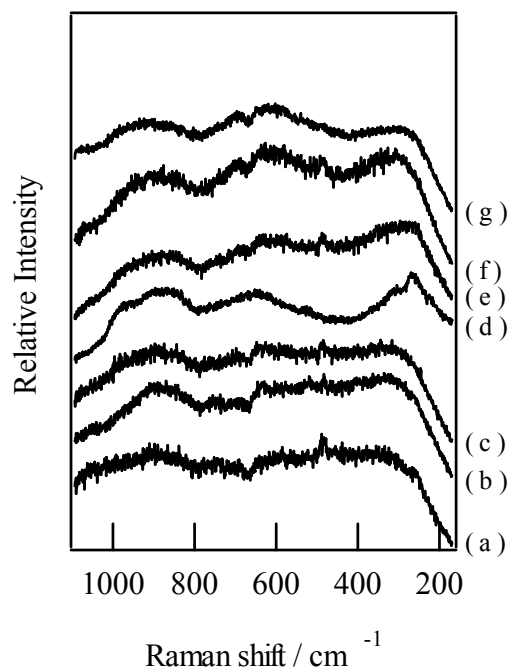
Figure 8. Raman spectra of Ta_2O_5/Al_2O_3 catalysts with various loadings. (a) 10 wt%,(b) 20 wt%, (c) 30 wt%, (d) 33 wt%, (e) 35 wt%, (f) 40 wt%, and (g) 50 wt%. Calcination temperature: 1223 K,

Moreover, no band for adsorbed lutidine was observed in the IR spectrum of T-Ta_2O_5 exposed to lutidine, indicating that both Brønsted and Lewis acid sites are absent on T-Ta_2O_5. Based on these results, it can be thought that the formation of inert T-Ta_2O_5 phase reduced the catalytic activity by increasing the mass fraction of Ta_2O_5. Onfloy et al. reported that Nb_2O_5/TiO_2 and WO_3/TiO_2 exhibit Brønsted acid property when crystallites of Nb_2O_5 and WO_3 did not formed.[29] Recently, we also found that Nb_2O_5/Al_2O_3 exhibit Brønsted acid property when crystallite of Nb_2O_5 did not formed.[16,17] Similarly, XRD patterns and Raman spectra of Ta_2O_5/Al_2O_3 indicate that amorphous Ta_2O_5 supported on Al_2O_3 exhibit Brønsted acid property.

XPS measurements and analysis

The valence of tantalum cation of Ta_2O_5/Al_2O_3 catalyst surface was evaluated by using XPS. Binding energy of Ta 4f peaks of Ta_2O_5/Al_2O_3 was independent of Ta_2O_5 loadings (Figure 9). The Ta $4f_{7/2}$ peak at 26.2 eV is assignable to Ta^{5+}. Figure 10 shows the surface Ta/Al ratio estimated from the areas of Ta 4f and Al 2p XPS. The surface Ta/Al ratio shows a linear increase with loading of Ta_2O_5 up to 33 wt% but then it becomes slightly gradual. This value (33 wt% of Ta_2O_5) was slightly larger than the calculated value of formation of Ta_2O_5 monolayer (28 wt%) based on the cross-section area of TaO_6 octahedral unit and surface area of support.
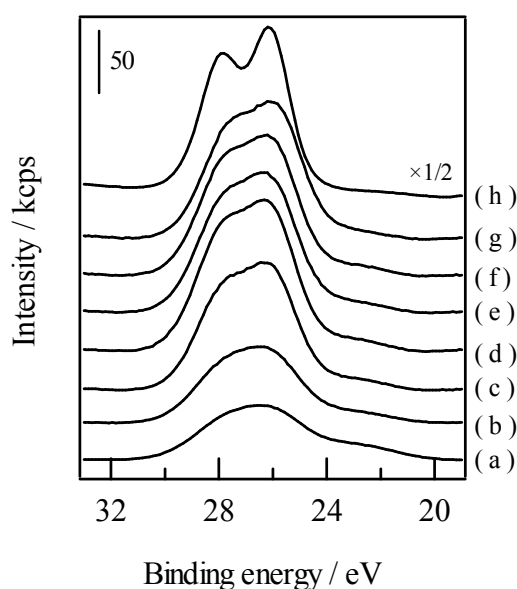

Figure 9. Ta 4f XPS of Ta_2O_5/Al_2O_3 with various loadings. (a) 10 wt%, (b) 20 wt%, (c) 30 wt%, (d) 33 wt%, (e) 35 wt%, (f) 40 wt%, (g) 50 wt%, and (h) T-Ta_2O_5. Calcination temperature: 1223 K.

This suggests that the surface of 33 wt% Ta_2O_5/Al_2O_3 was fully covered with monolayer of tantalum oxide and that a small cluster of Ta_2O_5 coexists on the surface. In the case of 33 wt% Ta_2O_5/Al_2O_3 catalyst, the surface density of Ta atom was estimated to 5.8 Ta atoms nm^{-2}. Bell et al.[30] and Iwasawa et al.[16] reported that the surface density of Nb atom at monolayer coverage was 6.3 Nb atoms nm^{-2}. Because ionic radius of Ta^{5+} is almost similar to that of Nb^{5+}, it seems that this surface density of Ta atom is almost similar to the estimated value of 33 wt% Ta_2O_5/Al_2O_3 catalyst strongly suggest that a monolayer of tantalum acid-like compound was formed over 33 wt% Ta_2O_5/Al_2O_3. Combining this result with the fact that the catalyst exhibited the highest activity at around 33 wt% of loading, it appears that Brønsted acid site are generated on a stabilized two-dimensional tantalum acid-like compound over Al_2O_3.
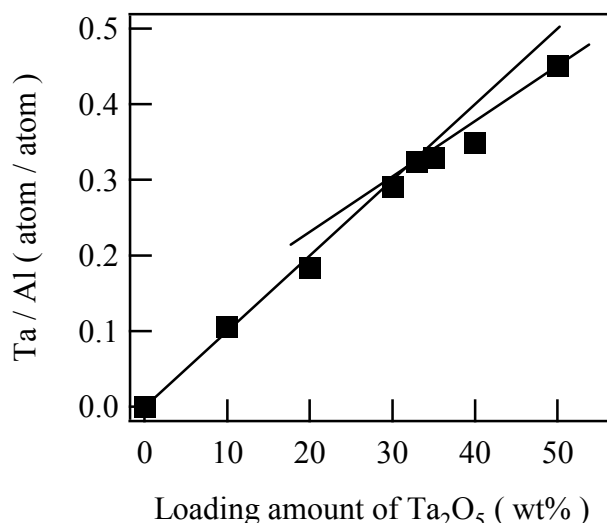
Fig. 10. The change in surface Ta/Al ratio with loading amount. Calcination temperature:1223 K.

Ta L_1-edge XANES spectra and analysis

The coordination environment of tantalum in Ta_2O_5/Al_2O_3 catalysts was investigated by Ta L_1 and L_3-edges XAFS spectra. Figure 11 shows Ta L_1-edge XANES spectra of reference samples and Ta_2O_5/Al_2O_3 catalysts with various loadings. The local symmetry of tantalum atom is figured by a pre-edge peak area of Ta L_1-edge XANES due to 2s to 5d transition. This transition is the dipole forbidden transition for regular octahedral site-symmetry such as Sr_2GaTaO_6. The dipole forbidden transition is partially allowed by the distortion of octahedral environment, because p orbitals are mixed with d orbitals caused by the breakdown of inversion symmetry due to structure distortion.[31] Therefore, tantalum atom with tetrahedral symmetry like $YTaO_4$ exhibits relatively large preedge

peak area. In order to examine the local symmetry of tantalum cation, the pre-edge peak areas at 11678 eV of Ta_2O_5/Al_2O_3 catalysts were evaluated and summarized in Figure 12. As shown in Figure 12, pre-edge peak areas of Ta_2O_5/Al_2O_3 catalysts were smaller than $YTaO_4$, which had tetrahedral symmetry, and larger than Sr_2GaTaO_6 having regular octahedral symmetry. Furthermore, this value of Ta_2O_5/Al_2O_3 catalyst was slightly larger than $T-Ta_2O_5$, but almost similar to tantalum acid having distorted octahedral symmetry, suggesting that TaO_6 unit in Ta_2O_5/Al_2O_3 catalyst had distorted octahedral symmetry like tantalum acid. This value was almost constant up to 50 wt% of Ta_2O_5 loading.
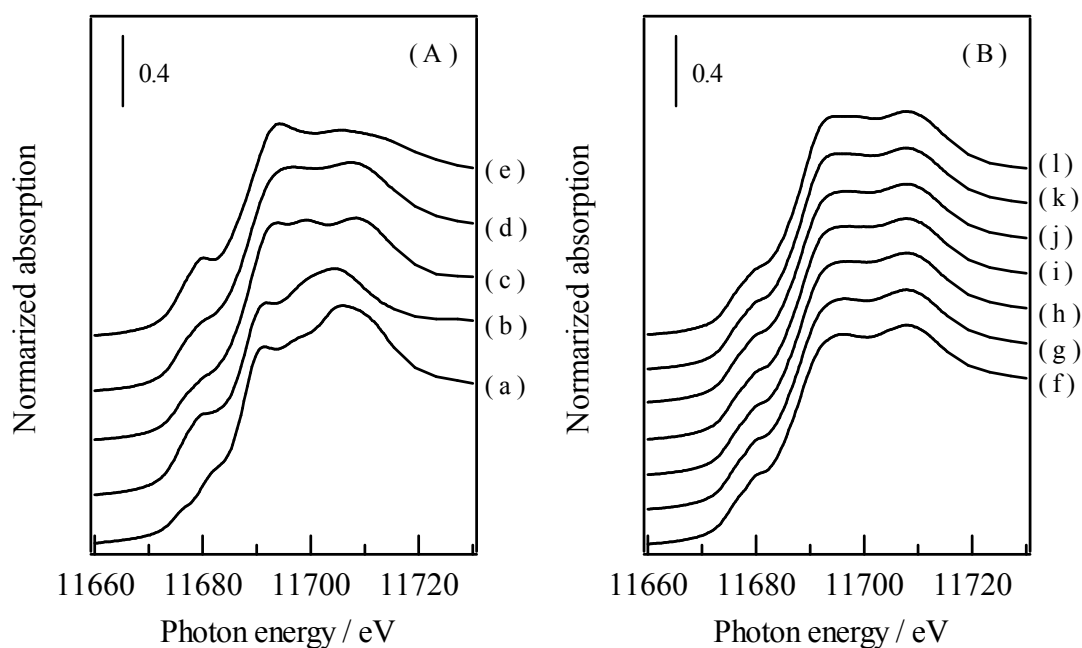
Figure 11. Ta L_1-edge XANES spectra of (A) references and (B) Ta_2O_5/Al_2O_3 catalysts with various loadings. (a) Sr_2GaTaO_6, (b) $T-Ta_2O_5$, (c) $Ta_2O_5 \cdot nH_2O$, (d) $AlTaO_4$, (e) $YTaO_4$, (f) 10 wt%, (g) 20 wt%, (h) 30 wt%, (i) 33 wt%, (j) 35 wt%, (k) 40 wt%, and (l) 50 wt%. Calcination temperature: 1223 K.
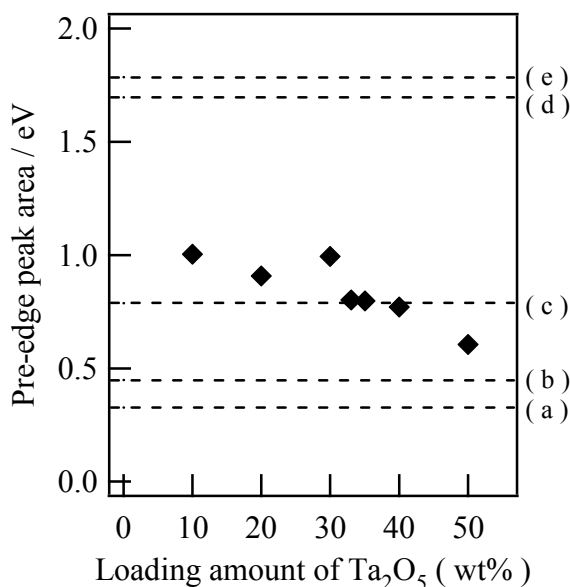
Figure 12. The change in the pre-edge peak areas of Ta_2O_5/Al_2O_3 catalysts with loadings. (a) Sr_2GaTaO_6, (b) $T-Ta_2O_5$, (c) $Ta_2O_5 \cdot nH_2O$, (d) $AlTaO_4$, and (e) $YTaO_4$. Calcination temperature: 1223 K.

Ta L_3-edge EXAFS spectra and analysis

The Ta L_3-edge EXAFS oscillations of Ta_2O_5/Al_2O_3 catalysts with various loadings are shown in Figure 13. In the high k region (>9 $Å^{-1}$), the amplitude of the EXAFS oscillations of Ta_2O_5/Al_2O_3 catalysts with loading of Ta_2O_5 up to 30 wt% was weak. Above 35 wt%, the amplitude of the EXAFS oscillations in this region gradually grew with increasing the Ta_2O_5 loading and the period of the oscillation was similar to that of $T-Ta_2O_5$. This indicates that the local structure of tantalum cation of Ta_2O_5/Al_2O_3 catalysts with loading of Ta_2O_5 below 30 wt% was similar to that of tantalum acid, that is, distorted octahedral TaO_6 unit. On the other hand, above 35 wt%, the amorphous Ta_2O_5 supported on $\gamma-Al_2O_3$ crystallized to $T-Ta_2O_5$ gradually and the crystallite size increased.

Fourier Transforms of Ta L_3-edge EXAFS are shown in Figure 14. The peak in the range 1-2 Å due to Ta–O shell and the peak around 3 Å due to Ta–O–Ta (or Ta–O–Al) were appear. When the loading was higher than 35 wt%, the amplitude of the second was stronger than those of catalysts with loading up to 30 wt%. These results strongly suggest that $T-Ta_2O_5$ over catalysts with higher loading than 35 wt% has a three-dimensional structure, whereas TaO_6 unit over catalysts loading below 33 wt% has mainly a two-dimensional structure. These results agree with the results of XPS
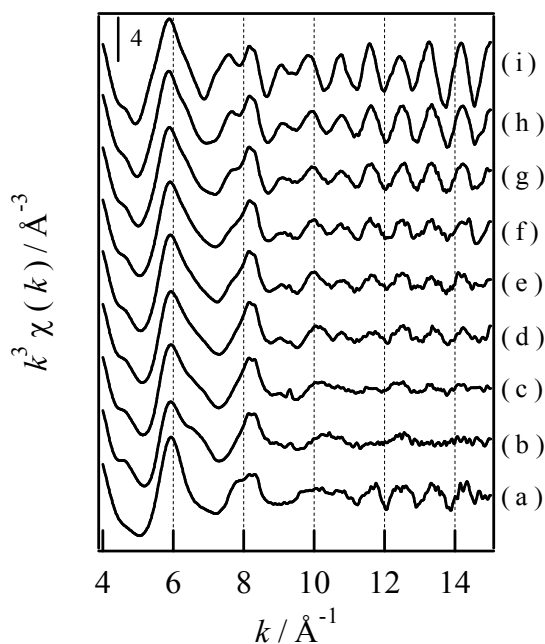
Figure 13. k^3-weighted Ta L$_3$-edge EXAFS oscillations of references and Ta$_2$O$_5$/Al$_2$O$_3$ catalysts with various loadings. (a) Ta$_2$O$_5$•nH$_2$O, (b) 10 wt%, (c) 20 wt%, (d) 30 wt%, (e) 33 wt%, (f) 35 wt%, (g) 40 wt%, (h) 50 wt%, and (i) T-Ta$_2$O$_5$. Calcination temperature: 1223 K.

Figure 14. Fourier transforms of k^3-weighted Ta L$_3$-edge EXAFS of references and Ta$_2$O$_5$/Al$_2$O$_3$ catalysts with various loadings. (a) Ta$_2$O$_5$•nH$_2$O, (b) 10 wt%, (c) 20 wt%, (d) 30 wt%, (e) 33 wt%, (f) 35 wt%, (g) 40 wt%, (h) 50 wt%, and (i) T-Ta$_2$O$_5$. Calcination temperature: 1223 K.
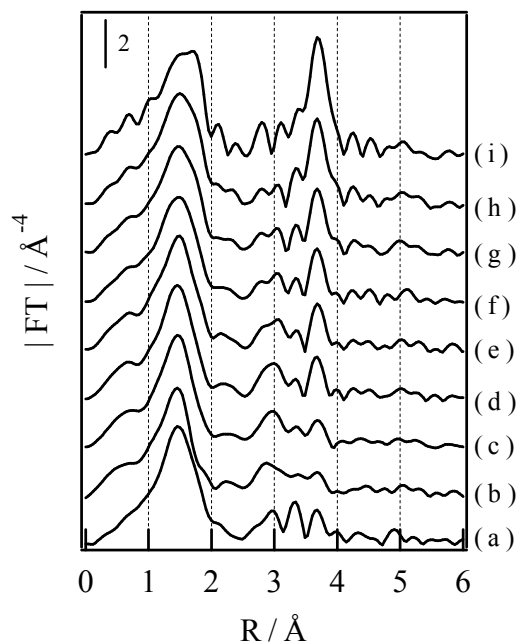
measurement. According to the results mentioned above, it appears that the monolayer of tantalum acid-like is stabilized over the Ta_2O_5/Al_2O_3 catalysts with around 33 wt% Ta_2O_5 loading. In this monolayer, TaO_6 unit having distorted octahedral symmetry forms a two-dimensional Ta–O–Ta network. This Ta–O–Ta network may have an important role in the generation of Brønsted acid sites.

Conclusions

We found that the Ta_2O_5/Al_2O_3 catalysts calcined at high temperatures were effective for Friedel–Crafts alkylation and isomerization of α-pinene. Among the Ta_2O_5/Al_2O_3 catalysts tested, 33 wt% Ta_2O_5/Al_2O_3 calcined at 1223 K showed the highest activity in both Frieadel–Crafts Alkylation and isomerization of α-pinene. The Ta_2O_5/Al_2O_3 catalyst exhibits the Brønsted acidity despite calcination at such high temperatures. It is concluded that a monolayer of tantalum acid-like compound, which have distorted octahedral symmetry, were stabilized over 33 wt% Ta_2O_5/Al_2O_3 catalyst calcined at 1223 K. The stabilized tantalum acid-like compound which has two-dimensional Ta-O-Ta network probably accounts for the generation of Brønsted acid. The formation of an inert $AlTaO_4$ and $T-Ta_2O_5$ phases resulted in the decreasing the Brønsted acidity

References

(1)   Ushikubo, T.; Wada, K. *Chem. Lett.,* **1988**, 1573.

(2)   Ushikubo, T.; Wada, K. *Appl. Catal.,* **1990**, *67*, 25.

(3)   Iizuka, T.; Ogasawara, K.; Tanabe, K. *Bull. Chem. Soc. Jpn.,* **1983**, *56*, 2927.

(4)   Tanabe, K. *Catal. Today,* **2003**, *78*, 65.

(5)   Tanabe, K.; Okazaki, S. *Appl. Catal. A-Gen.,* **1995**, *133*, 191.

(6)   Nowak, I.; Ziolek, M. *Chem. Rev.* **1999**, *99*, 3603.

(7)   Okuhara, T. *Chem. Rev.* **2002**, *102*, 3641.

(8)   Ohuchi, T.; Miyatake, T.; Hitomi, Y.; Tanaka, T. *Catal. Today* **2007**, *120,* 233.

(9)   Corma, A. *Chem. Rev.* **1997**, *97*, 2373.

(10)   Corma, A. *Chem. Rev.* **1995**, *95*, 559.

(11)   Arata, K.; Matsuhashi, H.; Hino, M.; Nakamura, H. *Catal. Today,* **2003**, *81*, 17.

(12)   Katada, N; Ishiguro, H; Muto, K; Niwa, M. *Chem. Vap. Ceposition,* **1995**, *1*, 54.

(13)   Takagaki, A.; Sugisawa, M.; Lu, D. L.; Kondo, J. N.; Hara, M.; Domen, K.; Hayashi, S. *J. Am. Chem. Soc.* **2003**, *125*, 5479.

(14)   Tagusagawa, C.; Takagaki, A.; Hayashi, S.; Domen, K. *J. Am. Chem. Soc.,* **2008**, *130*, 7230.

(15)   Takagaki, A.; Tagusagawa, C.; Hayashi, S.; Hara, M.; Domen, K. *Energy Environ. Sci.* **2010**, *3*, 82.

(16)   Shishido, T.; Kitano, T.; Teramura, K.; Tanaka, T. *Catal. Lett.,* **2009**, *129*, 383.

(17)   Shishido, T.; Kitano, T.; Teramura, K.; Tanaka, T. *Top. Catal.,* **2010**, *53*, 672.

(18)   Kitano, T.; Okazaki, S.; Shishido, T.; Teramura, K.; Tanaka, T. *Chem. Lett.,* **2011**, *40*, 1332.

(19)   Tamaguchi, O; Tomihisa, D; Uegaki, T; Shimizu, K. *J. Am. Ceram. Soc.,* **1987**, *70*, C335.

(20)   Onfloy, T; Clet, G; Houalla, M. *Micropor. Mesopor. Mater.,* **2005**, *82*, 99.

(21)   Ankudinov, A. L.; Ravel, B.; Rehr, J. J.; Conradson, S. D. *Phys. Rev. B* **1998**, *58*, 7565.

(22)   Okumura, K.; Yamashita, K.; Hirano, M.; Niwa, M. *Chem. Lett.* **2005**, *34*, 716.

(23)   Okumura, K.; Yamashita, K.; Hirano, M.; Niwa, M. *J. Catal.* **2005**, *234*, 300.

(24)   Yamashita, K.; Hirano, M.; Okumura, K.; Niwa, M. *Catal. Today* **2006**, *118*, 385.

(25)   de la Cruz, M. H. C.; da Silva, J. F. C.; Lachter, E. R. *Catal. Today* **2006**, *118*, 379.

(26)   de la Cruz, M. H. C.; Abdel-Rehim, M. A.; Rocha, A. S.; da Silva, J. F. C.; Faro, A. D.; Lachter, E. R. *Catal. Commun.* **2007**, *8*, 1650.

(27)   Morterra, C; Cerrato, G; Meligrana, G; *Langmuir,* **2001**, *17*, 7053.

(28)   Onfroy, T.; Clet, G.; Houalla, M. *J. Phys. Chem. B* **2005**, *109*, 14588.

(29)   Onfroy, T.; Clet, G.; Bukallah, S. B.; Visser, T.; Houalla, M. *Appl. Catal. A-Gen.* **2006**, *298*, 80.

(30)   Tanaka, T; Yoshida, T; Yoshida, H; Aritani, H; Funabiki, T; Yoshida, S; Jehng, J. M.; Wachs, I. E. *Catal. Today,* **1996**, *28*, 71.

(31)   Yamamoto, T. *X-ray Spectrom.,* **2008**, *37*, 572.

Chapter 5

Effect of High Temperature Calcination on Generation

of Brønsted Acid Sites of Alumina-Supported Tungsten Oxide

Abstract

The acid properties of alumina-supported tungsten oxide (WO_3/Al_2O_3) catalysts with loadings of 5-50 wt% WO_3 that were calcined at various temperatures were investigated by acid-catalyzed reactions (benzylation of anisole and isomerization of α-pinene), and Fourier transform infrared (FT-IR) spectroscopy. The relationships between acid properties, structures, and catalytic performances are evaluated. Both the catalytic activity and amount of Brønsted acid sites depend on calcination temperatures and WO_3 loading amount. High temperature calcination (1123 K) generated Brønsted acid property, and 20 wt% WO_3/Al_2O_3 calcined at 1123 K exhibited the highest activity of the catalysts tested. The activities for benzylation of anisole and α-pinene isomerization over WO_3/Al_2O_3 calcined at 1123 K were proportional to Brønsted acidity, indicating that these reactions occurred on the Brønsted acid sites. Tungsten oxide monolayer domains formed on the alumina support. When the WO_3 loading was sufficient to form two-dimensional tungsten oxide overlayers (> 20 wt%), some of the Brønsted acid sites on WO_3/Al_2O_3 were obscured by monoclinic WO_3 having no Brønsted acid site, resulting in a lowering of the catalytic activity. This suggests that Brønsted acid sites are generated at the boundaries between tungsten oxide monolayer domains.

Introduction

Tungsten compounds are widely used in various industrial processes such as oxidations, acid-base reactions, and photocatalytic reactions. Dodecatungstophosphoric acid is heteropoly acid that contains 12 tungsten (W) atoms, and is an active homogeneous acid catalysts for hydration of olefins and esterification.[1-3] Homogeneous acid catalysts are environmentally unfriendly because of their corrosive nature, difficulty of separation from solution, and necessity of neutralization, so use of heterogeneous acid catalysts in reactions are preferred. As a result, the acid properties of water-insoluble heteropoly compounds, such as heteropoly acids supported on silica ($H_3PW_{12}O_{40}/SiO_2$ and $H_4SiW_{12}O_{40}/SiO_2$) and salts with large monovalent ions ($Cs_{2.5}H_{0.5}PW_{12}O_{40}$), heve been studied.[4-10] $H_3PW_{12}O_{40}/SiO_2$, $H_4SiW_{12}O_{40}/SiO_2$, and $Cs_{2.5}H_{0.5}PW_{12}O_{40}$ are effective for various acid-base reactions such as esterification and hydration. However, these heteropoly acids possess some advantages. Leaching into polar solvents such as water and alcohols occurs in the case of supported heteropoly acids. Moreover, it is difficult to regenerate heteropoly acids by heat treatment at temperatures exceeding 773 K because heteropoly acid calcined at higher temperature than 773 K decomposes.[11,12] Tungsten oxide supported on zirconia, titania, and iron oxide (WO_3/ZrO_2, WO_3/TiO_2, and WO_3/Fe_2O_3) are known as solid superacid catalysts. The acid strength of WO_3/ZrO_2, WO_3/TiO_2, and WO_3/Fe_2O_3 is estimated to be $H_0 <$ -14.6, -13.1, and -12.5, respectively. These catalysts promote acid reactions requiring superacid sites, such as skeletal isomerization of butane.[13-18]

Niobic acid ($Nb_2O_5 \cdot nH_2O$, hydrated niobium oxide) is one of the useful solid acid catalysts and exhibits water-tolerance and strong Brønsted acid property.[8,19-22] However, $Nb_2O_5 \cdot nH_2O$ loses its acid properties when is calcined at 773 K because of phase transformation from amorphous to crystalline phases (TT- and T-phases).[22,23] In contrast, niobium oxide supported on alumina (Nb_2O_5/Al_2O_3) calcined at high temperature (1123 K) exhibits high activity for acid-catalyzed reactions such as benzylation of anisole, cumene cracking, and isomerization of α-pinene because of its Brønsted acid property.[24-26] Calcination temperature and loading amount of Nb_2O_5 strongly affect the acid property and structure of supported Nb_2O_5. 16 wt% Nb_2O_5/Al_2O_3 calcined at 1123 K showed the highest activity. The Brønsted acidity of this catalyst was not changed even after treatment at

1173 K under nitrogen flow, indicating that Brønsted acid sites generated on the Nb_2O_5/Al_2O_3 catalyst were thermally quite stable. Tantalum oxide also loses its acid property when the catalyst is heated at 1073 K,[22,27] but tantalum oxide supported on alumina (Ta_2O_5/Al_2O_3) calcined at high temperature (1223 K) exhibits catalytic activity for benzylation of anisole and isomerization of α-pinene, and Brønsted acid property.[28,29] These examples demonstrate that the alumina support stabilizes Brønsted acid sites during calcination at high temperatures, and that both Nb_2O_5/Al_2O_3 and Ta_2O_5/Al_2O_3 calcined at high temperatures work as thermally stable solid acid catalysts. High temperature calcination usually causes solid acid catalysts to lose their acid properties. Conventional solid acid catalysts, such as aluminosilicate, zeolite and binary oxides, lose their acid properties if pretreated at >1000 K. If a solid acid could be prepared by calcination at the high temperatures required to form ceramics, it would be useful as an acid-catalyst even under strict conditions because of its high stability. We proposed that supported niobium oxide and tantalum oxide form two-dimensional oxides, and that Brønsted acid sites are generated on. Such two-dimensional oxides may be an important factor in the generation of Brønsted acid sites.

The acid properties of tungsten oxide on alumina (WO_3/Al_2O_3) have also been investigated. Arata et al. reported that 5 and 10 wt% WO_3/Al_2O_3 exhibited high activity for cracking of cumene when the catalyst was calcined at temperatures higher than 1273 K.[30] Soled et al. also suggested that high temperature calcination increased the fraction of Brønsted acidity to total acidity for 10 wt% WO_3/Al_2O_3 calcined at 1173 K.[31] However, the relationship between the structure and acidic properties of WO_3/Al_2O_3 is still unclear and the structure of acid sites has not been clarified. In the present study, we characterized structural changes in a series of alumina-supported tungsten oxide catalysts with various loadings of WO_3 that are calcined at various temperatures to clarify the relationship between their acidic properties and local structures around tungsten species. A model structure of the acid sites in WO_3/Al_2O_3 is proposed.

Experimental

Preparation

A series of WO_3/Al_2O_3 catalysts were prepared by impregnation of γ-Al_2O_3 (JRC-ALO-8) with an aqueous solution of ammonium tungsten para pentahydrate (($NH_4)_{10}W_{12}O_{42} \cdot 5H_2O$)) at 353 K, dried overnight at 353 K, and then calcined at various temperature for 3 h in dry air. Aluminum tungstate, $Al_2W_3O_{12}$, was synthesized by heating mixture of Al_2O_3 and WO_3 at 1373 K for 12 h. WO_3 was obtained by calcination of $(NH_4)_{10}W_{12}O_{42} \cdot 5H_2O$ at 773 K for 3 h.

Reactions

Benzylation of anisole (Friedel-Crafts alkylation of anisole with benzylalcohol) and isomerization of α-pinene were used as test reactions to examine the acid properties of WO_3/Al_2O_3.

Benzylation of anisole was examined in the liquid phase. Catalysts (0.5 g) was pretreated in a N_2 flow at 473 K for 1 h and then added to a mixture of benzyl alcohol (6.25 mmol) and anisole (92.5 mmol) in a 100 mL flask. The reaction was carried out at 353 K for 1 h and the products were determined by GLC (GC-14B with a flame ionization detector, Shimadzu, Kyoto, Japan) and GC-MS (GC-MS QP-5050, Shimadzu), using a CBP10 column.

Isomerization of α-pinene was carried out under a dry N_2 atmosphere using a stirred batch reactor. Prior to each run, sample (0.1 g) was pretreated at various temperature under 13.3 kPa of O_2 for 1 h and then evacuated at the same temperature for 1 h. α-Pinene (12.5 mmol) was added to the reactor and stirred at 323 K for 3 h. The products were determined by GLC (GC-2014 with a flame ionization detector, Shimadzu), using a CBP20 column.

Characterizations

Brunauer-Emmett-Teller (BET) specific surface areas were estimated from N_2 isotherms measured at 77 K. N_2 adsorption isotherm measurements were carried out using an adsorption analyzer (BELSORP 28SA, BEL Japan, Osaka, Japan) at 77 K. Prior to the measurement, each sample was evacuated at 373 K for 2 h.

X-ray diffraction (XRD) patterns were obtained using a powder X-ray diffractometer (MultiFlex DR, Rigaku, Tokyo Japan) with Cu Kα radiation ($\chi = 1.5405$ Å).

Laser Raman spectra were obtained with a Raman spectrometer (NRS-2000, JASCO, Tokyo,

Japan), using the 514.5 nm line of an argon laser. The spectral resolution was 4 cm^{-1}.

FT-IR spectra were recorded using an FT-IR spectrometer (SPECTRUM ONE, Perkin-Elmer, Walthham, MA, USA) with a resolution of 4 cm^{-1}. Each sample (13 mg) was pressed into a self-supporting wafer with a diameter of 13 mm. Catalysts were pretreated under 6.7 kPa of O_2 for 1 h at 673 K and then evacuated for 1 h at 673 K. To determine the number of Brønsted and Lewis acid sites on WO_3/Al_2O_3, the wafer was exposed to 0.667 kPa of pyridine vapor at 298 K for 10 min and then evacuated at 423 K for 10 min.

X-ray photoelectron spectra (XPS) of the catalysts were acquired using an X-ray photoelectron spectrometer (5500MT, ULVAC PHI, Kanagawa, JAPAN) equipped with a hemispherical energy analyzer. Samples were mounted on indium foil and then transferred to the chamber of the spectrometer. The residual gas pressure in the chamber during data acquisition was less than 1.33×10^{-6} Pa. Spectra were measured at room temperature using Mg Kα radiation. The electron take-off angle was set at 45 deg. Binding energies were referenced to the O 1s level.

X-ray absorption experiments were carried out on the BL01B1 beamline at SPring-8 (Hyogo, Japan). The ring energy was 8 GeV, and the stored current was 99.5 mA. W L_1-edge (12.1 keV) and W L_3-edge (10.2 keV) X-ray absorption spectra were recorded in transmission mode in air or N_2 at room temperature. Si (311) and Si (111) two crystal monochromators were used to obtain a monochromatic X-ray beam. Data reduction was performed using the REX2000 Ver.2.5.9 (Rigaku) and FEFF8.40 programs.[32]

Results

Catalysis

Figure 1a shows the results for benzylation of anisole on 20 wt% WO_3/Al_2O_3 calcined at various temperatures. This reaction has been performed using various solid acid catalysts and is reported to occur on Brønsted acid sites.[33-39] The main products of this reaction were *p*- and *o*-benzyl anisole and dibenzyl ether was a minor product. No multiply-alkylated product formed. Dibenzyl ether is produced on Lewis acid sites by dehydration of two benzyl alcohols. The yield of dibenzyl ether was less than 0.18 mmol in all of reaction. The calcination temperature of the catalysts

significantly affects its activity. The maximum yield of benzyl anisole was obtained using catalyst calicned at 1123 K. The ratio of *p*-benzyl anisole to *o*-benzyl anisole was ca. 3/2 regardless of calcination temperature.

Isomerization of α-pinene was used as a test reaction to investigate the acid-base properties of the catalyst. The activity and selectivity of isomerization of α-pinene over 20 wt% WO_3/Al_2O_3 calcined at various temperature are summarized in Table 1. Many products were formed in the isomerization of α-pinene, and can be divided into three groups, 1) bicyclic compounds such as fenchene and camphene, 2) monocyclic compounds such as limonene, terpinene, and 3) β-pinene. (Scheme 1) β-pinene is produced on basic sites and bicyclic and monocyclic compounds are produced on acid sites. Ohnishi *et al.*[40] and Yamamoto *et al.*[41,42] reported that monocyclic and bicyclic compounds were produced on Brønsted acid sites and their ratio depended on the maximum acid strength of the catalyst.

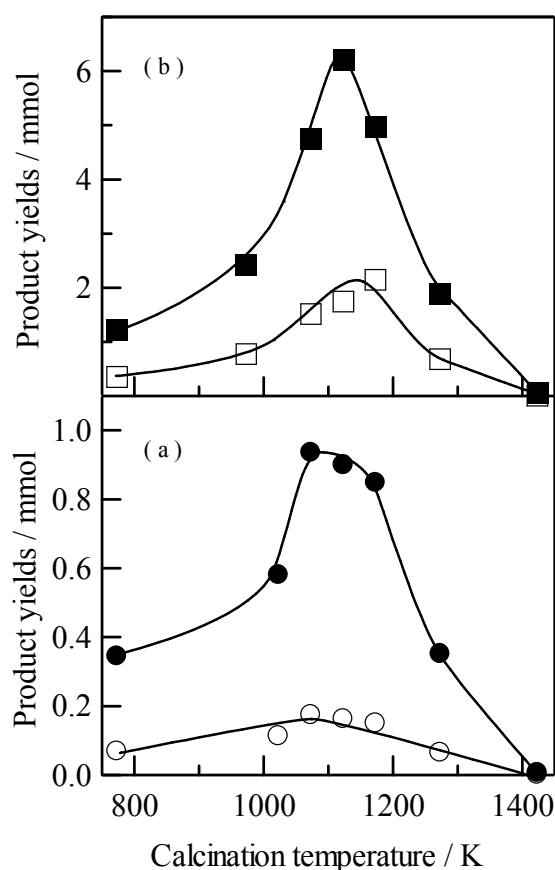**Figure 1**. Activity of 20 wt% WO_3/Al_2O_3 calcined at various temperature (a) for Friedel–Crafts alkylation ((●) benzyl anisole and (○) dibenzyl ether), (b) for isomerization of α-pinene ((■) camphene and (□) limonene). Pretreatment temperature : 473 K.

We also demonstrated that the yields of camphene and limonene correlate with the Brønsted acidity of Nb_2O_5/Al_2O_3 catalyst.[26] The main products of isomerization of α-pinene on WO_3/Al_2O_3 were camphene and limonene, with a selectivity of ca. 66% and 18%, respectively. This result suggests that isomerization of α-pinene to camphene and limonene occurred on Brønsted acid sites generated on WO_3/Al_2O_3 catalysts.

Table 1. Results for α-pinene isomerization on 20 wt% WO_3/Al_2O_3 calcined at various temperatures[a]

Calcination temperature / K	Conversion (%)	Selectivity[b] (%)							
		1	2	3	4	5	6	7	8
773	18.7	1	66	3	2	19	1	4	5
973	60.0	tr	68	1	2	21	1	5	3
1073	74.8	1	68	tr	2	21	tr	6	2
1123	94.5	2	66	tr	4	18	3	7	1
1173	77.7	1	61	tr	tr	26	tr	6	3
1273	36.3	1	65	1	2	23	1	5	3
1423	14.9	tr	76	20	tr	4	tr	tr	tr

[a] Pretreatment temperature : 473 K.
[b] 1 : α-fenchene, 2 : camphene, 3 : β-pinene, 4 : α-terpinene, 5 : limonene, 6 : γ-terpinene, 7 terpinolene, 8 others.
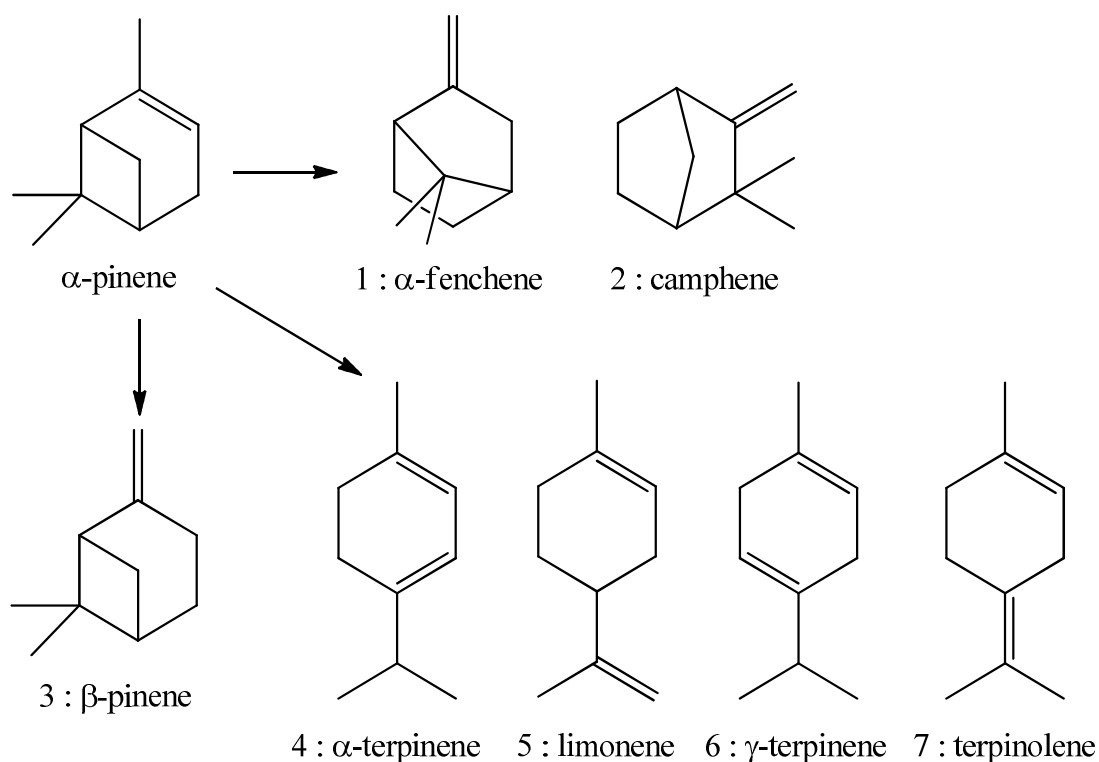
Scheme 1. α-Pinene isomerization.

Figure 1b shows the yield of camphene and limonene produced over 20 wt% WO_3/Al_2O_3 calcined at various temperatures. The yields increased with calcination temperature up to 1123 K and then decreased above 1123 K. The selectivities for camphene and limonene were almost constant up to 1273 K. Conversely, above 1273 K, the selectivities for camphene and β-pinene increased and that for limonene decreased. These results suggest that the number of acid sites increased up to 1273 K, although the acid strength remained constant. In contrast, calcinations above 1273 K may affect not only the number of acid sites but also the acid strength.

The results for benzylation of anisole over WO_3/Al_2O_3 calcined at 1123 K with various loadings of WO_3 are presented in Figure 2a. The loading amount of WO_3 significantly affected the yields of benzyl anisoles. Alumina and WO_3 alone were almost inactive. The catalytic activity suddenly increased from 10 wt% WO_3 and the maximum yield was obtained for 20 wt% WO_3. When the loading exceeded 20 wt%, the catalytic activity gradually decreased. The ratio of *p*-benzyl anisole to *o*-benzyl anisole was ca. 3/2 regardless of WO_3 loading amount.

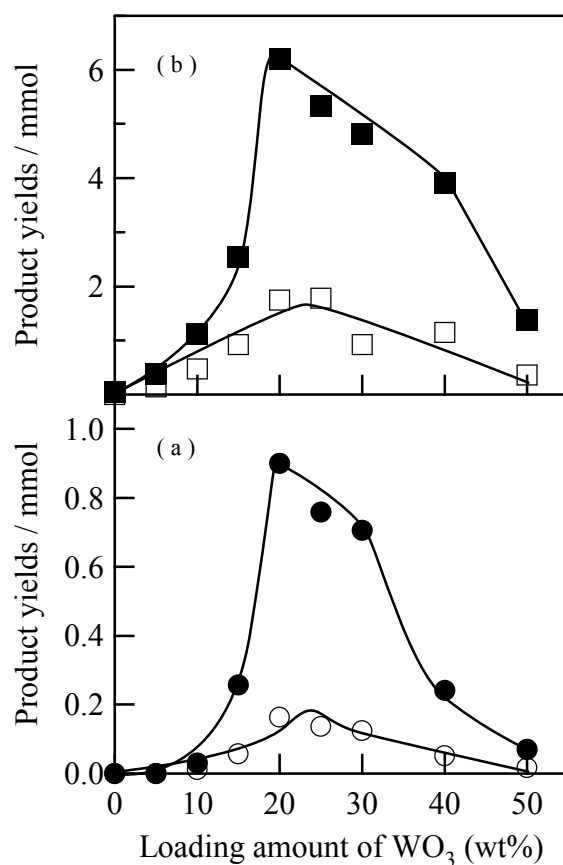**Figure 2.** Activity of WO_3/Al_2O_3 calcined at 1123 K with various loadings (a) for Friedel–Crafts alkylation ((●) benzyl anisole and (○) dibenzyl ether), (b) for isomerization of α-pinene ((■) camphene and (□) limonene). Pretreatment temperature : 473 K.

Such constant selectivity showed that the acid strength was independent of the WO_3 loading amount but the amount of acid sites varied.

The results of isomerization of α-pinene over WO_3/Al_2O_3 calcined at 1123 K with various WO_3 loadings are summarized in Table 2 and Figure 2b. The yields of camphene and limonene increased with loading up to 20 wt% WO_3. Over 20 wt% WO_3, the yield of these compounds decreased. On alumina alone, mainly camphene and β-pinene were produced. The selectivities for camphene and β-pinene decreased and that for limonene increased as the loading amount increased to 10 wt% WO_3. No significant change of selectivity was found in the range of 15–30 wt% WO_3, whereas the selectivity for camphene increased from 40 wt% WO_3. These results indicate that the number of acid sites changed, but the acid strength and acid type did not in the range of 10–30 wt% WO_3. Houalla et al.[43] investigated the effect of WO_3 loading amount on the acidity of WO_3/Al_2O_3 calcined at 1073 K and suggested that the number of Brønsted acid sites increased when the WO_3 loading exceeded 1.4 atoms of W/nm^2 (9.65 wt%). In this study, WO_3/Al_2O_3 calcined at 1123 K showed activity when the loading amount was 10 wt%, which is consisitent with their results.

Table 2. Results for α-pinene isomerization on WO_3/Al_2O_3 Calcined at 1123 K with various WO_3 loadings[a]

Loading amount of WO_3 (wt%)	Conversion (%)	Selectivity[b] (%)							
		1	2	3	4	5	6	7	8
0	15.9	tr	75	25	tr	tr	tr	tr	tr
5	7.6	tr	61	9	1	22	1	4	2
10	22.1	tr	60	3	2	25	1	5	4
15	37.4	1	64	tr	2	23	tr	6	3
20	94.5	2	66	tr	4	18	3	7	1
25	79.7	1	66	tr	3	22	tr	6	2
30	90.4	1	67	tr	3	19	tr	7	3
40	50.5	1	70	tr	2	20	tr	5	2
50	24.2	1	72	1	1	18	tr	5	2

[a] Pretreatment temperature : 473 K.
[b] 1 : α-fenchene, 2 : camphene, 3 : β-pinene, 4 : α-terpinene, 5 : limonene, 6 : γ-terpinene, 7 terpinolene, 8 others.

The effects of pretreatment temperature on isomerization of α-pinene over 20 wt% WO_3/Al_2O_3 calcined at 1123 K is presented in Figure 3. The highest yields of camphene and limonene were obtained when the catalyst was pretreated at 473 K. Although the yield of camphene decreased gradually as the pretreatment temperature increased, WO_3/Al_2O_3 showed activity even after evacuation at 1173 K (ca. 2/3 of the yield of that pretreated at 473 K), indicating that Brønsted acid sites on WO_3/Al_2O_3 are thermally stable. In the previous report, we reported that the activity of α-pinene isomerization over Nb_2O_5/Al_2O_3 pretreated at 1173 K was almost same to the activity pretreated at 673 K and Brønsted acid sites on Nb_2O_5/Al_2O_3 calcined at high temperature were thermally stable. In contrast, the activity over zeolites and silica-alumina decreased significantly following pretreatment at 1173 K.

Because benzylation of anisole and isomerization of α-pinene are reported to be promoted by Brønsted acid sites, and the catalytic activity of WO_3/Al_2O_3 strongly depended on the loading amount of WO_3 and calcination temperature, the Brønsted acidity of WO_3/Al_2O_3 prepared under various conditions was measured by pyridine adsorbed FT-IR spectra. Brønsted acid property was estimated from the specific amount of pyridinium ions adsorbed on each WO_3/Al_2O_3 samples, and Lewis acid property was estimated from the amount of pyridine coordinated to Lewis acid sites.
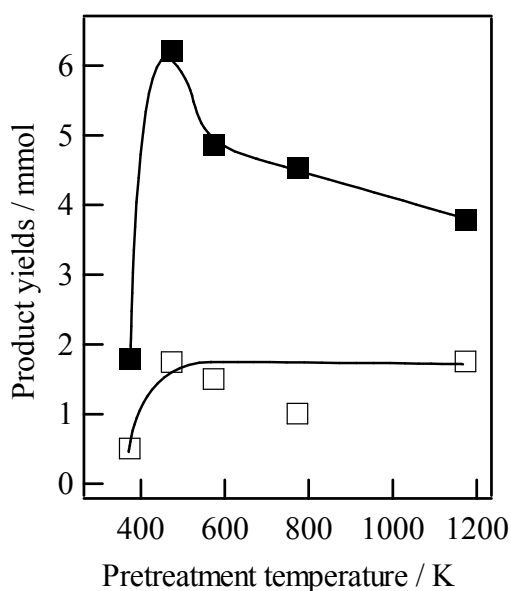

Figure 3. Activity of 20 wt% WO_3/Al_2O_3 calcined at 1123 K pretreated at various temperature for isomerization of α-pinene ((■) camphene and (□) limonene).

Figure 4 shows IR spectra of adsorbed pyridine on Al_2O_3 and 20 wt% WO_3/Al_2O_3 calcined at 1123 K. Four bands at 1447, 1490, 1578, and 1609 cm^{-1} were observed in the IR spectrum of alumina.[44-47] These four bands correspond to pyridine species adsorbed on Lewis acid sites. In contrast, WO_3/Al_2O_3 exhibited new bands at 1543 and 1640 cm^{-1} corresponding to pyridine species adsorbed on Brønsted acid sites. Therefore, the presence of WO_3 generates Brønsted acid sites. The specific amount of Brønsted acid sites determined from pyridinium ions was calculated using an integrated molar adsorption coefficient value of $\varepsilon = 1.67$ cm µmol^{-1} for the band area at 1545 cm^{-1} of protonated pyridinium ions.[46,47] The calculated Brønsted acidity of 20 wt% WO_3/Al_2O_3 calcined at various temperatures is shown in Figure 5. Brønsted acidity increased with calcination temperature up to 1123 K, while calcination at temperatures above 1123 K resulted in a reduction of Brønsted acidity. This result shows that high temperature calcination is important for generation of Brønsted acid sites. The Brønsted acidity of WO_3/Al_2O_3 calcined at 1123 K with various WO_3 loading amount is presented in Figure 6. No Brønsted acid sites were present on Al_2O_3, and Brønsted acidity increased with WO_3 loading up to 20 wt%. Above 10 wt%, Brønsted acidity increased sharply and 20 wt% WO_3/Al_2O_3 exhibited the highest Brønsted acidity of the catalysts. Brønsted acidity gradually decreased for samples with loadings over 20 wt%.
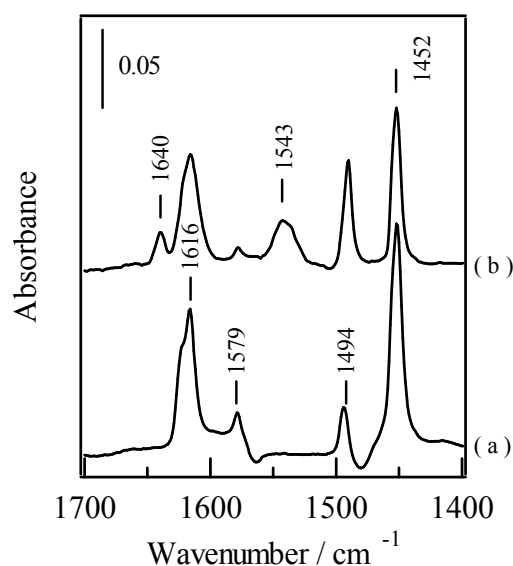
Figure 4. IR spectra of pyridine adsorbed on (a) γ-Al_2O_3 and (b) 20 wt% WO_3/Al_2O_3 calcined at 1123 K.

The yield of benzyl anisole, camphene and limonene are proportional to the Brønsted acidity of the catalyst (Figure 7), indicating that Friedel–Crafts reaction and isomerization of α-pinene occurred at the Brønsted acid sites.
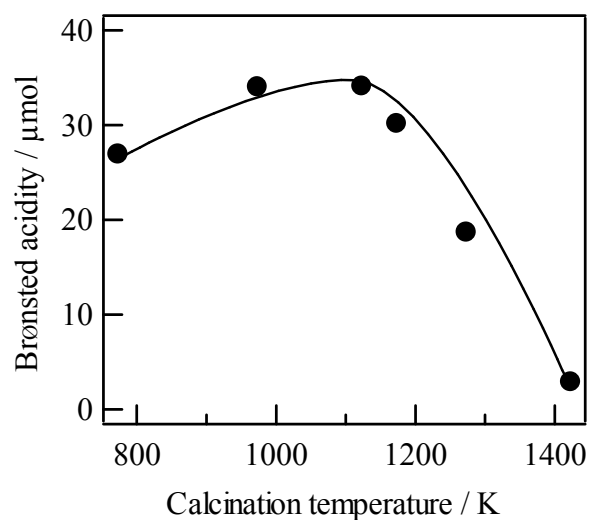
Figure 5. Brønsted acidity over 20 wt% WO_3/Al_2O_3 calcined at various temperature.

Figure 6. Brønsted acidity over WO_3/Al_2O_3 calcined at 1123 K with various loadings.
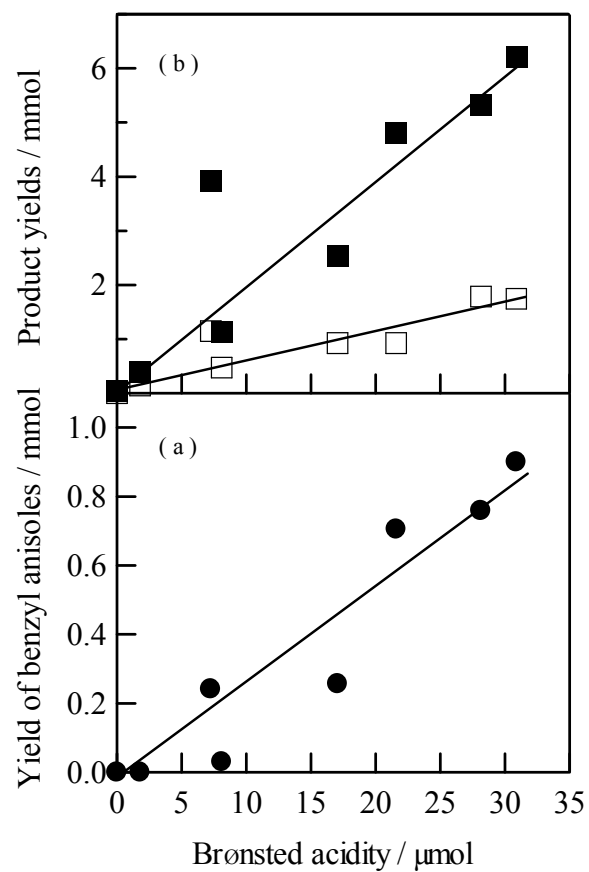
Figure 7. Correlation between catalytic activities over WO_3/Al_2O_3 calcined at 1123 K with various loadings and Brønsted acidity of samples.
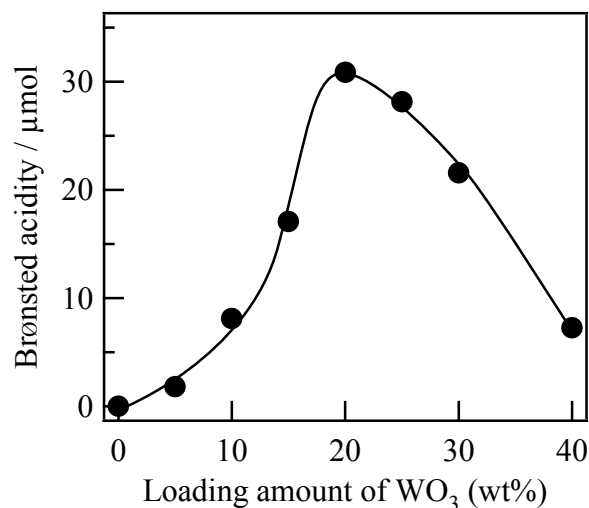(a) Benzylation of anisole, (b) isomerization of α-pinene ((■) camphene and (□) limonene).

Characterizations

Figure 8 and 9 show XRD patterns and Raman spectra, respectively, of 20 wt% WO_3/Al_2O_3 calcined at various temperatures. Diffraction lines consistent with γ-Al_2O_3 were observed for all 20 wt% WO_3/Al_2O_3. In contrast, crystalline WO_3 was not observed in WO_3/Al_2O_3 calcined below 1173 K. Monoclinic WO_3 (m-WO_3) was found in WO_3/Al_2O_3 calcined at 1173 K, which then transformed to $Al_2W_3O_{12}$ when the catalyst was calcined at 1273 K.
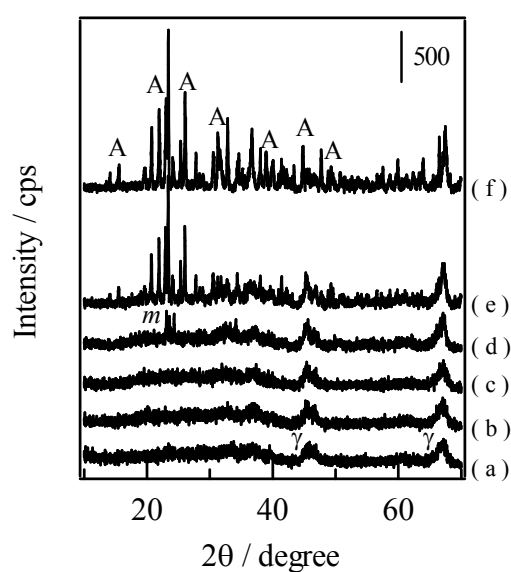
Figure 8. XRD patterns of 20 wt% WO_3/Al_2O_3 calcined at various temperatures. (a) 773 K, (b) 1073 K, (c) 1123 K, (d) 1173 K, (e) 1273 K, and (f) 1423 K. γ = γ-Al_2O_3; m = m-WO_3 ; A = $Al_2W_3O_{12}$
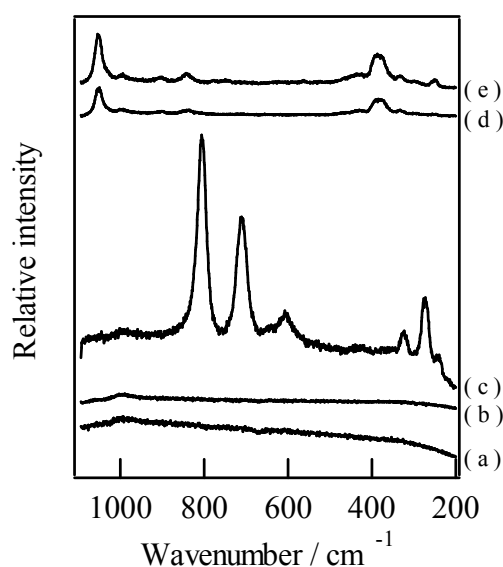
Figure 9. Raman spectra of 20 wt% WO_3/Al_2O_3 calcined at various temperatures. (a) 1073 K, (b) 1123 K, (c) 1173 K, (d) 1273 K, and (e) 1423 K.

Because m-WO$_3$ and Al$_2$W$_3$O$_{12}$ have no Brønsted acid sites and did not promote benzylation of anisole and isomerization of α-pinene, it is supposed that formation of m-WO$_3$ and Al$_2$W$_3$O$_{12}$ cause the number of Brønsted acid sites on WO$_3$/Al$_2$O$_3$ calcined at temperatures higher than 1123 K to decrease. XRD patterns and Raman spectra of WO$_3$/Al$_2$O$_3$ calcined at 1123 K with various WO$_3$ loadings were also measured (Figures 10 and 11, respectively).
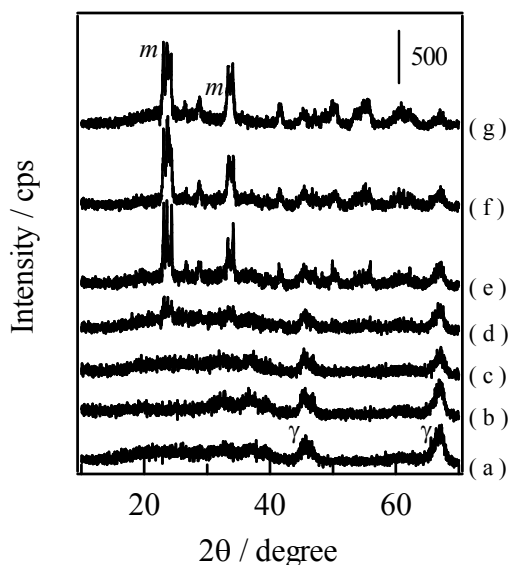
Figure 10. XRD patterns of WO$_3$/Al$_2$O$_3$ calcined at 1123 K with various loadings. (a) 5 wt%, (b) 15 wt%, (c) 20 wt%, (d) 25 wt%, (e) 30 wt%, (f) 40 wt%, and (g) 50 wt%. γ = γ-Al$_2$O$_3$; m = m-WO$_3$.
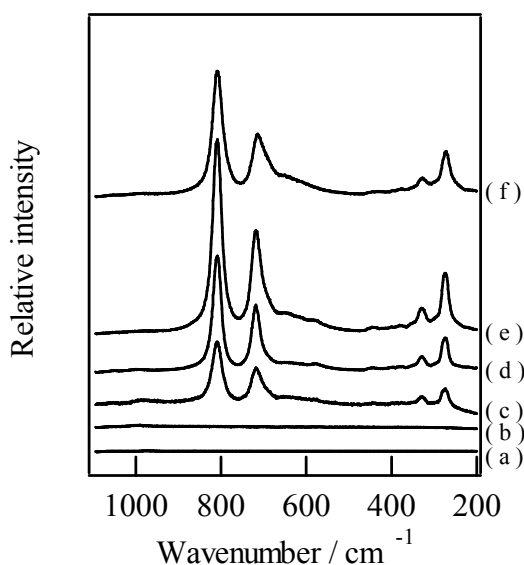
Figure 11. Raman spectra of WO$_3$/Al$_2$O$_3$ calcined at 1123 K with various loadings. (a) 10 wt%, (b) 20 wt%, (c) 25 wt%, (d) 30 wt%, (e) 40 wt%, and (f) 50 wt%.

20 wt% WO_3/Al_2O_3 did not show any diffraction peak or Raman shifts consistent with m-WO_3 or $Al_2W_3O_{12}$. m-WO_3 appeared for 25 wt% WO_3/Al_2O_3 and its contribution grew as the WO_3 loading increased. Considering the change in acid property related to formation of m-WO_3 and $Al_2W_3O_{12}$, the Brønsted acidity on WO_3/Al_2O_3 decreased with higher WO_3 loading above 20 wt%. These results suggest that amorphous tungsten oxide is the source of Brønsted acid sites.

The surface W/Al ratio on the catalysts was estimated from the areas of W 4f and Al 2p XPS. The binding energies of W $4f_{7/2}$ and W $4f_{5/2}$ peaks of WO_3/Al_2O_3 catalysts were found to be 35.5 and 37.6 eV, respectively. These binding energies were constant regardless of calcination temperature and loading amount of WO_3. This indicates that the valence of the tungsten cation of WO_3/Al_2O_3 catalyst was W^{6+} regardless of calcination temperature and WO_3 loading amount. The surface W/Al ratio for 20 wt% WO_3/Al_2O_3 calcined at various temperatures was constant, indicating that W atoms did not penetrate into the bulk structure independent of calcination temperature. Figure 12 shows the surface W/Al ratio of WO_3/Al_2O_3 calcined at 1123 K with various WO_3 loading. The surface W/Al ratio increased linearly with WO_3 loading up to 20 wt%, but then increased gradually. The cross-sectional area of a WO_6 octahedral unit is 0.22 nm^{-2}, so when WO_3 is loaded on alumina as 20 wt%, the surface of the catalyst is completely covered. This suggests that a monolayer of tungsten oxide was formed on 20 wt% WO_3/Al_2O_3. Because the maximum Brønsted acidity was observed for 20 wt% WO_3/Al_2O_3, a monolayer of tungsten oxide generated Brønsted acid sites.
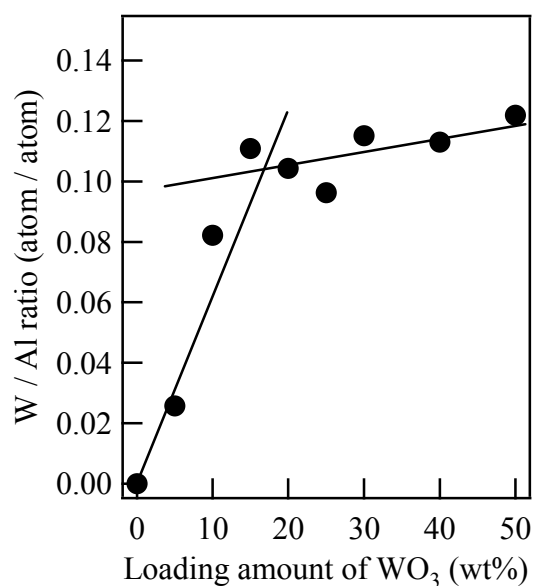
Figure 12. Atomic ratio of WO_3/Al_2O_3 calcined at 1123 K with various loadings.

The local structure of WO_3/Al_2O_3 catalysts was characterized by W L_1–edge and W L_3-edge XAFS spectra. Figure 13 shows W L_1-edge X-ray absorption near-edge structure (XANES) spectra of WO_3/Al_2O_3 calcined at 1123 K with various loadings along with reference samples. The pre-edge peak observed in W L_1-edge XANES spectra, which is assigned to the transition from 2s to d-p orbitals, is sensitive to the symmetry around W, [48-50] and can be used to provide information on local symmetry. The shapes of the spectra of WO_3/Al_2O_3 resemble to that of WO_3, indicating that the local structure of WO_3 supported on alumina is similar to that of WO_3. The tungsten oxide unit in WO_3/Al_2O_3 samples is distorted from ideal octahedral symmetry, because the pre-edge peak in the W L_1-edge XANES spectra is intense. Therefore the pre-edge peak of Na_2WO_4 (tetrahedral WO_4) is much more intense than that of tungsten oxide (distorted octahedral), and that of $SrCaWO_3$ (octahedral WO_6) is much less intense than that of tungsten oxide. When the WO_3 loading is lower than 20 wt%, the pre-edge peak area of WO_3/Al_2O_3 is larger than that of $SrCaWO_3$ and smaller than that of Na_2WO_4, indicating that the coordination symmetry of W species on WO_3/Al_2O_3 is distorted octahedral.
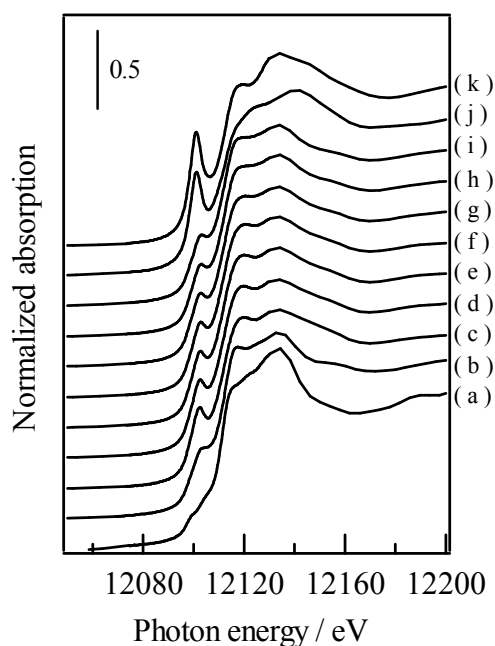
Figure 13. W L_1-edge XANES spectra of reference samples and WO_3/Al_2O_3 calcined at 1123 K with various loadings.
(a) Sr_2CaWO_6, (b) m-WO_3, (c) 5 wt%, (d) 10 wt%, (e) 15 wt%, (f) 20 wt%, (g) 25 wt%, (h) 30 wt%, (i) 40 wt%, (j) $Al_2W_3O_{12}$, and (k) Na_2WO_4.

The W L$_3$-edge k^3-weighted extended X-ray adsorption fine structure (EXAFS) oscillations of WO$_3$/Al$_2$O$_3$ catalysts with various loadings and reference samples are shown in Figure 14. The shape of the EXAFS oscillations of WO$_3$/Al$_2$O$_3$ catalysts with loading of WO$_3$ up to 20 wt% was constant. Over 20 wt%, the shape of the EXAFS oscillations of the WO$_3$/Al$_2$O$_3$ catalysts resemble in the range of 3–5 Å and 8–10 Å to that of WO$_3$ with increase of WO$_3$ loading than 20 wt%. This result indicates that amorphous WO$_3$ gradually transformed to crystaline WO$_3$ on the WO$_3$/Al$_2$O$_3$ catalysts with loadings of WO$_3$ above 20 wt%. Figure 15 shows Fourier transformed EXAFS oscillations of WO$_3$/Al$_2$O$_3$ catalysts with various loadings and reference samples. There were two peaks observed at 1.4 and 3.6 Å in the radial structure functions (RSFs) of WO$_3$ that correspond to W– O and W–(O)–W linkages, respectively. Until a WO$_3$ loading of 20 wt%, only one peak at 1.4 Å was found. A new peak at 3.6 Å appeared and increased in intensity for WO$_3$/Al$_2$O$_3$ with WO$_3$ loadings higher than 20 wt%. This indicates that W–(O)–W linkages of various length were formed on 20 wt% WO$_3$/Al$_2$O$_3$, and that W–(O)–W linkages with a certain length in WO$_3$ clusters were mixed and their length increased for WO$_3$/Al$_2$O$_3$ with WO$_3$ loading exceeding 20 wt%. These results imply that monolayer tungsten oxide domains are formed on the 20 wt% WO$_3$/Al$_2$O$_3$ catalyst. Considering that the 20 wt% WO$_3$/Al$_2$O$_3$ catalyst exhibits the highest Brønsted acidity, monolayer tungsten oxide domains having with m-WO$_3$ like structure may play an important role in the generation of Brønsted acid sites.

Figure 14. W L$_3$-edge k^3-weighted EXAFS of reference samples and WO$_3$/Al$_2$O$_3$ calcined at 1123 K with various loadings.

(a) m-WO$_3$, (b) 5 wt%, (c) 10 wt%, (d) 15 wt%, (e) 20 wt%, (f) 25 wt%, (g) 30 wt%, (h) 40 wt%, and (i) Al$_2$W$_3$O$_{12}$.

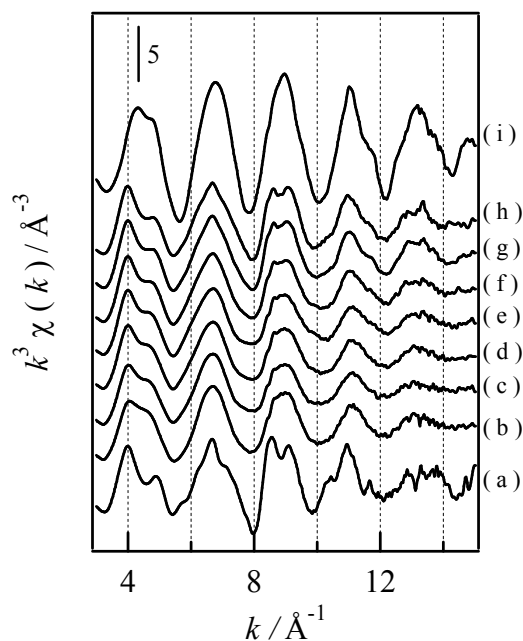**Figure 15.** Fourier transforms of W L$_3$-edge k^3-weighted EXAFS of reference samples and WO$_3$/Al$_2$O$_3$ calcined at 1123 K with various loadings.

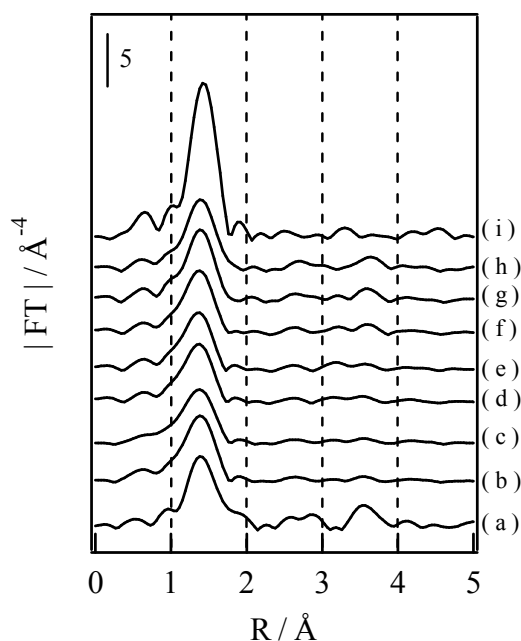(a) m-WO$_3$, (b) 5 wt%, (c) 10 wt%, (d) 15 wt%, (e) 20 wt%, (f) 25 wt%, (g) 30 wt%, (h) 40 wt%, and (i) Al$_2$W$_3$O$_{12}$.

The physical properties of WO_3/Al_2O_3 catalysts also depended on calcination temperature and loading amount of WO_3. The physical properties of WO_3/Al_2O_3 with various loadings are summarized in Table 3. The catalyst areas include that of the alumina support. S_0 is the surface area $g(Al_2O_3)^{-1}$ of a carrier, and was calculated from the BET specific surface area and WO_3 content. $S_{occupied}$ is the estimated area occupied by WO_6 units. It was assumed that all WO_3 was present as WO_6 octahedra and the area of each unit is 0.22 nm^2.[51] Increase the loading amount of WO_3 caused the surface are of WO_3/Al_2O_3 to decrease. It is supposed that shrinking of the Al_2O_3 support is a cause of this decrease. The areas of the alumina support (S_0) decreases and the area occupied by WO_6 units ($S_{occupied}$) increases with loading amount of WO_3, and $S_{occupied}$ becomes comparable to S_0 at 20 wt%. Considering the results of XPS, at just 20 wt%, WO_3 monolayer covered most of surface of the alumina support. The surface density of W atoms on 20 wt% WO_3/Al_2O_3 calcined at 1123 K is estimated to be 4.4 atoms nm^{-2}. Wachs and colleagues[52] reported that monolayer coverage of WO_3 on alumina corresponds to 4.0 atom nm^{-2}, which is comparable to our estimated value. These results mean that WO_3 is loaded as a two-dimensional monolayer at loadings less than 20 wt%. The acid properties of supported tungsten oxide have been investigated by a lot of researchers.

Table 3. Physical properties of WO_3/Al_2O_3 calcined at 1123 K

W content		$Area^b$ / m^2g^{-1}	S_0^c / m^2	$S^d_{occupied}$ / m^2 $g(cat)^{-1}$	$S^d_{occupied}$ / m^2 $g(Al_2O_3)^{-1}$
mmol $g(Al_2O_3)^{-1}$	$(wt\%)^a$				
0	0	124	124	0	0
0.22	5	131	138	28.6	30.1
0.48	10	120	133	57.1	63.4
0.76	15	119	140	85.7	101
1.08	20	118	148	114	143
1.44	25	101	135	143	191
1.85	30	93	133	171	244
2.88	40	85	142	229	382
4.31	50	51	102	286	572

[a] As WO_3
[b] BET specific surface area
[c] Surface area of $g(Al_2O_3)^{-1}$ carrier
[d] Occupied area by WO_3 unit (0.22 nm^2)

WO_3/ZrO_2 is one of the solid superacid catalysts and many researchers inspected the acid property and the structure of tungsten oxide supported on zirconia.[13-18,50,53-56] The acid properties of WO_3/ZrO_2 are also affected by calcination and loading amount of WO_3. It has been reported that WO_3/ZrO_2 shows the highest activity when the surface density of tungsten oxide is 7–8 atom nm^{-2}, which is a slightly larger than the loading amount at which a tungsten oxide monolayer cover the ZrO_2 support.[13,17,55] Moreover, some researchers reported that tungsten oxide is loaded as a monolayer on zirconia, and polymeric tungsten oxide plays a role in generating acid sites.[17,18] These results indicate that two-dimensional tungsten oxide is important in generation of acid sites.

In this study, the changes in acid properties and structure of WO_3/Al_2O_3 with WO_3 loading amount may be summarized as follows. (1) The activity for acid-catalyzed reactions and Brønsted acidity increased with loading amount up to 20 wt%. (2) The acid strength did not change with loading amount. (3) The ratio of Brønsted acidity to W atoms supported on WO_3/Al_2O_3 was quite small (0.04) for 20 wt% WO_3/Al_2O_3 calcined at 1123 K. (4) The surface was covered with a two-dimensional tungsten oxide monolayer up to 20 wt% loadings. Based on these results, we concluded that hydroxyl groups formed at the boundary of tungsten oxide monolayer domains act as Brønsted acid sites (Figure 16).
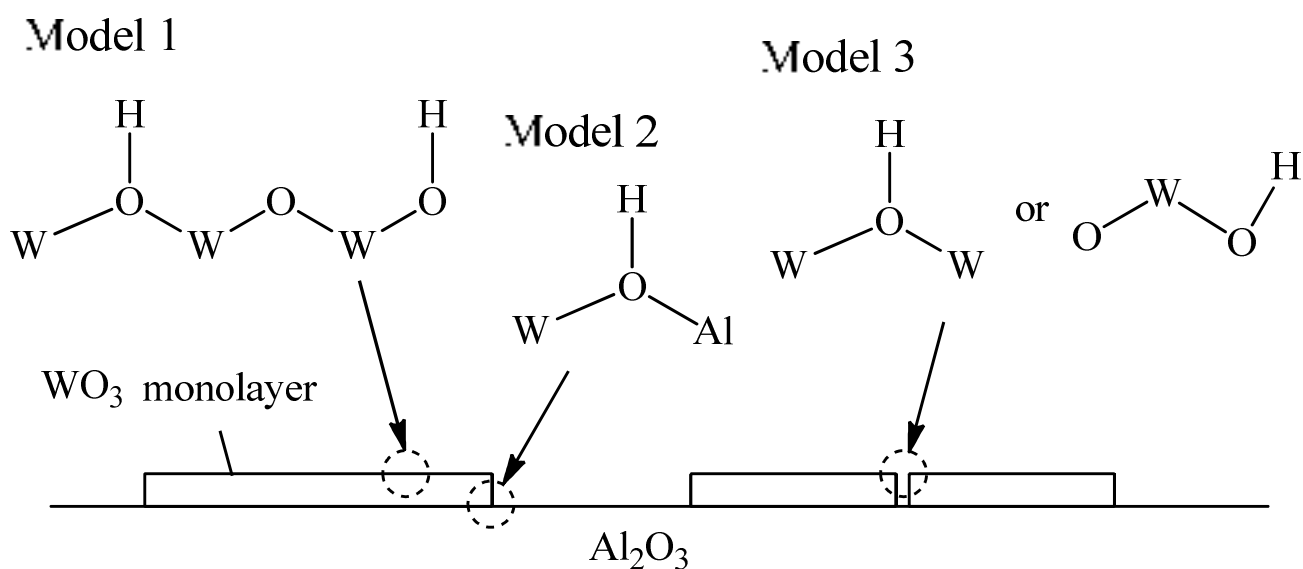

Figure 16. Structure models of Brønsted acid sites on WO_3/Al_2O_3.

First, tungsten monolayer domains are dispersed on alumina and few boundaries between domains are present. As the WO_3 loading amount increases, the number of monolayer domains and coverage increase, so boundaries between tungsten oxide monolayer domains form and simultaneously the number of Brønsted acid sites increase. Around 20 wt%, tungsten oxide monolayer domains cover most of the alumina surface, and the number of boundaries increased, resulting in a significant increase of Brønsted acidity. If Brønsted acid sites are generated on the tungsten oxide monolayer domains (W-OH or W-(OH)-W) or on the edges of tungsten oxide monolayer domains and alumina (W-(OH)-Al), the activity and Brønsted acidity would increase linearly with loading amount.

Figure 17 shows a model for the generation of Bronsted acid sites by high temperature calcination. The surface area of alumina decreased when alumina was calcined at high temperatures because the alumina shrunk. On WO_3/Al_2O_3 calcined at low temperatures such as 773 K, tungsten oxide monolayer domains are dispersed on alumina surface. In this case, the number of Brønsted acid sites is small because the number of boundaries between WO_3 monolayer domains is small. Upon increasing calcination temperature, tungsten oxide monolayer domains assemble and the number of boundaries increases because the alumina shrinks. As a result, Brønsted acidity increases with calcination temperature up to 1123 K. Calcination at temperatures higher than 1123 K causes the number of Brønsted acid sites to decrease because of aggregation of tungsten oxide monolayer domains to form inert crystalline WO_3 and $Al_2W_3O_{12}$.

We concluded that generation of Brønsted acid sites by calcination at high temperatures is related to (1) the formation of tungsten oxide monolayer domains on the surface of alumina, and (2) the formation of boundaries between domains of tungsten oxide monolayer. (3) The shrinkage of alumina upon calcination at high temperatures reduces its surface area. As a result, the distance between domains of tungsten oxide monolayer decreases, allowing boundaries between tungsten monolayer domains generate Brønsted acid sites.
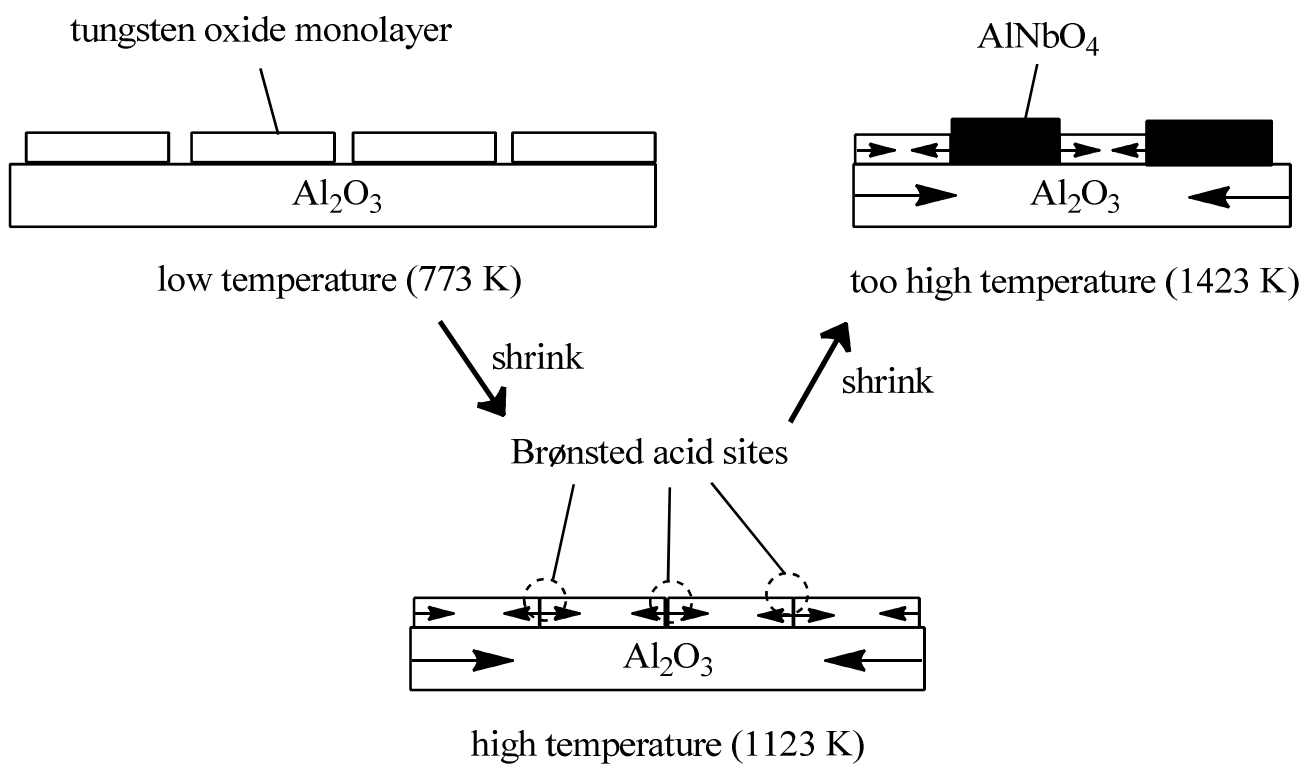
Figure 17. Generation mechanism of Brønsted acid sites on WO_3/Al_2O_3 calcined at high temperature.

Conclusions

WO$_3$/Al$_2$O$_3$ calcined at high temperature exhibited catalytic activities for benzylation of anisole and isomerization of α-pinene, and Brønsted acidity. Calcination temperature and loading amount of WO$_3$ affected the acid properties and structure of WO$_3$/Al$_2$O$_3$. 20 wt% WO$_3$/Al$_2$O$_3$ calcined at 1123 K exhibited both the highest reactivity and Brønsted acidity. WO$_3$/Al$_2$O$_3$ showed activity for isomerization of α-pinene even after evacuation at 1173 K, indicating that Brønsted acid sites generated on WO$_3$/Al$_2$O$_3$ were thermally stable. Tungsten oxide was loaded as two-dimensional monolayer domains below 20 wt% and these domains covered most of the alumina surface at 20 wt%. Additional loading of WO$_3$ cause the formation of inert WO$_3$ crystals and a decrease of Brønsted acidity. Brønsted acid sites are probably generated at the boundaries of tungsten oxide monolayer domains. A proposed generation mechanism of Brønsted acid sites is as follows: At low loading amount, tungsten oxide monolayer domains are dispersed on alumina and few boundaries are present between domains. As the WO$_3$ loading increases, the number of tungsten oxide monolayer domains increase and boundaries between domains form Brønsted acid sites. When tungsten oxide monolayer domains cover most of the alumina surface (20 wt% WO$_3$/Al$_2$O$_3$), the amount of boundaries between tungsten oxide monolayer domains is maximized, generating the largest number of Brønsted acid sites.

References

(1)   Okuhara, T.; Mizuno, N.; Misono, M. In *Advances In Catalysis*; 1996; Vol. 41; pp 113.

(2)   Lana, E. J. L.; Rocha, K. A. D.; Kozhevnikov, I. V.; Gusevskaya, E. V. *J. Mol. Catal. A,* **2006**, *243*, 258.

(3)   Lana, E. J. L.; da Silva Rocha, K. A.; Kozhevnikov, I. V.; Gusevskaya, E. V. *J. Mol. Catal. A,* **2006**, *259*, 99.

(4)   Zhang, J.; Kanno, M.; Wang, Y.; Nishii, H.; Miura, Y.; Kamiya, Y. *J.Phys. Chem. C,* **2011**, *115*, 14762.

(5)   Rafiee, E.; Rashidzadeh, S.; Azad, A. *J. Mol. Catal. A,* **2007**, *261*, 49.

(6)   Firouzabadi, H.; Iranpoor, N.; Jafari, A. A.; Jafari, M. R. *J. Mol. Catal. A,* **2006**, *247*, 14.

(7)   Nakato, T.; Kimura, M.; Nakata, S.; Okuhara, T. *Langmuir,* **1998**, *14*, 319.

(8)   Okuhara, T. *Chem. Rev.,* **2002**, *102*, 3641.

(9)   Izumi, Y.; Hasebe, R.; Urabe, K. *J. Catal.,* **1983**, *84*, 402.

(10)   Izumi, Y.; Ono, M.; Kitagawa, M.; Yoshida, M.; Urabe, K. *Microporous Mater.,* **1995**, *5*, 255.

(11)   Kozhevnikov, I. V. *Chem. Rev.,* **1998**, *98*, 171.

(12)   Jalil, P. A.; Tabet, N.; Faiz, M.; Hamdan, N. M.; Hussain, Z. *Appl. Catal. A-Gen.,* **2004**, *257*, 1.

(13)   Santiesteban, J. G.; Vartuli, J. C.; Han, S.; Bastian, R. D.; Chang, C. D. *J. Catal.,* **1997**, *168*, 431.

(14)   Arata, K. *Appl. Catal. A-Gen.,* **1996**, *146*, 3.

(15)   Arata, K.; Nakamura, H.; Shouji, M. *Appl. Catal. A-Gen.,* **2000**, *197*, 213.

(16)   Arata, K.; Matsuhashi, H.; Hino, M.; Nakamura, H. *Catal. Today,* **2003**, *81*, 17.

(17)   Barton, D. G.; Soled, S. L.; Meitzner, G. D.; Fuentes, G. A.; Iglesia, E. *J. Catal.,* **1999**, *181*, 57.

(18)   Naito, N.; Katada, N.; Niwa, M. *J. Phys. Chem. B,* **1999**, *103*, 7206.

(19)   Tanabe, K. *Catal. Today,* **1990**, *8*, 1.

(20)   Tanabe, K.; Okazaki, S. *Appl. Catal. A-Gen.,* **1995**, *133*, 191.

(21)   Tanabe, K. *Catal. Today,* **2003**, *78*, 65.

(22)   Ushikubo, T.; Wada, K. *Appl. Catal.,* **1990**, *67*, 25.

(23)   Ohuchi, T.; Miyatake, T.; Hitomi, Y.; Tanaka, T. *Catal. Today,* **2007**, *120*, 233.

(24)   Shishido, T.; Kitano, T.; Teramura, K.; Tanaka, T. *Catal. Lett.,* **2009**, *129*, 383.

(25)   Shishido, T.; Kitano, T.; Teramura, K.; Tanaka, T. *Top. Catal.,* **2010**, *53*, 672.

(26)   Kitano, T.; Shishido, T.; Teramura, K.; Tanaka, T. *J.Phys. Chem. C,* **2012**, *116*, 11615.

(27)   Ushikubo, T.; Wada, K. *Chem. Lett.,* **1988**, 1573.

(28)   Kitano, T.; Okazaki, S.; Shishido, T.; Teramura, K.; Tanaka, T. *Chem. Lett.,* **2011**, *40*, 1332.

(29)   Kitano, T.; Okazaki, S.; Shishido, T.; Teramura, K.; Tanaka, T. *Catal. Today,* **2012**, *192*, 189.

(30)   Hino, M.; Matsuhashi, H.; Arata, K. *Catal. Lett.,* **2006**, *107*, 161.

(31)   Soled, S. L.; McVicker, G. B.; Murrell, L. L.; Sherman, L. G.; Dispenziere, N. C.; Hsu, S. L.; Waldman, D. *J. Catal.,* **1988**, *111*, 286.

(32)   Ankudinov, A. L.; Ravel, B.; Rehr, J. J.; Conradson, S. D. *Phys. Rev. B,* **1998**, *58*, 7565.

(33)   de la Cruz, M. H. C.; da Silva, J. F. C.; Lachter, E. R. *Catal. Today,* **2006**, *118*, 379.

(34)   de la Cruz, M. H. C.; Abdel-Rehim, M. A.; Rocha, A. S.; da Silva, J. F. C.; Faro, A. D.; Lachter, E. R. *Catal. Commun.,* **2007**, *8*, 1650.

(35)   Yamashita, K.; Hirano, M.; Okumura, K.; Niwa, M. *Catal. Today,* **2006**, *118*, 385.

(36)   Okumura, K.; Yamashita, K.; Hirano, M.; Niwa, M. *Chem. Lett.,* **2005**, *34*, 716.

(37)   Okumura, K.; Yamashita, K.; Hirano, M.; Niwa, M. *J. Catal.,* **2005**, *234*, 300.

(38)   Cseri, T.; Bekassy, S.; Figueras, F.; Cseke, E.; Demenorval, L. C.; Dutartre, R. *Appl. Catal. A-Gen.,* **1995**, *132*, 141.

(39)   Tagusagawa, C.; Takagaki, A.; Hayashi, S.; Domen, K. *J. Am. Chem. Soc.,* **2008**, *130*, 7230.

(40)   Ohnishi, R.; Tanabe, K.; Morikawa, S.; Nishizak.T. *Bull. Chem. Soc. Jpn.,* **1974**, *47*, 571.

(41)   Yamamoto, T.; Tanaka, T.; Funabiki, T.; Yoshida, S. *J. Phys. Chem. B,* **1998**, *102*, 5830.

(42)   Yamamoto, T.; Tanaka, T.; Matsuyama, T.; Funabiki, T.; Yoshida, S. *J. Phys. Chem. B,* **2001**, *105*, 1908.

(43)   Chen, X.; Clet, G.; Thomas, K.; Houalla, M. *J. Catal.,* **2010**, *273*, 236.

(44)   Morterra, C.; Magnacca, G. *Catal. Today,* **1996**, *27*, 497.

(45)   Jacobs, P. A.; Leeman, H. E.; Uytterho.Jb. *J. Catal.,* **1974**, *33*, 17.

(46)   Barzetti, T.; Selli, E.; Moscotti, D.; Forni, L. *J. Chem. Soc.-Faraday Trans.,* **1996**, *92*, 1401.

(47)   Emeis, C. A. *J. Catal.,* **1993**, *141*, 347.

(48)   Yoshida, S.; Tanaka, T.; Hanada, T.; Hiraiwa, T.; Kanai, H.; Funabiki, T. *Catal. Lett.,* **1992**, *12*, 277.

(49)   Yoshida, H.; Tanaka, T.; Yoshida, T.; Funabiki, T.; Yoshida, S. *Catal. Today,* **1996**, *28*, 79.

(50)   Yamamoto, T.; Orita, A.; Tanaka, T. *X-Ray Spectrom.,* **2008**, *37*, 226.

(51)   Pfaff, C.; Zurita, M. J. P.; Scott, C.; Patino, P.; Goldwasser, M. R.; Goldwasser, J.; Mulcahy, F. M.; Houalla, M.; Hercules, D. M. *Catal. Lett.,* **1997**, *49*, 13.

(52)   Wachs, I. E. *Catal. Today,* **1996**, *27*, 437.

(53)   Ross-Medgaarden, E. I.; Knowles, W. V.; Kim, T.; Wong, M. S.; Zhou, W.; Kiely, C. J.;

Wachs, I. E. *J. Catal.,* **2008**, *256*, 108.

(54)   Zhou, W.; Ross-Medgaarden, E. I.; Knowles, W. V.; Wong, M. S.; Wachs, I. E.; Kiely, C. J. *Nat. Chem.,* **2009**, *1*, 722.

(55)   Scheithauer, M.; Grasselli, R. K.; Knozinger, H. *Langmuir,* **1998**, *14*, 3019.

(56)   Afanasiev, P.; Geantet, C.; Breysse, M.; Coudurier, G.; Vedrine, J. C. *J. Chem. Soc.-Faraday Trans.,* **1994**, *90*, 193.

Chapter 6

Brønsted Acid Generation of Alumina-Supported Molybdenum Oxide Calcined at High Temperatures: Characterization by Acid-Catalyzed Reactions and Spectroscopic Methods

Abstract

The acidic properties of alumina-supported molybdenum oxide (MoO_3/Al_2O_3) calcined at high temperatures, with MoO_3 loadings of 5-30 wt%, were investigated using acid-catalyzed reactions (benzylation of anisole and isomerization of α-pinene), and Fourier-transformed infrared spectroscopy. The structure of MoO_3 on Al_2O_3 was characterized by X-ray diffraction (XRD), Raman spectroscopy, X-ray photoelectron spectra (XPS), and X-ray absorption fine structure (XAFS) analysis. The correlation between acidic property and structure is discussed. Brønsted acid sites, where acid-catalyzed reactions take place, are generated on MoO_3/Al_2O_3 by calcination at high temperature. 11 wt% MoO_3/Al_2O_3 calcined at 1073 K exhibited the highest activity, and the largest numbers of Brønsted acid sites were generated. XPS and Mo K-edge XAFS revealed that molybdenum oxide monolayer domains with distorted MoO_6 units and small MoO_3 clusters are formed and molybdenum oxide monolayer domains are stabilized on alumina below 11 wt% of MoO_3 loading. Brønsted acid sites are probably generated at boundaries between molybdenum oxide monolayer domains and/or small MoO_3 clusters. When the MoO_3 loading was sufficient to form two-dimensional molybdenum oxide overlayers (> 11 wt%), some of the Brønsted acid sites on MoO_3/Al_2O_3 was covered with $Al_2Mo_3O_{12}$ having no Brønsted acid site, resulting in a lowering of the catalytic activity.

Introduction

Molybdenum oxide catalysts are used in the wide range of petrochemical industry. Molybdenum oxide is usually used with supported on an inorganic oxide support (TiO_2, SiO_2, Al_2O_3, and ZrO_2) to improve catalytic activity and selectivity, life, and mechanical strength. Supported molybdenum oxides often show a good catalytic performance for selective oxidation of hydrocarbons,[1] oxidative dehydrogenation of alkanes,[2] and metathesis of olefins.[3] In the case of MoO_3/ZrO_2, it was reported that the catalyst exhibited high activity for acid-base reactions such as cracking of hexane,[4] benzoylation of toluene,[5] and hydrolysis of ethyl acetate.[6,7] MoO_3/ZrO_2 exhibits unique acid property; Arata[8] reported that MoO_3/ZrO_2 was one of the solid superacid catalysts and showed the highest acid strength to be $H_0 \leq -13$. Okuhara[6,7] reported that the MoO_3/ZrO_2 catalyst exhibits hydrophobicity and the acid property was enhanced by addition of water. On the other hand, MoO_3/Al_2O_3 is active for epoxidation of allyl alcohol,[9] oxidative dehydrogenation of propane,[10,11] and hydrodesulfurization of thiophene.[12] The activity and the active sites for selective oxidation[13] and hydrodesulfurization[12] were investigated. However, there are few reports discussing the relation between structure and acidic property of acid sites on MoO_3/Al_2O_3.

Recently, we reported that Brønsted acid sites were generated on Nb_2O_5/Al_2O_3 and Ta_2O_5/Al_2O_3 calcined at 1123 K and 1223 K despite calcination at high temperatures, which usually caused disappearance of acidic property. Niobic acid ($Nb_2O_5 \cdot nH_2O$, hydrated niobium oxide) is effective for reactions that relate to aqueous media including esterification, olefin hydration, alcohol dehydration and exhibits Brønsted acid property.[14-19] However, niobic acid loses their acid property when calcined at 773 K due to phase transformation.[20] On the other hand, Nb_2O_5/Al_2O_3 calcined at high temperature such as 1123 K showed activity in benzylation of anisole, cumene cracking, and isomerization of α-pinene, which proceeded on Brønsted acid sites. In a series of Nb_2O_5/Al_2O_3 catalyst, 16 wt% Nb_2O_5/Al_2O_3 calcined at 1123 K exhibited the highest activity and Brønsted acidity.[21-23] Moreover, Nb_2O_5/Al_2O_3 calcined at 1123 K maintained the activity for isomerization of α-pinene even after pretreatment at 1173 K. The result means that the Brønsted acid sites generated on Nb_2O_5/Al_2O_3 calcined at 1123 K are thermally quite stable. Ta_2O_5/Al_2O_3 calcined at 1223 K also show activity for benzylation of anisole and isomerization of α-pinene and exhibited Brønsted acid

property.[24,25] Hydrated tantalum oxide shows mainly Lewis acid properties in the absence of water, but water treatment causes generation of Brønsted acid sites.[26,27] Hydrated tantalum oxide loses the acid property by calcination at 1073 K, but 33 wt% Ta_2O_5/Al_2O_3 calcined at 1223 K exhibited the highest Brønsted acid property. These facts strongly suggest that alumina support plays a role of generation of thermally stable Brønsted acid sites and Nb_2O_5/Al_2O_3 and Ta_2O_5/Al_2O_3 calcined at high temperature work as thermally stable solid acid catalysts. The acidic property of Nb_2O_5/Al_2O_3 and Ta_2O_5/Al_2O_3 depends on both calcination temperature and loading amount due to structural change of Nb_2O_5 and Ta_2O_5. Based on characterization of Nb_2O_5/Al_2O_3 and Ta_2O_5/Al_2O_3, we proposed that niobium oxide and tantalum oxide were loaded as monolayer on alumina and concerned with generation of Brønsted acid sites.

Many researchers investigated the structure of molybdenum oxide supported on alumina calcined at moderate temperatures (773 - 873 K).[9-11,13,28,29] Isolated tetrahedral species are formed at very low loading amount of MoO_3 (under 5 wt%). On the other hand, octahedral polymolybdates are produced at higher loading amount than 5 wt%. When the MoO_3 loading is sufficient to form two-dimensional molybdenum oxide overlayers, MoO_3 crystal or $Al_2Mo_3O_{12}$ are formed on alumina. However, few papers reported the structure of molybdenum oxide supported on alumina calcined at higher temperatures than 873 K. Furthermore, the relation between the structure of molybdenum and the activity for selective oxidation,[9] oxidative dehydrogenation,[11] and hydrodesulfurization[12] on MoO_3/Al_2O_3 has been often studied. The relation between the structure of molybdenum oxide and the acidic property is still unclear.

In the present study, we investigated structural change in a series of alumina-supported molybdenum oxide catalysts with various loadings of MoO_3 (5 – 30 wt%) and calcined at various temperatures (773 – 1123 K) to clarify the correlation between their acidic properties and local structures around molybdenum species.

Experimental

Preparation

A series of MoO_3/Al_2O_3 catalysts were prepared by impregnation of γ-Al_2O_3 (JRC-ALO-8)

with an aqueous solution of ammonium molybdate tetrahydrate ($(NH_4)_6Mo_7O_{24} \cdot 4H_2O$) at 353 K, dried overnight at 353 K, and calcined at various temperature for 3 h in a dry air. Aluminum molybdate, $Al_2Mo_3O_{12}$, was synthesized from $Al(NO_3)_3 \cdot 9H_2O$ and $(NH_4)_6Mo_7O_{24} \cdot 4H_2O$. $Al(NO_3)_3 \cdot 9H_2O$ was dissolved in an aqueous solution and then oxalic acid (Wako, Osaka, Japan) and 28% ammonia solution were added to pH of 1.0 and 3.0, respectively. An aqueous solution of $(NH_4)_6Mo_7O_{24} \cdot 4H_2O$ was added to an aluminum solution in a ratio of Al/Mo = 1.0, and refluxed at 413 K for 1 h. The white paste obtained by removing water was dried at 423 K for 15 h, and $Al_2Mo_3O_{12}$ was formed by calcination of the solid at 1023 K for 4 h. MoO_3 was obtained by calcination of $(NH_4)_6Mo_7O_{24} \cdot 4H_2O$ at 773 K for 3 h.

Ractions

Benzylation of anisole (Friedel-Crafts alkylation of anisole with benzylalcohol) and isomerization of γ-pinene were employed as test reactions to examine the acid properties of MoO_3/Al_2O_3.

Benzylation of anisole was examined in a liquid phase. The catalysts (0.2 g) was pretreated in a N_2 flow at 473 K for 1 h and added to a mixture of benzyl alcohol (6.25 mmol) and anisole (92.5 mmol) in a 100 ml flask. The reaction was carried out at 383 K for 0.5 h and the products were determined by GLC (GC-14B with a flame ionization detector, Shimadzu, Kyoto, Japan) and GC-MS (Shimadzu GC-MS QP-5050), using a CBP10 column.

Isomerization of α-pinene was carried out under a dry N_2 atmosphere using a stirred batch reactor. Prior to each run, 0.05 g of sample was pretreated at 673 K under 13.3 kPa of O_2 for 1 h and followed by evacuation at the same temperature for 1 h. α-Pinene (12.5 mmol) was added in the reactor and stirred at 323 K for 3 h. The products were determined by GLC (Shimadzu GC-2014 with a flame ionization detector), using a CBP20 column.

Characterizations

The Brunauer-Emmett-Teller (BET) specific surface area was estimated from N_2 isotherm at 77 K. The N_2 adsorption isotherm measurements were carried out using a BELSORP 28SA (BEL Japan, Osaka, Japan) at 77 K. Prior to the measurement, each sample was evacuated at 673 K for 2 h.

X-ray diffraction (XRD) patterns were obtained using a MultiFlex DR Powder X-ray diffractometer (Rigaku, Tokyo Japan), using Cu Kα radiation ($\chi = 1.5405$ Å).

Laser Raman spectra were obtained using a NRS-2000 Raman Spectrometer (JASCO, Tokyo, Japan), using 514.5 nm line of an argon laser. The spectral resolution was 4 cm^{-1}.

FT-IR spectra were recorded using a SPETRUM ONE FT-IR spectrometer (Perkin-Elmer, Walthham, MA) with a resolution of 4 cm^{-1}. Each sample (13 mg) was pressed into a self-supporting wafer (diameter 13 mm). The catalysts were pretreated under 6.7 kPa of O_2 for 1 h at 673 K and then evacuated for 1 h at 673 K. For determination of the number of Brønsted and Lewis acid sites on MoO_3/Al_2O_3, the wafer was exposed to 0.667 kPa of pyridine vaper at 298 K for 10 min followed by evacuation at 423 K for 10 min.

X-ray photoelectron spectra (XPS) of the catalysts were acquired using an ULVAC PHI 5500MT system equipped with a hemispherical energy analyzer. Samples were mounted on indium foil and then transferred to an XPS analyzer chamber. The residual gas presser in the chamber during data acquisition was less than 1.33×10^{-6} Pa. The spectra were measured at room temperature using Mg Kα radiation. The electron take-off angle was set at 45 deg. Binding energy were referenced to O 1s level.

X-ray absorption experiments were carried out on the BL01B1 at SPring-8 (Hyogo, Japan). The ring energy was 8 GeV, and the stored current was 99.5 mA. The Mo K-edge (20.0 keV) X-ray absorption spectra were recorded in transmission mode in air or in N_2 at room temperature. A Si (311) and a Si (111) two crystal monochromator were used to obtain monochromatic X-ray beam. The data reduction was performed by the REX2000 Ver.2.5.9 (Rigaku) and FEFF8.40 programs.[30]

Results and Discussions

Catalysis

Figure 1a shows the results of benzylation of anisole over 11 wt% MoO_3/Al_2O_3 calcined at various temperatures. In this reaction, *p*- and *o*-benzyl anisoles were mainly formed and dibenzyl ether was minor product. Formation of multiply alkylated products was not observed. This reaction takes place on Brønsted acid sites and benzyl anisole is produced.[31-37] Dibenzyl ether is produced on Lewis acid sites due to dehydration between two molecules of benzyl alcohol. The amount of dibenzyl ether was less than 0.08 mmol in every reaction. The yield of benzyl anisole strongly

depended on the calcination temperature and increased with increasing calcination temperature up to 1073 K. When the catalyst was calcined at 1123 K, the yield decreased. The ratio of *p*-benzyl anisole to *o*-benzyl anisole was ca. 8/7 regardless of the calcination temperature. The results of isomerization of α-pinene over 11 wt% MoO_3/Al_2O_3 calcined at various temperature is summarized in Table 1. Isomerization of α-pinene is used for a test reaction to investigate acid-base property and acid strength of the catalyst.[38-40] The main products over MoO_3/Al_2O_3 were camphene and limonene, and the selectivities to camphene and limonene were ca. 57% and 33%, respectively. The minor products were β-pinene, fenchene, α-terpinene, γ-terpinene, and terpinolene. Products are divined in three groups (Scheme 1). The first group is β-pinene, which is produced on basic sites. The second group is bicyclic compound such as camphene and fenchene, and the last group is monocyclic compound such as limonene, terpinolene, α-terpinene, and γ-terpinene.

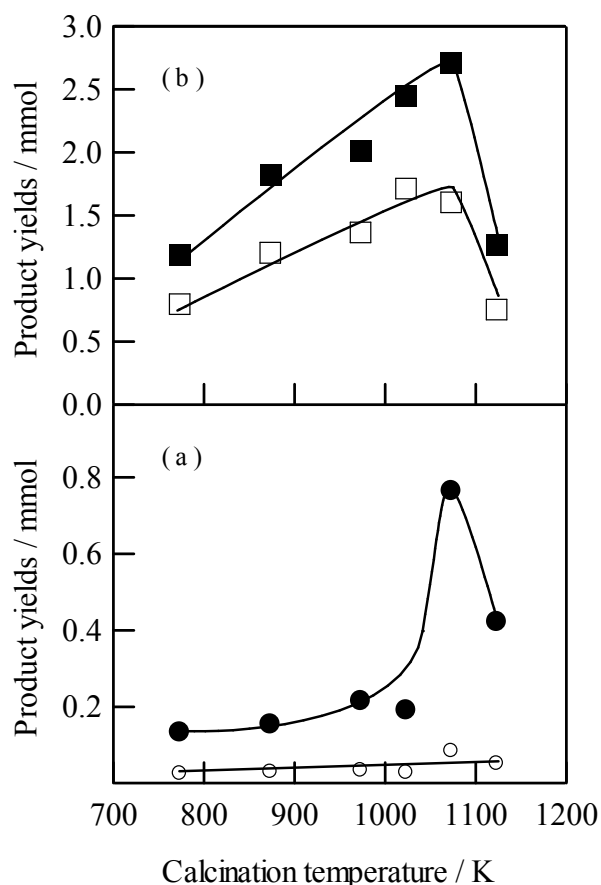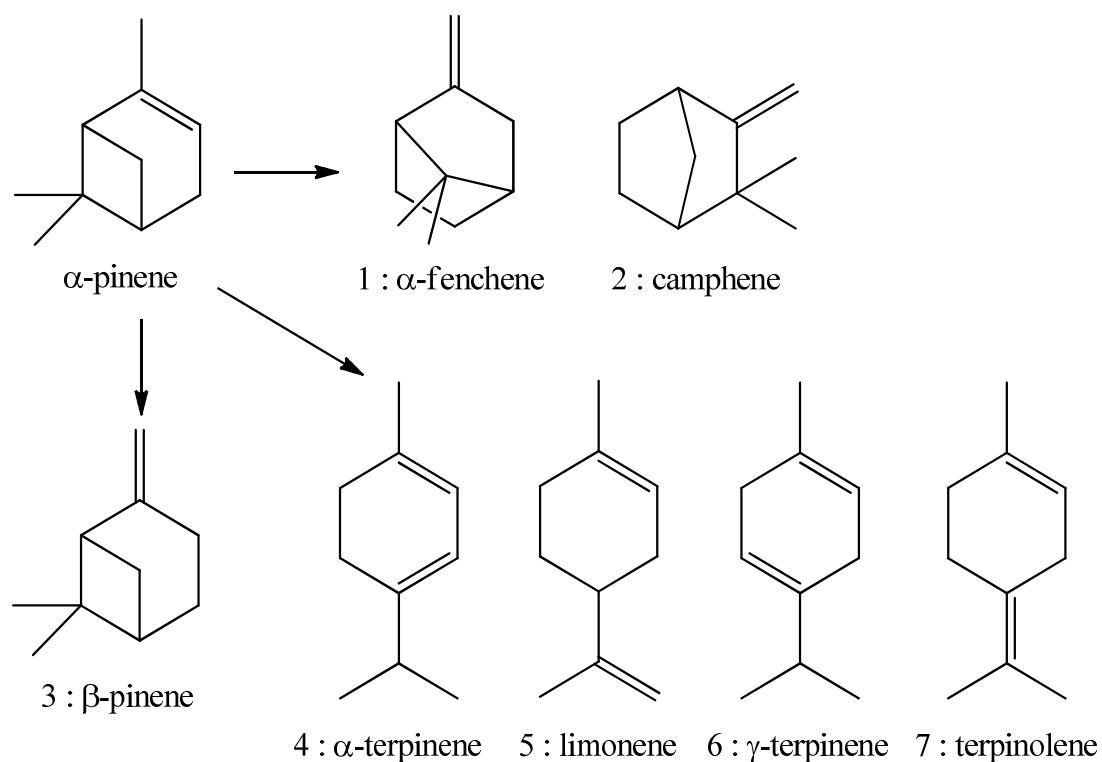
Figure 1. Activity of 11 wt% MoO_3/Al_2O_3 calcined at various temperature (a) for Friedel–Crafts alkylation ((●) benzyl anisole and (○) dibenzyl ether), (b) for isomerization of α-pinene ((■) camphene and (□) limonene).

Ohnishi[41] and Yamamoto[38,40] reported that monocyclic and bicyclic compound such as camphene and limonene were produced on Brønsted acid sites and the fraction was changed by the maximum strength of acid sites of the catalyst. The selectivity strongly depends on acidic and basic property of the catalyst. Because camphene and limonene were mainly produced on MoO_3/Al_2O_3, MoO_3/Al_2O_3 catalysts mainly exhibit Brønsted acid property.

Table 1. Results for α-pinene isomerization on 11 wt% MoO_3/Al_2O_3 calcined at various temperatures

Calcination temperature / K	Conversion (%)	Selectivity[a] (%)							
		1	2	3	4	5	6	7	8
773	20.8	2	52	tr	2	35	2	5	2
873	23.1	2	52	tr	2	35	2	5	2
973	31.3	2	53	tr	2	36	2	4	1
1023	44.4	tr	53	tr	2	37	2	5	1
1073	45.4	tr	57	tr	2	33	2	5	1
1123	30.8	1	55	tr	2	33	2	5	2

[a] 1 : α-fenchene, 2 : camphene, 3 : β-pinene, 4 : α-terpinene, 5 : limonene, 6 : γ-terpinene, 7 terpinolene, 8 others.

Scheme 1. α-Pinene isomerization.

Figure 1b show yields of camphene and limonene produced over 11 wt% MoO_3/Al_2O_3 calcined at various temperatures. The yields increased with raise of calcination temperature up to 1073 K as well as benzylation of anisole. The selectivity of camphene and limonene were almost constant with the change in calcination temperature. These results suggest that calcination temperature affects only the number of acid sites.

The results of benzylation of anisole over MoO_3/Al_2O_3 calcined at 1073 K with various MoO_3 loading are shown in Figure 2a. The yield of benzyl anisole was also strongly affected by loading amount of MoO_3. Alumina was almost inactive. And the yield of benzyl anisole rapidly increased with increase of MoO_3 loading above 8 wt%. The 11 wt% MoO_3/Al_2O_3 exhibited the highest activity and then activity decreased sharply over 11 wt%. The ratio of *p*-benzyl anisole to *o*-benzyl anisole was ca. 8/7 regardless of MoO_3 loading amount. This suggests that the acid strength was independent on the MoO_3 loading, whereas the number of acid sites varied.
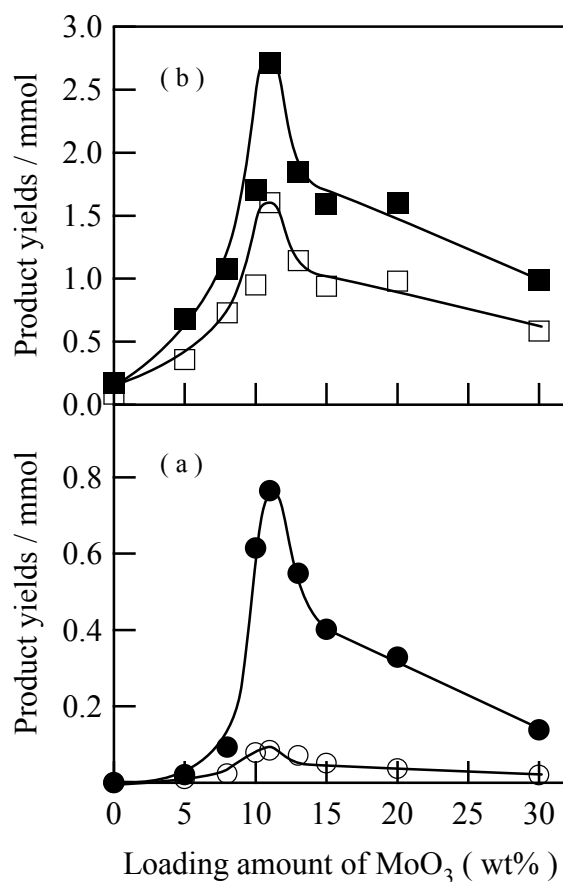

Figure 2. Activity of MoO_3/Al_2O_3 calcined at 1073 K with various loadings (a) for Friedel–Crafts alkylation ((●) benzyl anisole and (○) dibenzyl ether), (b) for isomerization of α-pinene ((■) camphene and (□) limonene).

Effects of MoO$_3$ loading amount on the activity of α-pinene isomerization were investigated. The change in yields and selectivities of camphene and limonene are shown in Figure 2b and Table 2. On alumina, the main products were camphene, limonene, and β-pinene, but activity is quite low. With increase of loading amount up to 8 wt%, the selectivities to camphene and limonene slightly increased and that to β-pinene decreased. The selectivity was almost constant from 8 wt% to 30 wt%. On the other hand, the conversion increased with rise of MoO$_3$ loading up to 11 wt% and then decreased. The yields of camphene and limonene changed sharply. The result shows the conversion strongly depends on loading amount. It is suggested that the acidity increased and the acid strength changed by increase of loading amount up to 8 wt%. And the retention of selectivity at 8 − 30 wt% indicates that only the number of acid sites increased or decreased without change in the acid strength with loading amount at 8 − 30 wt%.

Because calcination temperature and loading amount of MoO$_3$ strongly affected the activity for benzylation of anisole and isomerization of α-pinene, acidic property of MoO$_3$/Al$_2$O$_3$ catalyst was investigated by pyridine adsorbed FT-IR spectra. We evaluated the amount of acid sites from the specific amount of the adsorbed pyridinium ions for Brønsted acid sites and pyridine coordinated to Lewis acid sites over each MoO$_3$/Al$_2$O$_3$ catalyst.

Table 2. Results for α-pinene isomerization on MoO$_3$/Al$_2$O$_3$ calcined at 1073 K with various MoO$_3$ loadings

Loading amount of MoO$_3$ (wt%)	Conversion (%)	Selectivity[a] (%)							
		1	2	3	4	5	6	7	8
0	3.0	4	40	10	2	26	3	5	10
5	9.2	1	55	4	1	31	2	5	1
8	27.8	tr	54	tr	1	36	2	5	2
10	27.2	tr	58	tr	2	33	2	4	1
11	45.4	tr	57	tr	2	33	2	5	1
13	25.4	tr	56	tr	2	33	2	5	2
15	30.4	tr	56	tr	2	34	2	5	1
20	29.6	tr	56	tr	2	35	2	4	1
30	20.0	tr	57	tr	1	34	2	4	2

[a] 1 : α-fenchene, 2 : camphene, 3 : β-pinene, 4 : α-terpinene, 5 : limonene, 6 : γ-terpinene, 7 terpinolene, 8 others.

Figure 3 shows IR spectra of adsorbed pyridine on 11 wt% MoO_3/Al_2O_3 calcined at 1073 K and Al_2O_3, respectively. The spectrum of alumina exhibited four bands at 1447, 1490, 1578, and 1609 cm^{-1}. These four bands correspond to pyridine species adsorbed on Lewis acid site.[42,43] On the other hand, MoO_3/Al_2O_3 gave new bands at 1545 and 1639 cm^{-1} corresponding to pyridine species adsorbed on Brønsted acid sites and the bands at 1623, 1495, and 1455 cm^{-1} were shifted to 1613, 1490, and 1451 cm^{-1}, respectively. Appearance of bands at 1545 and 1639 cm^{-1} on MoO_3/Al_2O_3 means Brønsted acid sites are generated by the addition of molybdenum oxide on alumina and are maintained even after calcination at high temperatures.[42,43] Shifts of bands at 1623, 1495, and 1455 cm^{-1} indicated that Lewis acid property was changed by loading of molybdenum oxide.

To determine whether the activities for benzylation of anisole and isomerization of α-pinene were controlled by the amount of Brønsted acid sites, the specific amounts of pyridinium ion on Brønsted acid sites and of pyridine coordinated to Lewis acid sites on each MoO_3/Al_2O_3 catalyst were evaluated from the area of band of adsorbed pyridine. The number of Brønsted acid site was calculated using an integrated molar adsorption coefficient value of $\varepsilon = 1.67$ cm μmol^{-1} for the band area at 1545 cm^{-1} of protonated pyridinium ion.[44,45]
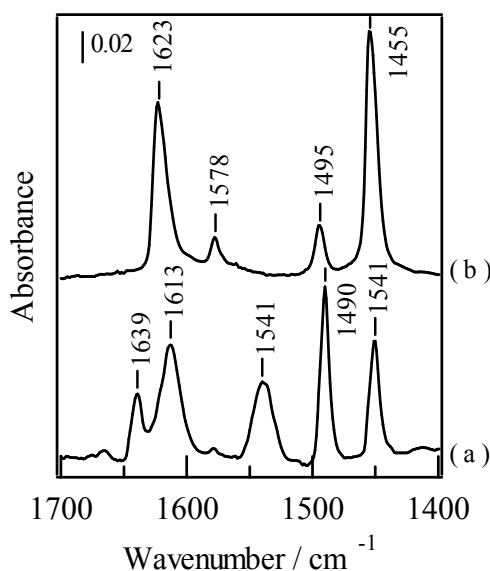

Figure 3. IR spectra of pyridine adsorbed on (a) 11 wt% MoO_3/Al_2O_3 calcined at 1073 K and (b) γ-Al_2O_3.

Figure 4 shows the number of Brønsted acid sites of 11 wt% MoO_3/Al_2O_3 calcined at various temperatures. The Brønsted acidity increased with increase of calcination temperature up to 1073 K and the calcination at 1123 K resulted in reduction of Brønsted acidity. This result showed that high temperature calcination is important for generation of Brønsted acid sites.

Figure 5 shows the Brønsted acidity of MoO_3/Al_2O_3 calcined at 1073 K with various MoO_3 loadings. Al_2O_3 did not exhibit Brønsted acid property. Brønsted acidity increased with rise of MoO_3 loading, and 11 wt% MoO_3/Al_2O_3 exhibited the highest Brønsted acidity.
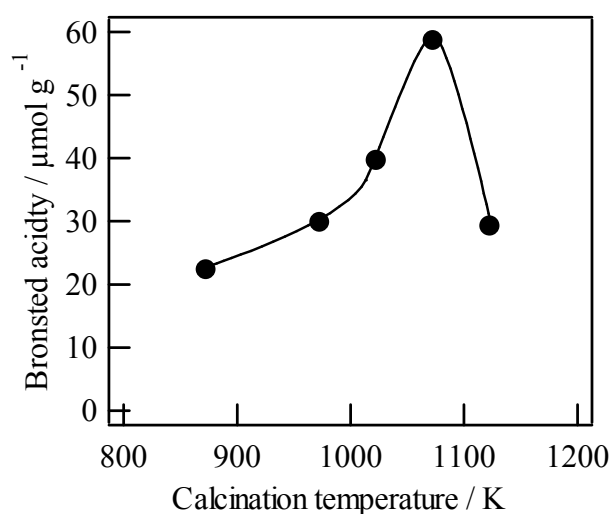

Figure 4. Brønsted acidity over 11 wt% MoO_3/Al_2O_3 calcined at various temperature.
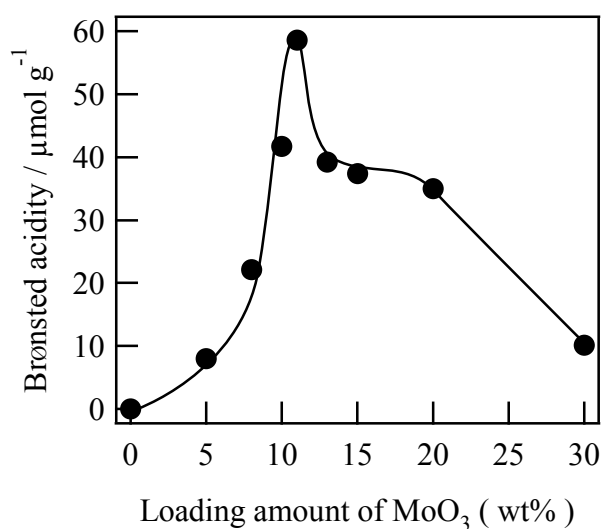

Figure 5. Brønsted acidity over MoO_3/Al_2O_3 calcined at 1073 K with various loadings.

Then Brønsted acidity decreased over 11 wt% loading. Figure 6 shows the correlation between the activities and number of Brønsted acid sites. The activities for benzylation of anisole and isomerization of α-pinene strongly depended on Brønsted acidity and a good correlation was shown between the activities and Brønsted acidity. These results exhibit that benzylation of anisole and α-pinene isomerization proceeded on Brønsted acid sites generated on MoO_3/Al_2O_3 calcined at high temperatures. The amount of Lewis acidity was calculated using an integrated molar adsorption coefficient value of $\varepsilon = 2.22$ cm μmol^{-1} for the band area at 1450 cm^{-1} of coordinated pyridine.[44,45] Lewis acidity decreased with increase of calcinations temperature and MoO_3 loading amount, indicating that no Lewis acid site concerned with these reactions. (Figure 7 and 8)
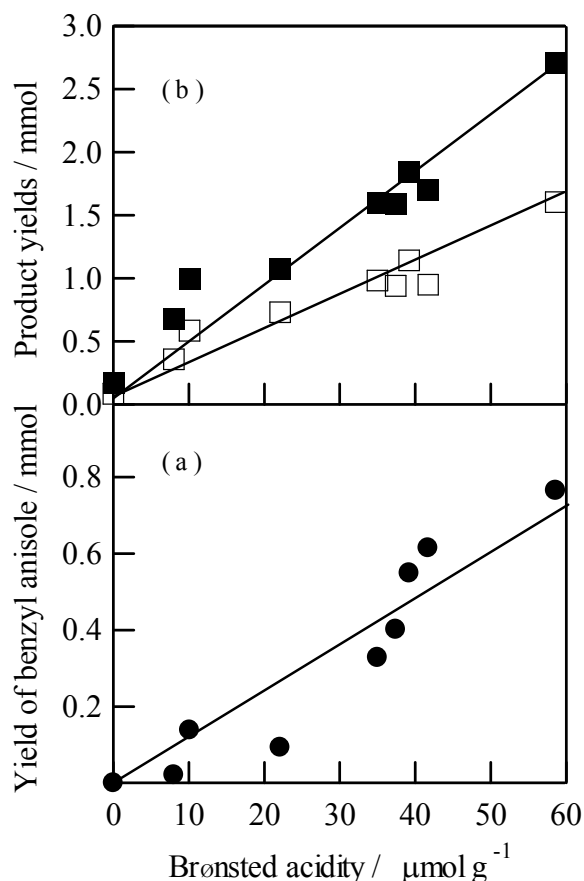
Figure 6. Correlation between catalytic activities over MoO_3/Al_2O_3 calcined at 1073 K with various loadings and Brønsted acidity of samples.
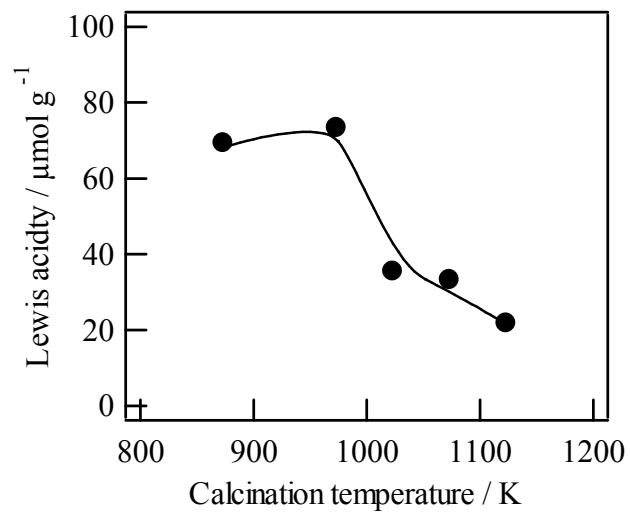(a) Benzylation of anisole, (b) isomerization of α-pinene ((■) camphene and (□) limonene).

Figure 7. Lewis acidity over 11 wt% MoO_3/Al_2O_3 calcined at various temperature.
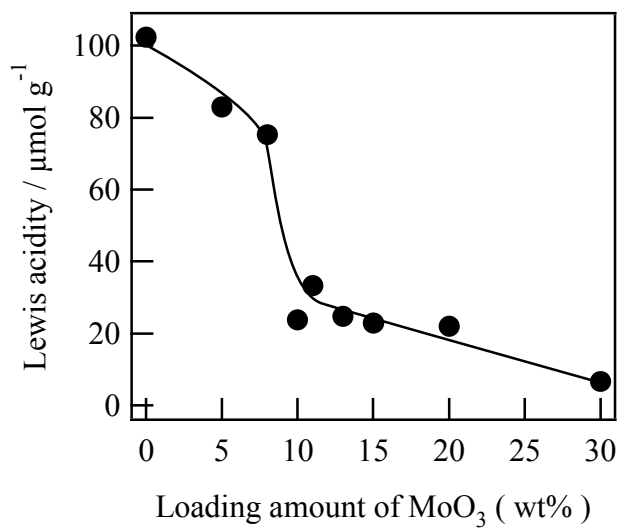
Figure 8. Lewis acidity over MoO_3/Al_2O_3 calcined at 1073 K with various loadings.

Characterizations

Figure 9 and 10 show XRD patterns and Raman spectra of 11 wt% MoO_3/Al_2O_3 calcined at various temperatures. Molybdenum oxide was not crystalized on MoO_3/Al_2O_3 calcined below 1123 K. $Al_2Mo_3O_{12}$ was formed on MoO_3/Al_2O_3 calcined at 1123 K. The results showed that MoO_3 was loaded as amorphous phase. Because benzylation of anisole and isomerization of α-pinene did not proceed on $Al_2Mo_3O_{12}$ and no Brønsted acid sites existed on $Al_2Mo_3O_{12}$, formation of $Al_2Mo_3O_{12}$ caused decrease of Brønsted acid sites on MoO_3/Al_2O_3 calcined at 1123 K.
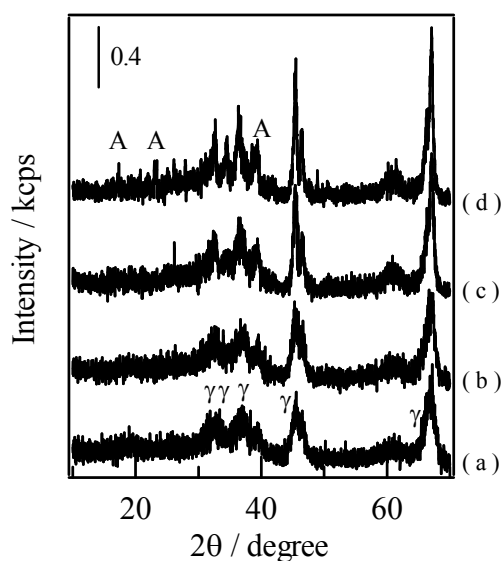
Figure 9. XRD patterns of 11 wt% MoO_3/Al_2O_3 calcined at various temperatures.
(a) 773 K, (b) 1023 K, (c) 1073 K, and (d) 1123 K. γ = γ-Al_2O_3; A = $Al_2Mo_3O_{12}$
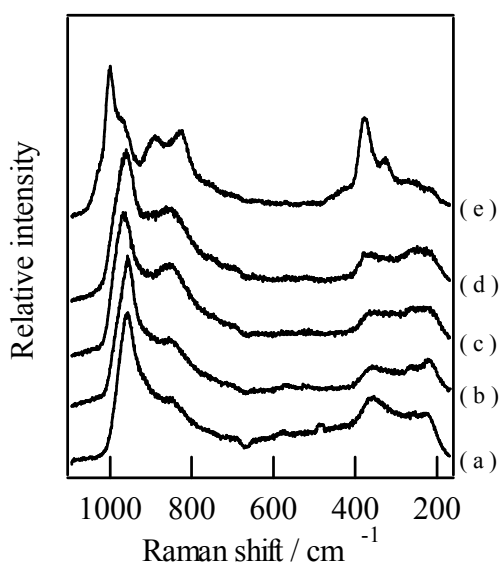
Figure 10. Raman spectra of 11 wt% MoO_3/Al_2O_3 calcined at various temperatures.
(a) 873 K, (b) 973 K, (c) 1023 K, (d) 1073 K, and (e) 1123 K.

Figure 11 and 12 show XRD patterns and Raman spectra of MoO_3/Al_2O_3 calcined at 1073 K with various MoO_3 loading. XRD patterns and Raman spectra of MoO_3/Al_2O_3 showed no diffraction pattern and Raman peak due to $Al_2Mo_3O_{12}$ crystalline until the MoO_3 reached 11 wt%. Above 13wt%, $Al_2Mo_3O_{12}$ appeared and $Al_2Mo_3O_{12}$ crystal grew with increase of loading amount. Considering the results of change in acid property, because of the formation of $Al_2Mo_3O_{12}$, Brønsted acid sites decreased over MoO_3/Al_2O_3 with higher MoO_3 loading than 11 wt%.
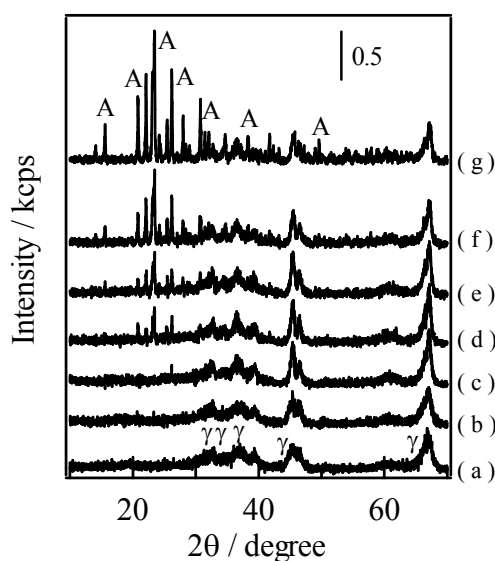
Figure 11. XRD patterns of MoO_3/Al_2O_3 calcined at 1073 K with various loadings.
(a) 5 wt%, (b) 8 wt%, (c) 11 wt%, (d) 13 wt%, (e) 15 wt%, (f) 20 wt%, and (g) 30 wt%.
$\gamma = \gamma\text{-}Al_2O_3$; A = $Al_2Mo_3O_{12}$.

Figure 12. Raman spectra of MoO_3/Al_2O_3 calcined at 1073 K with various loadings.
(a) 5 wt%, (b) 8 wt%, (c) 11 wt%, (d) 13 wt%, and (e) 30 wt%.

- 146 -

From these results, it can be thought that amorphous molybdenum oxide concern with generation of Brønsted acid sites.

The surface Mo/Al ratios on MoO_3/Al_2O_3 catalysts were estimated from the areas in the Mo 3d and Al 2p XP spectra. Bi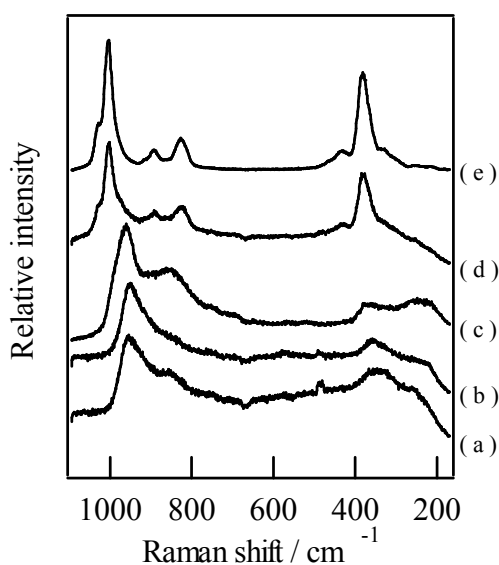nding energy of Mo $3d_{5/2}$ and Mo $3d_{3/2}$ peaks of the catalysts is 232.7 and 235.9 eV respectively and did not change regardless of calcination temperature and loading amount of MoO_3. This result indicates that the valence of molybdenum cation of MoO_3/Al_2O_3 catalyst were Mo^{6+} regardless of calcination temperature and MoO_3 loading amount. No significant change was shown in the surface Mo/Al ratio of 11 wt% MoO_3/Al_2O_3 calcined at various temperature, indicating Mo atoms were located on the surface regardless of calcination temperature without sublimination of MoO_3. Figure 13 shows the surface Mo/Al ratio of MoO_3/Al_2O_3 calcined at 1073 K with various MoO_3 loading. The surface Mo/Al ratio shows a linear increase with loading of MoO_3 up to 10 wt% then the line becomes gradual. The cross-section area of MoO_6 octahedral unit is 0.22 nm^{-2} and surface area of the catalyst.[11] It is estimated that the surface of MoO_3/Al_2O_3 is completely covered with monolayer of molybdenum oxide when the molybdenum content is 10 wt% as MoO_3. The results suggest that monolayer of molybdenum oxide was formed on 10 wt% MoO_3/Al_2O_3 and three-dimensional MoO_3 clusters seem to coexist above 10 wt%.
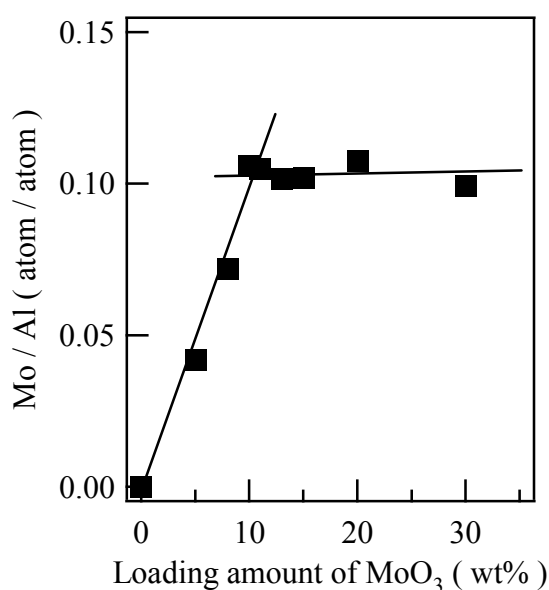

Figure 13. Atomic ratio of MoO_3/Al_2O_3 calcined at 1073 K with various loadings.

Considering the results of XRD and Raman spectra, two-dimensional molybdenum oxide domains are mainly formed and a little of three-dimensional MoO_3 clusters are contained on 11 wt% MoO_3/Al_2O_3. Three-dimensional MoO_3 clusters are transformed to $Al_2Mo_3O_{12}$ and $Al_2Mo_3O_{12}$ increases with increase of loading amount above 11 wt%. Taking into account the change in the number of Brønsted acid site, we concluded that stabilized monolayer of molybdenum oxide and small MoO_3 clusters account for the generation of Brønsted acid sites.

The local structure of MoO_3/Al_2O_3 catalysts was characterized by Mo K–edge XAFS spectra. Figure 14 shows Mo K-edge X-ray adsorption near-edge structure (XANES) spectra of MoO_3/Al_2O_3 calcined at 1073 K with various loading and reference samples. The pre-edge peak at Mo K-edge XANES, which is assigned to transition of 1s to d-p orbitals, is sensitive to the symmetry. X-ray absorptions have been often used to provide information on the local symmetry.[46-48] The molybdenum oxide unit on a sample is distorted from an ideal octahedral symmetry, the pre-edge peak of Mo K-edge XANES become intense. Therefore, a pre-edge peak of Na_2MoO_4 (MoO_4 tetrahedral) is much more intense than that of molybdenum oxide (distorted octahedral) is, and that of $SrCaMoO_3$ (MoO_3 octahedral) is much less intense than that of molybdenum oxide.
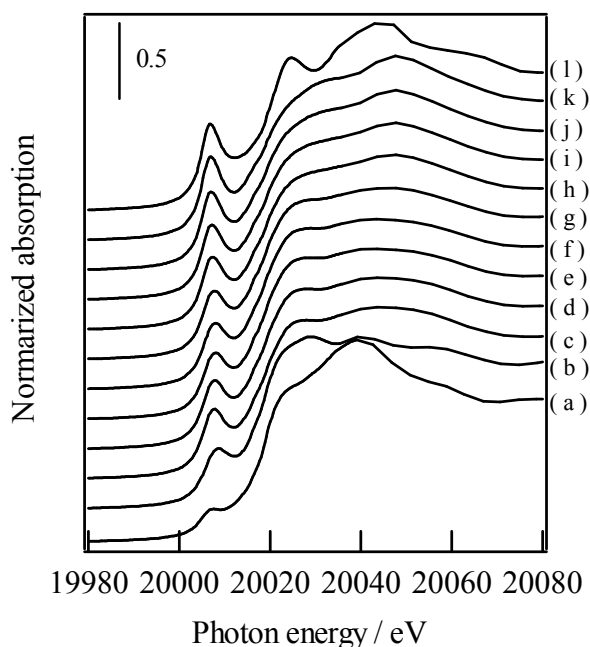

Figure 14. Mo K-edge XANES spectra of reference samples and MoO_3/Al_2O_3 calcined at 1073 K with various loadings.
(a) Sr_2CaMoO_6, (b) MoO_3, (c) 5 wt%, (d) 8 wt%, (e) 10 wt%, (f) 11 wt%, (g) 13 wt%, (h) 15 wt%, (i) 20 wt%, (j) 30 wt%, (k) $Al_2Mo_3O_{12}$, and (l) Na_2MoO_4.

- 148 -

The pre-edge peaks of MoO_3/Al_2O_3 are larger than that of MoO_3 and smaller than that of Na_2MoO_4, indicating that the coordination symmetry around Mo of MoO_3/Al_2O_3 is distorted octahedral symmetry. The area was slightly decreased up to 11 wt%. Above 13 wt%, this value gradually increased and approached to that of $Al_2Mo_3O_{12}$. The shape of spectra of 5 – 11 wt% MoO_3/Al_2O_3 in the range of 20.02 – 20.06 eV resemble each other. Above 13 wt%, the two peaks at around 20.25 and 20.45 eV grew with increase of loading amount. These results indicate that the formation of $Al_2Mo_3O_{12}$ proceeds when the MoO_3 loading was larger than 11 wt%.

The Mo K-edge k^3-weighted extended X-ray adsorption fine structure (EXAFS) oscillations of MoO_3/Al_2O_3 catalysts with various loadings and reference samples are shown in Figure 15. No significant changes in the EXAFS spectra of each MoO_3/Al_2O_3 catalyst appeared until the MoO_3 loading was 11 wt%. The oscillation amplitude decreased monotonically with k, suggesting that a smaller Mo–(O)–Mo contribution than that in bulk MoO_3. On the other hand, the configuration changed in EXAFS oscillations of 13 – 30 wt% MoO_3/Al_2O_3 catalysts. Appreciable oscillation appeared in the k region higher than 8 $Å^{-1}$, and the oscillation is similar to that of $Al_2Mo_3O_{12}$, indicating that there is a Mo–(O)–Al contribution on the catalyst.

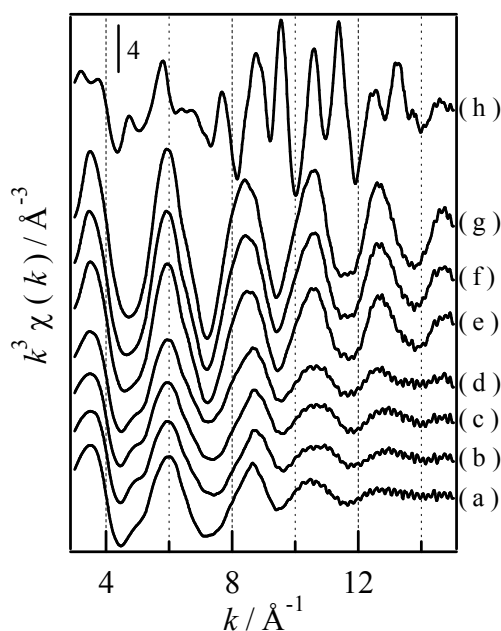**Figure 15.** Mo K-edge k^3-weighted EXAFS of reference samples and MoO_3/Al_2O_3 calcined at 1073 K with various loadings.
(a) 5 wt%, (b) 10 wt%, (c) 11 wt%, (d) 13 wt%, (e) 20 wt%, (f) 30 wt%, (g) $Al_2Mo_3O_{12}$, and (h) MoO_3.

The oscillation in the k region higher than 6 Å^{-1} grew remarkably in the EXAFS oscillation of 20 and 30 wt% MoO$_3$/Al$_2$O$_3$ catalysts, which indicates growth of Al$_2$Mo$_3$O$_{12}$ crystal. In the case of 13 wt% MoO$_3$/Al$_2$O$_3$ catalyst, it appears that a small amount of Al$_2$Mo$_3$O$_{12}$ was present together with monolayer of molybdenum oxide. Therefore, these results indicate that the local structure of molybdenum cation of MoO$_3$/Al$_2$O$_3$ catalysts with loading of MoO$_3$ up to 11 wt% is maintained and Al$_2$Mo$_3$O$_{12}$ crystal is mixed to the loaded molybdenum oxide with increase of MoO$_3$ loading over 11 wt%.

Figure 16 shows Fourier transformed EXAFS oscillations of MoO$_3$/Al$_2$O$_3$ catalysts with various loadings and reference samples. Until 11 wt%, only one peak at 1.3 Å was shown and new peak at 3.3 Å appeared and grew on MoO$_3$/Al$_2$O$_3$ with higher MoO$_3$ loading than 11 wt%. The two peaks at 1.3 and 3.3 Å are corresponded to Mo-O and Mo–(O)–Al linkages. The peak at 3.3 Å is assigned by analyzing the backscattering amplitudes and the phase shifts. Because the atomic numbers of Al (13) and Mo (42) is different, the back scattering amplitude of Al and the phase shift of the Mo–(O)–Al are different from those of the Mo–(O)–Mo pair.
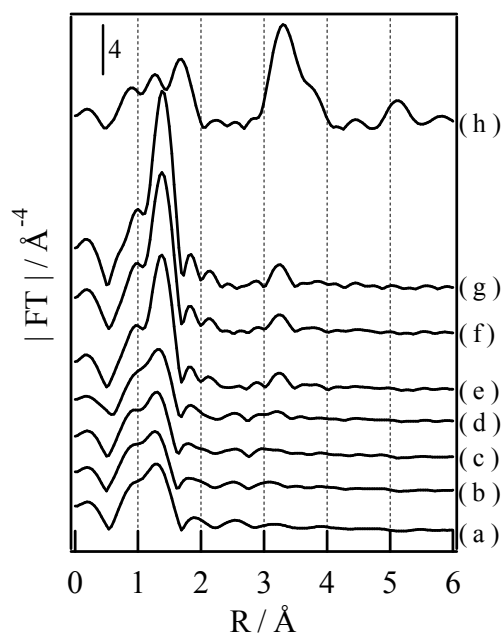

Figure 16. Fourier transforms of Mo K-edge k^3-weighted EXAFS of reference samples and MoO$_3$/Al$_2$O$_3$ calcined at 1073 K with various loadings.
(a) 5 wt%, (b) 10 wt%, (c) 11 wt%, (d) 13 wt%, (e) 20 wt%, (f) 30 wt%, (g) Al$_2$Mo$_3$O$_{12}$, and (h) MoO$_3$.

In the structure of $Al_2Mo_3O_{12}$ crystal, there is no Mo–(O)–Mo linkages but Mo–(O)–Al linkages and increase of the peak at 3.3 Å means that $Al_2Mo_3O_{12}$ crystal is mixed to the loaded molybdenum oxide with increase of MoO_3 loading over 11 wt%. These results agree with the results of XPS measurement.

Physical property of MoO_3/Al_2O_3 calcined at 1073 K is summarized in Table 3. The catalyst areas include that of the alumina carrier. S_0 is the surface area $g(Al_2O_3)^{-1}$ of a carrier, and was calculated from the BET specific surface area and MoO_3 content. $S_{occupied}$ is the estimated area occupied by MoO_6 unit (0.22 nm^2). It is assumed that all of MoO_3 is loaded as MoO_6 octahedra and the area of that is 0.22 nm^2. The surface area of MoO_3/Al_2O_3 decreased with loading amount of MoO_3 due to a shrink of alumina support and at sudden decrease of surface area was shown at 10 wt%. The areas of alumina support (S_0) decrease and the area occupied by MoO_6 units ($S_{occupied}$) increase with loading amount of MoO_3 and $S_{occupied}$ become larger than S_0 at 10 wt%. The surface density of Mo atom on 8 and 10 wt% MoO_3/Al_2O_3 calcined at 1073 K is estimated to be 2.8 and 5.6 atoms nm^{-2}, respectively.

Table 3. Physical properties of MoO_3/Al_2O_3 calcined at 1073 K

Mo content		Area[b] / m^{2}g^{-1}	S_0[c] / m^2	$S^d_{occupied}$ / m^2 g(cat)$^{-1}$	$S^d_{occupied}$ / m^2 g(Al_2O_3)$^{-1}$
mmol g(Al_2O_3)$^{-1}$	(wt%)[a]				
0	0	148	148	0	0
0.37	5	131	138	46.0	48.4
0.60	8	121	132	73.6	80.0
0.77	10	74.3	82.6	92.0	102
0.86	11	63.7	71.6	101	114
1.04	13	57.7	66.3	120	137
1.23	15	59.8	70.4	138	162
1.74	20	54.4	68.0	184	230
2.98	30	44.3	63.3	276	394

[a] As MoO_3
[b] BET specific surface area
[c] Surface area of g(Al_2O_3)$^{-1}$ carrier
[d] Occupied area by MoO_3 unit (0.22 nm^2)

Because some researchers suggested that the surface density of Mo atoms in monolayer coverage with MoO_3 was 4.5 atom nm^{-2} and the value was larger than the surface density of Mo atom on 8 wt% and a little smaller than 10 wt%,[10] these results mean that MoO_3 was loaded as two-dimensional molybdenum oxide until 8 wt% and formation of three-dimensional MoO_3 just started on 10 wt% MoO_3/Al_2O_3. In discussing where the Brønsted acid sites generated, there are some important points. (1) The activity and Brønsted acidity increased with loading amount, but the tendency of increase became larger up to 11 wt%. (2) Brønsted acidity is much smaller than the number of supported Mo atoms. (3) The Brønsted acidity strongly depended on loading amount, but the acid strength was not changed with loading amount. On the basis of the results above, we concluded that two-dimensional molybdenum oxide and a small cluster of MoO_3 were the keys to the generation of Brønsted acid sites. We assumed three models on the structure of Brønsted acid sites generated on MoO_3/Al_2O_3. (Figure 17) One is hydroxyl groups formed on molybdenum oxide monolayer domain and three-dimensional MoO_3 (Mo−OH or Mo−(OH)−Mo) work as Brønsted acid sites. And the second model means hydroxyl groups formed on the edges of molybdenum oxide monolayer domain and three-dimensional MoO_3 (molybdenum oxide domain; Mo−(OH)−Al) work as Brønsted acid sites. In the last model, they are located at the boundaries of molybdenum oxide monolayer domain and three-dimensional MoO_3. The relation between the number of Brønsted acid sites and the Mo content strongly suggests that model 3, isolated or bridged hydroxyl groups located at the boundaries of molybdenum oxide islands, is the most reliable among the proposed models. Until 8 wt%, only molybdenum monolayer was formed on alumina and small clusters of MoO_3 are mixed over 8 wt%. Because Brønsted acidity sharply increased from 8 wt%, Brønsted acid sites are generated on the boundary of both of molybdenum monolayer domain and small clusters of MoO_3. Generation of Brønsted acid sites by calcination at high temperatures is assumed to be due to (1) the formation of MoO_3 monolayer domains and small clusters of MoO_3 on the surface of alumina, and (2) the formation of boundaries of molybdenum oxide monolayer domains and MoO_3 small clusters. The shrink of alumina by calcination at high temperatures contributes to the reduction of surface area of alumina. As a result, the distance between domains of molybdenum oxide monolayer and small clusters of MoO_3 becomes shorter, and then, boundaries of molybdenum monolayer domain and small clusters of MoO_3 form to generate Brønsted acid sites.
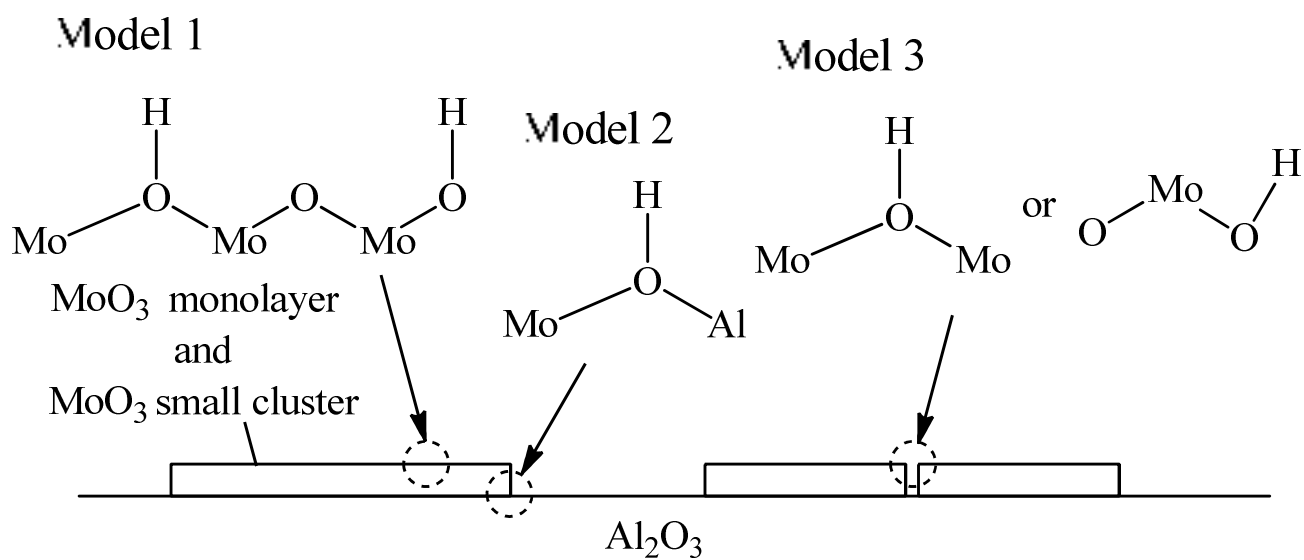
Figure 17. Structure models of Brønsted acid sites on MoO₃/Al₂O₃.

Conclusions

MoO_3/Al_2O_3 calcined at high temperature exhibited reaction acitivity (benzylation of anisole and isomerization of $\square$-pinene) and Brønsted acidity. The acid property of MoO_3/Al_2O_3 strongly depended on calcination temperature and MoO_3 loading and high calcination temperature (1073 K) was effective for generation of Brønsted acid sites. 11 wt% MoO_3/Al_2O_3 calcined at 1073 K exhibited the highest reactivity and Brønsted acidity. On the catalyst, molybdenum oxide monolayer domains and small clusters of MoO_3 were formed on alumina and covered the surface on this catalyst. Brønsted acid sites are generated on the boundary of molybdenum oxide monolayer domains and small clusters of MoO_3. Over 11 wt%, molybdenum oxide monolayer domains and small clusters of MoO_3 translated to inert $Al_2Mo_3O_{12}$ and Brønsted acid sites disappeared.

References

(1)   Liu, H. F.; Liu, R. S.; Liew, K. Y.; Johnson, R. E.; Lunsford, J. H. *J. Am. Chem. Soc.,* **1984**, *106*, 4117.

(2)   Wang, D. J.; Lunsford, J. H.; Rosynek, M. P. *J. Catal.,* **1997**, *169*, 347.

(3)   Thomas, R.; Moulijn, J. A.; Debeer, V. H. J.; Medema, J. *J. Mol. Catal.,* **1980**, *8*, 161.

(4)   Hino, M.; Arata, K. *Chem. Lett.,* **1989**, 971.

(5)   Arata, K.; Nakamura, H.; Shouji, M. *Appl. Catal. A-Gen.,* **2000**, *197*, 213.

(6)   Li, L. S.; Yoshinaga, Y.; Okuhara, T. *Phys. Chem. Chem. Phys.,* **1999**, *1*, 4913.

(7)   Li, L. S.; Yoshinaga, Y.; Okuhara, T. *Phys. Chem. Chem. Phys.,* **2002**, *4*, 6129.

(8)   Arata, K. *Appl. Catal. A-Gen.,* **1996**, *146*, 3.

(9)   Imamura, S.; Sasaki, H.; Shono, M.; Kanai, H. *J. Catal.,* **1998**, *177*, 72.

(10)   Chen, K.; Xie, S.; Bell, A. T.; Iglesia, E. *J. Catal.,* **2001**, *198*, 232.

(11)   Abello, M. C.; Gomez, M. F.; Ferretti, O. *Appl. Catal. A-Gen.,* **2001**, *207*, 421.

(12)   Okamoto, Y.; Tomioka, H.; Katoh, Y.; Imanaka, T.; Teranishi, S. *J. Phys. Chem.,* **1980**, *84*, 1833.

(13)   Hu, H. C.; Wachs, I. E. *J. Phys. Chem.,* **1995**, *99*, 10911.

(14)   Iizuka, T.; Ogasawara, K.; Tanabe, K. *Bull. Chem. Soc. Jpn.,* **1983**, *56*, 2927.

(15)   Tanabe, K. *Catal. Today,* **1990**, *8*, 1.

(16)   Tanabe, K.; Okazaki, S. *Appl. Catal. A-Gen.,* **1995**, *133*, 191.

(17)   Tanabe, K. *Catal. Today,* **2003**, *78*, 65.

(18)   Okuhara, T. *Chem. Rev.,* **2002**, *102*, 3641.

(19)   Nowak, I.; Ziolek, M. *Chem. Rev.,* **1999**, *99*, 3603.

(20)   Ohuchi, T.; Miyatake, T.; Hitomi, Y.; Tanaka, T. *Catal. Today,* **2007**, *120*, 233.

(21)   Shishido, T.; Kitano, T.; Teramura, K.; Tanaka, T. *Catal. Lett.,* **2009**, *129*, 383.

(22)   Shishido, T.; Kitano, T.; Teramura, K.; Tanaka, T. *Top Catal,* **2010**, *53*, 672.

(23)   Kitano, T.; Shishido, T.; Teramura, K.; Tanaka, T. *J. Phys. Chem. C,* **2012**, *116*, 11615.

(24)   Kitano, T.; Okazaki, S.; Shishido, T.; Teramura, K.; Tanaka, T. *Chem. Lett.,* **2011**, *40*, 1332.

(25)   Kitano, T.; Okazaki, S.; Shishido, T.; Teramura, K.; Tanaka, T. *Catal. Today,* **2012**, *192*, 189.

(26)   Ushikubo, T.; Wada, K. *Chem. Lett.,* **1988**, 1573.

(27)   Ushikubo, T.; Wada, K. *Appl. Catal.,* **1990**, *67*, 25.

(28)   Tian, H.; Roberts, C. A.; Wachs, I. E. *J. Phys. Chem. C,* **2010**, *114*, 14110.

(29)   Medema, J.; Vanstam, C.; Debeer, V. H. J.; Konings, A. J. A.; Koningsberger, D. C. *J. Catal.,* **1978**, *53*, 386.

(30)   Ankudinov, A. L.; Ravel, B.; Rehr, J. J.; Conradson, S. D. *Phys. Rev. B,* **1998**, *58*, 7565.

(31)   de la Cruz, M. H. C.; Abdel-Rehim, M. A.; Rocha, A. S.; da Silva, J. F. C.; Faro, A. D.; Lachter, E. R. *Catal. Commun.,* **2007**, *8*, 1650.

(32)   de la Cruz, M. H. C.; da Silva, J. F. C.; Lachter, E. R. *Catal. Today,* **2006**, *118*, 379.

(33)   Yamashita, K.; Hirano, M.; Okumura, K.; Niwa, M. *Catal. Today,* **2006**, *118*, 385.

(34)   Okumura, K.; Yamashita, K.; Hirano, M.; Niwa, M. *Chem. Lett.,* **2005**, *34*, 716.

(35)   Okumura, K.; Yamashita, K.; Hirano, M.; Niwa, M. *J. Catal.,* **2005**, *234*, 300.

(36)   Cseri, T.; Bekassy, S.; Figueras, F.; Cseke, E.; Demenorval, L. C.; Dutartre, R. *Appl. Catal. A-Gen.,* **1995**, *132*, 141.

(37)   Tagusagawa, C.; Takagaki, A.; Hayashi, S.; Domen, K. *J. Am. Chem. Soc.,* **2008**, *130*, 7230.

(38)   Yamamoto, T.; Tanaka, T.; Matsuyama, T.; Funabiki, T.; Yoshida, S. *J. Phys. Chem. B,* **2001**, *105*, 1908.

(39)   Tanaka, T.; Kumagai, H.; Hattori, H.; Kudo, M.; Hasegawa, S. *J. Catal.,* **1991**, *127*, 221.

(40)   Yamamoto, T.; Tanaka, T.; Funabiki, T.; Yoshida, S. *J. Phys. Chem. B,* **1998**, *102*, 5830.

(41)   Ohnishi, R.; Tanabe, K.; Morikawa, S.; Nishizak.T. *Bull. Chem. Soc. Jpn.,* **1974**, *47*, 571.

(42)   Parry, E. P. *J. Catal.,* **1963**, *2*, 371.

(43)   Jacobs, P. A.; Leeman, H. E.; Uytterho.Jb. *J. Catal.,* **1974**, *33*, 17.

(44)   Barzetti, T.; Selli, E.; Moscotti, D.; Forni, L. *J. Chem. Soc.-Faraday Trans.,* **1996**, *92*, 1401.

(45)   Emeis, C. A. *J. Catal.,* **1993**, *141*, 347.

(46)   Yoshida, H.; Tanaka, T.; Yoshida, T.; Funabiki, T.; Yoshida, S. *Catal. Today,* **1996**, *28*, 79.

(47)   Yamamoto, T.; Orita, A.; Tanaka, T. *X-Ray Spectrom.,* **2008**, *37*, 226.

(48)   Yoshida, S.; Tanaka, T.; Hanada, T.; Hiraiwa, T.; Kanai, H.; Funabiki, T. *Catal. Lett.,* **1992**, *12*, 277.

Chapter 7

Comparison between Brønsted Acid Property of Alumina-Supported Niobium Oxide, Tantalum Oxide, and Tungsten Oxide Calcined at High Temperatures

Abstract

The acid property and coordination environment of Brønsted acid sites on monolayer of niobium oxide, tantalum oxide, and tungsten oxide supported on alumina (16 wt% Nb_2O_5/Al_2O_3 calcined at 1123 K (16NbAl), 33 wt% Ta_2O_5/Al_2O_3 calcined at 1223 K (33TaAl), and 20 wt% WO_3/Al_2O_3 calcined at 1123 K (20WAl)) were investigated. The acid property was examined by acid-catalyzed reactions (benzylation of anisole and isomerization of α-pinene), and Fourier Transformed infrared spectroscopy (FT-IR). Characterization of coordination environment of Brønsted acid sites on these catalysts was performed by FT-IR. The Brønsted acid properties of 16NbAl, 33TaAl, and 20WAl were different from each other and both number and maximum acid strength of Brønsted acid sites were in order of 20WAl > 16NbAl > 33TaAl. The results of structural characterization of 16NbAl, 33TaAl, and 20WAl showed that hydroxyl groups formed between monolayer domains of niobium oxide, tantalum oxide, and tungsten oxide work as Brønsted acid sites, and the coordination environment of hydroxyl groups is different from each other. The difference of coordination environment probably results in the difference of Brønsted acid property of these catalysts.

Introduction

Recently, we reported that Brønsted acid sites were generated on Nb_2O_5/Al_2O_3, WO_3/Al_2O_3, and Ta_2O_5/Al_2O_3 calcined at high temperatures (1123 – 1223 K). Usually, high temperature calcination causes disappearance of acidic property. Niobic acid ($Nb_2O_5 \cdot nH_2O$, hydrated niobium oxide) shows catalytic activity for esterification, olefin hydration, alcohol dehydration, and exhibits Brønsted acid property.[1-6] However, niobic acid loses their acid property when calcined at 773 K due to phase transformation to T- and TT-phases.[7,8] On the other hand, Nb_2O_5/Al_2O_3 calcined at high temperature exhibited a high activity in benzylation of anisole, cumene cracking, and isomerization of α-pinene, which proceed on Brønsted acid sites.[9-11] The Brønsted acid property and catalytic activity strongly depended on both calcination temperature and loading amount of Nb_2O_5. In a series of Nb_2O_5/Al_2O_3 catalyst, 16 wt% Nb_2O_5/Al_2O_3 calcined at 1123 K exhibited the highest activity and Brønsted acidity. Moreover, Nb_2O_5/Al_2O_3 calcined at 1123 K maintained the activity for isomerization of α-pinene even after pretreatment at 1173 K. The result means that the Brønsted acid sites generated on Nb_2O_5/Al_2O_3 calcined at 1123 K are thermally stable. Ta_2O_5/Al_2O_3 calcined at 1223 K and WO_3/Al_2O_3 calcined at 1123 K also showed catalytic activity for benzylation of anisole and isomerization of α-pinene, and exhibited Brønsted acid property as well as Nb_2O_5/Al_2O_3 calcined at 1123 K.[12-14] For these catalysts, calcination temperature and loading amount strongly affected the Brønsted acid property and catalytic activity. 33 wt% Ta_2O_5/Al_2O_3 calcined at 1223 K and 20 wt% WO_3/Al_2O_3 calcined at 1123 K exhibited the highest Brønsted acid property among Ta_2O_5/Al_2O_3 and WO_3/Al_2O_3 tested, indicating that Nb_2O_5/Al_2O_3, Ta_2O_5/Al_2O_3, and WO_3/Al_2O_3 calcined at high temperature work as thermally stable solid acid catalysts. It appears that the acidic property of these catalysts was sensitive to structural change of supported metal oxides. Based on structural characterization of these catalysts, we revealed that on 16NbAl, 33TaAl, and 20WAl, niobium oxide, tantalum oxide, and tungsten oxide were loaded on alumina as two-dimensional monolayer domains, and proposed that Brønsted acid sites are generated on the boundaries between the monolayer domains of metal oxides on alumina.

Up to now, the difference of acid property between Nb_2O_5/Al_2O_3, Ta_2O_5/Al_2O_3, and WO_3/Al_2O_3 is still unclear. The clarification of the acid property and the coordination environment

of Brønsted acid sites is expected to provide the valuable information for construction of generation mechanism of acid sites on supported metal oxides exhibiting acid property. For this purpose, the investigation of hydroxyl groups using FT-IR is suitable method because a part of hydroxyl groups on metal oxide works as Brønsted acid sites. Hydroxyl groups on various metal oxides such as zeolites, Al_2O_3, SiO_2, TiO_2, and ZrO_2 have been investigated using FT-IR.[15-27]

In the present study, we investigated the acid property of Nb_2O_5/Al_2O_3, Ta_2O_5/Al_2O_3, and WO_3/Al_2O_3, and characterized the coordination environment of Brønsted acid sites on these catalysts by FT-IR. In addition, the effect of metal species (Group V: Nb and Ta, and Group VI, W) on the Brønsted acid property and coordination environment of Brønsted acid sites on these catalysts were discussed.

Experimental

Preparation

The precursors of Nb_2O_5/Al_2O_3 and WO_3/Al_2O_3 were prepared by impregnation of γ-Al_2O_3 (JRC-ALO-8) with an aqueous solution of ammonium niobium oxalic acid ($NH_4(NbO(C_2O_4)_2(H_2O))$) and tungsten para pentahydrate ($(NH_4)_{10}W_{12}O_{42} \cdot 5H_2O$)) at 353 K and dried overnight at 353 K. The precursor of Ta_2O_5/Al_2O_3 was prepared by impregnation of γ-Al_2O_3 (JRC-ALO-8) with ethanol tantalum ethoxide dissolving in at 353 K and dried overnight at 353 K. Nb_2O_5/Al_2O_3 and WO_3/Al_2O_3 were obtained by calcination of precursors at 1123 K for 3 h in a dry air. Ta_2O_5/Al_2O_3 was obtained by calcination of precursor at 1223 K for 3 h in a dry air.

Reactions

Benzylation of anisole (Friedel-Crafts alkylation of anisole with benzylalcohol) and isomerization of α-pinene were employed as test reactions to examine the acid properties.

Benzylation of anisole was examined in a liquid phase. The catalysts (0.1 – 0.2 g) were pretreated in a N_2 flow at 473 K for 1 h and added to a mixture of benzyl alcohol (6.25 mmol) and anisole (92.5 mmol) in a 100 ml flask. The reaction was carried out at 353-443 K and the products were determined by GLC (GC-14B with a flame ionization detector, Shimadzu, Kyoto, Japan) and GC-MS (Shimadzu GC-MS QP-5050), using a CBP10 column.

Isomerization of α-pinene was carried out under a dry N_2 atmosphere using a stirred batch reactor. Prior to each run, 0.05 – 0.2 g of sample was pretreated at 673 K under 13.3 kPa of O_2 for 1 h and followed by evacuation at the same temperature for 1 h. α-Pinene (12.5 mmol) was added in the reactor and stirred at 323 K for 2 h. The products were determined by GLC (Shimadzu GC-2014 with a flame ionization detector), using a CBP20 column.

Characterizations

FT-IR spectra were recorded using a SPETRUM ONE FT-IR spectrometer (Perkin-Elmer, Walthham, MA) with a resolution of 4 cm^{-1}. Each sample (13 mg) was pressed into a self-supporting wafer (diameter 13 mm). The catalysts were pretreated under 6.7 kPa of O_2 for 1 h at 673 K and then evacuated for 1 h at 673 K. For determination of the number of Brønsted and Lewis acid sites on WO_3/Al_2O_3, the wafer was exposed to 0.667 kPa of pyridine vaper at 298 K for 10 min followed by evacuation at 373 K, 423 K, 473 K, 523 K, and 573 K for 10 min.

Results and disccusions

Catalysis

In series of Nb_2O_5/Al_2O_3, Ta_2O_5/Al_2O_3, and WO_3/Al_2O_3, 16 wt% Nb_2O_5/Al_2O_3 calcined at 1123 K, 33 wt% Ta_2O_5/Al_2O_3 calcined at 1223 K, and 20 wt% WO_3/Al_2O_3 calcined at 1123 K exhibited the highest activity and Brønsted acidity, respectively.[9-13,28] On these catalysts, monolayer of metal oxides just covers most of alumina surface (Table 1).

Table 1. Physical property of 16NbAl, 33TaAl, and 20WAl

Catalyst	Loading amount (wt%)	Metal content / mmol g(Al_2O_3)$^{-1}$	Surface are^a / m^2 g(Al_2O_3)$^{-1}$	Metal density / nm^{-2}
16NbAl	16	1.43	126	6.8
33TaAl	33	2.23	154	8.7
20WAl	20	0.86	115	5.6

^{a} Surface area of g(Al_2O_3)$^{-1}$ carrier.

The activities of benzylation of anisole on 16NbAl, 33TaAl, and 20WAl were investigated. Figure 1 and Table 2 show the results of benzylation of anisole on the catalysts. Benzylation of anisole is performed for various solid acid catalysts and reported to proceed on Brønsted acid sites.[28-31] The main products were *p*- and *o*-benzyl anisole and the minor product was dibenzyl ether. Multiply product was not observed. Dibenzyl ether is produced on Lewis acid sites by dehydration of two molecules of benzyl alcohol. The reaction proceeded on the catalysts constantly and the yield of benzyl anisole increased linearly. The order of production rate of benzyl anisole on the catalysts was 20WAl >> 16NbAl > 33TaAl. These catalysts gave different selectivity (different ratio of *p*- to *o*-benzyl anisole), indicating that the acid strength of Brønsted acid sites is different from each other.
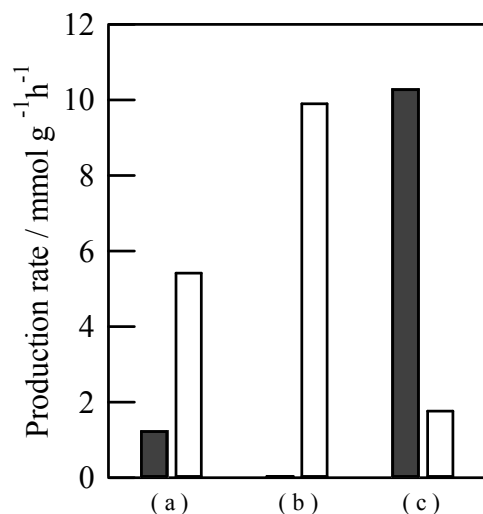

Figure 1. Production rate of benzyl anisole for benzylation of anisole on (a) 16 wt% Nb_2O_5/Al_2O_3 calcined at 1123 K reacted (reaction temperature : (■) 383 K and (□) 413 K), (b) 33 wt% Ta_2O_5/Al_2O_3 calcined at 1223 K (reaction temperature : (■) 383 K and (□) 433 K), and (c) 20 wt% WO_3/Al_2O_3 calcined at 1123 K (reaction temperature : (■) 383 K and (□) 353 K).

Table 2. Results for benzylation of anisole on the catalysts

Catalyst	Reaction temperature / K	Reaction rate / mmol g^{-1} h^{-1}	*p/o* ratio
Nb_2O_5/Al_2O_3	383	1.3	1.09
	413	5.5	1.34
Ta_2O_5/Al_2O_3	383	tr	—
	443	9.9	1.08
WO_3/Al_2O_3	383	10.3	1.29
	353	1.8	1.47

Benzylation of anisole proceeds on 33TaAl at 433 K, but 33TaAl did not promote the reaction at 383 K. The reaction rate of 20WAl at 353 K was higher than that of 16NbAl at 383 K. These facts indicate that the acid strength of Brønsted acid sites on 33TaAl is the weakest and that on 20WAl is the strongest. Figure 2 shows the reaction rate of isomerization of α-pinene on 16NbAl, 33TaAl, and 20WAl. The selectivity of isomerization of α-pinene on these catalysts is summarized in Table 3. Isomerization of α-pinene is used for test reaction to investigate acid-base property and acid strength of the catalyst. Many kinds of products were obtained from isomerization of α-pinene and the products are divided in three groups, β-pinene, bicyclic compound such as fenchene and camphene, and monocyclic compound such as limonene, terpinene, and terpinolene. (Scheme 1) β-pinene is produced on basic sites and bicyclic compound and monocyclic compound are produced on acid sites.
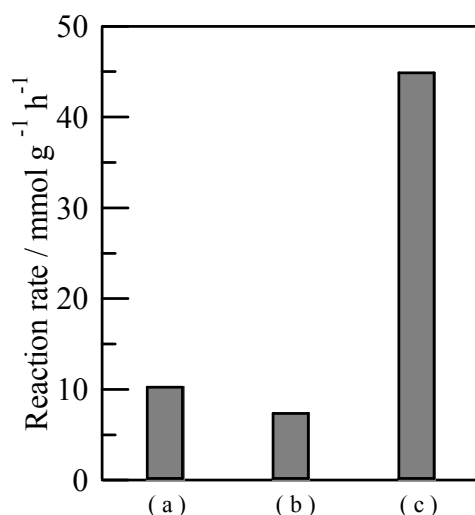

Figure 2. Reaction rate of α-pinene for isomerization on (a) 16 wt% Nb_2O_5/Al_2O_3 calcined at 1123 K, (b) 33 wt% Ta_2O_5/Al_2O_3 calcined at 1223 K, and (c) 20 wt% WO_3/Al_2O_3 calcined at 1123 K.

**Table 3.** Results for α-pinene isomerization on the catalysts

Catalyst	Reaction rate / mmol g⁻¹ h⁻¹	Selectivity[a] (%)							
		1	2	3	4	5	6	7	8
Nb_2O_5/Al_2O_3	10.4	3	40	2	3	35	4	13	5
Ta_2O_5/Al_2O_3	7.5	4	53	5	2	25	2	8	tr
WO_3/Al_2O_3	45.0	tr	63	tr	3	27	1	6	tr

[a] 1 : α-fenchene, 2 : camphene, 3 : β-pinene, 4 : α-terpinene, 5 : limonene, 6 : γ-terpinene, 7 terpinolene, 8 others.

Ohnishi[32] and Yamamoto[32,33] reported that monocyclic and bicyclic compound were produced on Brønsted acid sites and the fraction was changed by the max acid strength of the catalyst. The main products of isomerization of α-pinene on these catalysts were camphene and limonene, indicating these catalysts mainly exhibit Brønsted acid property. The order of reaction rate of α-pinene isomerization on the catalysts was 20WAl >> 16NbAl > 33TaAl. The selectivity on 16NbAl, 33TaAl, and 20WAl was a little different. The results of benzylation of anisole and isomerization of α-pinene also indicate that the Brønsted acid properties of 16NbAl, 33TaAl, and 20WAl were different.

It appears that these catalysts have Brønsted acid sites whose property is different, because 16NbAl, 33TaAl, and 20WAl showed different reaction activity and selectivity. To reveal the Brønsted acid property of these catalysts, pyridine adsorbed FT-IR spectra were measured. The Brønsted acidity was evaluated by the specific amounts of pyridinium ions adsorbed on Brønsted acid sites on these catalysts. The amount of Brønsted acid sites titrated by pyridine was calculated using an integrated molar adsorption coefficient value of $\varepsilon = 1.67$ cm μmol^{-1} for the band area at 1545 cm^{-1} of protonated pyridine.[34,35] Figure 3 shows the amount of Brønsted acid sites on the catalysts evacuated at 373 − 573 K. Since the stronger Brønsted acid sites have the stronger interaction with basic molecule (pyridine), the higher desorption temperature of adsorbed pyridine indicates the presence of stronger Brønsted acid sites.
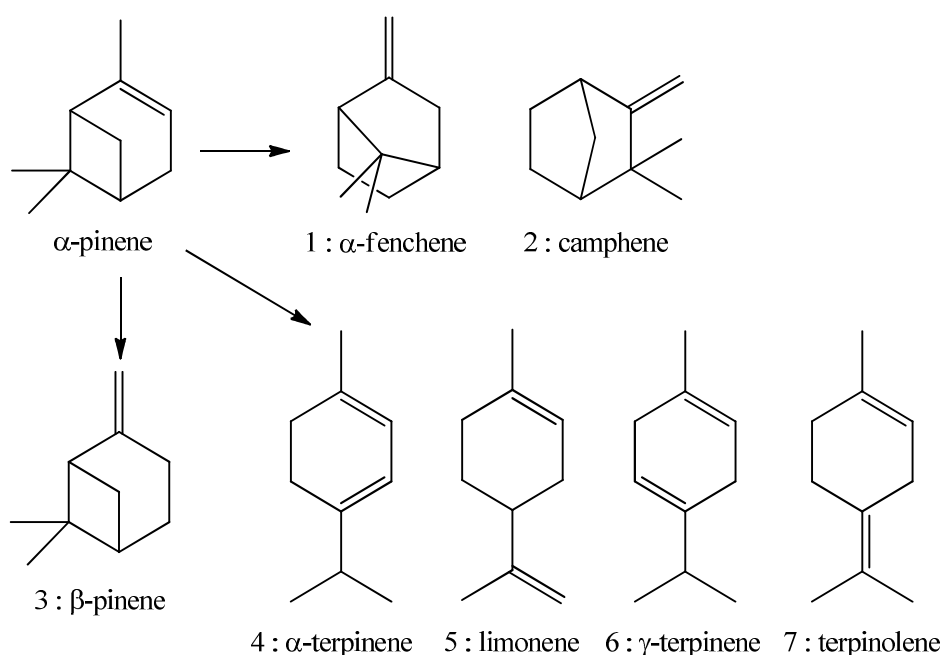
Scheme 1. α-pinene isomerization.

Brønsted acid sites on 20WAl evacuated at 523 K held pyridine. Pyridine desorbed from Brønsted acid sites on 16NbAl and 33TaAl when 16NbAl and 33TaAl were evacuated at 523 K and 473 K, respectively. These results indicates that the maximum acid strength of Brønsted acid sites was in order of 20WAl > 16NbAl > 33TaAl. On the other hand, the amount of Brønsted acid sites was in order of 20WAl > 16NbAl > 33TaAl at each evacuation temperature.

Table 4 summarizes the specific activities per Brønsted acid site of 16NbAl, 33TaAl, and 20WAl for benzylation of anisole and isomerization of α-pinene. The turnover number (TON) for benzylation of anisole is different from each other. The order is 20WAl > 16NbAl > 33TaAl.
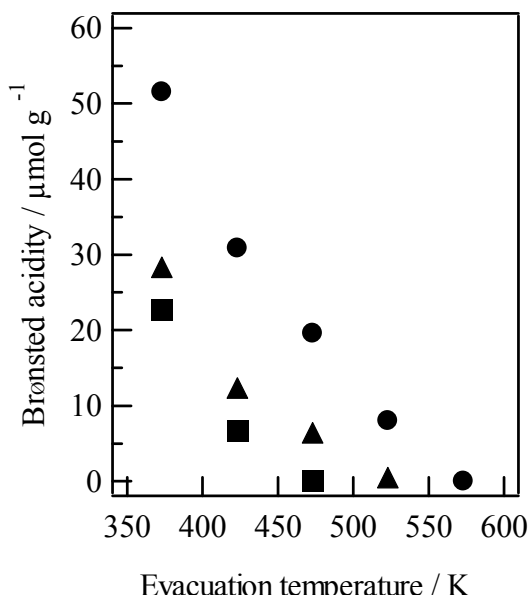

Figure 3. Brønsted acidity of the catalysts evacuated at each temperature. (▲) 16 wt% Nb_2O_5/Al_2O_3 calcined at 1123 K, (■) 33 wt% Ta_2O_5/Al_2O_3 calcined at 1223 K, and (●) 20 wt% WO_3/Al_2O_3 calcined at 1123 K.

Table 4. Specific activity per Brønsted acid site of 16NbAl, 33TaAl, and 20WAl in benzylation and α-pinene isomerization[a]

Catalyst	TON	
	benzylation of anisole[b]	α-pinene isomerization[c]
Nb_2O_5/Al_2O_3	110	1138
Ta_2O_5/Al_2O_3	0	1109
WO_3/Al_2O_3	334	1458

[a] Brønsted acidity was estimated from the amount of pyridine adsorbed on the catalyst evacuated at 423 K
[b] (Yield of benzyl anisole)/(Brønsted acidity)
[c] (Consumption of α-pinene)/(Brønsted acidity)

On the other hand, TON for α-pinene isomerization is similar to each other. These results suggest that benzylation of anisole is sensitive to the strength of Brønsted acid sites, and that the activity for α-pinene isomerization does not depend on the strength of Brønsted acid sites but on the amount of Brønsted acid sites. Therefore based on the results of reactions, it can be thought that 20WAl exhibit the strongest Brønsted acid property and the largest amount of Brønsted acid sites are generated on 20WAl. On the other hand, the strength of Brønsted acid sites on 33TaAl is the weakest and the amount is the smallest.

Characterizations

FT–IR spectra (OH region, 3650–3800 cm-1) of 16NbAl before and after pyridine adsorption are shown in Figure 4(A). A sharp band appeared at 3743 cm^{-1} and a broad band was observed around 3713 cm^{-1} and these bands became very small due to adsorption of pyridine and recovered progressively with increase of evacuation temperature. Figure 4(B) shows difference spectra from 3650 to 3800 cm^{-1} of adsorbed pyridine on 16NbAl. After adsorption of pyridine, negative bands appeared at 3743 and 3713 cm^{-1}. With increase of evacuation temperature, the intensity of the bands at 3743 and 3713 cm^{-1} recovered gradually. Hydroxyl groups at 3743 and 3713 cm^{-1} were almost recovered when was evacuated at 523 K. Figure 4(C) shows difference spectra from 1420 to 1560 cm^{-1} of IR spectra of pyridine adsorbed on 16NbAl. A band at 1545 cm^{-1} assigned to pyridinium ions adsorbed at Brønsted acid sites appeared, and the intensity of this band decreased as the evacuation temperature increased.[34,35] This band disappeared when the catalyst was evacuated at 523 K and the change in this band is in agreement with that in hydroxyl groups. These results indicate that the hydroxyl groups observed at 3713 and 3743 cm^{-1} on 16NbAl act as Brønsted acid sites.
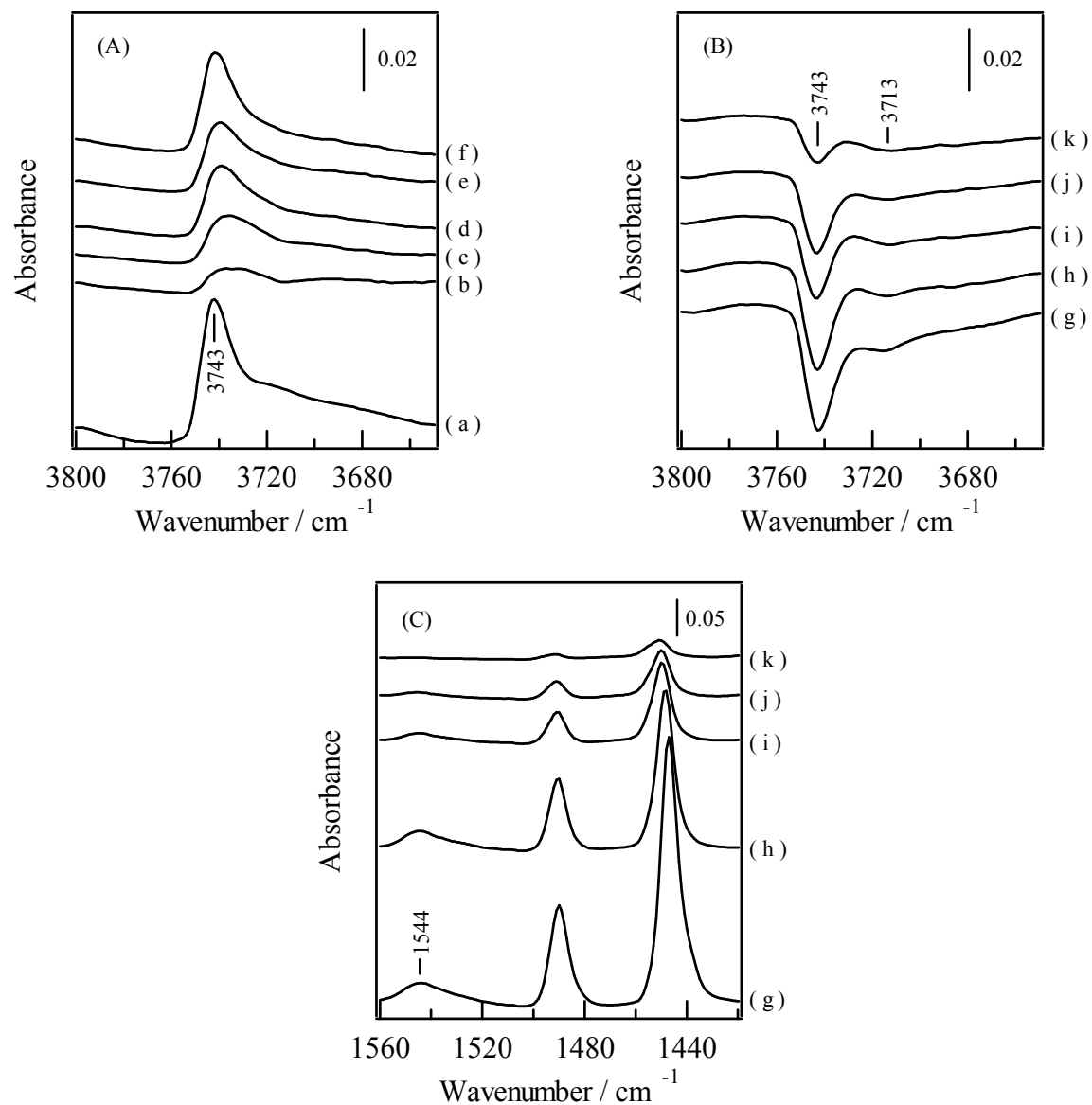
Figure 4. (A) FT-IR spectra of (a) 16 wt% Nb_2O_5/Al_2O_3 calcined at 1123 K, and 16 wt% Nb_2O_5/Al_2O_3 calcined at 1123 K with adsorbed pyridine and subsequent evacuation at (b) 298 K, (c) 373 K, (d) 423 K, (e) 473 K, and (f) 523 K. (B), (C) Difference spectra of pyridine adsorbed on 16 wt% Nb_2O_5/Al_2O_3 calcined at 1123 K (g): (b)-(a), (h): (c)-(a), (i): (d)-(a), (j): (e)-(a), and (k): (f)-(a).

In Figure 5(A), FT–IR spectra from 3550 to 3800 cm^{-1} of 33TaAl before and after pyridine adsorption were shown. A sharp band was shown in the spectra at 3742 cm^{-1} and disappeared when pyridine was introduced. A new band appeared and increased around 3680 cm^{-1} when the catalyst was evacuated at higher temperature than 298K. Figure 5(B) shows difference spectra from 3550 to 3800 cm^{-1} of adsorbed pyridine on 33TaAl. After adsorption of pyridine, a negative band appeared at 3742 cm^{-1}. The band at 3742 cm^{-1} a little recovered and the new band around 3680 cm^{-1} appeared and increased with increase of evacuation temperature. Figure 5(C) shows difference spectra from 1420 to 1560 cm^{-1} of IR spectra of pyridine adsorbed on 33TaAl. Pyridinium ions adsorbed on Brønsted acid sites appeared at 1543 cm^{-1}, and the intensity of this band decreased as the evacuation temperature increased. These results indicate that the hydroxyl groups observed at 3742 cm^{-1} on 33TaAl act as Brønsted acid sites. Incomplete recovery of the band at 3742 cm^{-1} when the catalyst was evacuated at 473 K was supposed to be caused by an interaction between pyridine adsorbed on Lewis acid sites and hydroxyl group existing near Lewis acid sites. A shift of the band assigned to hydroxyl groups from 3742 cm^{-1} to 3660 cm^{-1} by pyridine adsorption is supposed to be caused by the interaction.
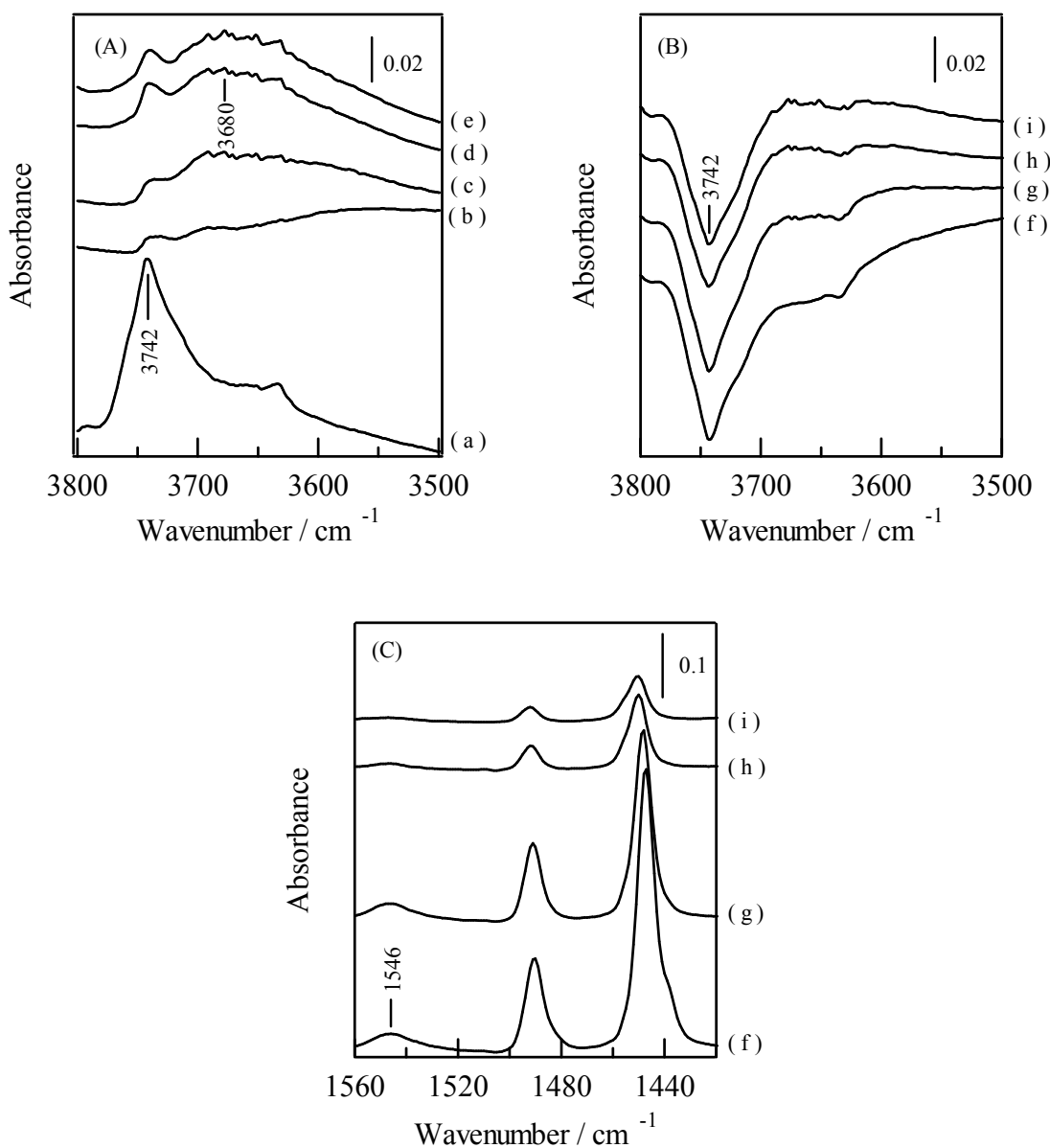
Figure 5. (A) FT-IR spectra of (a) 33 wt% Ta_2O_5/Al_2O_3 calcined at 1223 K, and 33 wt% Ta_2O_5/Al_2O_3 calcined at 1223 K with adsorbed pyridine and subsequent evacuation at (b) 298 K, (c) 373 K, (d) 423 K, and (e) 473 K. (B), (C) Difference spectra of pyridine adsorbed on 33 wt% Ta_2O_5/Al_2O_3 calcined at 1223 K (f): (b)-(a), (g): (c)-(a), (h): (d)-(a), and (i): (e)-(a).

FT–IR spectra from 3500 to 3800 cm^{-1} of 20WAl before and after pyridine adsorption were shown in Figure 6(A). A broad band appeared around 3658 cm^{-1}. Figure 6(B) shows difference spectra from 3500 to 3800 cm^{-1} of adsorbed pyridine on 20WAl. A negative band appeared around 3673 cm^{-1} after pyridine adsorption. With increase of evacuation temperature, the intensity of the bands around 3673 cm^{-1} recovered gradually and the band at 3673 cm^{-1} was shifted to around 3698 cm^{-1} when evacuated at 473 K. Figure 6(C) shows difference spectra from 1420 to 1560 cm^{-1} of IR spectra of pyridine adsorbed on 20WAl. A band at 1543 cm^{-1} assigned to pyridinium ions adsorbed at Brønsted acid sites appeared, and the intensity of this band decreased and the position of the band is shifted to 1546 cm^{-1} as the evacuation temperature increased. The change in the band at 1543 cm^{-1} is corresponding to that in hydroxyl groups. These results indicate that the hydroxyl groups observed around 3658 cm^{-1} on 20WAl act as Brønsted acid sites. The shift of the negative bands from 3673 cm^{-1} to 3698 cm^{-1} is supposed to be brought about by retention of pyridine only on strong Brønsted acid sites due to high temperature evacuation.
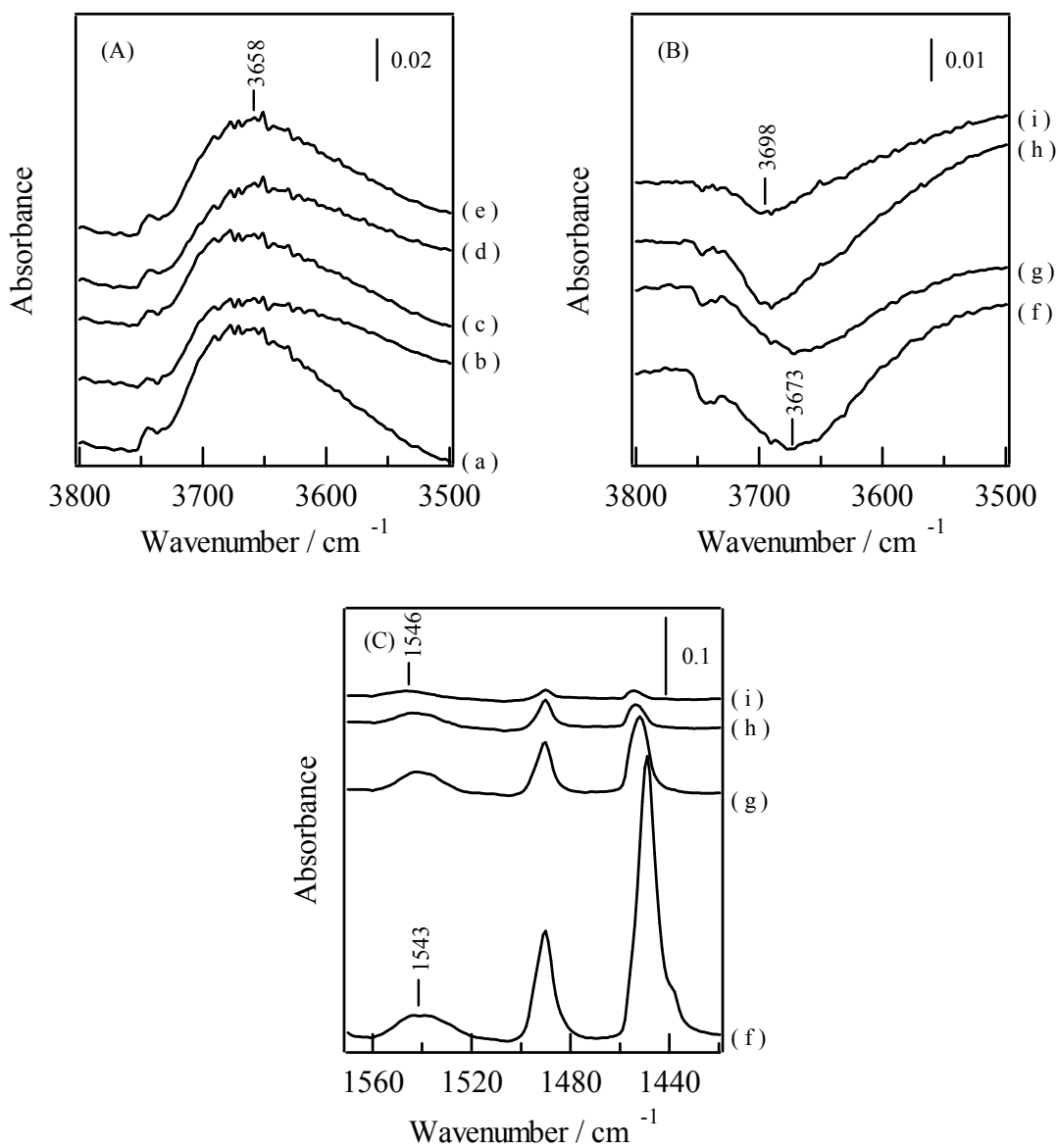
Figure 6. (A) FT-IR spectra of (a) 20 wt% WO$_3$/Al$_2$O$_3$ calcined at 1123 K, and 20 wt% WO$_3$/Al$_2$O$_3$ calcined at 1123 K with adsorbed pyridine and subsequent evacuation at (b) 298 K, (c) 423 K, (d) 473 K, (e) 523 K, and (f) 573 K. (B), (C) Difference spectra of pyridine adsorbed on 20 wt% WO$_3$/Al$_2$O$_3$ calcined at 1123 K (g): (b)-(a), (h): (c)-(a), (i): (d)-(a), (j): (e)-(a), and (k): (f)-(a).

In order to reveal the coordination environment of Brønsted acid sites on these catalysts, changes in hydroxyl groups with loading amount were investigated. In the previous report, from the pyridine adsorbed FT-IR spectra of Nb_2O_5/Al_2O_3 calcined at 1123 K with various Nb_2O_5 loading, we characterized the coordination environment of Brønsted acid sites on Nb_2O_5/Al_2O_3, and concluded that hydroxyl groups (Nb–OH–Nb) formed on the boundaries between niobium oxide monolayer domains act as Brønsted acid sites. Figure 7 shows IR spectra of hydroxyl groups on Ta_2O_5/Al_2O_3 calcined at 1223 K with various Ta_2O_5 loadings. As the Ta_2O_5 loading increased up to 33 wt%, the band at 3572, 3679, and 3727 cm^{-1} decreased in intensity and a new band appeared at 3742 cm^{-1}. The band at 3742 cm^{-1} increased in intensity with Ta_2O_5 loading up to 33 wt%. The band at 3742 cm^{-1} decreased in intensity at 40 wt% loading. In the previous report, we concluded that tantalum oxide monolayer domains are formed on Ta_2O_5/Al_2O_3 calcined at 1223 K with a Ta_2O_5 loading of up to 33 wt%.[12,13] When the Ta_2O_5 loading exceeds 33 wt%, Ta_2O_5 crystal, which has no hydroxyl groups and no Brønsted acid site, is formed. This results in a decrease of Brønsted acid sites. Figure 8 shows difference spectra of hydroxyl groups on Ta_2O_5/Al_2O_3 calcined at 1223 K with various loadings. A negative band at 3742 cm^{-1} increased in intensity with Ta_2O_5 loading up to 33 wt%, and then decreased in intensity at 40 wt%. Considering these results, this band at 3742 cm^{-1} is assigned to hydroxyl groups, which act as Brønsted acid sites, on tantalum oxide monolayer domains.
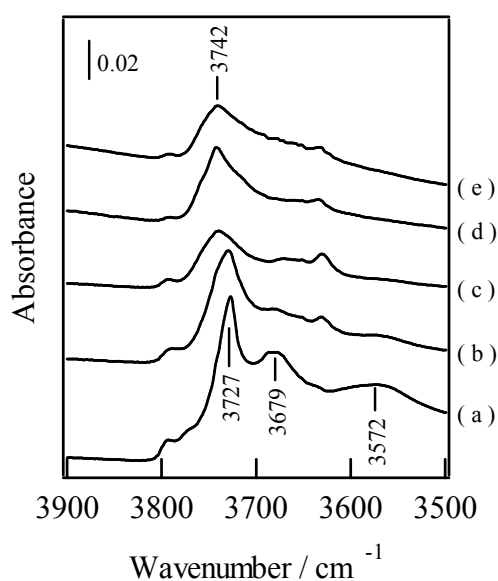

Figure 7. FT-IR spectra of Ta_2O_5/Al_2O_3 calcined at 1223 K with various Nb_2O_5 loadings. (a) γ-Al_2O_3, (b) 10 wt%, (c) 20 wt%, (d) 33 wt%, and (e) 40 wt% Ta_2O_5 loading.

IR spectra of hydroxyl groups on WO_3/Al_2O_3 calcined at 1123 K with various WO_3 loadings are shown in Figure 9. A band at 3726 cm^{-1} is shown in the spectrum of alumina and this band decreased as the WO_3 loading increased up to 20 wt%. On the other hand, a new band appeared at 3658 cm^{-1} and this band increased in intensity with WO_3 loading up to 20 wt%. Over 20 wt%, the band decreased in intensity.
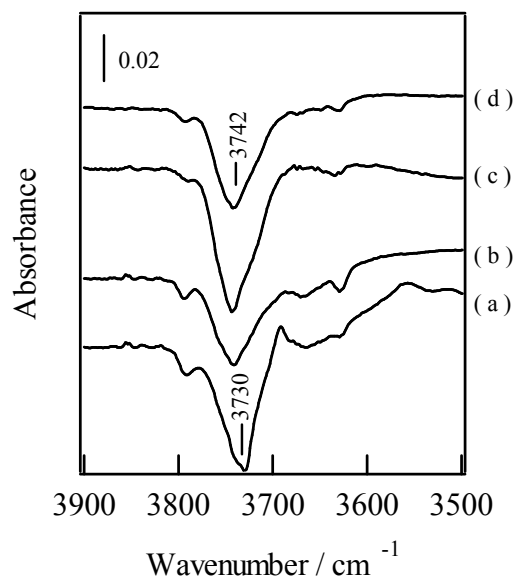

Figure 8. FT-IR spectra of Ta_2O_5/Al_2O_3 calcined at 1223 K with various Ta_2O_5 loadings after pyridine adsorption and subsequent evacuation at 423 K. (a) 10 wt%, (b) 20 wt%, (c) 33 wt%, and (d) 40 wt% Ta_2O_5 loading.
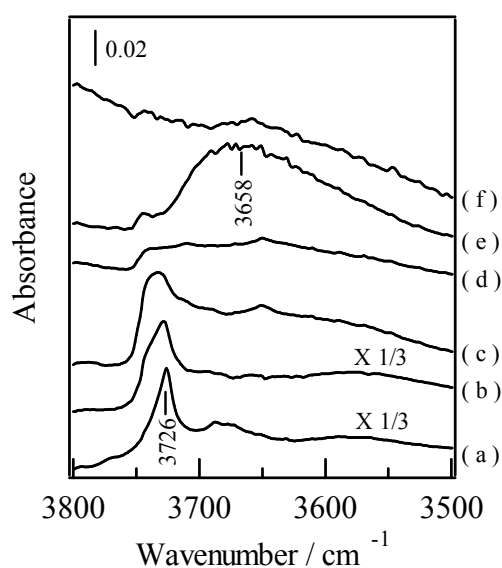

Figure 9. FT-IR spectra of WO_3/Al_2O_3 calcined at 1123 K with various WO_3 loadings. (a) γ-Al_2O_3, (b) 5 wt%, (c) 10 wt%, (d) 15 wt%, (e) 20 wt%, and (f) 30 wt% WO_3 loading.

We investigated the acid property of WO_3/Al_2O_3 prepared with various calcination temperature and WO_3 loading amount, and found that 20 wt% WO_3/Al_2O_3 calcined at 1123 K exhibited the highest reaction activity and Brønsted acidity. In addition, we concluded that WO_3 is loaded as monolayer domains on WO_3/Al_2O_3 calcined at 1123 K with WO_3 loading of up to 20 wt%. When the loading amount became over 20 wt%, monoclinic WO_3, which has no hydroxyl groups and Brønsted acid sites, is formed. This causes decrease of Brønsted acid sites above 20 wt%. Figure 10 shows difference spectra of hydroxyl groups on WO_3/Al_2O_3 calcined at 1123 K with various loadings. A negative band at 3673 cm^{-1} increased in intensity with WO_3 loading up to 20 wt%, and then decreased over 20 wt%. Taking account of the results about characterization of acid property and the structure of WO_3, the band at 3658 cm^{-1} is assigned to hydroxyl groups, which act as Brønsted acid sites, on tungsten oxide monolayer domains.
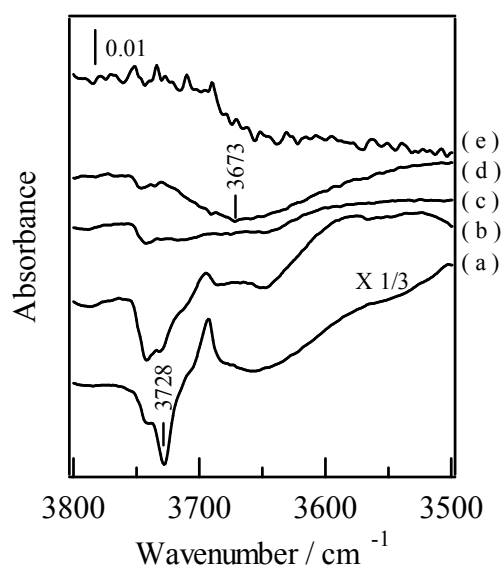

Figure 10. FT-IR spectra of WO_3/Al_2O_3 calcined at 1123 K with various WO_3 loadings after pyridine adsorption and subsequent evacuation at 423 K. (a) 5 wt%, (b) 10 wt%, (c) 15 wt%, (d) 20 wt%, and (e) 30 wt% WO_3 loading.

The results of pyridine adsorbed FT-IR spectra of Nb_2O_5/Al_2O_3, Ta_2O_5/Al_2O_3, and WO_3/Al_2O_3 demonstrate that different types of hydroxyl groups formed on these catalysts and work as Brønsted acid sites. Various metal oxides, such as TiO_2, SiO_2, ZrO_2, and Al_2O_3, possess several kinds of hydroxyl groups. TiO_2,[16-19] SiO_2,[19,20,22] and ZrO_2[23,24] show two types of isolated hydroxyl groups at $3670 - 3780$ cm^{-1}. In contrast, Al_2O_3 has five kinds of isolated hydroxyl groups with bands at 3800, 3775, 3745, 3730, and 3700 cm^{-1} that are assigned to terminal hydroxyl groups coordinated to a single octahedral Al cation, terminal hydroxyl groups coordinated to a single tetrahedral Al cation, bridging hydroxyl groups that link two octahedral Al cations, bridging hydroxyl groups that link one octahedral Al cation and one tetrahedral Al cation, and bridging hydroxyl groups that link three octahedral Al cations, respectively.[24,25] We proposed that the coordination environment of the hydroxyl groups on Nb_2O_5/Al_2O_3 with signals at 3743 and 3713 cm^{-1} are bridging hydroxyl groups that link two octahedral Nb cations (Nb_o), and those that link one octahedral Nb cation and one tetrahedral Nb cation (Nb_t), respectively. Similarly, hydroxyl groups on 33TaAl shown at 3742 cm^{-1} are assignable to bridging hydroxyl groups that link two Ta octahedral cations (Ta_o) and those on 20WAl shown at 3658 cm^{-1} are assigned to bridging hydroxyl groups that link three W cations. The results of characterization of Brønsted acid property (Figure 3 and Table 4) indicated that the order of the maximum strength and amount of Brønsted acid site was 20WAl > 16NbAl > 33TaAl. Niwa et al. reported that H-Y zeolite forms four kinds of hydroxyls working as Brønsted acid site and the strength of Brønsted acid sites differs.[26,27] The hydroxyls are formed on Si–(OH)–Al bonding in super cage, sodalite cage, and hexagonal prism and the coordination environment of the four hydroxyls are different from each other. Some researchers suggested that the difference of strength of Brønsted acid sites is mainly caused by the difference of bond angle of Si–(OH)–Al and the smaller the bond angle is, the stronger Brønsted acid site is.[36,37] It is found that niobic acid has water-tolerant Lewis acid site by Nakajima et al..[38] They explained that water-tolerant Lewis acid sites are generated not on NbO_6 octahedra but on NbO_4 tetrahedra on the surface of niobic acid. These examples show that coordination environment of hydroxyls decides the generation of Brønsted acid sites and strong Brønsted acid sites are generated when the distortion of coordination environment is large. Considering these facts, it is supposed that bridging hydroxyl groups that link three W cations and have large distortion due to linking three W cations on 20WAl are easy to

generate Brønsted acid sites and work as strong Brønsted acid sites and bridging hydroxyl groups that link two Ta octahedral cations and have small distortion due to linking two Ta octahedral cations on 33TaAl are difficult to generate Brønsted acid sites and work as weak Brønsted acid sites. The difference of coordination environment is expected to cause the difference of acid amount and strength of Brønsted acid sites on these catalysts.

Conclusions

Monolayer of niobium oxide, tantalum oxide, and tungsten oxide supported on alumina (16 wt% Nb_2O_5/Al_2O_3 calcined at 1123 K, 33 wt% Ta_2O_5/Al_2O_3 calcined at 1223 K, and 20 wt% WO_3/Al_2O_3 calcined at 1123 K) exhibited different reaction activity and Brønsted acid property. The number and maximum acid strength of Brønsted acid sites were in order of 20WAl > 16NbAl > 33TaAl. On each catalyst, hydroxyl groups formed on monolayer of these metal oxides on alumina act as Brønsted acid sites. On 16NbAl, bridging hydroxyl groups that link two octahedral Nb cations and those that link one octahedral Nb cation and one tetrahedral Nb cation worked as Brønsted acid sites. On the other hand, bridging hydroxyl groups that link two Ta octahedral cations act as Brønsted acid sites on 33TaAl and bridging hydroxyl groups that link three W cations act as Brønsted acid sites on 20WAl. The change in activity and Brønsted acid property was caused by difference of coordination environment of hydroxyl groups on monolayer of these metal oxides.

References

(1)   Tanabe, K. *Catal. Today,* **2003**, *78*, 65.

(2)   Tanabe, K.; Okazaki, S. *Appl. Catal. A-Gen.,* **1995**, *133*, 191.

(3)   Tanabe, K. *Catal. Today,* **1990**, *8*, 1.

(4)   Tanabe, K. *Mater. Chem. Phys.,* **1987**, *17*, 217.

(5)   Okuhara, T. *Chem. Rev.,* **2002**, *102*, 3641.

(6)   Iizuka, T.; Ogasawara, K.; Tanabe, K. *Bull. Chem. Soc. Jpn.,* **1983**, *56*, 2927.

(7)   Ohuchi, T.; Miyatake, T.; Hitomi, Y.; Tanaka, T. *Catal. Today,* **2007**, *120*, 233.

(8)   Ushikubo, T.; Wada, K. *Appl. Catal.,* **1990**, *67*, 25.

(9)   Shishido, T.; Kitano, T.; Teramura, K.; Tanaka, T. *Catal. Lett.,* **2009**, *129*, 383.

(10)   Shishido, T.; Kitano, T.; Teramura, K.; Tanaka, T. *Top. Catal.,* **2010**, *53*, 672.

(11)   Kitano, T.; Shishido, T.; Teramura, K.; Tanaka, T. *J. Phys. Chem. C,* **2012**, *116*, 11615.

(12)   Kitano, T.; Okazaki, S.; Shishido, T.; Teramura, K.; Tanaka, T. *Chem. Lett.,* **2011**, *40*, 1332.

(13)   Kitano, T.; Okazaki, S.; Shishido, T.; Teramura, K.; Tanaka, T. *Catal. Today,* **2012**, *192*, 189.

(14)   Kitano, T.; Tomohiro, H.; Toshio, U.; Shishido, T.; Teramura, K.; Tanaka, T. *to be submitted*.

(15)   Jackson, P.; Parfitt, G. D. *Trans. Faraday Soc.,* **1971**, *67*, 2469.

(16)   Yates, D. J. *J. Phys. Chem.,* **1961**, *65*, 746.

(17)   Primet, M.; Pichat, P.; Mathieu, M. V. *J. Phys. Chem.,* **1971**, *75*, 1216.

(18)   Tanaka, K.; White, J. M. *J. Phys. Chem.,* **1982**, *86*, 4708.

(19)   Morrow, B. A.; McFarlan, A. J. *Langmuir,* **1991**, *7*, 1695.

(20)   Morrow, B. A.; McFarlan, A. J. *J. Phys. Chem.,* **1992**, *96*, 1395.

(21)   Zecchina, A.; Bordiga, S.; Spoto, G.; Marchese, L.; Petrini, G.; Leofanti, G.; Padovan, M. *J. Phys. Chem.,* **1992**, *96*, 4991.

(22)   Agron, P. A.; Fuller, E. L.; Holmes, H. F. *J. Colloid Interf. Sci.,* **1975**, *52*, 553.

(23)   Yamaguchi, T.; Nakano, Y.; Tanabe, K. *Bull. Chem. Soc. Jpn.,* **1978**, *51*, 2482.

(24)   Morterra, C.; Magnacca, G. *Catal. Today,* **1996**, *27*, 497.

(25)   Knozinger, H.; Ratnasamy, P. *Catal. Rev.-Sci. Eng.,* **1978**, *17*, 31.

(26)   Suzuki, K.; Katada, N.; Niwa, M. *J. Phys. Chem. C,* **2007**, *111*, 894.

(27)   Sarria, F. R.; Marie, O.; Saussey, J.; Daturi, M. *J. Phys. Chem. B,* **2005**, *109*, 1660.

(28)   de la Cruz, M. H. C.; da Silva, J. F. C.; Lachter, E. R. *Catal. Today,* **2006**, *118*, 379.

(29)   de la Cruz, M. H. C.; Abdel-Rehim, M. A.; Rocha, A. S.; da Silva, J. F. C.; Faro, A. D.; Lachter, E. R. *Catal. Commun.,* **2007**, *8*, 1650.

(30)   Okumura, K.; Yamashita, K.; Hirano, M.; Niwa, M. *Chem. Lett.,* **2005**, *34*, 716.

(31)   Okumura, K.; Yamashita, K.; Hirano, M.; Niwa, M. *J. Catal.,* **2005**, *234*, 300.

(32)   Yamamoto, T.; Tanaka, T.; Funabiki, T.; Yoshida, S. *J. Phys. Chem. B,* **1998**, *102*, 5830.

(33)   Yamamoto, T.; Tanaka, T.; Matsuyama, T.; Funabiki, T.; Yoshida, S. *J. Phys. Chem. B,* **2001**, *105*, 1908.

(34)   Barzetti, T.; Selli, E.; Moscotti, D.; Forni, L. *J. Chem. Soc.-Faraday Trans.,* **1996**, *92*, 1401.

(35)   Emeis, C. A. *J. Catal.,* **1993**, *141*, 347.

(36)   Sastre, G.; Fornes, V.; Corma, A. *J. Phys. Chem. B,* **2000**, *104*, 4349.

(37)   Katada, N.; Suzuki, K.; Noda, T.; Sastre, G.; Niwa, M. *J. Phys. Chem. C,* **2009**, *113*, 19208.

(38)   Nakajima, K.; Baba, Y.; Noma, R.; Kitano, M.; Kondo, J. N.; Hayashi, S.; Hara, M. *J. Am. Chem. Soc.,* **2011**, *133*, 4224.

Summary

In this thesis, the author summarized the results of evaluation of acid property and structural characterization of alumina-supported transition metal oxide (Nb, Ta, Mo, and W). As the results of characterization, the author proposed a new generation mechanism of Brønsted acid sites on supported metal oxide.

In Chapter 1, the author reports that thermally stable Brønsted acid sites were generated on alumina-supported niobium oxide (Nb_2O_5/Al_2O_3) calcined at high temperature (1123 K) and the acid property strongly depended on calcination temperature and loading amount of Nb_2O_5. The catalyst promoted various reactions such as benzylation of anisole, cracking of cumene, and isomerzation of α-pinene, and the reaction activity and Brønsted acidity of the catalyst became the maximum when the calcination temperature was 1123 K and the loading amount was 16 wt%. On the catalyst prepared by the optimized condition, niobium oxide was supported as two-dimensional monolayer and covered most of alumina surface. The author concluded that Brønsted acid sites are generated on two-dimensional niobium oxide monolayer.

In Chapter 2, the author describes the detail structure of two-dimensional structured niobium oxide monolayer on Nb_2O_5/Al_2O_3 and generation mechanism of Brønsted acid sites. The results of structural characterization exhibited that niobium oxide monolayer domains were supported on alumina and the domains increased with increase of loading amount. The author suggested that bridging hydroxyl groups that link two octahedral Nb cations (Nb_o) and those that link one octahedral Nb cation and one tetrahedral Nb cation (Nb_t) were formed on the boundaries between niobium oxide monolayer domains and the hydroxyl groups worked as Brønsted acid sites.

In Chapter 3, the effect of niobium oxide monolayer domain size on the activity and Brønsted acid property of Nb_2O_5/Al_2O_3 is summarized. The pH value in the preparation solution of Nb_2O_5/Al_2O_3 strongly affects the activity and Brønsted acid property and Brønsted acidity became the largest when Nb_2O_5/Al_2O_3 was prepared by the preparation solution of pH 1.7. The results of structural characterization indicated that the niobium oxide domain size increased with raise of the pH value in the preparation solution. The author supposed that Brønsted acid sites were generated on

the boundaries between large niobium oxide monolayer domains and implied that the strong distortion of Nb–(OH)–Nb bond was necessary to generate Brønsted acid sites.

In Chapter 4, the acid property and structure of alumina-supported tantalum oxide (Ta_2O_5/Al_2O_3) calcined at high temperature (1223 K) are discussed. On Ta_2O_5/Al_2O_3, the activity and Brønsted acid property depended on calcination temperature and loading amount and the optimized condition was Ta_2O_5 loading of 33 wt% and calcination at 1223 K. The author concluded that tantalum oxide was loaded as two-dimensional monolayer and the tantalum oxide monolayer concerned with generation of Brønsted acid sites.

In Chapter 5, the author describes the acid property and structure of alumina-supported tungsten oxide (WO_3/Al_2O_3) calcined at high temperature (1123 K). Calcination temperature and loading amount largely affected the reaction activity and Brønsted acid property of WO_3/Al_2O_3 and 20 wt% WO_3/Al_2O_3 calcined at 1123 K showed the highest activity and Brønsted acidity. The results of structural characterization suggested that tungsten oxide was loaded as two-dimensional monolayer and the tungsten oxide monolayer concerned with generation of Brønsted acid sites.

In Chapter 6, the acid property and structure of alumina-supported molybdenum oxide (MoO_3/Al_2O_3) calcined at high temperature (1073 K) are characterized. The activity and Brønsted acid property of MoO_3/Al_2O_3 were also affected by calcination temperature and loading amount and the optimized condition was MoO_3 loading of 11 wt% and calcination at 1073 K. The author concluded that molybdenum oxide was loaded as two-dimensional monolayer or small three-dimensional cluster and the monolayer mainly concerned with generation of Brønsted acid sites.

In Chapter 7, comparison of Brønsted acid property and coordination state of hydroxyl groups working as Brønsted acid sites on Nb_2O_5/Al_2O_3, Ta_2O_5/Al_2O_3, and WO_3/Al_2O_3 is done. The amount and strength of Brønsted acid sites were different from each other and the order of amount and strength was WO_3/Al_2O_3 > Nb_2O_5/Al_2O_3 > Ta_2O_5/Al_2O_3. The author suggested that the coordination state of hydroxyls working as Brønsted acid sites differed from each other and the difference of coordination state caused the difference of amount of strength of Brønsted acid sites.

In short, the author found that transition metal oxide (Nb, Ta, Mo, and W) forms

two-dimensional monolayer on Nb_2O_5/Al_2O_3, Ta_2O_5/Al_2O_3, MoO_3/Al_2O_3, and WO_3/Al_2O_3 calcined at high temperature (1073 - 1223 K) and the monolayer of transition metal oxide concerned with generation of Brønsted acid sites. In addition, the author suggested that transition metal oxide was supported as domains and hydroxyls formed on the boundaries between monolayer domains are working as Brønsted acid sites, which were thermally stable. Generation of Brønsted acid sites is supposed to demand large monolayer domains. On Nb_2O_5/Al_2O_3, Ta_2O_5/Al_2O_3, MoO_3/Al_2O_3, and WO_3/Al_2O_3, the amount and strength of Brønsted acid sites were different from each other and the order of amount and strength was WO_3/Al_2O_3 > Nb_2O_5/Al_2O_3 > Ta_2O_5/Al_2O_3. The author suggested that the coordination state of hydroxyls working as Brønsted acid sites differed from each other and the difference of coordination state caused the difference of amount of strength of Brønsted acid sites. This generation mechanism of Brønsted acid sites is supposed to be one of the models of acid sites generation on other supported metal oxide exhibiting Brønsted acid property. Because clarification of the generation mechanism of acid sites on supported metal oxide must greatly contribute to the development of highly-efficient reaction process using supported metal oxide, this study is expected to play an important role for the development of highly-efficient reaction process.

List of Publications

Chapter1.

1. Brønsted Acid Generation over Alumina-Supported Niobia by Calcination at 1173 K
Tetsuya Shishido, Tomoyuki Kitano, Kentaro Teramura, and Tsunehiro Tanaka
Catalysis Letters, **2009,** *129,* 383-386.

2. Generation of Brønsted Acid Over Alumina-Supported Niobia by Calcination at High Temperatures
Tetsuya Shishido, Tomoyuki Kitano, Kentaro Teramura, and Tsunehiro Tanaka
Topics in Catalysis, **2010,** *53,* 672-677.

3. Brønsted Acid Property of Alumina-Supported Niobium Oxide Calcined at High Temperature : Characterization by Acid-Catalyzed Reactions and Spectroscopic Methods
Tomoyuki Kitano, Tetsuya Shishido, Kentaro Teramura, and Tsunehiro Tanaka
The Journal of Physical Chemistry C, **2012,** *116,* 11615-11625.

Chapter2.

4. Characterization of Thermally Stable Brønsted Acid Sites on Alumina-Supported Niobium Oxide Calcined at High Temperature
Tomoyuki Kitano, Tetsuya Shishido, Kentaro Teramura, and Tsunehiro Tanaka
To be submitted.

Chapter3.

5.   The Acid Property of Nb_2O_5/Al_2O_3 Prepared by Impregnation Method Using Niobium Oxalate Solution: Effect of pH of Solution on the Structure and Acid Property
Tomoyuki Kitano, Tetsuya Shishido, Kentaro Teramura, and Tsunehiro Tanaka
To be submitted.

Chapter4.

6.   Generation of Brønsted Acid Sites on Alumina-supported Tantalum(V) Oxide Calcined at 1223 K
Tomoyuki Kitano, Shota Okazaki, Tetsuya Shishido, Kentaro Teramura, and Tsunehiro Tanaka
Chemistry Letters, **2011,** *40,* 1332-1334.

7.   Generation of Brønsted acid sites on Al_2O_3-supported Ta_2O_5 Calcined at high temperatures
Tomoyuki Kitano, Shota Okazaki, Tetsuya Shishido, Kentaro Teramura, and Tsunehiro Tanaka
Catalysis Today, **2012,** *192,* 189-196.

Chapter5.

8.   Effect of High Temperature Calcination on Generation of Brønsted Acid Sites of WO_3/Al_2O_3
Tomoyuki Kitano, Tomohiro Hayashi, Toshio Uesaka, Tetsuya Shishido, Kentaro Teramura, and Tsunehiro Tanaka
The Journal of Physical Chemistry C, submitted

Chapter6.

9.   Brønsted Acid Generation of Alumina-Supported Molybdenum Oxide Calcined at High Temperatures: Characterization by Acid-Catalyzed Reactions and Spectroscopic Methods
Tomoyuki Kitano, Shota Okazaki, Tetsuya Shishido, Kentaro Teramura, and Tsunehiro Tanaka
Journal of Molecular Catalysis A: Chemical, in press.

Chapter7.

10.   Comparison between Brønsted Acid Property of Nb_2O_5/Al_2O_3, Ta_2O_5/Al_2O_3, and WO_3/Al_2O_3 Calcined at High Temperatures
Tomoyuki Kitano, Tomohiro Hayashi, Shota Okazaki, Tetsuya Shishido, Kentaro Teramura, and Tsunehiro Tanaka
To be submitted.